8-2020

Zebrafish as a Model to Understand the Impact of Inactivity and Neuromuscular Electrical Stimulation on Duchenne Muscular Dystrophy

Elisabeth Kilroy
University of Maine, elisabeth.kilroy@maine.edu

ZEBRAFISH AS A MODEL TO UNDERSTAND THE IMPACT OF INACTIVITY AND NEUROMUSCULAR ELECTRICAL STIMULATION ON DUCHENNE MUSCULAR DYSTROPHY

By

Elisabeth Ann Kilroy

B.S. College of Charleston, 2014

A DISSERTATION

Submitted in Partial Fulfillment of the

Requirements for the Degree of

Doctor of Philosophy

(in Biomedical Science)

The Graduate School

The University of Maine

August 2020

Advisory Committee:

Clarissa Henry, Professor of Biological Sciences, University of Maine, Advisor

Gregory Cox, Associate Professor, The Jackson Laboratory

Thane Fremouw, Associate Professor of Psychology, University of Maine

Roger Sher, Research Associate Professor of Neurobiology, Stony Brook University

Calvin Vary, Faculty Scientist III, Maine Medical Center Research Institute

ZEBRAFISH AS A MODEL TO UNDERSTAND THE IMPACT OF INACTIVITY AND NMES ON DUCHENNE MUSCULAR DYSTROPHY

By

Elisabeth Ann Kilroy

Dissertation Advisor: Dr. Clarissa Henry

An Abstract of the Dissertation Presented
in Partial Fulfillment of the Requirements for the
Degree of Doctor of Philosophy
(in Biomedical Science)
August 2020

Skeletal muscle plasticity is imperative for functional adaptation to changing demands in activity. Although a great deal is known about the structural and functional plasticity of healthy skeletal muscle, far less is known about plasticity in diseased muscle. Here, we combined the power of the zebrafish model with the adaptability of neuromuscular electrical stimulation (NMES) to study the basic mechanisms of plasticity in the zebrafish model of Duchenne Muscular Dystrophy (DMD). Four NMES paradigms, defined by their frequency, delay, and voltage, were designed to emulate the repetition and load schemes of human resistance training programs. Additionally, two inactivity paradigms were designed to emulate activity patterns in individuals with DMD. Three sessions of endurance NMES improve muscle structure, increase swim velocity and distance traveled, and extend survival. Endurance NMES significantly increased the number and length of branching for neuromuscular junctions. Nuclear surface area and volume also significantly increased following endurance NMES. Time-lapse imaging suggests less degeneration and improved regeneration of the fast-twitch muscle fibers. Conversely, three days of inactivity worsen muscle structure and decreases survival. Strikingly, inactivity followed by a single session of endurance or power NMES obliterates muscle resilience. Therefore, our data clearly indicate that, at least in the zebrafish model, some resistance training is beneficial

whereas inactivity is deleterious for dystrophic muscle. More importantly, though, our data provide a new methodology with which to study muscle plasticity in healthy and diseased muscle.

DEDICATION

To all the children and adults fighting back against muscular dystrophy, to their caregivers and to their advocates, this is for you. Your strength ignites a fiery passion inside me that will never, ever be dimmed until cures are found. Adapt and overcome, always.

ACKNOWLEDGEMENTS

To the Graduate School of Biomedical Science and Engineering, thank you. You provided me with a graduate experience that surpassed all of my expectations. You supported me as I ventured down unchartered territories in graduate education and professional development. To the Admissions Committee, thank you for looking past all the undergraduate courses I did not take and all the experiences I did not have. Thank you for believing in me and my mission to cure muscular dystrophy. If I had to choose to attend graduate school all over again, I would choose GSBSE always.

To my advisor, Dr. Clarissa Henry, and committee members, Drs. Greg Cox, Cal Vary, Roger Sher, and Thane Fremouw, thank you for challenging me, for teaching me how to ask questions, and for showing me how to confidently admit that I do not know the answer. Thank you for allowing me to chase this crazy idea of mine without any proof that it could work. Clarissa, thank you for all of the laughs and tears, and for the adventures in Italy and Costa Rica, including the bajillion hours spent in the airport. Thank you for pushing me to be independent from my very first day. Thank you for giving me time to pursue my passions for higher education, advocacy and spending time with those fighting muscular dystrophy. Thank you for always volunteering me for speaking engagements and tackling the toughest challenges. Finally, thank you for allowing me to have open access to your refrigerator, washer and dryer, hair brush, and snack drawer. I promise that you did not eat your snacks as fast as you thought you did.

To all those who assisted me on this project, these experiments would not be possible without you. To the members of the Henry Lab, both past and present, thank you for allowing me to share this space and grow into a scientist. I promise to never steal a pipette again. To all the undergraduate students that worked alongside me, especially Kaylee Brann, Devon Varney, Amelie Germond, and Claire Schaffer, thank you for bringing your energy, your stories, and your love for science to the lab each and every day. You are all exceptional human beings and I am

excited to continue watching you grow into the best versions of yourselves. Dr. Josh Kelley and Ahmed Almaghasilah, thank you for your image analysis expertise and providing me with superior methods for quantifying muscle health and neuromuscular junctions. Dr. Karissa Tilbury and Jordan Miner, thank you for sharing your biomedical engineering expertise with me and using SHG to provide an in-depth analysis of the sarcomeres. Drs. Ben King and Joy-El Talbot, and Kodey Silknitter, thank you for navigating the large data sets that accompanied the RNAseq experiment and providing me numerous pathways to chase. Drs. Jared Talbot and Susan Amacher, thank you for sharing your transgenic 3MuscleGlow zebrafish lines and making in vivo time-lapse analyses possible. To Mark Nilan, thank you for outstanding care and maintenance of the zebrafish facility. With your help I went from one male and one female zebrafish to way too many zebrafish.

To my mother and stepfather, Julie and Russ Moser, thank you. Thank you for the car and moped that got me to and from the laboratory. Thank you for allowing me to go grocery shopping in your refrigerator and pantry and for the hundreds of loads of laundry that I did at your house. Momma, thank you for giving me pep talks, for always encouraging me to keep my head down and focused on my goals, and for the jackets and wool socks that I borrowed and failed to return. Russ, thank you for finding the errors in my scripts, for the reminders to shut down my computer, and for the homemade beers and handcrafted furniture.

To my father, Dr. Timothy Kilroy, thank you for forcing me to apply to UMaine and paying for the application fee. Thank you for always showing me the importance of education, networking and professional growth. Thank you for reminding me to take breaks and to strive for progress over perfection. Let it be known that you are no longer the real Dr. Kilroy.

To my brothers, Killian, Keegan and Konlon Kilroy, thank you for shaping me into the competitive and committed teammate that I am today. Keegan, thank you for helping me design the NMES parameters and the gym. Thank you for always being one phone call away and offering your engineering expertise to help me move this project forward. Killian, thank you for

paying for my cell phone bill to make these critical phone calls. Konlon, thank you for allowing me to drive across the country with you. I love watching you grow and will never forget to turn up for the weekends.

To Gabriel Jensen, thank you for everything. Your daily support, passion for science, and ability to make me belly laugh filled my gratitude cup every single day. To think that you were once a stranger crashing on my couch to now my fiancé and best best friend is an incredible feeling. For over three years, we woke up together, went to lab together, took classes together, ate lunch together, and went home together. I never imagined spending that much time with a single human being. You helped me work through my data and experimental design, you cheered for me at every presentation, you cooked me dinner, and you understood that five minutes in lab could mean an hour or more. I cannot wait to spend the rest of my life with you.

To Scott Delcourt and Drs. Kody Varahramyan and Joan Ferrini-Mundy, thank you for providing me with everything I needed to succeed as a graduate student and in my journey to becoming the best researcher that I can be. The commitment that you three have to growing and improving graduate education at UMaine is beyond anything I have ever witnessed. Scott, thank you for teaching me how to be compassionate and how to be an exceptional mentor. Dr. Varahramyan, thank you for teaching me how to negotiate and how to see things from different perspectives. Dr. Ferrini-Mundy, thank you for showing me how to be a leader and how to be a powerful force in the STEM community. As I continue my journey in academia, I will continue to reflect on these moments we shared.

To Tawny Martin, thank you for being my soul sister. You put me on a never-ending journey to becoming my best self. You taught me to be patient with myself, to share my emotions with others, and to speak for what I believe in. It continues to amaze me that we have created an ever-lasting friendship from thousands of miles apart. Our time at MDA Summer Camp, in Las Vegas, and in the wilderness of the Pacific Northwest are some of my fondest memories. In the hardest times, I turn inward and ask myself what you would do, and that is

when I grab my yoga mat, make tea, and meditate. Thank you for teaching me how to manifest my dreams and recreate the stories I tell myself.

To the campers and counselors at MDA Summer Camp, thank you for being a part of the best week of my year. From the questionable food, the marshmallow shooters, the boat races to the talent show and the final dance, the stories and memories will never be fully understood by an outsider.

To Morgan and Chelsea Hoffmann, thank you for supporting my research. I will never forget watching professional golfers tee off in honor of those living with muscular dystrophy. I will never forget trying to explain what I do to Rickie Fowler. I am honored to be the recipient of the first ever research award from the Morgan Hoffmann Foundation. The DanioVision experiments presented in below would not be possible without this award.

To NSF GRFP, thank you for recognizing my ability to become an exceptional scientist, researcher, mentor, and human being. Being awarded the NSF GFRP was one of the best days of my life. Many individuals told me not to get my hopes up and that I would never be awarded such a prestigious award. The stipend and education allowance allowed me to dive deeper into my research and ask more questions. To all those who have doubters and haters telling them not to apply, I promise you need to apply.

To the students, faculty and staff of GSBSE and the Graduate School, thank you. Thank you for building an incredible network of support.

TABLE OF CONTENTS

LIST OF TABLES

LIST OF FIGURES

CHAPTER 1

REVIEW OF THE LITERATURE

1.1 Introduction

My research examines the impact of inactivity versus neuromuscular electrical stimulation (NMES) on disease progression in the zebrafish model of Duchenne muscular dystrophy (DMD). Before diving into the significance of this research, it is worthy to discuss skeletal muscle and the components that allow it to perform functions that are critical to organismal health. A special emphasis is placed on the dystrophin protein and the role it plays in maintaining the structural integrity of the muscle fiber. More importantly, though, dystrophin is discussed in the disease context, from both clinical and molecular perspectives, since DMD is the direct result of its absence. Lastly, an in-depth review of studies examining the role that inactivity and activity play in DMD disease progression is provided to demonstrate the need for more research as well as a new approach to this research question.

1.2 Skeletal Muscle Function

Unlike many organs in the body, most individuals are confident in defining what skeletal muscle is, identifying where it is located, and describing the roles it plays in the human body. However, the complexity of skeletal muscle's function in human health continues to grow as new proteins are identified, and new roles for previously identified proteins are uncovered. Throughout the hundreds of thousands of research papers investigating skeletal muscle, it is well-established that skeletal muscle is a highly dynamic tissue whose structural and molecular networks actively respond to changes in the demands imposed on it. The skeletal muscle's ability to adapt to these demands is critical to maintaining not only muscle health but the overall health of an individual.

Skeletal muscle's primary role in the human body is to generate movement. It allows us to navigate throughout our world and to interact with our surroundings. Additionally, skeletal muscle maintains our posture and allows us to breath. Functional independence in our daily lives is determined by how successfully our skeletal muscle functions. However, skeletal muscle contributes to human health beyond generating the force and power required for movement, and these contributions are often overlooked. Over the past decade, an upsurge in 'omic' technologies, including proteomics and metabolomics, painted a more detailed molecular picture of skeletal muscle. This picture now encompasses a myriad of interactions with other body systems through numerous players [1]. Most notably, skeletal muscle is now classified as an endocrine organ. Recently, it was established that skeletal muscle secretes cytokines and other peptides, consequently termed myokines, that play important roles in maintaining metabolic homeostasis [2,3] and inflammation [4,5]. Interestingly, these myokines are regulated by skeletal muscle contractions and activity levels [2,6–8]. Skeletal muscle is also a highly metabolic tissue. It is essential for basal energy metabolism by serving as a storage site for carbohydrates and glucose homeostasis [9]. Additionally, skeletal muscle is a reservoir for amino acids, housing 50-75% of proteins required by other tissues, including the skin, brain, and heart [9]. Lastly, a major role skeletal muscle plays in energy metabolism is the production of heat to maintain core temperature [9].

Since skeletal muscle plays an important role in human movement and a vast amount of other key aspects of human health, it is not surprising that research continues to demonstrate that it is one of the primary predictors of longevity and recovery from illness and injury. Specifically, reduced skeletal muscle mass impairs the body's ability to respond to and recover from stress and chronic illness [9]. This is best exemplified in aging, where the loss in skeletal muscle mass contributes to an overall decline in physical functioning, increased disability, and mortality [10]. Therefore, robust skeletal muscle mass is essential for whole-body homeostasis

[11], and it is important that research focuses on preserving this tissue in healthy and diseased states.

1.3 Skeletal Muscle Structure

There are over 650 named skeletal muscles within the human body, and each of them share the same underlying structure. Skeletal muscle structure is highly intricate but can be broken down into four main components: the nerves that signal muscle contraction, the individual muscle fibers that contract, the vasculature that delivers oxygen, and the metabolic machinery that supplies energy to power movement [1]. Each of these four components contain many subcomponents with intricate structures that play a critical role in maintaining the overall structure of the muscle and allow it to perform its many functions. Understanding the underlying structure of skeletal muscle brings to light how a small perturbation, such as the presence of a partially formed protein, can spiral into a vicious cycle of degeneration and weakness.

Skeletal muscle is best described as a cylindrical bundle of cylindrical bundles that are separated from one another by connective tissue sheaths. For example, if we build a biceps muscle, the muscle responsible for flexion of the elbow, we begin first with the myofilaments, which are actin and myosin. Actin and myosin are long cylindrical proteins that are found in series along the length of the muscle fiber. Together, they are surrounded by a plasma membrane, known as the sarcolemma. Individual muscle fibers are wrapped by a second connective tissue sheath, called the endomysium, and are arranged into bundles, called fascicles. Each individual fascicle is surrounded by a connective sheath, called the perimysium. Finally, these fascicles are bundled together to form the biceps muscle, which is surrounded by another layer of connective tissue known as the epimysium.

Skeletal muscle is not only highly organized but is highly vascularized and highly innervated. An elaborate network of arteries and veins create a rich lattice of vasculature that enmeshes the bundles of muscle fibers [1]. These networks ensure that muscle fibers are supplied with ample amounts of oxygen for energy production. Notably, the density of the

vasculature varies within and between muscles, and adapts to changes in energy demand [1]. Motor neurons innervate the muscle, carrying signals from the brain to the muscle. Unlike the vasculature, there is a one-to-one relationship between a muscle and the motor neurons innervating it [12]. That is, a motor neuron can only innervate one muscle. However, a single motor neuron can innervate multiple muscle fibers within that muscle, but a muscle fiber cannot be innervated by more than one motor neuron [12]. The muscle fibers innervated by a single motor neuron is collectively called a motor unit [12]. The size of the motor unit, or the number of muscle fibers innervated by the motor neuron, is dependent upon the movements performed by the muscle. For example, motor units are small for muscles of the hands and fingers in order to carry out their highly coordinated, more delicate movements. Conversely, motor units are extremely large for the muscles of the thigh since highly coordinated movements are not required [12].

1.3.1 The Muscle Fiber

Individual muscle fibers themselves are highly organized and contain a plethora of intricate structural and regulatory components. Unlike other cells in the body, muscle fibers are multi-nucleated and post-mitotic [9], meaning multiple nuclei are found along the length of an individual muscle fiber and the muscle fiber is unable to divide to form a sister cell. Muscle fibers exhibit a range of diameters and lengths, but are, on average, 100 micrometers in diameter and 1 cm in length [9]. Therefore, having nuclei spread along the length of the muscle fiber ensures that specific proteins are synthesized and readily available to meet the demands of the muscle fiber within each region [13]. Similar to the nuclei, mitochondria are located strategically throughout the entire muscle fiber to allow for maximum oxygen delivery to the mitochondria, which in turn, allows for maximum energy production by the mitochondria [14]. Specifically, individual mitochondria are positioned close to the sarcolemma to reduce oxygen's diffusion distance from the vasculature as well as in the intermyofibrillar space to enhance the delivery of

ATP to the contractile machinery. Notably, changes in the demands imposed on skeletal muscle result in significant changes to these three structural components [9].

Individual muscle fibers drive skeletal muscle contraction and force generation required for locomotion, breathing, and postural stability. Muscle contraction is carried out and supported by five basic units: the neuromuscular junction (NMJ), the excitation-contraction coupling machinery, the sarcomere, the extracellular matrix (ECM), and the cytoskeleton [1]. The NMJ serves as the junction between the innervating motor neuron carrying the signal for contraction, the excitation-contraction coupling machinery then transforms the electrical impulse from this neuron into a mechanical contraction, the sarcomere is the contractile apparatus responsible for force generation while the ECM and cytoskeleton protect the muscle by providing mechanical support and force transmission. Together, this units allow the muscle to sustain rapid cycles of contraction and relaxation. The following sections below provide more detail on the these structural components.

1.3.2 The Neuromuscular Junction

The NMJ is the chemical synapse that transmits the electrical impulse from the innervating motor neuron to the muscle fiber. It is comprised of three major regions: the presynaptic region, the synaptic space, and the postsynaptic region. Within the presynaptic region is the nerve terminal that houses synaptic vesicles containing the neurotransmitter, acetylcholine [15,16]. Synaptic vesicles fuse to the presynaptic membrane and release acetylcholine into the synaptic space [17]. The synaptic space is the space between the pre- and post-synaptic membranes through which acetylcholine diffuses. Within the postsynaptic region are the junctional folds, which serve to amplify both the space occupied by and the volume of the postsynaptic membrane area [1]. The crests of these junctional folds are packed with nicotinic acetylcholine receptors [18], which become activated by the diffusing acetylcholine. Muscle contraction is discussed in more detail in 1.4.

1.3.3 The Excitation-Contraction Coupling Machinery

The excitation-contraction coupling machinery is composed of the transverse tubular (T tubule) system and the sarcoplasmic reticulum [9]. The T tubule system conducts the electrical signal received from the motor neuron to the interior of the muscle fiber [19]. T tubules are invaginations of the sarcolemma that ensure information from the innervating neuron is spread uniformly throughout the fiber [19] and that contractions are coordinated events. The sarcoplasmic reticulum is responsible for the storage, release and reuptake of calcium during muscle contractions [9]. The ends of the sarcoplasmic reticulum, termed terminal cisternae, are responsible for storing calcium and form triads with the T tubule system [9].

1.3.4 The Sarcomere

The sarcomere is the basic unit of the muscle fiber and it is the site of rapid force generation that brings above movement. Sarcomeres are intricate structures composed of two main alternating sets of protein filaments: thin filaments and thick filaments. Thin and thick filaments run parallel to the muscle fiber axis and are made up of actin and myosin, respectively, as well as their associated proteins [1]. Using transmission electron microscopy, the hallmark features of the sarcomere are easily visualized and distinguished by their light and dark appearance. At each end of the sarcomere is a dark narrow line called the Z disk, which is shared between adjacent sarcomeres and bisects the lighter I band [1]. The Z disk is responsible for holding together the thin filaments. Conversely, at the center of the sarcomere is a dark narrow line called the M line, which bisects the darker A band [1]. The M line is responsible for holding together the thick filaments [1].

The sarcomere is home to a diverse array of proteins whose roles include structural stability, excitation-contraction coupling, energy release, and the generation of force and power [20]. For example the troponin complex (including troponins C, I and T, which are the calcium, inhibitory, and tropomyosin binding subunits, respectively) and tropomyosin are associated with the actin filament and play a major regulatory role in the activation of excitation-contraction

coupling and force generation [9]. Two major structural proteins are titin and nebulin [20]. Titin is a large elastic protein anchored to the Z disk and the myosin filaments while nebulin is integrated within the actin filaments [21]. Both titin and nebulin serve as molecular templates, ensuring the precise length and organization of the myosin and actin filaments, respectively [22]. Additionally, titin and nebulin stabilize the sarcomere and maintain its integrity [20] through their contribution to the ever evolving passive tension and stiffness required by individual muscle fibers [9]. Myomesin is present at the M-line to serve as an additional strain sensor [23], while creatine kinase serves as a spatial ATP buffer and maintains energy homeostasis [24,25].

1.3.5 The Extracellular Matrix

As mentioned in the discussion of skeletal muscle structure, there are three discrete but interconnected connective tissue sheaths that surround and protein the muscle fibers, fascicles, and whole muscle: the endomysium, the perimysium, and the epimysium, respectively. These sheaths represent the extracellular matrices within skeletal muscle. The focus of this section, though, is on the endomysium and its interface with the sarcolemma. At the heart of this interface, is a specialized basement membrane [1], which is becoming more appreciated as research continues to demonstrate its multi-functional roles in protecting the integrity of the muscle fiber. For the remainder of this section and dissertation, ECM will be used to refer to this interface.

The ECM is highly involved in the modulation of mechanical homeostasis and cell-matrix interactions [26,27]. It provides the necessary uniform distribution and transmission of force across muscle fibers, which is mostly achieved through its cytoskeleton-ECM linkage via the dystrophin glycoprotein complex [26]. Additionally, the ECM serves as a scaffold for focal adhesions that are necessary for initiating biological responses to changes in the cellular environment [27]. Most importantly, though, several proteins residing in the ECM serve as important signaling mediators during recovery from injury and regeneration [28–30].

The multitude of proteins that construct the ECM primarily fall within one of three main classes: collagens, non-collagenous glycoproteins, and proteoglycans [1]. Collagens are the largest fraction of ECM proteins within skeletal muscle [31,32], and play major roles in structural stability. Specifically, collagen I exhibits a range of biomechanical properties, including tensile strength and load bearing [1], while collagen VI and IV create a network of fine filaments and integrate laminins, nidogens and other proteins into a stable structure [33,34]. Lastly, collagens I, III, V, and XI form fibrils to further enhance the structural stability of the ECM [1]. Working alongside the collagens, is fibronectin. Fibronectin is described as a master organizer, playing a major role in aiding fibril organization and serving as a bridge for proteins such as integrins, collagen IV, and other focal adhesion molecules [35]. Matrix assembly and modulation of cell-matrix interactions are regulated by several ECM proteins, including nidogens, periostin, and osteopontin [1]. Additionally, matrix metalloproteinases (MMPs) and their inhibitors (TIMP1 and TIMP2) are ECM-associated enzymes that maintain the integrity of the ECM by regulating ECM protein degradation [36,37]. The ECM is a dynamic structure in the sense that it responds to changes to the intra- and extracellular environments via a host of growth factors that signal the production or maintenance of ECM proteins [38]. The dynamic nature of the ECM is especially important for monitoring and responding to changes in muscle activity.

1.3.6 The Cytoskeleton and the Dystrophin Glycoprotein Complex

Sarcomeres are supported structurally by the muscle cytoskeleton [1]. This cytoskeleton is composed of various protein networks that form a lattice called the costamere [39]. The costamere functions to transmit force produced by the sarcomere both laterally and longitudinally [40–42]. Ultimately, this allows contractions to be unified from one tendon to the other while maintaining the integrity of the muscle fiber. It is estimated that as much as 70% of the force produced by the sarcomere is transmitted laterally through the costamere [42–44]. One of the most important components of the costamere, and arguably one of the most important structural complexes within the entirety of the skeletal muscle, is a multi-protein

complex known as the dystrophin glycoprotein complex (DGC) or the dystrophin-associated protein complex (DAPC). The DGC is physically connected to the internal myofilament structure through filamentous actin as well as the external extracellular matrix through laminin [45,46]. Proteins that make up the DGC are divided into three groups based on their cellular localization [47,48]. Cytoplasmic proteins include dystrophin, α-dystrobrevin, syntrophins, and nNOS. Transmembrane proteins include β-dystroglycan, sarcoglycans, sarcospan, and caveolin-3. Finally, the extracellular proteins include α-dystroglycan and laminin. The DGC is extremely important for maintaining the structural integrity of the muscle fiber, which is clearly demonstrated by how the partial or complete absence of a single protein within the complex results in muscular dystrophy [49,50]. Additionally, through the multiple binding sites and domains present within the individual proteins that construct it, the DGC serves as a scaffold for various signaling and channel proteins as well as an anchoring point for signaling molecules near their sites of action [47]. A more detailed discussion about the roles of these individual proteins is provided below.

Dystrophin is an extremely large (427 kDa) sub-sarcolemmal cytoskeletal protein organized into four distinct domains: (1) the actin-binding amino-terminal domain; (2) the central rod domain; (3) the cysteine-rich domain; and (4) the carboxy-terminal domain [48]. The actin-binding amino terminal domain houses binding sites for filamentous actin [51], connecting dystrophin to the sub-sarcolemmal actin network [52]. Additionally, this domain supports dystrophin's interaction with cytokeratin-19, a costamere-enriched intermediate filament [53,54], connecting dystrophin to the sarcomere. The central rod domain is made up of 24 spectrin repeats consisting of homologous triple helical repeats and four hinge domains [55]. A second actin-binding motif [56] and interaction sites for microtubules [57,58] are located within this domain, creating a strong lateral association with actin filaments [59] and providing an organizational framework for the microtubules [57,58]. The hinge domains provide elasticity to

the overall structure of the protein [55]. The cysteine-rich domain resides between the central rod and the carboxy terminus domains. This domain houses binding sites for beta-dystroglycan and calmodulin [60–63] as well as ankyrin-B [64] and synemin [65]. Ankyrin-B is an adaptor protein that helps retain dystrophin at the sarcolemma [64], while synemin is an intermediate filament protein, whose interaction with dystrophin helps strengthen the link between the costameres and myofibrils [65]. Lastly, the carboxy-terminus domain harbors binding sites for α-dystrobrevin and the syntrophins [66,67], which assists in their localization to the sarcolemma [68]. Ultimately, these intra- and extracellular linkages allow dystrophin to play a crucial role in stabilizing the sarcolemma against mechanical forces endured during muscle contraction [39,69–77] and in serving as a molecular shock absorber duration muscle contractions [78].

α-Dystroglycan is an extensively glycosylated extracellular protein [79,80] with a dumbbell-like shape from its two globular domains that are connected by an extensible portion [81,82]. One of these globular domains houses binding sites for multiple extracellular matrix components including laminins, agrin, perlecan, and biglycan [83], while the other houses a binding domain for β-dystroglycan [84,85]. β-dystroglycan is a single transmembrane protein with an extracellular amino-terminal domain that binds with α-dystroglycan and a carboxy-terminal domain that binds with dystrophin [86,87] and caveolin-3 [88]. The dystroglycan complex is responsible for transducing extracellular-mediated signals that direct cell polarity, matrix organization, and mechanical stability of tissues to the cytoskeleton [89–91]. Additionally, β-dystroglycan binds agrin at the NMJ, suggesting a role for β-dystroglycan in acetylcholine receptor clustering [92].

Syntrophins are intracellular membrane-associated adaptor proteins believed to recruit and regulate signal-transduction complexes [93]. Specifically, the syntrophins harbor numerous binding sites for dystrophin, α-dystrobrevin [94], calmodulin [95,96], heterotrimeric G-proteins [97], nNOS [98–100], voltage-gated sodium channels [101], non-voltage gated calcium channels

(specifically TRPC) [102], and aquaporin-4 [93]. Therefore, it is suggested that syntrophins play an important role in recruiting, organizing and anchoring a signaling complex to the dystrophin scaffold [93].

The sarcoglycan complex is composed of four sarcoglycan isoforms [103–106] and sarcospan [107]. Each of the sarcoglycan proteins are single transmembrane glycoproteins whose amino-terminal domains are housed either extracellularly (α-sarcoglycan) or intracellularly (β-, γ-, δ-sarcoglycan) [103–106]. While the purpose of the sarcoglycan complex is not fully understood, early studies predict that it has both mechanical and non-mechanical roles. Specifically, this complex may strengthen the interaction between β- and α-dystroglycan as well as β-dystroglycan and dystrophin [108]. Further, the sarcolgycan complex may regulate cell-cell adhesion through its interactions with the integrin complex and focal adhesion proteins [109,110]. Tightly associated with the sarcoglycan complex is sarcospan, which houses four transmembrane spanning helices [111]. Studies suggest an important role for sarcospan in upregulating the cell surface expression of the major laminin-binding complexes in the muscle, including the DGC, the utrophin-glycoprotein complex and integrin-α7β1 complexes [112]. Utrophin is a dystrophin-related protein with significant sequence homology to dystrophin and shares structural similarities with dystrophin that allow it to provide mechanical protection to skeletal muscle [66,113,114]. Integrin-α7β1 and its associated proteins, including talin, viniculin, and paxillin [1], are critical components of the costamere.

α-Dystrobrevin is a cytoplasmic dystrophin-related protein that binds directly to dystrophin, utrophin, and the syntrophins [115,116]. Unlike other members of the DGC whose roles are critical to sarcolemmal integrity and signaling, α-dystrobrevin may be critical to the distribution and stability of acetylcholine receptors at the NMJ [117,118]. Specifically, α-dystrobrevin may serve as a hub for assembling signaling complexes that are critical to the organization of the postsynaptic machinery, specifically the acetylcholine receptors [119].

Caveolin-3 is a critical structural protein located within flask-shaped invaginations of the plasma membrane, or caveolae [120]. Caveolin-3 interacts with a number of signaling molecules, including heterotrimeric G-proteins, c-SRC and SRC-like kinases [121], and may play a role in the formation of the T tubule system during muscle development [122] as well as in the regulation of energy metabolism [123]. Additionally, caveolin-3 interacts with nNOS and may negatively regulate its enzymatic activity [124,125]. nNOS is associated with the DGC through dystrophin and controls local blood flow [126].

1.3.7 Skeletal Muscle Fiber Types

Skeletal muscle fibers exhibit a high degree of heterogeneity, harboring unique biochemical, mechanical and metabolic phenotypes that allow them to meet the demands imposed on them [9]. Ultimately, this allows muscles within the human body to participate in activities that require different metabolic and mechanical demands, such as running a marathon or holding a plank, due to the unique distributions of various fiber types [9].

For the past few decades the classification of muscle fibers has evolved to incorporate new research that defines multiple subtypes or isoforms of specific proteins. Traditionally, muscle fibers are classified based on color (red vs white), which correlates to myoglobin content, or contraction speed during a single muscle twitch (fast vs slow) [127]. Muscle fibers are further classified based on their degree of fatigability during sustained activation (fatigable vs fatigue-resistant), their dominating metabolic pathway (oxidative vs glycolytic), as well as their histochemical stain reactions (ATPase or succinate dehydrogenase) [127]. More recently, muscle fibers are classified based on their calcium handling properties by the sarcoplasmic reticulum (slow vs fast) [128] and protein isoform expression, such as troponin T isoforms [129] and myosin isoforms. Regardless, human skeletal muscle is most frequently described as having three muscle fiber types: type I (slow, oxidative, fatigue-resistant), type IIa, (fast, oxidative, intermediate metabolic properties), and type IIb (fast, glycolytic, fatigable). Here, the

speed of contraction (fast vs slow) correlates with the sarcoplasmic reticulum and calcium handling, while the metabolic properties (oxidative vs glycolytic) and tolerability of fatigue (fatigue-resistant vs fatigable) correlate with the mitochondrial content [9]. Phenotypically, type I muscle fibers are highly vascularized and saturated with mitochondria, which allow them to remain active for longer periods of time but with low force output [1]. Muscles from elite endurance athletes, such as marathon runners, have a higher type I muscle fiber composition. Alternatively, type II fibers contract faster and fatigue much easier than type I fibers as a result of their higher glycolytic capacity and accelerated ATP hydrolysis [1]. Muscles from elite sprinters and power lifters have a higher proportion of type II fibers.

1.4 Skeletal Muscle Contraction

The stability and integrity of the skeletal muscle structure is critical to the survivability of the muscle fiber during muscle contraction. The absence or partial functioning of the above mentioned proteins in the ECM or DGC negatively affects the fiber's ability to withstand the movement and force generated during contraction. Muscle contraction occurs via a series of coordinated events that are repeated until movement ceases or until the muscle can no longer supply energy to support contraction. This series of events is properly named excitation-contraction coupling (ECC) and consists of three main events: the transmission of the nerve impulse to the muscle, the release of calcium from the sarcoplasmic reticulum, and the formation of a cross-bridge between myosin and actin [9]. Visually, we see the whole muscle contract, such as the biceps contracting to lift a cup of coffee to the mouth. However, the whole muscle contracts as a result of what occurs at the molecular level between the myosin heads and the actin filaments.

First, an action potential from the innervating motor neuron arrives at the presynaptic membrane, or nerve terminal. The arrival of the action potential stimulates the fusion of synaptic vesicles housing acetylcholine to the presynaptic membrane at the active zones, or visually dense zones at the presynaptic membrane that contain specialized proteins associated with

vesicle docking and fusion, exocytosis and vesicle recovery [130]. Exocytosis of acetylcholine into the synaptic space is tightly orchestrated by Ca^{+2} and its respective voltage-gated calcium channels [1]. This entire process is suggested to depend on both the muscle type and the stimulus [131,132]. Acetylcholine then readily diffuses across the synaptic space and binds with nicotinic acetylcholine receptors on the sarcolemma, creating a local depolarization event [1]. Following exocytosis, the synaptic vesicles and the associated vesicular membrane proteins are rapidly recycled via endocytosis to sustain further exocytosis [1]. Additionally, acetylcholinesterase immediately begins to hydrolyze the diffusing acetylcholine, promoting the cessation of this signal [133].

The local depolarization event at the sarcolemma activates the voltage-gated sodium channels that are concentrated within the junctional folds, which drives an action potential along the length of the muscle fiber and through its interior via the T tubule system [134]. When this action potential arrives at the triad, a voltage sensor subunit of the dihydropyridine receptor on the T tubule opens, allowing a flood of calcium to enter [135], which consequently triggers the ryanodine receptors within the terminal cisternae of the sarcoplasmic reticulum to open and large amounts of Ca^{+2} to enter the sarcoplasm. Ca^{+2} then binds to troponin C, a regulatory protein located on the actin filaments, which initiates a series of conformational changes that moves tropomyosin away from the myosin active sites on the actin filament [136]. With the active site now exposed, the head of the myosin molecule binds to actin at a 45 degree angle relative to actin [137]. This position is called the rigor state [137]. ATP molecules located near the myosin head bind to myosin, briefly dissociating myosin from actin [137]. These ATP molecules immediately become hydrolyzed by ATPase to ADP and inorganic phosphate, which facilitates the re-binding of the myosin head to actin but at a 90 degree angle relative to actin, forming a cross-bridge [137]. Upon release of inorganic phosphate, the power stroke is initiated, and the myosin head rotates on its hinge, pushing the actin filament towards the M-band. This sliding of actin and myosin generates muscle force [138,139]. Once the power stroke is

completed, ADP is released from the myosin head and the myosin head is repositioned into its rigor state at a new position along the actin filament [137]. This cycle continues until ATP is no longer available.

Since cross-bridges are formed along the entire length of the muscle fiber, forces are transmitted longitudinally and laterally throughout the fiber via the costameres [9]. However, movement is not produced until these forces reach the myotendinous junction, where the muscle and tendon interact, and then transmitted through the tendon to the bone [9]. The force that a muscle generates is dependent on several factors including the extent of activation of the innervating motor neuron, the size of the muscle fibers, the number of cross-bridges formed, the force generated by each cross-bridge, and most importantly, the space between the myofilaments [9]. The space between actin and myosin is extremely important, as highlighted by the force-length relationship, which states that at lengths longer and shorter than the optimal length of the sarcomere, there is sub-optimal overlap between actin and myosin during cross-bridge formation, which limits force generation.

Even though muscles generate force using the same mechanisms detailed above, muscles are capable of producing three types of contractions: isometric, concentric and eccentric [9]. During an isometric contraction, force is generated but there is no movement of the joint or limb. An example of an isometric contraction is pushing against a wall, where the resistance of the wall is greater than the force generated. Concentric and eccentric contractions occur to complete a full range of motion. Specifically, concentric contractions result in the shortening of the muscle and the movement brings the muscle's origin and insertion points closer together. An example of a concentric contraction is the biceps muscle contracting to flex the elbow. In contrast, eccentric contractions result in lengthening of the muscle as its origin and insertion points move away from each other. An example of an eccentric contraction is the biceps muscle lengthening to extend the elbow and return it to resting position. The lengthening of the muscle during an eccentric contraction can be associated with muscle damage [140].

As demonstrated above, muscle contraction requires ATP for cross-bridge formation. A contracting muscle fiber receives energy through three basic pathways: ATP and creatine phosphate (CP) stored in the muscle, anaerobic glycolysis, and oxidative phosphorylation [9]. The energy pathway used is dependent on the intensity and duration of the activity. It should be noted, though, that these pathways are not an all-or-none phenomenon but actively overlap at different time points throughout the activity. ATP and CP stored in the muscle provide energy for the first few seconds of activity since these reserves are extremely limited. Once ATP and CP stores are depleted, anaerobic glycolysis produces ATP quickly to sustain muscle contractions. The primary fuel source that supports this pathway is plasma glucose [141]. However, anaerobic glycolysis can only provide energy for a couple of minutes since glycolysis also produces H^+ and lactate, both of which impair muscle function and are associated with muscle fatigue [9]. The final energy pathway that produces ATP is oxidative phosphorylation. Oxidative phosphorylation occurs within the mitochondrial network and ATP is shuttled throughout the muscle fiber to sustain muscle contractions for minutes to hours. The primary fuel sources that support this pathway free fatty acids within the plasma as well as glycogen and triglycerides stored within the muscle [141].

1.5 Skeletal Muscle Repair and Regeneration

Skeletal muscle undergoes multiple bouts of damage throughout its lifetime from daily use and injury. For example, the physical movement of actin sliding past myosin may result in microlesions within the sarcolemma of a single muscle fiber while acute ischemia may result in widespread damage throughout the entire muscle. The muscle fiber's ability to reseal its sarcolemma to prevent cell death as well as the entire muscle's ability to regenerate following extensive damage are hallmarks of skeletal muscle tissue [1]. Below are brief overviews of the repair and regenerative processes following injury to the sarcolemma and to the whole muscle, respectively.

A highly-orchestrated membrane repair machinery patches microlesions endured by the sarcolemma during contraction-relaxation cycles, and allow the muscle fiber to continue meeting the functional demands of the muscle. This membrane-repair machinery is constructed by various proteins, including dysferlin [142–145], caveolin-3 [146], calpain-3 [147], AHNAK [148,149], and annexin A1 and A2 [148,150]. Immediately after a tear in the sarcolemma occurs, calcium rapidly enters the muscle fiber, activating and strengthening the binding properties of these repair proteins [151] such that the annexins bind with dysferlin and phospholipids while dysferlin binds additional phospholipids [152]. These binding events encourage the recruitment of intracellular vesicles, such as lysosomes and enlargeosomes, to the sarcolemma [153,154]. An additional protein, mitsgumin 53, also plays a role in translocating these vesicles [155–159]. These intracellular vesicles accumulate beneath the damaged sarcolemma, and then undergo exocytosis to fuse with the sarcolemma, creating a patch of new membrane and sealing the damaged area [152]. Intracellular vesicle fusion is made possible by the SNARE proteins [160] and synaptotagmins [161]. Finally, the membrane repair complex is deactivated through calpain-dependent cleavage of the annexins and AHNAK [151]. This rapid membrane repair mechanism occurs within seconds of activation [162].

In the event that the membrane damage is too extensive and cannot be repaired via the patch repair mechanism, sarcolemmal injuries may trigger an inflammatory response [163–165] and activate the satellite cells. Satellite cells are located along the length of the muscle fiber tucked between the sarcolemma and the basal lamina [166,167]. These cells represent the adult stem cell niche in skeletal muscle and are responsible for muscle growth and regeneration [166,167]. Upon unresolved injury, fiber necrosis occurs, which activates the complement cascade, stimulating the infiltration of leukocytes, neutrophils, and eventually macrophages [1]. These macrophages clear the damaged muscle fibers and send the initial signals for satellite cell migration and proliferation [168]. The ability to regenerate is governed not only by the

satellite cells [169] but by the microenvironment [170]. This microenvironment, or niche, is home to growth factors, extracellular matrix proteins, fibro-adipogenic progenitors (FAPs), chemokines, and MMPs [1]. Additional components within and around this niche include the local interstitial cells, motor neurons, the vasculature [171,172], and chemo-attractants and cytokines from local and infiltrating inflammatory cells [173–179]. These components provide scaffolding for cell migration and cues for the regenerative processes. There are many shared components between embryonic myogenesis and muscle regeneration [180], including the transcription factors and signaling molecules that orchestrate the activation and migration of satellite cells to the site of injury as well as their proliferation and differentiation into muscle fibers [1]. Within days of the initial injury, damaged muscle is completely regenerated [151]. Most importantly, though, skeletal muscle's regenerative capacity is governed by its ability to reactivate the satellite cell pool when necessary [151].

1.6 Skeletal Muscle Plasticity

Alongside the muscle's ability to repair and regenerate is its profound ability to respond to changes in its physiological environment. In fact, skeletal muscle is one of the most dynamic and plastic tissues within the human body [9]. Skeletal muscle fibers are capable of changing their size and type, metabolic profiles, calcium handling properties, and more. Skeletal muscle is constantly sensing, transducing, and integrating neuronal, mechanical, metabolic and hormonal signals in order to produce a systemic physiological adaptation that would allow it to perform more optimally, whether it is to maintain new postures, to run longer distances or to perform finer movements with the fingers. These adaptations occur at the level of gene activation, mRNA processing, as well as protein synthesis and assembly (reviewed in [181]).

Skeletal muscle plasticity is best understood in the context of skeletal muscle size in response to completing a resistance training program versus enduring bedrest or limb immobilization. The maintenance of skeletal muscle size is the direct result of the synergy of the signaling pathways for anabolic and catabolic processes such that myofibrillar proteins are

continuously being synthesized and degraded. However, when the functional demands change, one pathway dominates over the other. For example, during periods of increased contractile activity, such as during an exercise program, muscle growth, or hypertrophy, is initiated by enhancing protein synthesis. Conversely, during periods of decreased contractile activity, such as during bed rest, muscle wasting, or atrophy, is initiated by enhancing protein degradation. Interestingly, studying these two mechanisms on a cellular and molecular level has proven difficult because there is not one specific signaling pathway that initiates a hypertrophic versus atrophic program, but rather an overlap between inhibition and activation of various molecular players [181]. For example, growth hormone, IGF-1 and insulin are recognized most in the initiation of muscle growth, while myostatin is the primary initiator of muscle wasting, but these proteins act via the same molecular mediators [181]. In lieu of discussing these pathways, a discussion on the phenotypic changes observed in response to exercise training and inactivity will be provided below.

1.6.1 Benefits of Exercise

There are more than 100,000 studies showing positive associations between the terms ‘exercise’ and ‘health’ [182]. In fact, health-related physical fitness is among the most powerful predictors of morbidity and mortality [183–185], and lifelong exercise is associated with a longer health span by targeting the four components of physical fitness: (1) cardiovascular fitness, (2) musculoskeletal fitness, (3) body composition and (4) metabolism. Exercise training leads to extensively documented improvements in a myriad of systems with the most profound being in cardiorespiratory function, muscle oxidative capacity, metabolic health, glucose and lipid homeostasis, adiposity, inflammatory burden, muscle mass and strength, joint pain, bone density, mobility function, depression, anxiety, and cognition [186,187]. These clear and profound benefits of exercise allow it to be prescribed as the primary prevention and secondary intervention strategies for over 40 conditions and chronic diseases, including cardiovascular disease, chronic obstructive pulmonary disease, obesity, diabetes, cancer, and sarcopenia

[182]. Many individuals assume that all exercise is created equal. However, the body's response to exercise is highly specific to the type of exercise that it is performed. This is especially true for skeletal muscle, which will be the focus of the discussion below.

1.6.2 Aerobic Exercise

Aerobic exercise training targets cardiorespiratory fitness by activating large muscle groups to perform continuous, rhythmical movements for a prolonged period of time [9,186]. It is designed to improve the capacity and efficiency of the aerobic energy-producing systems, specifically oxidative phosphorylation [186]. Examples of aerobic exercises include running, biking, or swimming.

Disruptions in cellular homeostasis occur during aerobic exercise and these disruptions are responsible for driving the positive adaptations [188,189] that ultimately lead to enhanced metabolic capacity [9]. Specifically, there is an increase in the capillary supply to the active muscles to facilitate oxygen delivery [190]. The number and size of the mitochondria are also increased to enhance the production of ATP [190]. Additionally, fat and glycogen storage as well as the availability of oxidative enzymes are increased to further enhance ATP production [191,192]. It should be noted that aerobic exercise most often does not result in changes in muscle size or force generating capacity [9].

1.6.3 Resistance Training

In contrast to aerobic training, resistance training is a series of exercises that require individual muscles or targeted muscle groups to exert or resist force using free weights, weight machines, or elastic bands [186]. Resistance training is broken down into four types that are defined by their targeted goals for muscular fitness: local muscular endurance training, hypertrophy training, strength training, and power training. Local muscular endurance training utilizes high repetitions and submaximal loads with short rest intervals to improve the muscle's resistance to fatigue. Hypertrophy training utilizes moderate repetitions and moderate to heavy loads to increase the size of the muscle. Strength and power training are very similar, utilizing a

very low number of repetitions and maximal loads to increase the amount of resistance that the muscle can effectively move and to improve the speed at which this load is moved, respectively.

Within the four training programs, there are acute variables that influence training adaptations further [193,194]. These physiological adaptations are specific to the muscle actions involved [195], the speed of movement [196], the range of motion [197], the muscle groups trained [198], the energy systems involved [199,200], and the intensity and volume of training [201–203]. Regardless, though, these adaptations occur as a result of the cross talk between the nervous and muscular systems. Specifically, the early increases in strength are brought about by improvements in motor unit recruitment, firing rate, and synchronization [204]. Then, within about 4 to 8 weeks of training, muscle hypertrophy becomes evident [205–207] as a result of changes in the quality of proteins [207], transitioning between fiber types [205,207], and the rate of protein synthesis [206]. As training progresses, there is further interplay between neural adaptations and muscular hypertrophy that drive acute changes in muscular strength [204].

1.6.4 Inactivity

Physical inactivity is arguably one of the most important concerns to human health in the 21st century [208]. Even more so, it was a great concern for early Greek philosophers. Plato once said that the "lack of activity destroys the good condition of every human being, while movement and methodical physical exercise save it and preserve it." Similarly, Socrates once stated that “and is not the bodily habit spoiled by rest and idleness, but preserved for a long time by motion and exercise?” These negative impacts of physical inactivity on overall health are now well-established. Specifically, it is one of the main risk factors of a number of diseases including obesity, cardiovascular diseases, stroke, diabetes, and colon cancer [209,210], and is the largest preventable risk factors for Alzheimer’s disease in the United States [211,212]. Unfortunately, skeletal muscle is one of the major body systems that is influenced immediately by inactivity.

Physical inactivity is modeled in humans using strict bed rest, 24 hours a day, in a head-down position at -6 degrees [213]. Short-term bed rest for 2, 8 or 12 days does not result in significant effects on muscle mass or strength [214], but long-term bed rest for 35 or 90 days results in a large decrease in muscle force and power generation of the lower limb muscles [215,216]. These decreases are caused by muscle atrophy of both type I and type II muscle fibers [217]. Additionally, inactivity leads to lower work capacity (peak oxygen consumption) [218], hypovolemia and negative water balance [219–221], decreased orthostatic tolerance [222], changes in resting metabolic rate, poor body composition, including decreased lean body mass, increased fat mass, and reduced bone mineral density [223–229], limited muscular strength and endurance [222,224,225], changes in thermoregulation [230,231], impaired immune response [226], and altered mood and neuropsychological performance [232]. Further, proteolysis pathways are significantly upregulated, especially the ubiquitin-proteasome pathway and autophagy [233,234], which negatively affects the quality of the muscle proteins [235]. Similarly, in rodent models, inactivity is achieved through hindlimb suspension, where the hindlimbs are elevated to produce a 30-degree head-down tilt [236]. This position restricts animals to using only their forelimbs [236]. Regardless, hindlimb suspension for 1 to 2 weeks negatively affects body and muscle mass [237], myosin heavy chain expression and fiber type switching [238,239], functional muscle strength [240], protein synthesis and degradation pathways [241], and bone mechanical strength [242]. Most importantly, though, these negative consequences may be reversed upon resuming normal activity [243].

1.7 Muscular Dystrophy

Knowing the complexity of muscle structure and function as well as its response to exercise and inactivity, what happens when a protein is not present or functioning properly and how does the muscle now respond to changing demands imposed on it? A slight perturbation in muscle structure due to the absence of a protein, or even the presence of a partially formed

protein, can wreak havoc on the entire muscular system. This is often visualized as the loss in muscle fibers and reduced motor output [1]. One of the most common groups of diseases affecting skeletal muscle is muscular dystrophy. Muscular dystrophy is caused by the absence or dysfunction of a muscle protein involved in maintaining the integrity of the sarcolemma, repairing the sarcolemma after damage, or constructing the extracellular matrix or nuclear envelope. Muscular dystrophies are inheritable (or occasionally spontaneous) diseases that vary in their severity and age of onset, but share the same two features: progressive loss of muscle mass and function. There are over 50 genetically distinct muscular dystrophies [244] that can affect both males and/or females. Unfortunately, though, many individuals are diagnosed as having an unknown variant, meaning the missing or non-functional protein wreaking havoc on their muscular system has not been identified. Regardless, because muscular dystrophy leads to skeletal muscle degeneration, walking, breathing, and swallowing become extremely difficult and functional independence is lost.

1.7.1 Duchenne Muscular Dystrophy

In the realm of muscular dystrophy research, DMD is the most common type of muscular dystrophy and most frequent genetic disease of childhood, affecting 1 in 5000 male births [245]. Sadly, it is also the most lethal genetic disease of childhood [246]. Individuals with DMD harbor mutations in the gene encoding the protein dystrophin, which is located on the X chromosome, hence why females carry the mutation and are asymptomatic while males are symptomatic. The dystrophin gene is the largest known gene in the human genome spanning at least 2,300 kilobases [247–249]. Remarkably, though, 99.4% of this gene is comprised of introns while only a tiny percentage, representing 14 kilobases make up the 79 exons that encode the protein [61,247,250]. Most notably, it takes approximately 12 hours to transcribe 1,770 kilobases via RT-PCR, estimating at least 16 hours to complete the entire gene [251]. Further, the high molecular weight protein that is formed spans 3685 amino acids [61]. Mutations in the dystrophin gene lead to a truncated, non-functional dystrophin protein. Exon deletions and

duplications account for about 65% and between 6 to 11%, respectively, of all mutations while deep intronic mutations account for less than 7% of mutations [245].

1.7.2 Clinical Presentation of DMD

DMD is first diagnosed between the ages of 2 and 5 years. Symptoms are typically manifested as delayed milestones, including delayed onset of ambulation, difficulty standing unaided [252], and gait abnormalities [245]. When parents alert clinicians of these motor delays, the next step is testing for serum creatine kinase levels [245]. Elevated levels of serum creatine kinase is a major indicator of muscular dystrophy, and begins the genetic testing process. As the disease progresses, muscle wasting overpowers the regenerative capacity of the muscle, and performing activities of daily living become difficult [252]. As the paravertebral muscles weaken, individuals will exhibit a progressive lumbar curvature of the spine [246]. This curvature results in postural compensations as well as a change in the distribution of weight bearing from the heels to the toes [246]. Additionally, the calf muscles experience extensive fibrosis, leading to the development of contractures that limit plantar flexion [246]. Fibrosis and fatty tissue overwhelm the calf muscles, creating a pseudohypertrophy [246]. As a consequence of these changes, most individuals with DMD become wheelchair bound between the ages of 11 and 13 years old [252]. The progressive loss in muscle mass and strength is not only present in the limb muscles but also in respiratory and bulbar muscles, increasing the risk for respiratory failure [245]. Cardiac muscle is also affected by the absence of dystrophin, and exhibits progressive fibrosis, leading to subclinical and eventually dilated cardiomyopathy and heart failure [245]. These complications and the extremely progressive nature of this disease result in premature death before the age of 30 [253].

DMD muscle experiences increased fatigability, fibrosis, and fat deposition as well as defects in regeneration, vasoregulation, metabolism and synaptic structure and function [126,254–264]. Magnetic resonance spectroscopy of multiple muscles from individuals with DMD highlight the extensive reductions in muscle mass, and the infiltration of fatty tissue [265].

Further, muscle biopsies stained with hematoxylin and eosin reveal large accumulations of connective tissue separating the individual muscle fibers as well as the infiltration of immune cells within the interstitial tissue and near the blood vessels [266]. Individual muscle fibers also show a significant variability in their cross-sectional areas [266]. Electron microscopy shows an extensive number of lesions in the sarcolemma, some large enough to permit unrestricted movement of molecules into the muscle fiber [267].

1.7.3 Molecular Mechanisms of DMD

Dystrophin provides a link between the actin cytoskeleton and the extracellular matrix and serves as a scaffold for the assembly of the DGC within the sarcolemma. The mechanical defect hypothesis states that the progressive muscle weakness and wasting in DMD is caused by the lack of this link and the disruption of the DGC, which mechanically weakens the sarcolemma [268,269]. Stress placed on a mechanically weakened sarcolemma can cause microlesions to develop along the sarcolemma [270]. These microlesion allow excessive calcium entry, altering calcium homeostasis [271,272]. An increase in calcium permeability impairs different cellular processes, such as excitation-contraction coupling [272], and ultimately activates proteases to breakdown different cellular components. Therefore, the end result is an increase in muscle protein degradation, muscle fiber necrosis, and significant decreases in muscle strength and tolerance for physical activity [272,273].

However, some features of disease pathology in individuals with DMD cannot be explained by the mechanical defect hypothesis [246]. The immune system also plays a major role in amplifying the pathology of DMD as well as in determining disease severity [246]. Upon damage to healthy muscle, an inflammatory response is initiated to clear the damaged muscle fibers and begin regeneration. This response subsides within several hours or days, depending on the extent of damage. However, in DMD muscle, the inflammatory response is prolonged, and the microenvironment is more conducive to further promoting an inflammatory response. By manipulating specific inflammatory cell populations, studies suggest that these cells are

responsible for an extensive amount of damage to DMD muscle [274]. Specifically, pro-inflammatory macrophages accumulate, and there is an increase in pro-inflammatory cytokines, including TNF-α and TGF-β, as well as free radicals that lead to further muscle damage and fibrosis [275]. Therefore, the initial invasion of macrophages in response to acute muscle damage may actually amplify such damage and promote a chronic immune response [246]. Additional immune cells, including cytotoxic T lymphocytes, eosinophils, mast cells, and neutrophils, further exacerbate this immune response (reviewed in [246]). Ultimately, these ongoing cycles of degeneration and limited regeneration lead to premature senescence of muscle stem cells and the inability for muscle to repair itself when further damaged [272,276].

More recent studies suggest a critical role of nNOS in the progression of DMD. Nitric oxide (NO) is a potent vasodilator during exercise and is involved in the metabolism of free radicals. Its function is highly dependent on the dynamic regulation of its enzyme, nitric oxide synthase. In individuals with DMD, NO levels are decreased. It is suggested that, in the absence of dystrophin, nNOS is not recruited to the sub-sarcolemmal space, leading to aberrant nNOS signaling [274]. This aberrant signaling negatively impacts the maintenance of muscle mass as well as force generation and fatigability [277], which may be the result of the increased oxidative stress in dystrophic muscle [260,278]. Notably, overexpression of nNOS ameliorates the dystrophic phenotype [274].

1.7.4 Current Treatment Options for DMD

The first clinical description of DMD was recorded in the 1860s. In 1986, the DMD gene was identified, and in 1987, the protein product was identified [279–281]. Unfortunately, scientific advances are not paralleled by discoveries of effective therapeutic tools thus far as there is still no cure for DMD. One of the major obstacles in designing gene therapies for DMD is the size of the dystrophin gene itself as well as the protein product. Much attention is given to the development of gene delivery, gene editing, exon skipping, and stem cell-based approaches that restore the full-length or truncated, but functional, dystrophin protein constructs [282].

However, a number of hurdles have been reached, including tissue delivery, low efficiency, and an inability to target all DMD mutations [282]. Currently, there are three different micro-dystrophin gene therapies (sponsored by Solid Biosciences, Sarepta Therapeutics, and Pfizer) undergoing clinical testing [283]. Each of these therapies use a viral cDNA construct that code for a truncated micro-dystrophin protein. This micro-dystrophin lacks the internal repeating motifs but retain the critical binding domains for filamentous actin and β-dystroglycan [283,284]. This theoretically allows the micro-dystrophin protein to anchor the actin cytoskeleton to the sarcolemma and ECM, providing a greater level of stability to the muscle fibers. Additionally, antisense phosphorodiamidate morpholino oligomers (PMOs), such as eteplirsen, are promising. Eteplirsen is designed to alter the splicing of the dystrophin mRNA such that exon 51 is excluded, making it applicable to multiple mutations [245]. Current research demonstrates that eteplirsen restores a relatively small amount of dystrophin, but improves ambulation and respiratory effects [285,286].

It should be highlighted that dystrophic muscle maintains a limited ability to adapt to muscle contractions and this is through the compensatory upregulation of various proteins such as integrin-α7β1, utrophin, talin, vinculin, and γ-actin [287–289]. The upregulation of these proteins suggests a compensatory mechanism to reinforce the compromised costamere and preserve muscle structure [290]. Therefore, these proteins are emerging as targets for potential therapies [290]. Additionally, surrogate genes that may serve as a substitute for dystrophin function are being developed as an alternate mechanism for viral gene therapy. For example, GALGT2 is a protein responsible for the terminal glycosylation of dystroglycan [291]. As described previously, dystroglycan is a member of the DGC, and is critical to the maintenance of the NMJ and myotendinous junctions. The exogenous delivery of GALGT2 via a viral vector in mdx mouse models increased utrophin's expression throughout the muscle fiber and improved overall muscle health [292,293]. Pilot studies in humans are now underway [245].

More recently, genetic modifiers have been identified in human data and subsequent follow up studies using the mdx mouse model suggest they may also serve as potential therapeutic targets to modulate disease [294]. Genetic modifiers alter the clinical severity of DMD, including muscle strength and ambulation [294]. These modifiers include myostatin, osteopontin, latent transforming growth factor β binding protein 4, and annexin A6 [294]. Ultimately, these pathways represent additional mechanisms to improve sarcolemmal stability and repair as well as to reduce fibrosis in DMD [294].

Currently, individuals with DMD must rely on symptomatic treatments that aim to preserve functional abilities for as long as possible [295]. Specifically, the main goals for symptomatic treatment are to maintain ambulation, prevent scoliosis, delay the development of respiratory problems, and prolong survival [296]. The first international guidelines for the care and management of DMD were published in 2010 [252,297]. One popular treatment is chronic corticosteroid use, such as prednisone and deflazacort [298–300]. Corticosteroids act as immunosuppressors, and multiple studies confirmed that their use increases muscle strength and delays the progression of muscle weakness, allowing individuals with DMD to remain ambulatory for 2 to 5 years longer compared to non-treated individuals [252,297,301–304]. This supports the above hypothesis that inflammation promotes DMD pathology [246]. However, corticosteroids, especially chronic use of corticosteroids, are accompanied by a variety of side-effects that may be detrimental to disease progression, including weight gain, immunosuppression, hypertension, bone loss, and behavior changes [299,305]. These side-effects may ultimately lead to an increased energy demand to maintain muscle function. More importantly, though, the optimal dosing regimen that maximizes the beneficial effects while minimizing the negative side effects has not been established and research continues to address the importance of this [306–308].

As a component of the symptomatic treatment plan, physical activity has been under intense consideration since DMD was first characterized. In healthy children, muscle strength increases with age but in individuals with DMD, this relationship is not sustained [309]. The progressive decrease in muscle strength and endurance in individuals with DMD results in the partial and then complete loss of functional abilities [310]. Interestingly, lower-limb strength is one of the most important predictors of functional ambulation and independence in individuals with DMD [311,312]. Few studies have looked at activity levels, but all of them demonstrate that these individuals have lower physical activity levels compared to healthy counterparts beginning at a very young age [313,314]. Specifically, boys aged 5 to 13 years old wore a step activity monitor on the right ankle to track right steps or complete gait cycles. Those with DMD spent 40% fewer minutes performing high levels of activity (>30 steps/minute) compared to age-matched controls and spent a greater proportion of their days inactive or performing low levels of activity (<15 steps/minute). Further, these individuals spend fewer minutes at a moderate and high step rate compared to their healthy counterparts [313,314]. Gait velocity is a strong predictor of the amount of time before an individual becomes wheelchair dependent [312]. Specifically, in 51 individuals with DMD, 89% of boys who walked 10 meters in less than 6 seconds did not become wheelchair dependent for 2 or more years while 100% of those who walked 10 meters in greater than 12 seconds were wheelchair dependent in less than 1 year [312]. These reduced levels of activity are often the consequence of loss of functional muscle tissue, muscle disuse, overuse injury, cardiopulmonary involvement, increased fat mass, contractures, reduced efficiency of locomotion, reduced motivation, less social reinforcement for activity, increased depression, and increased societal barriers [315]. Ultimately, this progressive disuse of both the musculoskeletal and cardiorespiratory systems may lead to secondary deterioration of the muscle [315,316], similar to what is observed in healthy individuals.

1.8 Current Understanding of Exercise and Inactivity in DMD

While skeletal muscle plasticity is well-studied in healthy muscle, very little research is available on the adaptability of dystrophic muscle to exercise or inactivity. Currently, there are five proposed mechanisms described in the literature that render dystrophic muscle vulnerable to exercise [317]. These include weakening of the sarcolemma, increased calcium influx and oxidative stress, recurrent muscle ischemia, and aberrant signaling to both the nerves and immune cells (reviewed in more detail in [317]). Further, it is postulated that weaker muscles are more susceptible to exercise-induced damage because their maximal limits may be reduced [318]. The experiments performed in this dissertation were designed to investigate the role that exercise and inactivity play in the progression of DMD. Before discussing these experiments, a detailed review of studies addressing this same question is provided to shed light on the limitations of these studies and the need for more research.

1.8.1 Exercise in Human DMD

Current international care guidelines recommend that individuals with DMD participate in regular submaximal activities [297]. However, no randomized control trials are available that discuss what these activities entail or the timeframe for performing these activities. The first study that explores the effect of exercise on DMD was conducted by Vignos and Watkins in 1966 [319]. Twenty-eight boys with DMD, ages 5 to 10 years old, participated in a 12-month at home exercise program (n = 14 in exercise group; n = 14 in non-exercise control group) that included active-assistive or active-resistive movements. Individuals underwent monthly assessments that included a manual muscle test, a series of functional tests, and serum adolase and urinary creatine-creatinine excretion measurements. In the year leading up to the study, muscle strength was also measured, declining with time in both the exercise and non-exercised groups. Within the first four months of exercise, muscle strength improved each month, but functional tests did not parallel these improvements. However, at the conclusion of one year, the exercise group significantly improved overall strength, while the non-exercised

group continued to lose muscle strength. Ultimately, the authors conclude that a resistance exercise program is most effective if instituted early in the disease and the degree of improvement is dependent on the initial strength of the exercised muscle. In 1979, de Lateur and Giaconi [320] measured changes in maximal isokinetic strength across a 24-month period. Participants used a Cybex isokinetic exerciser to perform controlled extension of a single knee from 90 degrees to full extension. The contralateral leg served as the control. A greater maximal torque in the exercised leg was recorded both during and after training, and the authors conclude that submaximal exercise does not negatively affect strength in DMD muscle but may be of limited value for increasing strength. In 1981, Scott and colleagues [321] investigated the impact of two exercise programs on multiple outcome measures for muscle strength and function in 18 boys with DMD. For 6 months, Group 1 performed a series of exercises against manually applied resistance for 15 minutes each day while Group 2 performed a series of exercises in response to oral commands for 15 minutes each day. Total muscle strength, torque output, locomotor ability and walking times were negatively affected by both exercise programs, with Group 1 exhibiting greater difficulty in performing movements and taking longer to walk the predetermined distance. Here, the authors conclude that a pre-treatment phase is necessary to establish the rate of physical deterioration and that the study should be extended to determine the long-term impact of exercise. Regardless of the outcomes of these studies, exercise continued to be frowned upon and further studies using human subjects were not conducted.

However, in 2013, Jansen et al. [310] studied the impact of assisted bicycle training on various functional measures, range-of-motion, and strength. In this study, 30 boys with DMD were divided into either the intervention (n = 17) or control group (n = 13). The intervention group included 8 weeks of baseline measurements followed by 24 weeks of training, and 28 weeks of post-training measurements. Conversely, the control group included 8 weeks of baseline measurements, followed by 24 weeks of control (normal activity), and then 24 weeks of intervention and 4 weeks of post-training measurements. During the intervention period,

participants completed a 15-minute session on an assisted bicycle ergometer using both arms and legs. Sessions were completed 5 days per week. The authors confidently conclude that their results contradict the longstanding consensus that exercise accelerates disease progression but support the notion that dystrophic muscle obeys the adage “use it or lose it.” Lastly, in 2015, Alemdaroglu and colleagues [296] examined the effects of upper extremity exercise training on disease progression. Twenty-four boys, ages 8 to 15 years, were separated into the study group (n = 12) or control group (n = 12). The study group exercised with an electronic arm ergometer for 45 minutes each day, 3 days per week, while the control group performed strengthening range-of-motion exercises. Function performance, strength and endurance of the upper extremity were assessed as well as ambulatory status. Muscle strength was significantly improved for the right wrist flexor muscle as well as for the total forearm muscles of the right side in the control group. Grip strength also improved in the right hand of the control group. However, functional tests and timed performance tests were significantly different, in favor of the study group. The authors conclude that arm ergometer training had positive effects on muscular endurance, performance of daily activities, arm function, and ambulation status and should be included in rehabilitation programs early in the disease course.

While these studies suggest a positive effect of exercise, they are extremely limited not only in number but the overall design of the studies. First, these studies have extremely small sample sizes, and participants exhibited a range of severities and ages at the time of intervention. Studies also lacked valid experimental controls. For example, in one study, participants performed a movement using their limbs on one side of their body while their contralateral limbs served as a control. However, voluntary strength on the contralateral side can increase due to a phenomenon known as cross-education [322]. Secondly, the exercise regimes across the studies are different, including the type of exercise and the duration of the intervention, making it hard to compare these studies. Lastly, the outcome measures used to assess the impact of exercise varied across studies as well as the timeframe in which

measurements were taken. All of these variables markedly influence changes in muscle strength and function, and may not uphold to a population effect.

1.8.2 Exercise in mdx Mouse Model

To overcome the limitations of human studies, some researchers turned to the mdx mouse model. Pre-clinical animal models are critical for understanding a disease and unraveling mechanistic pathways. The mdx mouse model is the most researched DMD model. It arose from a spontaneous mutation in the premature stop codon which terminated exon 23 in the C57BL/10ScSnJ mouse over 30 years ago [323,324]. The mdx mouse displays the hallmark symptoms of DMD, including muscle weakness, respiratory insufficiency, cardiomyopathy, and changes in skeletal muscle histology [325,326]. Therefore, it is used to understand the pathophysiology of DMD and test therapeutic strategies, including the impact of exercise on dystrophic muscle. However, it should be noted that the mdx mouse model does not completely recapitulate the human disease, and the severity of its pathology is much less compared to humans [325].

Due to the large number of studies examining the effects of exercise on mdx muscle, detailed descriptions of each study will not be provided here but are highlighted in Tables 1 through 4. Instead, the major conclusions from these studies will be discussed. Notably, the purpose of these studies were in and of the same, with authors describing their goal or goals to determine the impact of exercise on muscle force and fatigue, oxidative stress, and evaluate the extent of trauma endured by the muscle. Based on these studies, exercise in mdx mice is beneficial or detrimental depending on the mode, duration, age at intervention, and intensity of the exercise protocol. Studies used either treadmill running, voluntary wheel running, or swimming as the mode of exercise. The duration of a single session, independent of the mode of exercise, ranged from 10 minutes to 2 hours, while the duration of experiments ranged from 1 week to 52 weeks. The age at which exercise began ranged from 3 weeks to 96 weeks old. This is important to highlight because mdx mice exhibit very little muscle weakness during the first

year of life, yet this is the time frame in which most studies are conducted, making it difficult to extrapolate these results to humans [327]. The intensity of exercise ranged from at will for voluntary wheel running to between 4 and 23 meters per minute for treadmill running at a decline between 0 and 18 degrees. Collectively, studies demonstrate either improvements in twitch tension and decreased necrosis [328], or reduced muscle strength and increased edema and inflammation [329]. Similarly, studies either demonstrate improvements in anti-oxidant capacities and oxidative enzyme activities [330–332] or detrimental increases in reactive oxygen species [333] and lipid peroxidation [334]. Further, most studies measured specific outcomes on individual muscles of the hindlimb, the diaphragm, or the heart. Unfortunately, these muscles are not equally affected by the absence of dystrophin [335], and therefore, likely respond differently to exercise.

Table 1: Studies examining treadmill exercise in mdx mice.

Study	Age	Duration of Study	Exercise Program	Results	Study's Conclusions
[328]	3 weeks	3 weeks	7 days/week Time = 25 min Incline = 18 degrees Speed = 4 m/min	Compared to WT, MDX-ex exhibited: ↓ BW ↓ muscle size ↓ twitch tension in EDL and SOL ↓ rate of relaxation ↑ mean fiber size, degree of hypertrophy, fiber variability in SOL type I fibers ↔ mean fiber size in SOL type II fibers ↓ internal nuclei in EDL and SOL ↓ inflammation in EDL ↓ fibrosis in SOL ↓ split fibers in SOL MDX exhibited less dragging of hind limbs and appeared less cachectic and atrophied.	Exercise is beneficial based on clinical performance, contractile properties of the SOL, and histochemical analysis in both SOL and EDL muscles.
[336]	2 months	3 days	3 days Time = 10 min Incline = -15 degrees Speed = 10 m/min	MDX-sed: 14.9 ± 0.62% TB damage 5.54 ± 0.27% BB damage >13% EDL and GASTROC damage <3% SOL and TA damage Compared to MDX-sed, MDX-ex exhibited: ↑muscle fiber damage in SOL (+10.04%), GASTROC (+9.92%), BB (+24.37%), TB (+8.02%) ↑ 27% DIA damage distribution of damaged fibers was similar limited hindlimb injuries (↑<11%)	Sarcolemma damage correlated with magnitude of mechanical stress during contraction rather than the number of activations Exercise could cause muscle wasting, weakness, dystrophy, fibrosis, and degeneration
[334]	4 weeks or 16 weeks	6 weeks	7 days/week Time = 2 x 30 min Incline = 0 degrees Speed = 8.3 m/min (8 day adaptation period prior to training): Time = 2 x 5 min Speed = 4 m/min then 8 m/min	**4 weeks** Compared to MDX-sed, MDX-ex exhibited: ↑ plasma CK (+85%) ↑ lipofuscin accumulation (+29%) ↑ TBARS (+48%) ↔ P/O ratios ↔ SOD activity ↓ O2 uptake state 3+4 (-52% and -23% respectively) ↓ RCI ratio (-27%) ↓ alpha-tocopherol ↓ GSH-Px activity (-12%; but ↑ in WT-ex (+60%)) ↓ alpha-tocopherol	Exercise affects mdx mitochondria differently based on age. Low intensity treadmill exercise is detrimental to muscle mitochondria of 4 week mdx mice. Adult mdx mice exhibited a higher mitochondrial adaptive capacity to low-intensity exercise and this could be due to increase in regenerating fibers.

Table 1 continued

				16 weeks Compared to MDX-sed, MDX-ex exhibited: ↔ plasma CK activity ↔ RCI and P/O ratios No differences in other measures.	
[337]	6 weeks	10 weeks	2x/week <u>Exercised</u> First 5 weeks Time = 60 min Incline = 7 degrees Speed = 15 m/min Last 5 weeks Time = 60 min Incline = 7 degrees Speed = 23 m/min <u>Non-exercised</u> Time = 60 min Incline = 0 degrees Speed = 2 m/min	Compared to MDX non-exercise, MDX-ex exhibited: ↑ heart weight (not significant) ↑ ratio heart:body weight ↑interstitial fibrosis and adipose tissue in cardiac muscle (fiber disorganization observed) ↑ infiltration of inflammatory cells ↑% dystrophic lesion in myocardium ↑basal level of [p-ERK1/2 and calcineurin] ↔ body weight ↓p-JNK1 in cardiac muscle ↑p-38 MAPK in heart MDX-ex + non-exercise: ↑immunoreactivity with antibodies against p-p38 MAPK, p-ERK1/2, calcineurin in degenerative fibers around the fibrotic change, infiltration of inflammatory cells	Physical exercise induces dystrophic features in mdx cardiac muscle. Future studies should look at the effects of inhibitors of p38 MAPK, ERK or calcineurin on exercised mdx mice in order to elucidate mechanism of progression of the dystrophic change in heart muscle
Nakamura et al. 2005 [338]	6 weeks	10 weeks	2x/week <u>Exercised</u> First 5 weeks Time = 60 min Incline = 7 degrees Speed = 15 m/min Last 5 weeks Time = 60 min Incline = 7 degrees Speed = 23 m/min	↔ overt necrosis, fibrosis, inflammatory cell invasion in skeletal muscle in MDX-ex. MDX-ex compared to MDX-sed: ↑ratio protein level of p-ERK1/2 to pan ERK1/2 (4 fold) ↑ratio of p-p38 MAPK to pan p38 MAPK (1.8 fold) ↑ratio of protein level of p-JNK2 to pan JNK2 (2.3 fold) ↑ MMP-9 (1.3 fold) ↔ ratio of protein level of p-JNK1 to pan JNK1 among any group	Treadmill exercise training ↑ phosphorylation of ERK1/2, p38 MAPK, and JNK2 in mdx GASTROC muscle. This may play a role in the degeneration and regeneration process of dystrophic features. No pathological change compared to previous results in cardiac muscle. Difference may be explained by the degeneration-regeneration cycle after exercise or by factors which modify muscle degeneration in *mdx* skeletal muscle but not cardiac muscle. JNK2 and p38 MAPK may be associated with the degeneration mechanism of dystrophin-deficient skeletal muscle.

Table 1 continued

					MMP-9- possible role in disruption of the integrity of muscle fibers or in the inflammatory response and the activation of satellite cells associated with regeneration. Not known if upregulation after exercise is associated with degeneration or regeneration in mdx skeletal muscle.
[339]	6 weeks N = 10 mdx male mice	10 weeks	2x/week First 5 weeks Time = 60 min Incline = 7 degrees Speed = 15 m/min Last 5 weeks Time = 60 min Incline = 7 degrees Speed = 23 m/min	MDX had difficulty completing protocol (fatigued, need for gentle stimulation or rest) MDX-Ex compared to MDX-sed: ↔ fiber size distribution ↔ intramuscular collagen (suggesting ↔ perimysial and endomysial fibrosis) ↑ population of smaller sized fibers (<20 um) ↓ # of large-sized DRG in sol/gas/quadriceps ↓ level of Igf-1 expression ↓ level of myod1 expression Type III collagen mainly localized in perimysium IGF-1 localized to early regenerating fibers with large round nuclei (moderately or fully regenerated, centrally nucleated fibers were not positively stained) IGF-1 absent in small regenerated fibers with compacted, centrally located nuclei	MDX skeletal muscles temporarily cope with work-induced injury by enhancing muscle regeneration and repair. Chronic exercise may accelerate active cycle of degeneration-regeneration, which may be an advantage for coping with exercise. Early ↓ of IGF-1 will accelerate age-dependent muscle wasting and weakness in the later stage of life. Mdx mice vulnerable to exercise, which may result in fiber necrosis earlier/more drastically; however, data show that necrosis can be repaired in exercise mice. Exercise may shorten the active degeneration-regeneration period in mdx mice and mdx muscle fibers more resistant to necrosis after undergoing one cycle of regeneration. Chronic exercise in the active degenerative-regenerative period will accelerate age-dependent dystrophic processes in mdx mice, leading to a shortening of the natural course of mdx skeletal muscles.
[273]	28 days	8 weeks	2x/week Time = 30 min Incline = 0 degrees Speed = 9 m/min	**Oxidative Damage** ↔ MDA, protein carbonyls in MDX-ex ↓MDA (38%) in MDX-ex ↓protein carbonyl (44%) in white muscle of MDX-ex	Low intensity exercise training decreases oxidative stress markers (protein carbonyls and MDA) in white GASTROC of mdx mice and does not

Table 1 continued

				Antioxidant Enzymes No effects of exercise on SOD, MnSOD, or CAT in MDX-ex **Mitochondrial Enzymes** ↔COX between MDX-ex and MDX-sed **Muscle Damage** ↔ internalized muscle nuclei per total muscle fiber area between MDX-ex and MDX-SED	detrimentally affect mdx mice. Oxidative stress may contribute to muscle degeneration in mdx mice but low intensity exercise training decreases ROS generation in skeletal muscle of trained mdx mice. Propose that when calcium homeostasis is improved, ROS generation is decreased which causes a decline in markers of oxidative stress in skeletal muscle MDX-ex. Lower protein carbonyls and MDA levels following exercise in MDX suggest that several pathways are involved in alleviating the effect: 1. Activation of nNOS and up-regulation of NO formation that results in lower generation of peroxynitrite 2. Improved calcium homeostasis that results in decreased ROS generation 3. Acceleration of the regeneration phase and transformation from fast to slow twitch fibers 4. Other unknown factors
[340]	8 weeks for 4 week study 12 weeks for single session	1 session vs 4 weeks	**Protocol A** single 30 minute session **Protocol B** 2x/week for 4 weeks **Treadmill Settings** Warm Up: Time = 2 min Incline = 0 degrees Speed = 4 m/min Followed by: Time = 8 min Incline = 0 degrees Speed = 8 m/min Main Exercise: Time = 30 min	**Protocol A** ~45% of 12-week old untrained mdx mice could not complete main exercise despite 5 rest times. MDX-ex and MDX-sed had high variation in the amount of myofiber necrosis but exercise significantly increased amount in both 24h and 48h samples ↑ mRNA levels of IL-1beta in MDX-ex after at 2h and IL-6 at 0h + 2h but ↔ at 24h ↓mRNA levels of TNF in MDX-ex	Protocol A is a suitable screening protocol for assessing therapeutic interventions in adult mdx mice. To visualize the increase in myofiber necrosis following treadmill exercise, the muscles must be sampled between 24 and 48 h. Large n is needed due to variation, and muscle choice is critical to assessing impact of exercise induced damage.

Table 1 continued

			Incline = 0 degrees Speed = 12 m/min *If one mouse fatigued, all four mice on treadmill were allowed to rest for 2 min then gradually increased speed*	↑protein thiol oxidation in MDX-ex at 0h + 2h but ↔ at 24h ↔ MDA in MDX-ex **Protocol B** ↓ avg # of rests needed to complete exercise throughout 4week period ↑rests for in Protocol A compared to Protocol B ↓ absolute and normalized change in forelimb grip strength in MDX-ex ↑myofiber necrosis in QUAD, TB, DIA, and TA in MDX-ex at 24h and ↑necrosis in MDX-ex at 0h ↔ myofiber necrosis in MDX-ex 96h post exercise ↑blood serum CK levels in MDX-ex at 24h but ↔ at 96h ↔ mRNA for IL-1beta or IL-6 in MDX-ex at 0h and ↓ at 96h ↓TNF mRNA in MDX-ex at 0h but ↔ for at 24h ↑protein thiol oxidation in MDX-ex at 0h but ↔ at 24h	Protocol A was damaging enough to render myofibers leaky, but not damaging enough to cause widespread myofiber necrosis in muscles except for the quadriceps. The mdx mice may have adapted to the treadmill exercise overtime, as shown by relatively stable IL-6 mRNA. Increased IL-6 following exercise may inhibit TNF, which is involved with the pathology of mdx mice and blockade of TNF can reduce necrosis. Potential therapeutic drugs for DMD should be chronically tested in order to examine efficiency and possible negative effects
[341]	4-5 weeks	4 weeks (T4) or 12 weeks (T12)	2x/week Time = 30 min Incline = 0 degrees Speed = 12 m/min 48 or 72 hr break between each exercise session Exercised for either 4 or 12 weeks	↔ BM in MDX-ex ↓absolute and normalized strength in T4 in MDX-ex and maintained up to T12 ↓ distance (30-40%) in MDX-ex at T4 + T12 compared to WT-ex ↑ fatigue in MDX-ex at T4 and T12 **Exercise-Related Genes** ↔ Pgc-1alpha gene in MDX-ex at T4 ↓Pgc-1alpha gene in MDX-ex at T12 ↔Sirt1 in MDX-ex at T4, but ↓in MDX-ex at T12 ↓Ppar-gamma in MDX-ex at T12 **Pgc-1alpha Target Genes**	GASTROC muscle was studied due to the resemblances in composition with human muscle. Exercise protocol does not produce metabolic adaptation in healthy muscle Genes primarily involved in harmful signaling in dystrophic skeletal muscles are kept deregulated in MDX-ex, while the expression of genes involved in protective programs and upregulated in basal conditions is markedly impaired. Exercise that is able to produce a myofiber adaptation in WT muscle

Table 1 continued

				↔ in Cox4 and Cs for MDX-ex at T4 ↔ in utrophin in MDX-ex at T4 or T12 exercise **Myofiber Phenotype Genes** ↔ Mhc isoforms in MDX-ex at T4 ↓Mhc1 in MDX-ex at T12 ↑Mhc2b in MDX-ex at T12 ↔ Serca1 in MDX-ex at T4 or T12 ↔ Serca2 in MDX-ex T4 but ↓Serca2 in MDX-ex at T12 ↑Mef2c (not significant) in MDX-ex at T12 ↓Hdac5 in MDX-ex at T4 and T12 **Regeneration-Related Genes** ↓Myog and Fst in MDX-ex at T12 ↔ Igf-1 in MDX-ex at T12 **Muscle Damage Related Genes** ↓Mstn in mdx mus at both ages (no effects of exercise) ↔ Atrogin1 in any experimental condition ↓adiponectin in MDX-ex at T12 **Autophagy Genes** ↓Bnip3 in MDX-ex at T12 ↓Pgc-1alpha, Sirt1, Fst, and Mhc1 in EDL of MDX-ex	may cause more damage in mdx muscle.
[342]	4 weeks	4 weeks	2x/week Time = 30 min Incline = 0 degrees Speed = 12 m/min No more than 48-72 h between each session Excluded mice that did not complete all sessions	MDX-ex compared to mdx SED: ↓TTEs and basal O2 consumption ↔max O2 consumption ↑oxidative stress in QUAD and AB ↑hydroxyproline deposition in QUAD and heart tissues ↔hydroxyproline in AB ↑collagen scarring in heart ↑collagen-I scar amounts ↑levels of dying myocytes (not significant) (indicated by intracellular IgG accumulation) ↔IgG staining in QUAD	Exercise is deleterious to mdx mice, and exacerbates disease pathology and alters exercise capacity. Forced treadmill exercise increases dystrophic severity. Intensity and modality of exercise affect how dystrophic muscle responds to exercise. This protocol exacerbated the pathology of mdx mice. Decrease in basal oxygen consumption could indicate that exercise produced disruptive changes in O2 consumption.

Table 1 continued

					Unlike the anti-fibrotic effects observed in healthy muscle following exercise, exercise increases fibrotic scar damage in quadriceps muscles, abdominal muscles, and heart in dystrophic muscle. No control conditions were used to assess the possibility that mdx mice incurred muscle damage during the maximal exercise test, which might further confound indices of muscle damage. Dystrophic muscle does not favorably adapt to exercise in regard to oxidant buffering and redox homeostasis.
[343]	8 weeks	60 days	3x/week **Low intensity training** Time = 30 min Incline = 0 degrees Speed = 9 m/min	MDX-ex compared to MDX-sed: ↑intramuscular area of collagen III (and ↑ than WT) ↔ BM ↔ % of centrally-located nuclei ↔ minimal Feret's diameter ↔ intramuscular area of collagen I ↓ collagen fibers mean values (but similar to WT)	Exercise did not influence muscle injuries resulting from membrane fragility in MDX mice. Exercise provoked adaptations on extracellular matrix bringing higher elastic features to mdx muscle tissue. Exercise delayed the aberrant muscle repair at the studied age. At 16 weeks old, regeneration was more present than fibrosis in both MDX-sed and MDX-ex but exercise decreased the progression of muscular fibrosis.
[344]	4-5 months	6 months	3x/week Time = 30 min Incline = 0 degrees Speed = 4 m/min (low intensity) vs 8 m/min (moderate intensity). Speed gradually increased over the first 7.5 min to reach training speeds.	MDX-low and MDX-mod compared to MDX-sed: ↑grip strength ↑max force generated by TA ↔ TA cross sectional analysis among groups dose-dependent ↑ in proportion of type IIa fibers ↑Pgc1a gene expression GASTROC ↑minute volume with aerobic exercise ↔ HR between groups ↔QRS duration throughout the study ↓rate of decline in fractional shortening and stroke volume	Progression of cardiomyopathy was delayed with aerobic exercise with no adverse effects on electrical function of dystrophic heart. Function of dystrophic heart and muscle was improved with exercise without a significant increase in fibrosis, centrally nucleated fibers, or serum CK Translate into human setting by defining biomarkers for skeletal and

Table 1 continued

				in an exercise dependent manner ↓heart mass with ↑ exercise intensity ↑Pgc1a in the hearts ↔picrosirius red staining (# and size of fibrotic regions in heart, DIA, GASTROC) ↔% of centrally located nuclei ↔serum CK during exercise program ↑serum and adipocyte concentrations of adiponectin ↓cross sectional area of adipocytes ↓in left ventricle internal diameter thickness during diastole and the left ventricle posterior wall thickness at month 6 Inspiratory time (Ti): ↑7% in MDX-sed ↑1% in MDX-mod ↓6% in MDX-low Expiratory time (Te): ↑43% in MDX-sed ↑13% in MDX-mod and MDX-low Ti and Te inversely related to disease progression ↑avg activity level (months 4+5) in MDX-mod compared to MDX-sed and MDX-low	cardiac dystrophic muscle to help define low and moderate exercises.
[345]	4-5 weeks 16 weeks for single session	~4 weeks vs >12 weeks vs 30 min	2x/week Time = 30 min Incline = 0 degrees Speed = 12 m/min Long (>12 weeks), short (~4 weeks) and acute (1 session) protocols	MDX-short and MDX-long compared to MDX-sed: ↓absolute and normalized strength after 4 week and impairment maintained up to 12 weeks ↓twitch and tetanic force of mdx DIA but no DIA fatigue ↓contractile force (to 10%) of EDL in MDX-short and becomes significant in MDX-long ↔ effects of eccentric contractions of EDL ↓PCG-1alpha, ↓MYH1, and ↓ basal upregulation of SIRT1 ↑AChR1 (twofold) in MDX-long protocol	There is a complex equilibrium between adaptation and maladaptation in MDX mice.

Table 1 continued

				↑NOX2 and Tuba-1b and ↓ in Fst ↑total damage (40%) in MDX-long protocol (sum of necrosis, infiltration and non-muscle area) ↔% of centrally located nuclei ↔mmp9 In response to single bout of exercise: ↓normalized twitch and tetanic tension in MDX-acute ↔contraction kinetics or fatigue ↓twitch and tetanic contractions of EDL in MDX-acute ↓time to peak tension and half-relaxation time for MDX-acute ↔ fatigue	

Table 2: Studies examining ad libitum wheel running in mdx mice.

Study	Age	Duration of Study	Results	Study's Conclusions
[346]	**Young group** ~4 weeks **Adult group** ~6 months	4 weeks	**Adult Mice** ↓running in MDX-ex compared to WT-ex CK ↓65% in MDX-ex ↑BW for MDX-ex ↓BW for WT-ex ↑SOL weight for MDX-ex and WT-ex but ↔EDL weight ↑CSA in SOL and EDL for MDX-ex and WT-ex ↓tetanic tension in SOL and EDL of MDX-ex and WT-ex ↔fatigue response in SOL of MDX-ex **Young Mice** ↔ running in MDX-ex and WT-ex due to high inter-mouse variability ↔CK levels in MDX-ex ↔ in BW between MDX-ex and WT-ex ↑SOL weight for MDX-ex and WT-ex but ↔EDL weight ↑CSA in SOL of MDX-ex but ↔EDL ↓tetanic tension in SOL and EDL in MDX-ex ↔fatigue response in SOL of MDX-ex ↔ on histology of MDX-ex	Force does not ↑ at same rate as the CSA. Could be because strangely branched and/or split fibers in MDX and/or ↑ in % of non-contractile elements such as connective tissue EDL and SOL from young and adult MDX showed slight injury b/c of exercise.
[347]	4 weeks	16 weeks	↔ avg week distance + daily speed for 2 weeks. Then ↓ avg distance and daily speed for MDX-ex compared to WT-ex in all weeks after 3 weeks except week 8 ↔ avg run hours per week in MDX-ex vs WT-ex running ↑ abs. mass of SOL in MDX-ex but ↔ in EDL + PL ↔ in EDL + PL contractile properties in MDX-ex	↓ in distance run MDX-ex vs WT-ex due to ↓ speed in MDX After exercise, ↑ fatigue resistance, proportion of oxidative fibers + improvement in muscle force production

Table 2 continued

			↑ abs. twitch + tetanic tensions of SOL in MDX-ex ↑ resistance to fatigue in EDL + SOL of MDX-ex but ↔ fatigue resistance in PL of MDX-ex ↑ type I + ↓ type IIa fibers in SOL but ↑ type IIa + ↓ type IIb in EDL of MDX-ex	
[348]	6 months	1 year	MDX-ex ran 55% of daily distance of WT-ex ↔ EDL weight but ↑ SOL weight in MDX-ex ↔ tetanic tension for EDL or SOL in MDX-ex ↑ fatigue resistance in EDL of MDX-ex	Hypothesis that long-term ad libitum exercise having beneficial effects on WT and deleterious effects on MDX was not supported by data MDX-sed show high muscle damage but MDX-ex respond beneficially to low levels of voluntary running Reason for atrophy in MDX mice is unknown but ould be due to ↓ physical activity, ↓ satellite cell proliferation., and/or ↑ catabolism Long-term exercise does not have deleterious effects on MDX EDL, and slightly improves SOL
[330]	21 days male	3 weeks	Run distance dependent on diet: MDX-ex-GTE ran total distance 128% ↑ than MDX-ex over course of study. Interestingly, MDX-ex-GTE total distance was equal to WT-ex ↑ tetanic stress in MDX-ex and MDX-ex-GTE and ↑active stiffness in MDX-ex and MDX-ex-GTE ↑abs. myosin content, total muscle protein to muscle mass, total contractile protein to total muscle protein in EDL of MDX-ex and MDX-ex-GTE ↑ type I and IIa fibers and ↓ type IIb fibers of EDL in MDX-ex but ↔ in MDX-ex-GTE ↑ antioxidant capacity in MDX-ex and MDX-ex-GTE ↓ Lipid peroxidation in GASTROC and heart of MDX-ex and MDX-ex-GTE ↓CK levels in MDX-ex and MDX-ex-GTE ↑CS activity in QUAD and heart of MDX-ex and MDX-ex-GTE	GTE, MDX-ex and MDX-ex-GTE was beneficial and no obvious deleterious outcomes EX + GTE diet ↑ muscle function in MDX ↑ EDL tetanic stress output could be due to ↑ stability of contractile proteins, shift in fiber type, and ↑ membrane integrity

Table 2 continued

			↑ B-oxidation activity in QUAD and heart of MDX-ex and MDX-ex-GTE	
[349]	4 weeks	8 weeks	↓ distance + time on wheel in MDX-ex than WT-ex ↔ BM in MDX-ex ↑percentage of type IIa fibers and ↓ percentage of type type IIb in EDL of MDX-ex Leftward shift in CSA distribution of EDL and SOL in MDX-ex ↔ in central nuclei in MDX-ex	MDX can remodel in response to exercise. MDX mice engage in physical activity when given the opportunity. Exercise may prevent secondary unwanted consequences. Appears to be an intensity threshold for inducing beneficial vs deleterious adaptations.
[290]	4-5 weeks	12 weeks	↓ BM in MDX-ex (no resistance) and MDX-resist (resistance increased by 1 g per week) ↓ mean daily distance in MDX-resist vs MDX-ex ↑ external work per week in MDX-resist vs MDX-ex during weeks 2-12 ↔ max. dorsiflexion torque in MDX-resist vs MDX-ex but ↑ during duration of study ↑ grip strength in MDX-ex + MDX-resist ↔ whole body tension in MDX-ex + MDX-resist ↔ abs. twitch, tetanic, or eccentric forces by SOL in MDX-ex + MDX-resist ↔ passive + active stiffness in in MDX-ex + MDX-resist ↔ in force loss during + following eccentric injury in in MDX-ex + MDX-resist ↔ in muscle masses in MDX-ex + MDX-resist ↔ CK in MDX-ex + MDX-resist ↑ beta-dystroglycan content in GASTROC of MDX-ex ↑ vinculin content in SOL of MDX-ex	↔ in functional measurements by wheel running 12 weeks of voluntary wheel running ↑ muscle strength in SOL and ↑ grip strength 2 modes of exercise differing in intensity are capable of inducing comparable adaptations in skeletal muscle of MDX mice. Dystrophic muscle can adapt to a resistance-type exercise Hypertrophy was not the underlying cause of improvement. Minimal changes in cytoskeletal proteins with wheel running. Did not observe a benefit with regard to susceptibility to injury. Data collected indicates that a threshold must be surpassed regarding cytoskeletal protein expression to observe functional benefits, and wheel running did not overtly elicit this adaptation in mice.

Table 2 continued

[332]	4 weeks	12 weeks	Voluntary wheel running does not induce physical inactivity in MDX-ex but mice ↓ voluntary activity during 30 min after forced running on wheel. ↔ CK in MDX-ex ↔ BM in MDX-ex ↑heart mass but ↔ GASTROC and TA in MDX-ex ↑ maximal isometric torque in MDX-ex Plantarflexor muscles beneficially adapted to daily running with ↑ sub-maximal torque MDX-ex but ↔ in concentric torques ↑% of peak torque in MDX-ex ↑ PCG-1alpha protein in GASTROC of MDX-ex ↑ COX IV protein in GASTROC of MDX-ex ↔ percent of central nuclei in TA or diaphragm but ↓ in central nuclei in GASTROC of MDX-ex	in vivo muscle strength + fatigue resistance ↑ in MDX-ex. Mitochondrial adaptations contribute to the beneficial exercise-induced skeletal muscle remodeling. Strength gains occurred at functionally-relevant, sub-maximal frequencies. Duration is an important exercise design parameter. Mode + intensity are also important.
[350]	10-12 weeks	2 weeks	Daily distances run by individual mice diverged over time. **Mouse 1** Pattern: intermittent running + resting throughout most of the dark hours **Mouse 2** Pattern: intermittent running + resting throughout most of the dark hours **Mouse 3** Pattern: intermittent running + resting throughout most of the dark hours **Mouse 4** Pattern: intermittent running + resting throughout most of the dark hours **Mouse 5** Pattern: intermittent running + resting throughout most of the dark hours. More breaks in last 4-6 hours of night **Mouse 6** Pattern: ran intermediate-high overnight distances, although these were variable by up to 3 km per night Ran mostly in first 6 hours per night, with almost no running activity in second 6 hours **Mouse 7** Pattern: intermittent running + resting throughout most of the dark hours Total Distance: 0.04 km **Mouse 8**	Extensive variation in voluntary wheel running in MDX adults. ↓# of bouts + ↑ bout distance promoted muscle damage. Data strongly indicates that a detailed analysis of individual mouse running behavior is essential when utilizing voluntary wheel running.

Table 2 continued

			Pattern: intermittent running + resting throughout most of the dark hours Total Distance: 7.65 km **Mouse 9** Pattern: ran intermediate-high overnight distances, although these were variable by up to 3 km per night Ran mostly in first 6 hours per night, with almost no running activity in second 6 hours **Mouse 10** Pattern: intermittent running + resting throughout most of the dark hours. More breaks in last 4-6 hours of night Total Distance: 67.24 km **Mouse 11** Pattern: ran intermediate-high overnight distances, although these were variable by up to 3 km per night Ran mostly in first 6 hours per night, with almost no running activity in second 6 hours Total Distance: 62.68 km Avg time spent running on running wheel per bout ranged from 1.04 min (mouse 7) to 10.52 min (mouse 11) Running bouts ↓ for mouse 4, 7, and 8, and ↑ for mouse 11 in comparison with group avg Mouse 7 + 11 had rest times ↑ than all other mice From slowest to fastest average running rate: mouse 7 + 8, mouse 1 + 4, mouse 2 +3, mouse 5 + 6, and mice 9-11. Mouse 8 ran ↑ # of bouts but ↓ avg rate. Mice 6 + 9-11 ran ↓ # of bouts but ↑ avg rate. ↑ in tissue necrosis in QUAD of mdx-ex. Shift towards larger fiber CSA in QUAD and GASTROC in MDX-ex. Mean distance covered in individual running bouts showed a positive correlation with percent of tissue necrosis in QUAD. Total # of running bouts showed an inverse correlation with tissue necrosis. Mean nightly + total # of running bouts also showed an inverse correlation with necrosis in GASTROC.	

Table 2 continued

			Mean running bout distance correlated with percent of centrally nucleated myofibers. Total + mean rest times showed positive correlation with necrosis in GASTROC. Total run time had negative correlation with necrosis in GASTROC. Only running parameter that was a significant positive indicator for myofiber CSA was total cumulative rest time.	
[351]	Sed MDX: 5 months Run MDX: 4-5 weeks Run CT: 4 weeks	Sed MDX: 2 weeks Run MDX: 4-4.5 months Run CT: 3 months	**Inactivity** ↓ specific maximal force in MDX+staple ↓ absolute maximal force in CT + MDX. ↓ force after 3rd, 6th, and 9th lengthening contraction in MDX-staple, indicating increased susceptibility to contraction-induced injury with inactivity ↑ expression of MHC-2b protein and GDF8, Stim1 and Jph1 gene expression in MDX+staple ↔ in Bnip3, LC3, and astrogin-1 expression in MDX-staple **Activity** ↑ specific maximal force, abs. maximal force, and muscle weight in MDX-ex lower force ↓ after 3rd, 6th, and 9th lengthening contraction in MDX-ex, indicating a decreased susceptibility to contraction-induced injury ↔ in gene expression except for ↑ in MHC-2a protein + ↓ in Actg1 ↔ fibrosis in MDX-ex	inactivity aggravates muscle weakness + susceptibility to contraction-induced injury. Possible that GDF8 decreases contractile protein contents because it is known to inhibit protein synthesis. Fast fibers have ↑ fragile than slow fibers Inactivity can worsen dystrophic features and be more harmful to DMD vs healthy muscle. Activity ↓ muscle weakness + susceptibility to contraction-induced injury. Data suggests that muscle weakness + susceptibility to contraction-induced injury in dystrophic muscle could be partly attributable to inactivity.
[352]	4 weeks	52 weeks	↑ BM in MDX-ex Running distance peaked at weeks 3+4 of study, and steeply declined after. ↑abs. plantarflexor, GASTROC and SOL, and heart masses in MDX-ex ↑CSA and tetanic force in SOL of MDX-ex	1 year of wheel running caused heart remodeling but diaphragm function was severely impaired in MDX-ex. Likely that ↑ rate of respiration + workload required to support exercise accelerated disease progression in diaphragm. Mice tend to perform intermittent sprints instead of maintaining a

Table 2 continued

			↑heart ↑ Left ventricular end diastolic and systolic dimensions, and systolic volume in MDX-ex ↑stroke volume + cardiac output in MDX-ex	steady pace which could ↑ diaphragm injury +↓ function
[353]			Note: mice are from Baltgalvis et al. 2012 ↑ total utrophin protein in QUAD of MDX-ex but ↔ in SOL ↔CSA or muscle fiber CSA variability ↑percentage of small central nuclei % in MDX-ex	Previous reports show utrophin protein translation is regulated by signaling pathways activated by aerobic exercise.
[354]	7 months	3 months	↔ in running between male + female MDX-ex ↔ force drop after 9 lengthening contractions ↔ in specific maximal force ↑ abs. maximal force in female MDX-ex but ↔ in males ↔ left ventricular function + structural heart dimensions ↔ in expression in cardiac gene markers of inflammation/fibrosis (Col1a1, Col3a1, Ctgf, and TgfB1) and cardiac remodeling (Bnp and Myh7)	Voluntary activity initiated at 7 months was not detrimental for hindlimb skeletal muscle in MDX mice and does not improve susceptibility contraction-induced injury in female MDX mice.

Table 3: Studies examining swimming in mdx mice.

Study	Age	Duration of Study	Exercise Program	Results	Study's Conclusions
[355]	5 weeks	15 weeks	Time was ↑ daily until total swim time was 2 hours continuously. Program continues by attaching weights (5% of body weight) to tail during 2 hour swim-period. Resisted swim continued for 5 more weeks until 20 weeks of age was reached	MDX-ex compared to MDX-sed: ↓ mass of SOL + EDL ↓ SOL CSA ↓ EDL CSA ↑ normalized twitch tension ↑ fatigue resistance in SOL and EDL ↑ type I fibers in EDL	Improvement in fatigue resistance of skeletal muscles in MDX-ex, improvements in muscle oxidative capacity, and transformation towards less-fatigable fibers renders muscle less vulnerable to damage. Combining exercise and an anabolic agent may improve muscle mass and offer greater benefits.
[356]	same mice from Hayes et al. 1993	15 weeks	same mice + protocol from Hayes et al. 1993	MDX-ex compared to MDX-sed: ↓ # of type IIa fibers and ↑ # of intermediate fibers **EDL** Type IIa fibers displayed steeper force-pCa and force-pSr Type IIb fibers showed ↓ threshold for contraction by Ca2+ and a ↓ Ca2+ sensitivity **SOL** ↔ differences existed for Ca2+, sensitivity of type I fibers to Ca2+, or force-pCa curve steepness Type IIa fibers had force-pCa curves that were significantly right shifted and displayed higher values for contraction threshold and sensitivity. ↓ force-pCa curve steepness values	Swimming affected some contractile properties of MDX skeletal muscle fibers. Fast-twitch fibers isolated from MDX-ex had ↓ sensitivity to Ca2+ and Sr2+. This ↓in sensitivity to activating ions may be a protective mechanism that prevents the ↑ resting Ca2+ in these fibers from exceeding contraction threshold.
[327]	8-10 months or 24 months	10 weeks	Free swimming for as long as possible once daily. Rest day after 2 consecutive days of swimming.	24-month mice were unable to swim continuously for > 25 min. For swimming, ↔BM or muscle mass in 24-month mdx mice ↔ absolute forces produced but ↑ in peak tension normalized to muscle mass and tetanic tension normalized to muscle mass in 8-10 month mdx mice vs 24-month mdx mice	Contractile properties of old MDX mice can still be altered by very low-intensity swimming. Low levels of controlled, non-weight-bearing activity can be beneficial for dystrophic muscle.

Table 3 continued

				↑ force-generating capacity in 24-month mdx mice ↔ fatigue properties of 24-month mdx mice	
[357]	4 weeks	4 weeks	exercised 4 days per week (M, T, Th, F) for 30 min/day. Mice were not forced to swim and were free to stand.	MDX-ex compared to MDX-sed: ↑ grip strength ↔ total protein carbonylation level but ↓ carbonylation of voltage-dependent anion-selective channel protein 1, fast isoforms of troponin T + MyBP-C, and phosphoglucomutase-1 ↑ expression of respiratory chain proteins, fast isoforms of troponin T and MyBP-C, UTP-glucose-1-phosphate uridylytransferase and carbonic anhydrase 3 ↓carbonylation of ATP synthase subunit alpha, fast isoform of troponin T and GP ↑expression of tubulin, vimentin, and associated proteins, and stress response proteins. Two ATP synthase complexes absent in MDX-sed muscle were restored in MDX-ex. ↑ expression of slow isoforms	Proteins involved in muscle contraction and glycogen metabolism were both over carbonylated and downregulated in MDX Sed. Swimming rescued, at least in part, MDX muscle at protein level. Specifically, proteins from mitochondria, muscle contraction, and glycogen metabolism that were highly carbonylated and downregulated in MDX-sed muscle were less carbonylated and highly expressed in MDX-ex. This suggests that protein carbonylation could cause a functional impairment in mdx muscle.

Table 4: Studies examining Rota-Rod training in mdx mice.

Study	Age	Duration of Study	Exercise Program	Results	Study's Conclusions
[358]	8 weeks	6 weeks	5 days/week at progressively increase number of rotations (16 to 24 rotations/minute) and duration (15 to 60 minutes).	MDX-ex compared to MDX-sed: between 1 and 3 weeks of training, ↓forelimb strength and insignificant ↓ of forelimb fatigue at weeks 3 and 4 of training. ↔ fatigue resistance ↓ inflammatory-necrotic areas in GASTRO and QUAD (not significant for mice that exercised for 15 days but significant for mice that exercised for 30 and 45 days) ↓ Cx39 protein in GASTRO and QUAD (not significant for mice that exercised for 15 days but significant for mice that exercised for 30 + 45 days)	Exercise did not improve muscle function in MDX-ex but there is improvements in muscle morphology Exercise intensity could have been too low to induce significant physiological adaptation in MDX-ex.
[359]			Same mice as first study.	4 spots showed modulation in protein levels in MDX-ex, including 3 CA3 isoforms and SODC. Levels appeared to return to WT levels. ↓ CA3 in MDX-ex ↑ SODC in MDX-ex	Reduced expression of CA3 and parallel increase in expression of SODC protein suggest improved oxidative stress and restored anti-oxidative response, indicating a possible mechanism by which exercise may reduce muscle degeneration in MDX Exercise may in part contribute to lower muscle degeneration in MDX muscles.
[360]			Same mice as first study.	↔ in total area of necrosis-regeneration in DIA in MDX-ex but ↑ area of active regeneration and ↓ area of necrosis when evaluated separately at both 30 and 45 days ↔ difference in Cx39, Hsp60, Hsp70 at 30 and 45 days ↓ NF-kB levels at 45 days in MDX-ex	Trend for regeneration areas to be larger than necrosis areas in diaphragm of MDX-ex. Similar Cx39 protein levels in diaphragm of MDX-sed and MDX-ex cannot be explained by inflammation in regenerating areas but stable levels of Cx39 and NF-kB may indicate that training was not detrimental to the diaphragm of MDX mice.

Early investigations on exercise and dystrophic muscle centered on determining the susceptibility of dystrophic muscle to eccentric contraction-induced injury. These studies subjected mice to a single or multiple sessions of eccentric exercise, either via electrically stimulated lengthening contractions or downhill treadmill running. In healthy muscle, it is well established that eccentric contractions produce greater exercise-induced damage and promote negative functional consequences [361]. Damage arises from the higher force required by the reduced number of activated muscle fibers, leading to high mechanical stresses and microlesions within the sarcolemma [362] as well as disruptions in the components of the extracellular matrix and connective tissue [363,364]. This is important to highlight because these studies clearly demonstrate that dystrophic muscles endure more damage from eccentric contraction compared to their wild-type counterparts [69,70,74,76,365–367]. Specifically, there is an increase in membrane breakdown in the rectus femoris and EDL muscles [365,366], and serum creatine kinase [74,368]. Thus, authors urged researchers and clinicians that because a single bout of eccentric contractions negatively affects dystrophic muscle, exercise should be completely avoided by those with DMD [76].

These studies led researchers to propose that eccentric exercise regimens could be used to make the mdx mouse model a better clinical model for DMD and become a more reliable model for testing novel therapies [74]. Specifically, because of the lesser severity in mdx muscle, many studies have used exercise to exacerbate the phenotype prior to administering the therapy. Since these studies further supported the above hypothesis that exercise exacerbates disease progression, researchers and clinicians air on the side of caution and advise their patients to not participate in exercise. It should be noted, though, the only conclusion that can be drawn from these experiments is that inappropriate exercise and forceful muscle contractions are, in fact, detrimental to mdx muscle [317].

Lastly, due to the biomechanical differences between mouse and humans, there is only one study that evaluated the impact of “resistance training” on mdx muscle. To emulate resistance training, Call and colleagues (2010) [290] progressively increased the resistance of the running wheel by adding weights to the running wheel. For 12 weeks, mdx mice where given access to a running wheel ad libitum. Resistance increased each week from 1 gram (which is 6% of body mass) to 7 grams. Additionally, a second group of mdx mice had ad libitum access to a running wheel whose resistance remained set at 1 gram and a third group that did not have access to a running wheel but maintained normal cage activities. Mice running on the resistance wheel did not display increased skeletal muscle damage nor higher creatine kinase levels when compared with mice that ran on the normal running wheel. From these results, the authors conclude that dystrophic skeletal muscle can positively adapt to resistance training.

The major shortcomings of studies on exercise and individuals with DMD are also evident in the mdx research. The lack of uniformity among the protocols of these studies severely hinders the ability to draw conclusions and translate results to humans [369]. In 2008, TREAT-NMD published standard operating procedures for experiments evaluating dystrophic muscle’s response to activity in order to improve comparability between studies (http://www.treat-nmd.eu/research/preclinical/dmd-sops/). These documents provide detailed protocols for both the mode, intensity, and duration of exercise. For example, to worsen the mdx phenotype and/or to evaluate the efficacy of therapeutic interventions, mdx mice should run at a speed of 12 meters per minute for 30 minutes twice a week (SOP DMD_M.2.1.001). Additionally, this SOP states that mdx mice can barely tolerate downhill running and this should only be used for proof-of-concept approaches. However, there is no published SOP for studying the impact of aerobic exercise on disease progression. Lastly, while similar studies use the same outcome measures, such as maximum twitch or tetanic tension and fatigue resistance, the protocols used to collect these data were extremely different. Differences in these parameters make it difficult to compare results across studies, leading to contradicting results

and further delay in understanding how exercise impacts the progression of DMD. SOPs are now available in order to limit these differences across all preclinical studies.

Voluntary wheel running as the primary mode of exercise for mdx mice should be addressed as a study limitation, especially because it leads to inconsistent results in the literature. For studies that used voluntary wheel running with various lengths of ad libitum access (4 weeks vs 16 weeks vs 1 year), force-generating capacity and fatigue resistance of the soleus and EDL muscles differed across studies [346–348,370]. For example, following 16 weeks and 1 year of voluntary running, the soleus muscles demonstrated greater force-generating capacities while the EDL muscle exhibited a greater fatigue resistance compared to sedentary mdx mice [347,348]. Conversely, no effect was observed on these same properties following 4 weeks and 1 year of voluntary wheel running in another set of studies [346,370]. These differences most likely arise from differences in the running activity of individual mice across the four studies. Specifically, in the two studies reporting positive benefits from wheel running, mdx mice ran an average weekly distance of 29.8 $\pm$ 2.6 km [347] and about 25.2 km based on the reported average daily distance [348]. For the two studies reporting no effects of wheel running, the average weekly distance ran by mdx mice was estimated to be 33 km based on data presented in the graphs [370] and an estimated 4.5 km based on data presented in the graphs [346]. Recently, Smythe and White (2012) [350], demonstrated that voluntary wheel running differentially affects the muscles depending on the time interval between and the duration of each individual bout of running, rather than on the total daily or weekly distance. Ultimately, when using wheel running as the mode of exercise, a large number of animals is required to tease apart these inter-individual differences.

1.8.3 Inactivity in DMD

Even with extremely low activity levels in boys with DMD and a limited understanding of the potential role that exercise plays in disease progression, very few studies have been done to understand the role that inactivity plays in disease progression. While there are no human data,

studies using the mdx mouse model are available [73,75,351] and their conclusions are contradicting. Following an injection of tetanus toxin into the right gastrocnemius muscle, 3-week-old mdx mice were subjected to sustained dorsiflexion of the right ankle joint for 2 to 56 days [73]. Compared with un-injected control mdx mice, the soleus and EDL muscles exhibited a significantly reduced number of muscle fibers with centrally located nuclei, leading the authors to suggest that muscle necrosis is facilitated by muscle movement and can be prevented through immobilization. Similarly, in 3-week-old mdx mice, when a metal splint was applied to the right hindlimb to prevent contractions for 14 days, evidence of early stage necrosis in the soleus and EDL muscle was absent [75]. Additionally, the cross sectional areas of muscle fibers were noticeably reduced [75]. Here, the authors conclude that, while muscle necrosis may occur from muscle contractions, early atrophy from immobilization and the requirement of the respiratory muscles to be permanently active eliminates any therapeutic potential of these results to slow the progression of disease in individuals with DMD [75]. Lastly, following 2 weeks of leg immobilization, inactivity was found to aggravate muscle weakness and increase its susceptibility to contraction-induced injury in 5-month-old mdx mice [351]. These deficits could not be explained by changes in the expression of genes involved in autophagy, proteolysis or fibrosis [351]. Here, the authors conclude that inactivity may be more harmful for dystrophic muscle than for healthy muscle [351]. Unfortunately, none of these studies examined the long-term impact of inactive periods on disease progression.

1.9 Recommendations for Future Research

Many authors who conduct reviews on the potential impact of exercise on DMD muscle draw the same conclusions: more research is necessary and study design must be improved [317,369,371–373]. To improve study design, authors suggests that studies include not only participants of similar age but with similar disease severity, be of longitudinal design rather than cross-sectional design, be of sufficient duration to capture all potential effects, implement outcome measures that are standardized, reliable and systematic across studies [371,372], and

assess respiratory, cardiac, and limb muscles simultaneously [369,372]. This is of utmost concern because there are several major questions that still need to be addressed, including: does exercise lessen or exacerbate muscle loss and contractures in DMD patients, when is exercise more likely to beneficial or injurious during the disease, how does exercise interact with other treatment modalities, what are the short (initial days or weeks), the intermediate (several weeks to months) and the long term (many months to years) effects of exercise on disease progression, and to what extent does exercise influence tissue reorganization [372]? More importantly, though, there is a need for establishing a model that not only allows the assessment of various exercise interventions both safely and effectively but permits longitudinal assessment of dynamic variables [372].

1.10 Purpose of our Research

Skeletal muscle plasticity in diseased muscle, specifically in muscle lacking dystrophin, is incredibly understudied. While healthy individuals are capable of adapting and overcoming changes in muscle activity, how exercise or the phenomenon “use it or lose it” applies to dystrophic muscle are not clear. Therefore, it is critical that research goes back to step one, and fundamentally assesses the short- and long-term impact of muscle contractions on the structure, function and survivability of dystrophic muscle.

The purpose of our research is to evaluate the impact of inactivity and NMES on muscle structure, function and survival using the zebrafish model of DMD in order to gain insight into the delicate equilibrium between adaptation and maladaptation in DMD muscle. Zebrafish are a well-established model for studying muscle diseases and offer several advantages to understanding disease progression, which are highlighted throughout our experiments. More importantly, though, studying the impact of activity on DMD muscle must go beyond measures of muscle strength and function and delve deeper into the molecular and cellular changes occurring across multiple systems that interact and support muscle health. As demonstrated above, most studies on humans and mouse models are limited in these assessments.

Leveraging the zebrafish model of DMD allows us to address many of these limitations both in vivo and across time. We hypothesize that inactivity lowers the threshold for contraction-induced injury in dystrophic muscle and accelerates disease progression. Conversely, we hypothesize that there is an intensity threshold for NMES, where it crosses from a therapeutic intervention to one of accelerated pathology. As novel treatment strategies become available and allow individuals with DMD to become more active, it is critical that we understand the basic mechanisms of skeletal muscle plasticity and define these thresholds.

CHAPTER 2

VARIATION IN DISEASE PROGRESSION IN A ZEBRAFISH MODEL OF DMD

2.1 Relevant Background

2.1.1 Zebrafish as a Model to Understand the Pathological Mechanisms of Muscular Dystrophy

Zebrafish harbor orthologous genes with more than 70% of all human genes and more than 80% of human disease-causing genes [374]. Included in these genes are those responsible for various types of muscular dystrophy (reviewed by [375,376]). Interestingly, multiple zebrafish models for these muscular dystrophies more closely resemble the severity of the pathology observed in humans than the corresponding mouse models [376–378]. Zebrafish are an attractive model for studying skeletal muscle and muscle diseases, especially because they generate a large number of offspring, develop rapidly ex utero, have optically transparent embryos and larvae, and can be genetically manipulated more easily [379,380]. Additionally, skeletal muscle is the largest and most prominent system in zebrafish larvae, allowing it to be easily visualized and accessible [375]. Further, many molecular, ultrastructural and histological features are shared between zebrafish and human muscle, including components of the DGC, the excitation-contraction coupling machinery, and the contractile apparatus [381–385]. However, one fundamental difference between zebrafish and human muscle is the anatomical separation of the fast- and slow-twitch muscle fibers. Specifically, the bulk of the fast muscle fibers are located close to the axis while the slow muscle fibers reside just under the skin. A second fundamental difference is that zebrafish harbor short muscle fibers attached serially to the myotendinous junctions. This structural difference increases the relative number of possible failure points per unit muscle length compared to mammalian limb muscles [386]. Lastly, zebrafish exhibit reproducible, quantitative motor behaviors beginning at 1 dpf [387], providing simple and non-invasive measures of muscle function. Therefore, numerous studies have leveraged the zebrafish model to perform large drug screening assays to identify potential

therapies for muscular dystrophies as well as to investigate potential mechanisms of disease progression.

2.1.2 The Zebrafish Model of DMD

Dystrophin-deficient zebrafish, known as sapje$^{ta222a/ta222a}$, and referred to as *dmd* mutants throughout this dissertation, are the smallest vertebrate model of DMD. These zebrafish were isolated in a forward genetic screen [388] and subsequently identified as carrying a non-sense mutation in exon 4 of the dystrophin gene. This mutation is autosomal recessive, affecting about 25% of the offspring from a heterozygous cross. Zebrafish *dmd* mutants are an excellent example of how the zebrafish model better captures the severity of the human disease than the mouse model [324,389]. For example, zebrafish larvae exhibit severe structural and functional deficits by 4 days post fertilization (dpf), and die prematurely by their second week [377,390]. Conversely, mdx mice have very mild structural and motor deficits with little impact on survival [324,389]. Upon histological characterization of *dmd* mutants, there is extensive muscle fiber degeneration and fibrosis, as well as infiltration of inflammatory cells and activation of muscle satellite cells [377]. Additionally, muscle fiber cross-sectional areas exhibit significant variation, with the proportion of small muscle fibers being significantly higher compared to wild-type siblings. However, at 7, 14, and 21 dpf, the area covered by muscle fibers with large cross-sectional areas is significantly greater in *dmd* mutants compared to wild-type siblings, and the percentage of muscle fibers with centrally-located nuclei is significantly reduced [377]. BrdU and Pax7 labeling also reveal significantly higher levels of proliferation throughout development in *dmd* mutants, especially for the satellite cell population [377]. Lastly, twitch and tetanic forces are significantly decreased in *dmd* mutants compared to wild-type siblings, with a 50% deficit in normalized twitch force and a 40% deficit in normalized tetanic force [386]. Therefore, while *dmd* mutants are well-characterized as a whole, longitudinal studies to elucidate variation in the severity of muscle degeneration as well as the dynamics of degeneration-regeneration cycles in

individual zebrafish have not been conducted. The goal for this chapter is to test a longitudinal approach for studying variation in the zebrafish model of DMD.

2.2 Experiment Overview

Unlike most zebrafish studies in which embryos are treated as a collective whole, we followed embryos individually throughout each experiment so that disease progression could be monitored throughout time. Experiments began at disease onset, which is 2 dpf. At disease onset, zebrafish were identified via birefringence as a *dmd* mutant or healthy wild-type sibling. Wild-type siblings had myotomes with organized, parallel muscle fibers that appear bright white while *dmd* mutants had myotomes with disorganized and detached muscle fibers that appear gray to black [389]. After separating *dmd* mutants from wild-type siblings, zebrafish were prepared for birefringence imaging (protocol in Appendix B.2). Zebrafish were imaged one by one, and housed one fish per well in 12-well plates with 3 mL of 1X ERM per well. Upon imaging, each individual zebrafish was assigned a number that was used to track the zebrafish and its corresponding birefringence images throughout the entire study. Birefringence images were taken at the same time every day beginning at 2 dpf. In addition to birefringence, DanioVision was used to analyze swimming activity as a metric of muscle function (protocol in Appendix B.3). Following birefringence imaging at 3, 5 and 8 dpf, swimming was analyzed. DanioVision was not performed at 2 dpf since zebrafish exhibit extremely low activity levels. At the conclusion of the experiment, birefringence images and DanioVision data were analyzed for each individual zebrafish. An overview of the experimental workflow is shown in Figure 1A.

2.3 Results

2.3.1 Longitudinal Studies Indicate that Muscle Structure, Degeneration, and Regeneration in *dmd* Mutant Zebrafish are Variable

All birefringence data were also normalized to the average WT birefringence in each imaging session (Fig. 1A). Birefringence clearly visualizes healthy muscle in WT larvae (Figure 1B, white arrowhead in B3 denotes a healthy muscle segment). While the average mean gray

value for a group of wild-type embryos is always 100% (see Figure 1E1), mean gray value of individual wild-type embryos varies day-by-day but hovers around 100% (see Figure 1E2). At the onset of muscle degeneration in *dmd* mutants, there was drastic variation in muscle structure: ranging from 35% to 135% of the average wild-type values (in Figure 1E1, note the large standard deviation; see Figure 14 for individual values). Mutants were categorized as either mild or severe at the onset of muscle degeneration (2 dpf) with mild *dmd* mutants having a mean gray value of ≥ 86% of wild-type birefringence and severe *dmd* mutants having a mean gray value of ≤ 85.99%. Although mild and severe mutants had indistinguishable muscle degeneration at 8 dpf (Figure 1E1), they took different paths to get there. Mild *dmd* mutants had better muscle structure at 2 and 3dpf than severe mutants (compare Figure 1C2, red arrowheads point to a couple muscle segments with degeneration versus the near complete degeneration in severe mutants in Figure 1D1). This improved muscle structure was reflected in significantly higher mean gray values at 2 and 3 dpf compared to severe *dmd* mutants, but at 5 and 6 dpf, severe *dmd* mutants had significantly higher mean gray values. These data indicate that *dmd* mild mutants undergo extensive degeneration for the first three days after disease onset followed by a period of slight regeneration. In contrast, muscle in severe *dmd* mutants regenerated throughout the study. These data clearly indicate that there is phenotypic variation in the zebrafish *dmd* mutants and that this variation can be quantified with birefringence.

2.3.2 Longitudinal Studies Indicate that Muscle Function in *dmd* Mutants is Variable

The above birefringence data indicate that general muscle structure at 8 dpf was not significantly different in mild versus severe *dmd* mutants. However, the path to muscle structure at 8 dpf differed between mild and severe mutants with mild mutants undergoing degeneration/slight regeneration and severe mutants regenerating. We thus asked whether muscle function, as assayed by swimming activity, was different in mild versus severe mutants. We analyzed motility with DanioVision and found that mild mutants swam a significantly greater

distance with significantly faster velocity than severe mutants at 3 and 5 dpf (Figure 15). Surprisingly, even though birefringence was similar between mild and severe mutants at 8 dpf, swimming activity remained significantly higher in mild *dmd* mutants at this time (Figure 1F). These results suggest that muscle structure early in development (2 dpf) correlates with function throughout development (8 dpf). Additionally, these data suggest that improving muscle structure may not coincide with improving function.

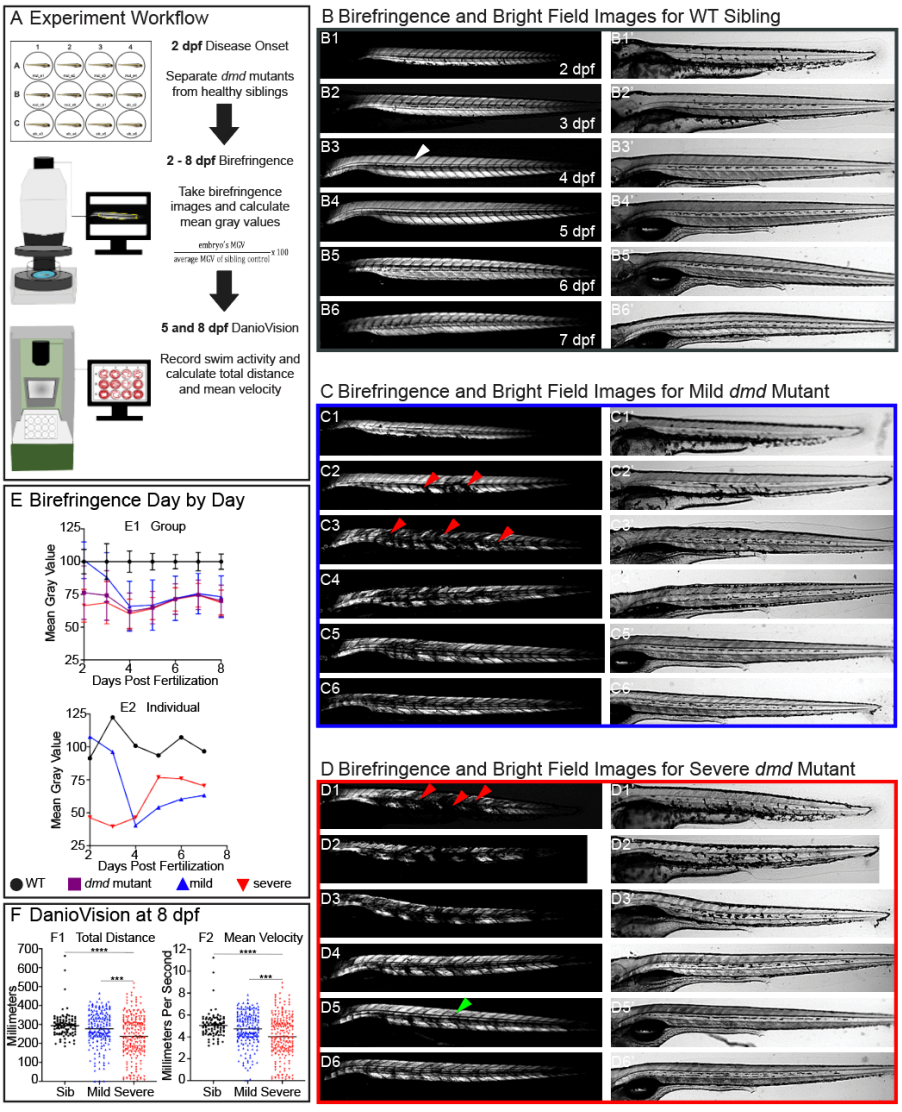

Figure 1: Variation in the *dmd* mutant phenotype determines disease progression.

(A) We created an experiment workflow to assess disease progression from 2 to 8 dpf. At 2 dpf, birefringence is used to separate *dmd* mutants from WT siblings. Zebrafish are placed in

individual wells of a 12-well plate and assigned a number, which is used to track individual zebrafish for the duration of the experiment. Each day, from 2 dpf to 8 dpf, birefringence images are taken. Birefringence (white) reflects normally organized muscle tissue. Loss of birefringence (grey to black) reflects areas of degeneration and myotomes with detached muscle fibers. Mean gray value is used to quantify birefringence and is presented as a percentage of WT sibling controls. Following birefringence imaging at 8 dpf, swimming activity is recorded using DanioVision. Total distance and mean velocity is calculated during the active (dark) periods. (B - D) Anterior left, dorsal top, side mounted. (B) Birefringence and bright field images of a WT sibling from 2 to 7 dpf. (C - D) At disease onset, zebrafish exhibit two levels of severity. (C) Birefringence and bright field images for a mild *dmd* mutant. Mild *dmd* mutants have mean gray values greater than 86% of WT siblings at 2 dpf. (D) Birefringence and bright field images for a severe *dmd* mutant. Severe *dmd* mutants have mean gray values less than 85.99% of WT siblings at 2 dpf. (E) Mild and severe *dmd* mutants exhibit variation in disease progression. (E1) Average mean gray values for WT siblings (black circles) do not change across time, remaining at 100%. However, mild *dmd* mutants (blue upward facing triangles) undergo extensive degeneration for the first three days followed by a period of slight regeneration. Conversely, severe *dmd* mutants (red downward facing triangles) regenerate throughout the study. (E2) Individual mean gray values for zebrafish presented in B - D highlight the vast degeneration that mild *dmd* mutants experience compared to the regeneration that occurs in severe *dmd* mutants. (F) Swimming activity is significantly different in mild versus severe *dmd* mutants. Total distance (F1) and mean velocity (F2) are significantly lower in severe *dmd* mutants compared to mild *dmd* mutants and WT siblings at 8 dpf. Each data point represents a single time point for an individual zebrafish. Each zebrafish has a total of 15 points. DanioVision data were analyzed using an ordinary one-way ANOVA with Tukey's multiple comparisons test. *** $p < 0.001$, **** $p < 0.0001$.

2.4 Perspective

The clinical presentation of muscular dystrophies is frequently variable: ranging from severe, congenital muscle weakness to mild, adult-onset limb girdle muscular dystrophies. Similarly, variability across individuals with the same disease-causing allele is common. This variability likely keeps clinicians from accurately informing patients as to how their disease will progress and/or respond to therapies. One roadblock to understanding the phenotypic spectrum of muscular dystrophies is that the basic biological mechanisms of variability in musculoskeletal development and disease are not well understood. This is especially true for DMD, which is one of the most studied types of muscular dystrophies, but still has no cure. The development of effective disease-modifying therapies that withstand the critical evaluation and exhaustive testing at the pre-clinical and clinical levels proves difficult. These difficulties likely arise from variation in disease severity, which is often not addressed in preliminary drug-screening studies due to the failure of identifying variation in these animal models. Additionally, due to the variation in both severity and disease progression in *dmd* mutants, it is possible that gene expression profiles may be different at these different stages, which could impact response to treatment. A preliminary study to unveil potential mechanisms for variation is addressed in Chapter 6.

Recognizing that there are differences in muscle homeostasis between mild and severe *dmd* mutants, we chose to conduct future studies identically so that variables such as treatment duration, disease stage at time of treatment, and disease stage at time of evaluation do not change. We also chose to examine mild and severe *dmd* mutants separately to identify that observed changes are occurring simultaneously in both phenotypes. Further, the above study demonstrates that changes in muscle structure, whether beneficial or detrimental, are not always reflected in muscle function. That is, muscle regeneration may be evident but these regenerating fibers may not improve muscle function, which was observed in severe *dmd* mutants. Conversely, muscle degeneration may be evident but these degenerating fibers may

not worsen muscle function, which is evident in mild *dmd* mutants. Therefore, it is critical that our future studies addressed muscle health using a combinatorial approach rather than focusing on demonstrating improvements/detriments in structure versus function.

CHAPTER 3

IMPACT OF INACTIVITY IN *DMD* MUTANT ZEBRAFISH

3.1 Relevant Background

In healthy individuals, prolonged inactivity stimulates muscle atrophy and hinders multiple components of overall health, especially muscular strength and endurance. Limitations in muscular strength and endurance lead to further inactivity, which leads to heightened muscle wasting and larger reductions in muscle strength and endurance. Ultimately, diminished muscle strength and endurance lead to persistent inactivity. However, even though muscle wasting and weakness are hallmarks of DMD, the impacts of inactivity on DMD disease progression are not entirely known. Of the three studies looking at the immediate effects of inactivity in mdx mice, meaning that the limb was immobilized until analyses began, two studies suggest that inactivity may prevent muscle damage that occurs as result of the absence of dystrophin [73,75], while the third study suggests that inactivity may increase susceptibility to this same damage [351]. No study to our knowledge examines how a prolonged period of inactivity, however this may be defined, followed by the resumption of normal activity affects disease progression in dystrophin-deficient muscle. As individuals with DMD are being advised to refrain from activities beyond that of their daily living, it is possible that they may be entering the vicious cycle of muscle wasting and weakness seen in inactive, healthy individuals. The goal of this chapter is to evaluate the longitudinal effects of two inactivity paradigms on neuromuscular plasticity in *dmd* mutants.

3.2 Experiment Overview

For intermittent inactivity, zebrafish were placed in a low dose of tricaine (MS-222; 306 μM in 1X ERM) overnight for 12 hours each day for three days beginning at disease onset (2, 3, and 4 dpf) (Figure 2A1). The total time that zebrafish were inactive was 36 hours. For extended inactivity, zebrafish were placed in the same dose of tricaine for 72 hours beginning at disease

onset (2, 3, and 4 dpf), and were removed from tricaine at the start of 5 dpf (Figure 2B1). Birefringence images were taken at disease onset, immediately prior to removal from tricaine at 5 dpf, and three days following removal at 8 dpf. DanioVision was used to evaluate swim function in response to intermittent or extended inactivity, and was performed 4 hours and 3 days following removal from tricaine (5 and 8 dpf, respectively). Following DanioVision, zebrafish were either fixed for further analyses of muscle health via immunostaining or followed daily for survival. Throughout the experiment, zebrafish were single-housed in individual wells of a 12-well plate with 3 mL of 1X ERM (or 3 mL of tricaine solution). A more detailed description of these methods is found in Appendix B.2 and B.3.

3.3 Results

3.3.1 Intermittent Inactivity Negatively Impacts Swimming Activity but no Effect on Structure or Survival

Birefringence was used as a metric to assess changes in muscle structure across time. Inactive *dmd* mutants exhibit lower mean gray values beginning at 4 dpf compared to control *dmd* mutants but follow similar trend of regeneration from 5 to 8 dpf (Figure 2A4). We chose to look specifically at the change in mean gray value from 5 to 8 dpf as a measure of recovery from inactivity. These data indicate that three intermittent periods of inactivity did not affect muscle structure (Figure 2A6). We fixed and stained *dmd* mutants with phalloidin at the end of the experiment (8 dpf) to determine whether there were any dramatic changes in muscle fiber structure, specifically the percent of muscle segments with detachments. These analyses also indicated that intermittent inactivity did not have major effects on muscle fiber organization (data not shown). Interestingly, however, *dmd* mutants subjected to intermittent inactivity swam more slowly and covered less distance at 8 dpf (Figure 2A8 and A9). These data indicate that early intermittent inactivity can have negative impacts on swimming activity later in development. However, survival was not negatively impacted (Figure 2A10).

3.3.2 Extended Inactivity Improves Swimming but Decreases Muscle Structure and Lifespan

In contrast to intermittent inactivity, extended inactivity from 2 dpf through the morning of 5 dpf had deleterious impacts later in development. Immobilized larvae initially show improved muscle structure at 5dpf (compare Fig. 2B3a to Fig. 2B2a, and Fig. 2B3b to Fig. 2B2b, quantification in Fig. 2B4). However, this improvement was short lived. Specifically, there was a significant decline in birefringence of inactive *dmd* mutants 3 days after removal from tricaine (compare Figure 2B3 5 dpf to 8 dpf, quantified in Figure 2B4). These data indicate that while muscle structure was preserved during the inactive period, it became more susceptible to damage upon reinstatement of normal activity, which is indicated by the significant decrease in mean gray value from 5 to 8 dpf (Figure 2B6) and poor muscle fiber organization (Fig. 2B7d, red arrowheads denote short disorganized muscle segments, red arrow points to a degenerating fiber). Surprisingly, even though muscle structure was improved upon removal from tricaine, inactive *dmd* mutants swam a significantly lower total distance and at a significantly slower mean velocity compared to control *dmd* mutants 4 hours after removal from tricaine (Figure 15). However, after three days of recovery in ERM, swim function in inactive *dmd* mutants was significantly improved, and *dmd* mutants that were inactive for three days swam a significantly higher total distance and at a significantly faster mean velocity compared to *dmd* mutant controls (Figure 2B8 and B9). Strikingly, this improved swim function did not correlate with survival: although extended inactivity increased swimming at 8 dpf, survival was negatively impacted in inactive *dmd* mutants (Figure 2B10). Thus, despite overall neutral effects on muscle structure at 8 dpf and improved swimming at 8 dpf, extended inactivity decreases lifespan.

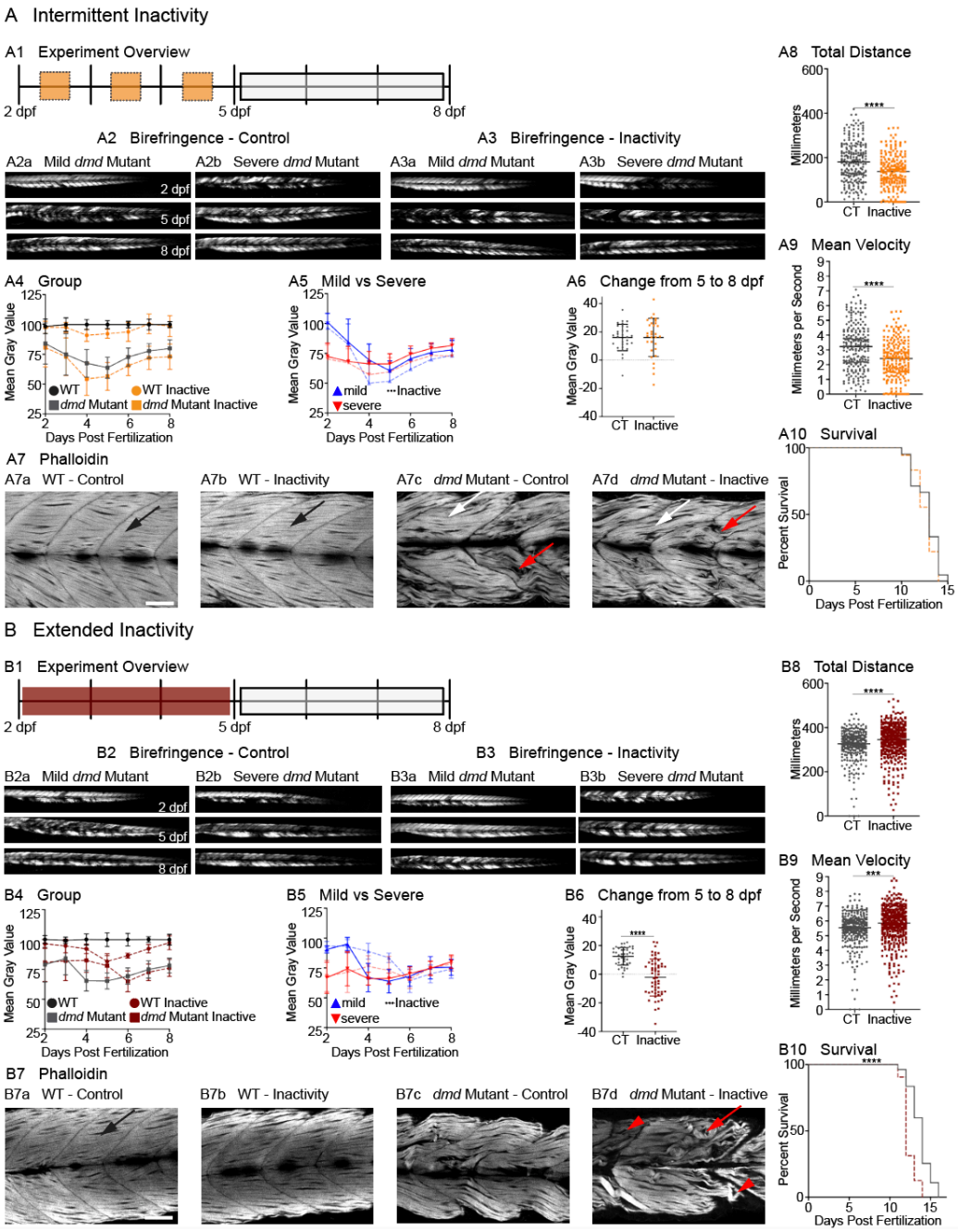

Figure 2: Inactivity in *dmd* mutants differentially affects muscle structure, function, and survival.

(A1) Experiment overview for intermittent inactivity. Zebrafish are housed in a low dose of tricaine for 12 hours overnight (orange boxes) at 2, 3, and 4 dpf. Upon removal from tricaine at 5 dpf, zebrafish are allowed to recover in ERM (white box) for the remainder of the experiment. (A2 - A3) Anterior left, dorsal top, side mounted. (A2) Birefringence images at 2, 5, and 8 dpf for

mild (A2a) and severe (A2b) *dmd* mutant controls housed in ERM. (A3) Birefringence images at 2, 5, and 8 dpf for mild (A3a) and severe (A3b) *dmd* mutants housed in tricaine for 12 hours overnight for 3 nights. (A4) Average mean gray values for WT sibling controls (black circles) remain consistent across time. However, WT siblings that were inactive (orange circles) experience a decrease in mean gray values at 4, 5 and 6 dpf, but recover to WT sibling control values by 8 dpf. Conversely, *dmd* mutants that were inactive (orange squares) experience a decrease in mean gray values compared to *dmd* mutant controls (gray squares) beginning at 4 dpf but do not recover to *dmd* control values at 8 dpf. (A5) Mild (blue upward facing triangles) and severe (red downward facing triangles) *dmd* mutants that were inactive (dashed lines) have lower mean gray values compared to their respective controls (solid lines) beginning at 4 dpf. Inactive mild *dmd* mutants experience a more dramatic decrease in mean gray values compared to mild control and inactive severe *dmd* mutants. (A6) Change in mean gray value from 5 to 8 dpf is not different in control versus inactive *dmd* mutants. (A7) Anterior left, dorsal top, side mounted. Scale bar is 50 micrometers. Phalloidin staining at 8 dpf suggests no change in muscle fiber structure following inactivity in *dmd* mutants (A7d) compared to *dmd* mutant controls (A7c). Total distance (A8) and mean velocity (A9) at 8 dpf are significantly lower in inactive *dmd* mutants compared to *dmd* mutant controls. Each data point represents a single time point for an individual zebrafish. Each zebrafish has a total of 15 points. (A10) Survival is not affected by intermittent inactivity. (B1) Experiment overview for extended inactivity. Zebrafish are housed in a low dose of tricaine (dark red box) for 72 hours beginning at 2 dpf. Upon removal from tricaine at 5 dpf, zebrafish recover in ERM (white box) for the remainder of the experiment. (B2) Birefringence images at 2, 5, and 8 dpf for mild (B2a) and severe (B2b) *dmd* mutant controls housed in ERM. (B3) Birefringence images at 2, 5, and 8 dpf for mild (B3a) and severe (B3b) *dmd* mutants housed in tricaine for 72 hours. (B4) Average mean gray values for WT sibling controls (black circles) remain consistent across time at 100%. However, WT siblings that were inactive (dark red circles) experience a dramatic decrease in mean gray value

beginning at 4 dpf and continuing through 7 dpf, but return to control values by 8 dpf. Conversely, *dmd* mutants that were inactive (dark red squares) have higher mean gray values at 4 and 5 dpf compared to *dmd* mutant controls (gray squares). However, upon return to ERM, inactive *dmd* mutants experience a decrease in mean gray values but regenerate to *dmd* mutant control values. (B5) Mild (blue upward facing triangles) and severe (red downward facing triangles) *dmd* mutants that were inactive (dashed lines) have higher mean gray values compared to control *dmd* mutants (solid lines) at 4 and 5 dpf. Inactive mild *dmd* mutants experience a more dramatic decrease in mean gray values compared to inactive severe *dmd* mutants at 6 dpf. (B6) Change in mean gray value from 5 to 8 dpf is significantly lower in inactive versus control *dmd* mutants. (B7) Anterior left, dorsal top, side mounted. Scale bar is 50 micrometers. Phalloidin staining at 8 dpf suggests that inactivity negatively affects muscle structure in *dmd* mutants (B7d) compared to *dmd* mutant controls (B7c). Total distance (B8) and mean velocity (B9) at 8 dpf are significantly higher in inactive *dmd* mutants compared to *dmd* mutant controls. Each data point represents a single time point for an individual zebrafish. Each zebrafish has a total of 15 points. (B10) Survival is negatively affected by extended inactivity. Birefringence and DanioVision data were analyzed using two-sided t tests. Survival data were analyzed using a Mantel-Cox test. *** $p < 0.001$, **** $p < 0.0001$.

3.3.3 Extended Inactivity Diminishes *dmd* Muscle Resilience to Neuromuscular Electrical Stimulation

The above data confirm previous data that inactivity improves muscle structure in *dmd* mutants while they remain inactive [377]. However, our data show that this beneficial effect does not perdure. These results raise the question of why the seemingly improved muscle structure is not stable and immediately affects muscle function upon reinstatement of normal activity at 5 dpf. To answer this question we turned to NMES, which was previously adapted for use in zebrafish larvae [391]. NMES uses trains of electrical pulses to evoke muscle

contractions and thus allows comparison of muscle structure in multiple larvae subjected to the same stimulus. Specifically, NMES would allow us to determine whether extended inactivity (1) obscured latent defects in muscle resilience because the muscle was not being used and thus did not degenerate, or (2) improved muscle fiber resilience but the resilience was not maintained for the next few days. In order to distinguish between these possibilities, we asked whether inactive larvae were uniquely susceptible to activity (NMES) immediately upon removal from tricaine.

For this experiment, *dmd* mutants were placed in tricaine for three days. In the morning of 5 dpf, a birefringence image was taken as a baseline measure of muscle structure (see Figure 3A). Next, larvae were subjected to a session of NMES using one of two stimulation paradigms. These stimulation paradigms were defined as high frequency, low voltage (NMES Paradigm 1), which requires the muscle to contract continuously but very subtly, or low frequency, high voltage (NMES Paradigm 2), which requires the muscle to contract more forcefully but less frequently. Birefringence images were taken immediately following this NMES session. A detailed description of how NMES was performed is provided in Appendix B.5. Finally, larvae resumed normal activity in 1X ERM for three days similar to the above experiment. At the end of this recovery period (8 dpf), birefringence images were taken and zebrafish were fixed for further structural analyses (see Figure 3A for experiment overview). Control *dmd* mutants, which were removed from tricaine and allowed to swim while experimental larvae were receiving NMES, sometimes showed increased degeneration just after swimming (Fig. 3B2b after) compared to immediately prior to removal from tricaine (Fig. 3B2a before). However, at a population level although there was a slight trend that inactive larvae showed more damage, there was not a significant increase in degeneration (Fig. 3B3). In contrast, both NMES paradigms significantly worsened mean gray values immediately after stimulation (Fig. 3C2, D2, yellow arrows denote new areas of degeneration after NMES, Fig. C3

and D3). Larvae that underwent three days of inactivity were unable to recover from this single session of NMES (Figure), and exhibited more fiber detachments, especially following NMES Paradigm 2 (Figure 3H2). More importantly, though, *dmd* mutants that underwent three days of inactivity were unable to recover from this single session of NMES. Specifically, *dmd* mutants exhibited a negative change in mean gray value from the birefringence measurement after NMES to three days following NMES, indicating extensive muscle deterioration (data not shown). Further, these larvae exhibited more fiber detachments especially following NMES Paradigm 2 (Figure 3H2). Therefore, these data suggest that inactivity for an extended period of time may cause *dmd* muscle to become more susceptible to contraction-induced injury.

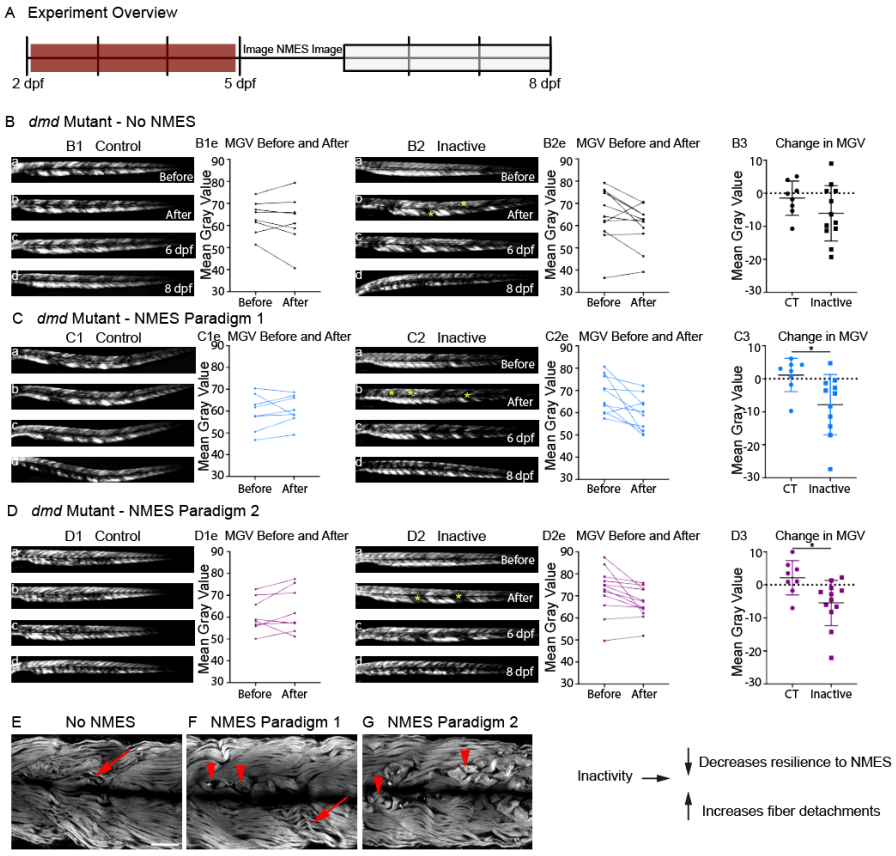

Figure 3: Extended inactivity increases susceptibility to injury in *dmd* mutants.

(A) Experiment overview. Zebrafish are housed in a low dose of tricaine for 72 hours (dark red box) beginning at 2 dpf. At 5 dpf, zebrafish receive a single session of NMES (either Paradigm 1

or Paradigm 2) and are then allowed to recover in ERM (white box) for the remainder of the experiment. (B, C, D) Anterior left, dorsal top, side mounted birefringence images. (B1) Birefringence for the first (a) and second (b) imaging session, and at 6 (c) and 8 (d) dpf for a *dmd* mutant control that did not receive NMES. (B1e) Individual mean gray values for *dmd* mutant controls for the first and second imaging session. (B2) Birefringence for the first (a) and second (b) imaging session, and at 6 (c) and 8 (d) dpf for an inactive *dmd* mutant that did not receive NMES. (B2e) Individual mean gray values for inactive *dmd* mutants for the first and second imaging sessions. (B3) Change in mean gray values between the first and second imaging session are lower in the inactive *dmd* mutants, indicating that upon removal from tricaine, muscle immediately begins degenerating. (C1) Birefringence before (a) and after (b) NMES Paradigm 1, and at 6 (c) and 8 (d) dpf for a *dmd* mutant control. (C1e) Individual mean gray values for *dmd* mutant controls before and after NMES Paradigm 1. (C2) Birefringence before (a) and after (b) NMES Paradigm 1, and at 6 (c) and 8 (d) dpf for an inactive *dmd* mutant. (C2e) Individual mean gray values for inactive *dmd* mutants before and after NMES Paradigm 1. (C3) Change in mean gray values before versus after NMES Paradigm 1 are significantly lower in inactive *dmd* mutants, indicating *dmd* muscle fibers are less resilient following extended inactivity. (D1) Birefringence before (a) and after (b) NMES Paradigm 2, and at 6 (c) and 8 (d) dpf for a *dmd* mutant control. (D1e) Individual mean gray values for *dmd* mutant controls before and after stimulation. (D2) Birefringence before (a) and after (b) NMES Paradigm 2, and at 6 (c) and 8 (d) dpf for an inactive *dmd* mutant. (D2e) Individual mean gray values for inactive *dmd* mutants before and after NMES Paradigm 2. (D3) Change in mean gray values before versus after NMES Paradigm 2 are significantly lower in inactive *dmd* mutants, further indicating that muscle fibers are less resilient after inactivity. (E-G) Anterior left, dorsal top, side mounted phalloidin staining. Scale bar is 50 micrometers. A single session of NMES Paradigm 1 negatively affects muscle structure in inactive *dmd* mutants (F) compared to inactive *dmd* mutants that did not receive stimulation (E). Similarly, a single session of NMES Paradigm 2

negatively affects muscle structure in inactive *dmd* mutants by increasing the number of visibly detached fibers (G) compared to inactive *dmd* mutant controls. Each data point represents a single zebrafish. Birefringence data were analyzed using two-sided t tests. * $p < 0.05$, ** $p < 0.01$.

3.4 Perspective

Step activity patterns from individuals with DMD indicate that activity levels are extremely low and infrequent in the years leading up to wheelchair dependency. This loss in activity is addressed as a clear consequence of muscle wasting in the absence of dystrophin. Based on the above data, it is critical that the consequences of prolonged reductions in activity are evaluated in human patients, especially in the realm of muscle resilience. This is especially a major concern for those individuals who participate in physical therapy or aquatic therapy programs on non-consecutive days throughout the week or sporadically throughout the month, where there may be large periods of reduced activity followed by a short, more intense session of activity.

In terms of neuromuscular plasticity in diseased muscle, these studies suggest that dmd muscle exhibits a more delicate, intricate equilibrium with more factors at play compared to healthy muscle. In healthy muscle we see improvements in structure correspond with improvements in function and these functional improvements prolong survival. Similarly, the consequences of muscle structure breakdown are decreases in function and reduced survival. Therefore, neuromuscular plasticity is linear and the consequences of change are easily predicted. However, based on the above data, neuromuscular plasticity in dmd muscle is not linear. That is, muscle structure does not predict function and function does not predict survival. There are more factors at play, and we need to identify these factors in order to better understand disease progression and elucidate mechanistic pathways that target improvements in structure, function, and survival. To begin to elucidate these mechanisms, it is important to ask what are the underlying mechanisms protecting (or preserving) muscle structure in dmd

muscle during extended inactivity but simultaneously breaking down muscle in healthy wild-type siblings? What mechanisms occur immediately upon return to ERM and normal activity, and how do these influence improvements in structure but reduced function? A more in-depth discussion of these questions is provided in Chapter 6 as inactivity and activity are discussed together.

CHAPTER 4

NMES AS A MODEL OF NEUROMUSCULAR PLASTICITY IN DMD MUTANT ZEBRAFISH

4.1 Relevant Background

Knowing that extended inactivity negatively impacts muscle health and survival in *dmd* mutants, we next asked whether there is there a better recommendation for care as researchers continue searching for a cure. Resistance training is an excellent approach to combatting muscle wasting and weakness in healthy individuals. Using zebrafish larvae as a model for lifting weights is not feasible, so we asked whether we could use NMES as an alternate means to stimulate muscle activity and combat muscle wasting and weakness in *dmd* mutants.

Numerous studies have demonstrated that skeletal muscle fibers are highly influenced by the activity pattern imposed upon them, whether via the innervating neuron or electrical stimulation [392]. Neuronal activity plays a vital role in determining both the biochemical and physiological characteristics of individual skeletal muscles and their muscle fibers [393]. NMES was introduced in the clinical setting to maintain and preserve neuromuscular function during disuse or the aging process, to restore neuromuscular function after disuse, or to enhance neuromuscular function in able-bodied individuals, especially athletes [394–409]. NMES delivers a series of waveforms of electrical current that is characterized by frequency, amplitude, and pulse width (or pulse duration) [410]. Frequency defines the rate at which the pulses are delivered and determines the pattern of temporal summation [410]. Both amplitude and pulse width describe how much voltage (or current) and for how long the pulse is being delivered and determines the number of muscle fibers that are activated [410]. These three parameters dictate the strength of the muscle contraction and the amount of force that is generated. Specifically, by increasing the pulse duration or the amplitude, the amount of muscle force generated will be greater [410]. The main advantage of NMES is its ability to activate muscle fibers, regardless of their type, without requiring high-effort voluntary force generation [403,411].

4.1.1 NMES in DMD

Guilluame Benjamin Amand Duchenne, the French neurologist who first described DMD, suggested NMES as a potential therapy for dystrophic muscle [412]. Immature muscle [413] and prolonged contraction and relaxation times [413–416] are characteristic features observed in individuals with DMD. Therefore, it was proposed that super-imposing slow frequency electrical stimulation on the muscles would initiate maturation of existing muscle fibers and support newly regenerated muscle fibers [417,418], and ultimately delay disease severity and progression. However, only a few studies have examined the impact of NMES on muscle strength and function in both humans and the mouse model of DMD.

In 14 boys with DMD, ages 5 to 12 years old, the TA muscle was stimulated (contralateral leg served as control) at 5 to 8 Hz continuously or intermittently (1.5 seconds on, 1.5 seconds off) for 1 hour each session with 3 sessions per day for 7 to 11 weeks [309]. Following the stimulation period, older boys exhibited no significant change in maximum voluntary contraction, but younger boys showed a mean increase of 47%. Notably, the stimulated muscles in the younger children were significantly stronger one month after stimulation was stopped. However, during a 6 month follow up, significant declines in physical characteristics and functional ability were evident. The authors conclude that DMD muscles respond positively to electrical stimulation if it is applied early in the disease. In a follow up study, Scott and colleagues (1990) [393] investigated the long-term effects of electrical stimulation on the quadriceps femoris muscle. Fifteen boys with DMD, ages 2 to 13 years old, received 3 hours of electrical stimulation 6 days per week for 7 to 11 weeks. After 10 weeks of stimulation, stimulated muscles exhibited a small but significant increase in overall strength but no functional improvements were observed. When stimulation was applied to the TA muscles intermittently (6 seconds on, 6 seconds off) for 1 hour twice a day with a frequency of 8 Hz in 7 boys with DMD and 2 boys with BMD between the ages of 6 and 10 years old, 4 participants exhibited no significant changes after 3 months and stopped the program while 5 participants

exhibited favorable changes and continued the program for 9 months [419]. These favorable changes included greater torque measurements of the stimulated muscles. The author concludes that electrical stimulation cannot prevent muscle degeneration but may slow its progression. In a follow-up study, similar results were found, including an average increase in torque of 17.1% on the stimulated leg and a decrease of 3.4% on the non-stimulated leg. Interestingly, the largest benefits were observed in the youngest participants [420].

Similarly, in the mdx model, NMES may exert beneficial effects on stimulated muscles. In mdx mice, ages 3 to 5 months, electrical stimulation was applied through implanted electrodes on either side of the lateral popliteal nerve of the hindlimb at 10 Hz for 30 minutes, 6 times per day for 9 and 28 days. Stimulation visibly improved ankle dorsiflexion and gait [421]. These improvements were accompanied by higher maximum tension development in the stimulated TA and EDL muscles, an increase in the number of muscle fibers in the stimulated EDL muscles, and an increase in the intensity of SDH staining in the stimulated muscles [421]. Vrbova & Ward (1981) [422] applied the same methods and found similar improvements in tension development of the TA muscles and increased fatigue resistance in the EDL muscles. However, the authors noticed that these functional improvements were only observed in severely affected muscles [422], contradicting what was observed in humans. More importantly, in a study examining the short- and long-term effects of electrical stimulation, these positive benefits disappeared once the NMES program ended. Specifically, four weeks after the completion of electrical stimulation, the maximum force generated by TA muscles was similar to the initial forces generated by the muscles of the contralateral side, indicating that any force output that was gained during the program was no longer present [423]. However, this was not observed in the EDL muscles for these muscles displayed significantly greater force compared to the unstimulated, contralateral side [423], suggesting that muscles may respond differently to stimulation. Ultimately, the mechanisms by which electrical stimulation may benefit dystrophic muscle are unknown, but authors suggest that it may slow degeneration of the existing muscle

fibers, support the growth of regenerating fibers, and develop and maintain characteristics of the slow fiber phenotype.

Given these beneficial effects observed in humans and mdx mice, we asked whether NMES could benefit muscle in *dmd* mutants, especially in comparison to inactivity. There are four types of strength training – endurance, hypertrophy, strength and power – and each are designed to elicit specific responses in the muscle by altering the number of repetitions performed and the load, or resistance, used. We designed four unique NMES paradigms ranging from high frequency/low voltage pulse trains to lower frequency/higher voltage pulse trains (Figure 4C and D). To easily differentiate these paradigms from each other, and because they were conceptually based on strength training paradigms, we named these paradigms endurance-NMES (eNMES), hypertrophy-NMES (hNMES), strength-NMES (sNMES), and power-NMES (pNMES). The goal for this chapter is to understand how dystrophic muscle responds to these four NMES paradigms at the structural and functional levels.

4.2 Experiment Overview

To assess the impact of each NMES program without introducing confounding variables, we created a training program, similar to the experimental workflow used to study the impact of inactivity on dmd muscle. Specifically, this training program was divided into two periods: the training period and the recovery period (Figure 5A). During the training period zebrafish completed three sessions of NMES, each session lasting one minute, on three consecutive days (2, 3, and 4 dpf). Following these three training days, zebrafish entered the recovery period (5, 6, 7 and 8 dpf). A complete protocol for how NMES was performed is provided in Appendix B.5. Throughout the training program, birefringence was used to assess muscle structure while DanioVision was used to measure swim function. Terminal outcome measures were performed at the conclusion of the recovery period, including various immunostaining to look at components of muscle health. The recovery period was also extended to track survival. Therefore, only the NMES paradigms changed during these studies.

4.3 Results

4.3.1 NMES Does Not Result in Immediate Damage to the Sarcolemma

Our first question was whether these four NMES paradigms elicit unique tail bend patterns that vary in how many times the tail bends as well as how hard it bends. As would be expected, eNMES with high frequency/low voltage pulse trains elicited a fast but subtle tail beat. Conversely, with pNMES, the tail beat infrequently but bent to a much greater degree. Next, we next asked if our NMES paradigms result in dramatic damage to the sarcolemma. As mentioned previously, one of the major reasons why strength training is not recommended for individuals with DMD is due to the fragility of the sarcolemma and its susceptibility to contraction-induced damage. We did this by asking whether increased Evans Blue Dye (EBD) was observed in muscle after one session of NMES. EBD is a membrane impermeable dye commonly used for examining sarcolemmal damage in skeletal muscle fibers. If the sarcolemma is damaged during NMES, it will become permeable to EBD and its accumulation can be easily quantified. At 2 dpf, EBD was injected into the peri-cardial space at disease onset and allowed to circulate for 4 hours (protocol in Appendix B.4). Then, images of EBD in the zebrafish musculature were taken immediately prior to and after one session of NMES (Figure 4A). Birefringence and EBD images of the same embryos before and after NMES are shown in Figure 4. The yellow stars denote the same position in the embryo before and after stimulation. Mean gray values were calculated to determine the amount of EBD entry into the muscle fibers. Both wild-type and *dmd* mutant control larvae are similar when imaged prior to and after the experimental larvae received NMES (Figure 4E, F, K1, and K2). None of the NMES paradigms consistently caused a dramatic change in either birefringence (data not shown) or EBD infiltration after one session (Figure 4G-K). These results indicate that the four NMES paradigms do not cause immediate dramatic damage to the sarcolemma.

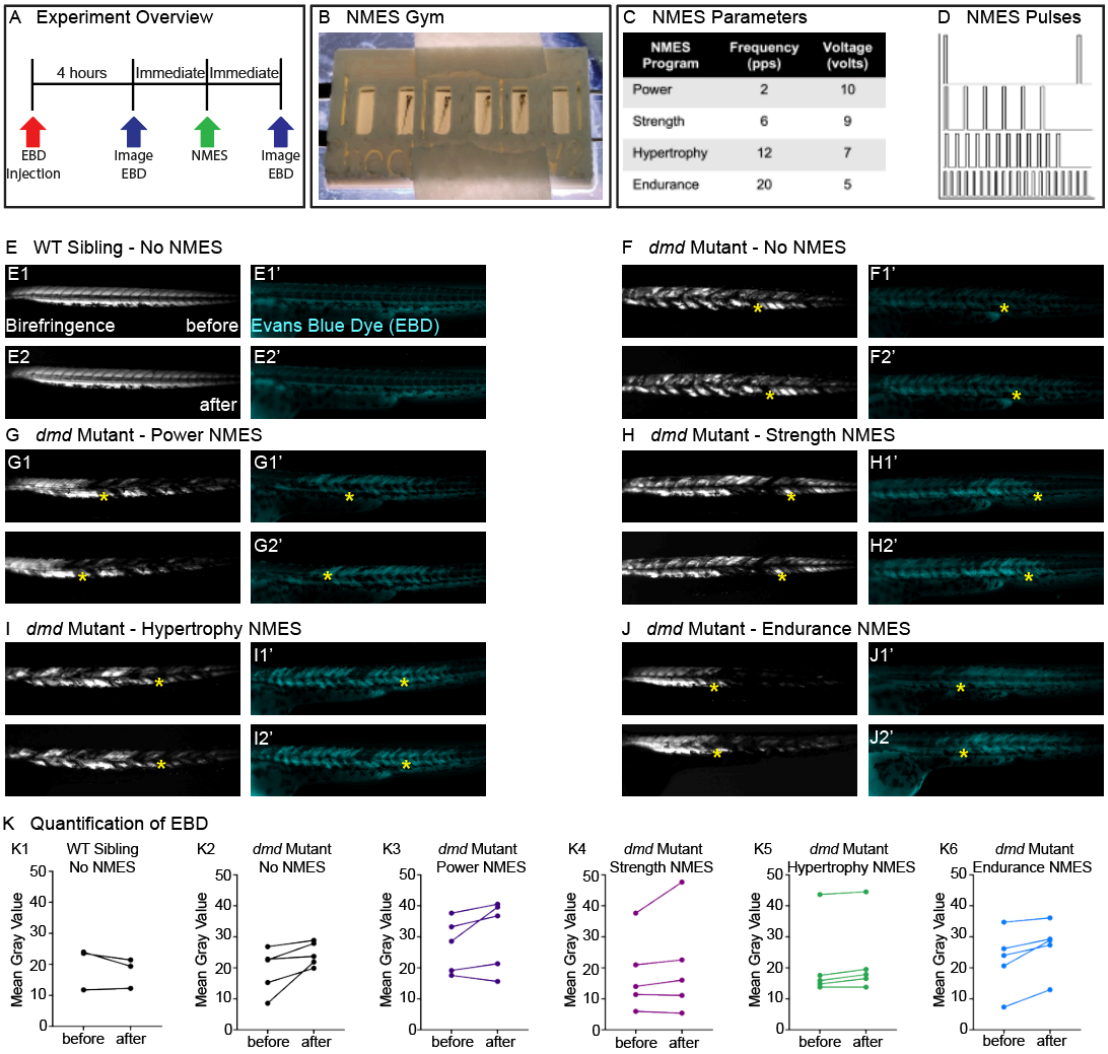

Figure 4: Four NMES paradigms do not result in immediate damage to the sarcolemma.

(A) Experiment overview. At 2 dpf, WT siblings and *dmd* mutants were injected with EBD. Four hours later, zebrafish were imaged for birefringence and EBD before and after a single session of NMES. (B) For NMES, zebrafish are placed in a 3D printed gym with their heads towards the positive electrode and tails towards the negative electrode. (C - D) NMES delivers a series of square wave pulses that vary in frequency and voltage. We named these paradigms after weightlifting regimes. (E-J) Anterior left, dorsal top, side mounted birefringence and EBD fluorescent images. Yellow asterisks denote the same position in embryos before and after NMES. (E) WT sibling control exhibits healthy muscle segments (E1, E2) and no dye entry in the muscle (E1', E2') during the first and second imaging session. (F) *dmd* mutant control has

significant areas of degenerated muscle (F1) and dye entry (F1') but no new areas of degeneration or dye entry during the second imaging session (F2, F2'). (G-J) Similar to the *dmd* mutant control, *dmd* mutants that receive NMES have significant areas of degenerated muscle and dye entry prior to NMES but no new areas of degeneration or dye entry during following NMES. (K) Quantification of EBD during the first and second imaging session.

4.3.2 Different NMES Differentially Impacts *dmd* Muscle Structure, Function, and Survival

During our initial assessment of each NMES paradigm, we took birefringence images of each zebrafish prior to the first NMES session at 2 dpf, 24 hours after the third NMES session at 5 dpf, and four days after this third session at 8 dpf, and calculated mean gray value to assess the extent of degeneration/regeneration. As was done for inactivity, we focused on the change in mean gray value from 5 to 8 dpf because that change represents how the muscle responds to and recovers from 3 sessions of NMES. Wild-type larvae with all 4 NMES paradigms were unaffected (Figure 5B1, C1, D1, E1 and data not shown). Control *dmd* larvae for each NMES paradigm were similar to larvae shown in Figure 1, with mild larvae degenerating between 2 and 5 dpf (Fig. 5B2,C2,D2,E2, red arrowheads denote degeneration from the previous time point, green arrowheads denote regeneration from the previous time point) and severe larvae regenerating between 2 and 5 dpf (Fig. 5 B3,C3,D3,E3). Between 5 and 8 dpf, as shown in Figure 1, birefringence levels for both mild and severe larvae trend towards slight improvement (Fig. 5B6, C6, D6, E6). The eNMES and pNMES paradigms improved muscle structure in *dmd* mutants. pNMES resulted in a slight but significant increase in birefringence compared to controls (Fig. 5B6, note also green arrows in Fig. 5B4 and 5B5). eNMES also increased regeneration between 5 and 8 dpf (Fig. 5E6, note green arrows in Fig. 5E4, E5). In contrast, *dmd* mutants that underwent sNMES exhibited significantly lower changes in mean gray values compared to control *dmd* mutants (Figure 5C6) while hNMES trended towards lowering birefringence (Figure 5D6). These data indicate that, at least at a gross level, different NMES

paradigms do have different effects on muscle structure in zebrafish larvae. To further look at the extent of deterioration in our NMES groups, we calculated the percentage of fish that deproved, meaning the fish exhibited a negative change in birefringence from 5 to 8 dpf (Figure 16). These data further indicate that the percent of *dmd* mutants in the endurance and power NMES groups deteriorating between 5 and 8 dpf is much lower than that of control *dmd* mutants. Conversely, sNMES and inactivity have higher percentages of *dmd* mutants that deprove and undergo muscle deterioration during this 5 to 8 dpf period.

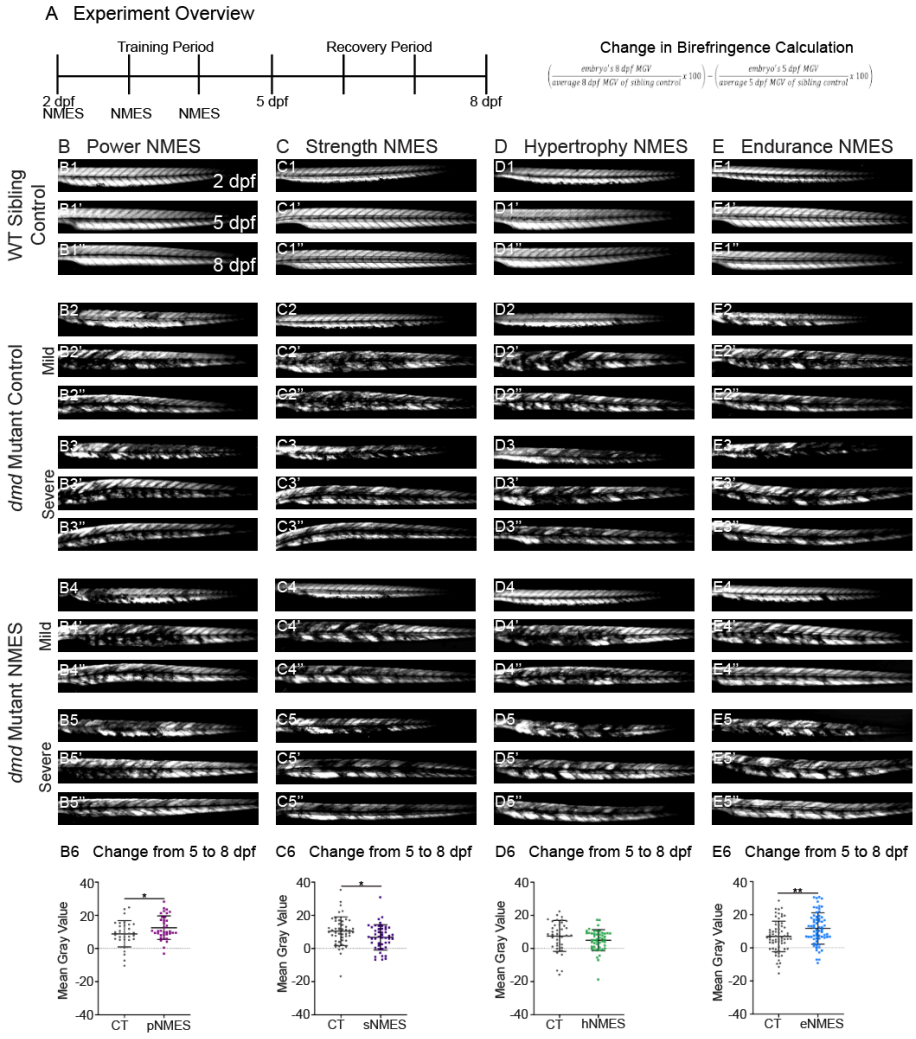

Figure 5: Birefringence is used as an initial measure of muscle structure following NMES. (A) Experiment overview and calculation of change in mean gray value from 5 to 8 dpf. At 2 dpf, birefringence images are taken followed by the first session of NMES. At 3 and 4 dpf, zebrafish

undergo the second and third sessions of NMES, respectively. Birefringence images are taken at 5 and 8 dpf. The training program is divided into the training period (2 to 4 dpf) and the recovery period (5 to 8 dpf). (B - E) Anterior left, dorsal top, side mounted birefringence images for WT sibling controls (B1 - E1), mild (B2 - E2) and severe (B3 - E3) *dmd* mutant controls, and mild and severe *dmd* mutants that received pNMES (B4 and B5), sNMES (C4 and C5), hNMES (D4 and D5), or eNMES (E4 and E5). (B6, C6, D6, and E6) Change in mean gray values from 5 dpf to 8 dpf represent how the muscle responds to and recovers from 3 sessions of NMES. Positive changes indicate improvements in muscle structure while negative changes indicate deterioration in muscle structure. Red arrowheads denote degeneration from the previous point, green arrowheads denote regeneration from the previous time point. Power (B6, maroon squares) and endurance (E6, blue squares) NMES significantly improve muscle structure in *dmd* mutants compared to *dmd* mutant controls (gray circles). Strength (C6, purple squares) NMES significantly worsens muscle structure in *dmd* mutants while hypertrophy NMES (D6, green squares) trends to decrease muscle structure compared to *dmd* mutant controls. Each data point represents a single zebrafish. Birefringence data were analyzed using two-sided t tests. * < 0.05, ** p < 0.01.

To gain a better understanding of the impacts of NMES on muscle structure, we stained zebrafish for phalloidin, which binds to f actin, allowing individual muscle fibers to be visualized. Muscle fibers in WT zebrafish are highly organized and linear (Figure 6A). In contrast, many fibers in *dmd* mutants are disorganized while others are compressed and/or detached from their extracellular matrix (Figure 6B). We quantified the percentage of muscle segments with fiber detachments and found that, similar to the results observed with birefringence, eNMES and pNMES resulted in fewer fiber detachments compared to control *dmd* mutants (Figure 6C2 and F2). Taken together, the above data indicate that eNMES and pNMES improve muscle structure in *dmd* larvae.

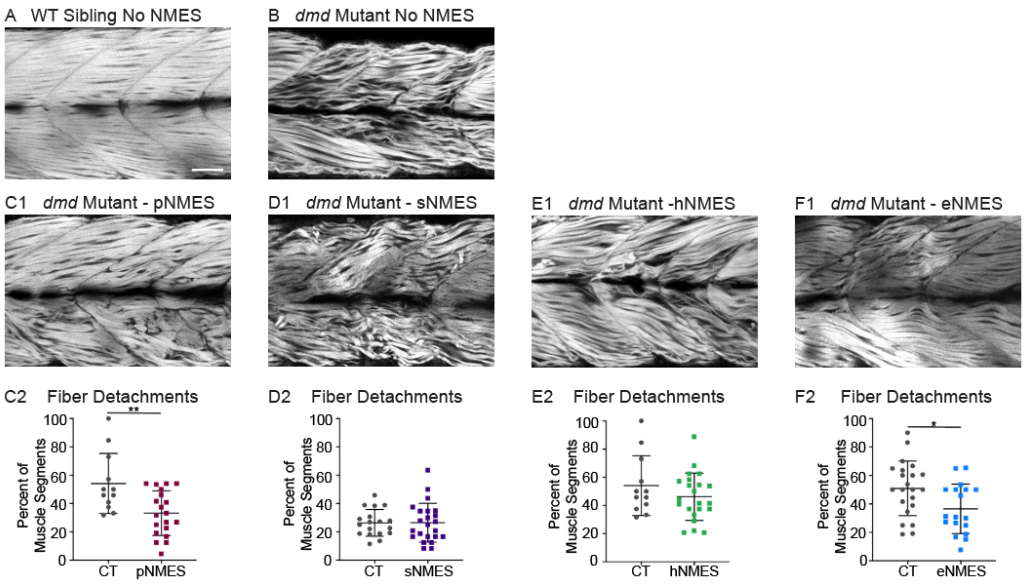

Figure 6: Phalloidin staining provides more details on how *dmd* muscle responds to NMES at the structural level.

Phalloidin staining for F-actin at 8 dpf allows for visualization of individual muscle fibers and the ability to count detached fibers in *dmd* mutants. Anterior left, dorsal top, side mounted. Scale bar is 50 micrometers. (A) Representative image of WT sibling demonstrates organized muscle fibers with well-defined myotome boundaries. (B) Representative image of *dmd* mutants demonstrates disorganized, wavy muscle fibers with poorly defined myotome boundaries and empty space between individual muscle fibers. (C1) Representative image of *dmd* mutant that received pNMES demonstrates less muscle fiber waviness, lack of empty space between muscle fibers but visible detached fibers. (D1) Representative image of *dmd* mutant that received sNMES demonstrates massive deterioration of muscle fiber structure, disorganized myotomes with poorly defined boundaries. (E1) Representative image of *dmd* mutant that received hNMES demonstrates improved muscle fiber organization with more defined myotome boundaries but visibly detached muscle fibers and empty space between fibers. (F1) Representative image of *dmd* mutant that received eNMES demonstrates healthy myotomes with clearly defined boundaries, organized muscle fibers with very few wavy fibers, and lack of

empty space between fibers. Quantification of the percentage of muscle segments with detachments indicates that pNMES (C2) and eNMES (F2) significantly reduce fiber detachments in *dmd* mutants. Strength NMES (D2) and hNMES (E2) do not impact the percent of muscle segments with detachments. Each data point represents a single fish. A muscle segment is defined as half of a myotome. Muscle detachment data were analyzed using two-sided t tests.* $p < 0.05$, ** $p < 0.01$.

We hypothesized that improved muscle structure would correlate with improved function. We tested this hypothesis by assessing swim activity as a gross readout of muscle function. Swim activity was tested using DanioVision at 8 dpf. As predicted, eNMES resulted in increased distance and mean velocity compared to control *dmd* larvae (Figure 7A4 and B4). Surprisingly, though, pNMES negatively affected swimming activity (Figure 7A1 and B1). Similarly, sNMES significantly reduced total distance and mean velocity (Figure 7A2 and B2) while hNMES did not affect these two measures (Figure 7A3 and B3).

Because improvements in muscle structure in response to different NMES paradigms did not strictly correlate to changes in swimming, we asked whether neuromuscular junction (NMJ) morphology changed with NMES. We analyzed NMJ morphology by using the SV2 antibody to label presynaptic structures and alpha-bungarotoxin to stain postsynaptic AChR. We focused on analyzing fast-twitch muscle fiber innervation, which is called distributed innervation (the rich network of NMJs in between the chevron shaped slow-twitch muscle innervation at the myotendinous junctions (MTJs), Figure 7C1).

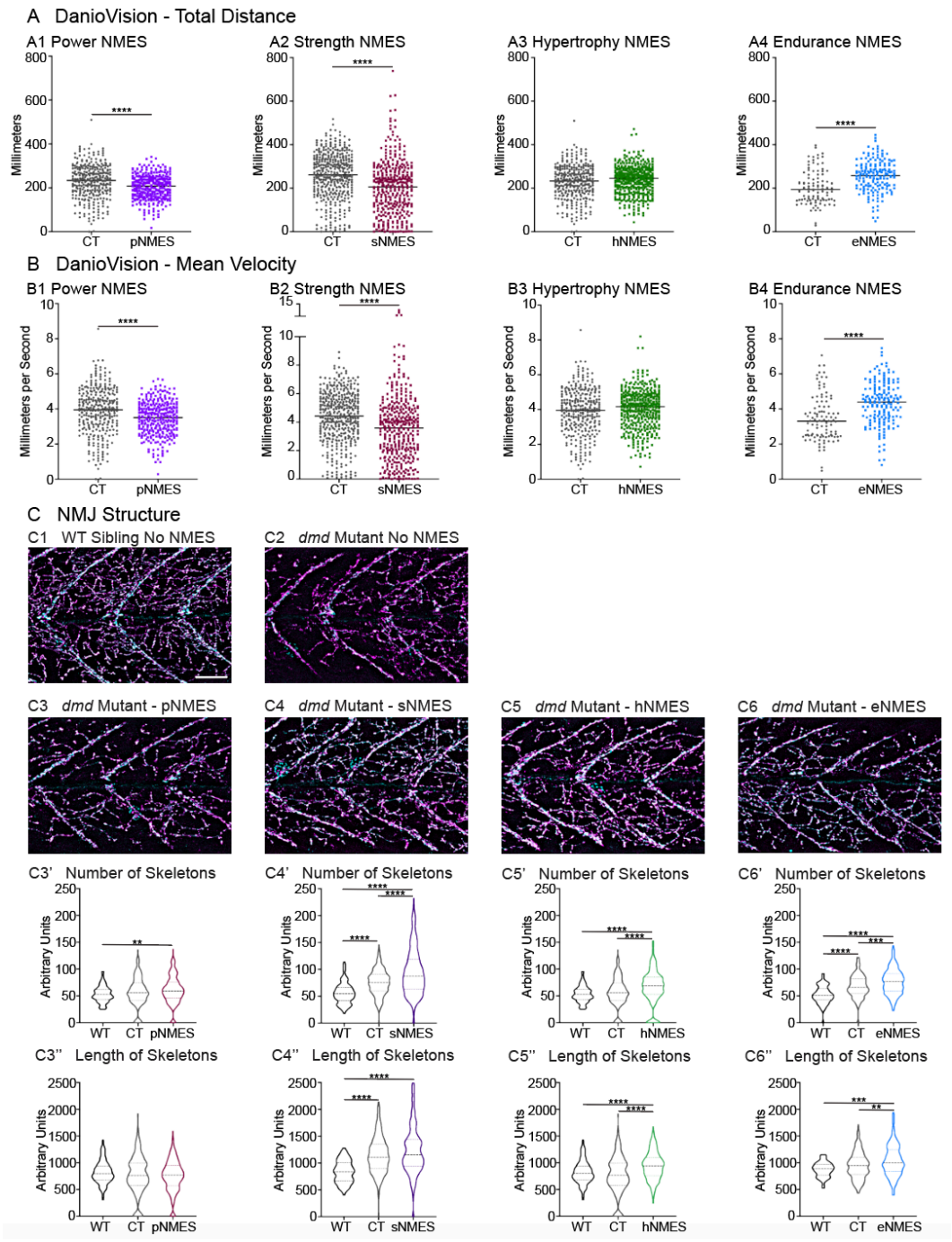

Figure 7: NMJ abundance does not correlate with swim function.

DanioVision was used to assess the impact of NMES on total distance (A) and (B) mean velocity. Measurements were made at 8 dpf. (A1, B1) *dmd* mutants that completed pNMES exhibited significant reductions in total distance and mean velocity compared to *dmd* mutants in the control group. (A2, B2) Strength NMES also negatively affected swimming activity in *dmd*

mutants compared to control *dmd* mutants. (A3, B3) No change in total distance or mean velocity is observed following hNMES. (A4, B4) *dmd* mutants that completed eNMES swam a significantly greater total distance and at a significantly faster mean velocity compared to *dmd* mutants in the control group. Each data point represents a single time point for an individual zebrafish. Each zebrafish has a total of 15 points. (C) anti-SV2 (cyan) and a-Bungarotoxin (AChR; magenta) antibodies are used to visualize the pre- and post-synaptic components of the NMJ. (C1) Representative image of WT sibling has muscle segments that are vastly innervated by both SV2 and AChR. (C2) Representative image of *dmd* mutant demonstrates a visible reduction in innervation, with relatively large portions of the muscle segments lacking innervation, especially by SV2. (C3, C4, C5, and C6) Representative images of *dmd* mutants that completed three sessions of pNMES, sNMES, hNMES, or eNMES demonstrate visible increases in innervation by both SV2 and AChR. The number of NMJs (skeleton number) within the muscle segments is significantly increased in *dmd* mutants compared to both WT siblings and *dmd* mutant controls following sNMES (C4'), hNMES (C5''), and eNMES (C6'). Skeleton length is also increased in *dmd* mutants that completed three sessions of hNMES (C5'') and eNMES (C6'') compared to both WT siblings and *dmd* mutant controls. (C3', C3'') Power NMES did not change the number or length of skeletons compared to *dmd* mutant controls. DanioVision data were analyzed using two-sided t tests. NMJ data were analyzed using either an ordinary one-way ANOVA with Tukey's multiple comparisons test or a Kruskal-Wallis test with Dunn's multiple-comparison test.** $p < 0.01$, *** $p < 0.001$, **** $p < 0.0001$.

Lastly, survival was tracked in dmd mutants treated with NMES. Survival checks were performed twice daily. Three sessions of eNMES, sNMES, and pNMES slightly but significantly extended the median age of survival for dmd mutants compared to unstimulated dmd mutants (Figure 8A, B, D); with eNMES having the largest beneficial effect. Three sessions of hNMES, however, did not affect median survival age (Figure 8C). Taken together, these data indicate

that different NMES paradigms elicit different neuromuscular responses. Furthermore, out of the four NMES paradigms we tested, only eNMES improves neuromuscular structure, swimming, and lifespan. Ultimately, these data further support the need to examine multiple components of muscle health in order to understand how an intervention affects disease severity and progression. More importantly, though, these data suggest that there are additional mechanisms underlying neuromuscular plasticity in *dmd* mutants that are not captured by changes in muscle structure and function.

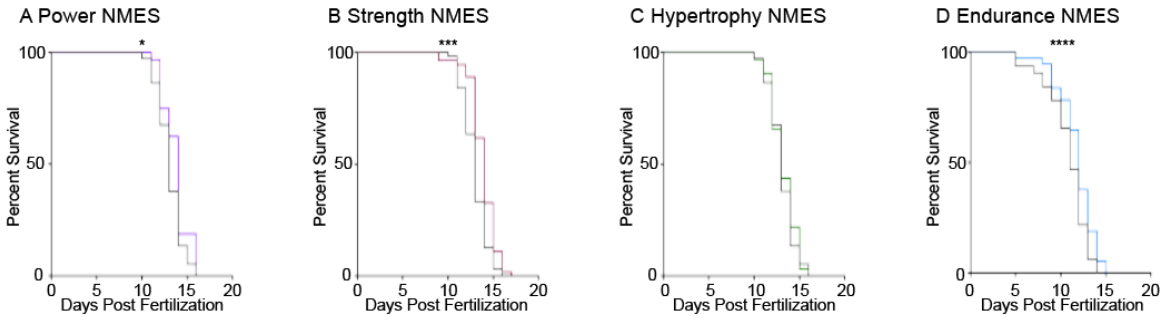

Figure 8: Changes in muscle health and swim activity do not predict survival. Survival was tracked following completion of the three NMES sessions. Survival was significantly improved in *dmd* mutants that completed power (C1), strength (C2), and endurance (C4) NMES. (C3) Hypertrophy NMES had no effect on survival in *dmd* mutants. DanioVision data were analyzed using two-sided t tests. Survival data were analyzed using a Mantel-Cox test. * $p < 0.05$, *** $p < 0.001$, **** $p < 0.0001$.

4.4 Perspective

Currently, individuals with DMD are advised to refrain from resistance training since the loss of dystrophin causes the DGC to become unstable and the integrity of the sarcolemma to be weakened. This long-standing consensus stems from the hypothesis that muscle fiber degeneration would be initiated sooner and greatly accelerated since the magnitude of tensile forces experienced by the sarcolemma would be increased. From the data presented in the

Chapter 2, *dmd* mutants exposed to extended periods of inactivity experience negative consequences on disease progression, especially regarding muscle structure and survival. Therefore, this limited understanding of how resistance training affects the structural integrity of dystrophic muscle may actually be accelerating disease progression. Using NMES as a mechanism to emulate the four types of resistance training, we found that these four NMES paradigms do not result in immediate damage the sarcolemma nor negatively affect survival, suggesting that NMES may be a better recommendation for care. However, these four NMES paradigms differentially affect muscle structure and function, supporting our idea that neuromuscular plasticity is a delicate balance between numerous components that may not be reflected in muscle fiber structure.

Our understanding of neuromuscular plasticity in healthy muscle encompasses this idea that improvements in structure are likely to lead to improvements in muscle function. Thus, if muscle structure becomes compromised, it will likely lead to compromised muscle function. However, in *dmd* mutants, the above data suggest that neuromuscular plasticity may not share this same relationship. Previous studies often expect improvements in structural components to translate into improvements in functional components but, based on our initial investigations with inactivity and NMES, this is not the case. Collectively, our experiments suggest that *dmd* muscle exhibits a delicate, intricate equilibrium with several factors influencing muscle structure, swimming activity and survival. Therefore, we next asked what are these additional factors? What additional components of muscle and organism health are at play in defining improvements in function and survival? To begin to answer these questions, we examined the effects of eNMES in more detail since this paradigm positively improved all three outcome measures.

CHAPTER 5

MECHANISMS MEDIATING IMPROVEMENT FOLLOWING ENDURANCE NMES IN *DMD* MUTANT ZEBRAFISH

5.1 Relevant Background

While previous studies have found positive benefits of NMES on dystrophic muscle in humans and in mdx mice, the cellular and molecular mechanisms underlying these improvements are poorly understood. In muscle atrophy studies, NMES is capable of preventing decreases in muscle mass and muscle fiber cross-sectional area, and it is suggested that these improvements are due to the absence of the typical slow to fast heavy chain isoform transitioning observed with muscle atrophy as well as the decrease in expression of atrophy-related genes [424]. In aging studies, NMES significantly improved functional tests and increased the diameter of fast muscle fibers, which may be driven by an upregulation in markers for satellite cell activation (myogenin, miR-206 and miR-1), muscle growth (IGF-1), and cell adhesion (collagen I, III, and VI), but, more importantly, the down-regulation of markers for atrophy-related ubiquitin ligases (MuRF-1) [425]. Lastly, in active versus sedentary males, 8 weeks of NMES training (3 sessions per week) significantly increased maximum voluntary contraction force, neural activation, and muscle fiber cross-sectional area for both slow and fast muscle fibers, which was likely achieved through enhanced gene and protein expression patterns indicative of both resistance and endurance training, including oxidative and glycolytic metabolism, antioxidant defense systems, and myofibrillar proteins [403,426]. Further, NMES demonstrated profound effects on elements of the contractile apparatus, excitation-contraction coupling machinery, ion homeostasis, metabolism, and the NMJ [427,428]. The goal for this chapter is to dive deeper into understanding the mechanisms that underly the improvements in muscle structure, function and survival following eNMES.

5.2 Experiment Overview

We used a multi-discipline approach to understand the basic biology of neuromuscular plasticity observed in *dmd* mutants following eNMES. We leveraged the unparalleled imaging capabilities of the zebrafish larval model to shed light on the structural mechanisms that may lead to the increased birefringence and decreased muscle detachments following eNMES. In most zebrafish studies, muscle detachments are counted as a method to quantify changes in muscle health. When we quantified the percentage of muscle segments with detachments, we observed that eNMES significantly reduced this percentage in *dmd* mutants (Figure 6F2). While these data suggest that muscle fiber health is improved, we elected to capture a more detailed assessment of muscle fiber organization after noticing that while some muscle segments did not have visibly detached fibers, these segments contained disorganized muscle fibers with a characteristic 'waviness'. Therefore, we elected to use machine learning and trained the computer to identify, pixel-by-pixel, 'healthy' versus 'sick' with 97% accuracy. Next, we asked the computer to identify the percentage of healthy muscle in the same phalloidin images in which fiber detachments were counted on. A detailed description of the methodology used for machine learning is provided in Appendix B.9.

We used second harmonic generation (SHG) imaging as a label-free mechanism to visualize sarcomeres at 8 dpf. SHG is a nonlinear optical microscopy technique that captures highly polarizable matter in a non-centrosymmetric molecular organization (Plotnikov et al. 2005). One such structure is the rod domain of myosin that constructs the sarcomere. A detailed description on how zebrafish were prepared for SHG imaging is provided in Appendix B.8.

We also utilized two types of time-lapse analyses, the taco time-lapse and the longitudinal time-lapse, to follow the extent of degeneration/regeneration occurring in each *dmd* mutant as well as the health of their muscle nuclei during the training and recovery periods. For these experiments we used transgenic 3MuscleGlow *dmd* mutants (sapje^{ta222a}; myog:H2B-mRFP; mylpfa:lyn-Cyan; smyhc1:EGFP) to visualize fast and slow muscle fibers and muscle

nuclei (Hromowyk et al. 2020). For this zebrafish line, disease onset is at 3 dpf rather than 2 dpf even though both lines harbor the same point-mutation. Therefore, NMES was performed at 3, 4 and 5 dpf, and the recovery period ensued from 6 to 9 dpf. A detailed description on how zebrafish were prepared for live imaging is provided in Appendix B.7 and how muscle nuclei were quantified is provided in Appendix B.9. For the taco time-lapse experiments, imaging began at the same time each day and each zebrafish was imaged at least three times. During the training period, imaging began immediately following the NMES session. Once all zebrafish were imaged, the second round of imaging began followed by the third and/or fourth round. Zebrafish were imaged each day from 3 to 7 dpf. For the longitudinal time-lapse experiments, imaging began immediately after the NMES session and zebrafish were imaged continuously for 12 hours.

Alongside these imaging experiments, we performed RNAseq to uncover potential molecular mechanisms that may be eliciting the improvements observed in dmd muscle following eNMES. At 7 dpf, RNA was extracted from two zebrafish per tube. In each tube, zebrafish were paired according to their initial mean gray value (severe versus mild) as well as their change in mean gray value from 5 to 7 dpf. The protocol for RNA extraction and data analysis are presented in Appendix B.11.

5.3 Results

5.3.1 eNMES Improves Muscle Structure and Sarcomere Length

As demonstrated previously, eNMES significantly reduced the percentage of muscle segments with muscle fiber detachments, suggesting that muscle fiber health is improved. However, after noticing that while some muscle segments did not have visibly detached fibers, these segments contained disorganized muscle fibers with a characteristic ‘waviness’, we elected to use machine learning to better capture muscle health. We observed that *dmd* mutants completing three sessions of eNMES trend towards having higher percentages of health muscle compared to control *dmd* mutants (Figure 9A4). The contribution of these

disorganized, wavy muscle fibers to overall muscle structure and function in *dmd* mutants is currently unknown.

Using SHG microscopy, we analyzed muscle fibers at the level of the sarcomeres. The length of a sarcomere is extremely important to muscle function [429]. As described previously, a sarcomere produces force through the cross-bridges formed between actin and myosin, and the amount of force generated is dependent upon the amount of overlap between these thick and thin filaments. More specifically, force production can be predicted using the force-length relationship, which states that there is an optimal sarcomere length required for maximal force and power production [430]. At 8 dpf, wild-type siblings exhibited a mean sarcomere length of 1.853 ± 0.1071 micrometers (Figure 9B4), matching lengths previously published in 3 dpf wild-type zebrafish (1.86 ± 0.15 micrometers; [431]). Compared to wild-type siblings, *dmd* mutants have significantly shorter sarcomeres with a mean length of 1.575 ± 0.1567 micrometers (Figure 9B4). While no study has directly measured sarcomere lengths using SHG imaging in *dmd* mutants, other studies have reported shorter sarcomere lengths in mutants versus wild-type siblings [386]. Notably, three sessions of eNMES significantly increased mean sarcomere lengths (1.707 ± 0.1710) compared to *dmd* mutant controls, and these values are nearing wild-type lengths, but still significantly shorter (Figure 9B4). These data suggest that eNMES may improve muscle structure and function by restoring sarcomere lengths to more optimal lengths, which may allow stronger cross-bridges to form and more success in generating force and power.

5.3.2 Muscle Nuclei Return to a More Ellipsoidal Shape With eNMES

The above improvements in sarcomere lengths prompted us to next ask whether muscle nuclei are also changing in response to eNMES. The role of myonuclear size and shape on muscle health is becoming more prevalent especially since changes in these parameters as well as their positioning are becoming more evident in skeletal muscle diseases [13,432,433]. We

measured three components of nuclear size and shape: volume, surface area, and filament index. Filament index is a measure that quantifies the departure of an object from a circle. Specifically, a circle has a filament index of 1 and a higher filament index indicates a departure to a more ellipsoidal shape. Therefore, in terms of muscle nuclei, a higher filament index suggests that the nuclei are more elongated, which is suggested to be healthier [434]. Muscle nuclei in *dmd* mutants have significantly lower volumes, surface areas, and filament indices compared to wild-type siblings (Figure 9C4-C6). Interestingly, eNMES significantly increased these measures, especially for filament index, which is restored to wild-type values (Figure 9C6). Additionally, these nuclei appear more organized along the length of individual muscle fibers, similar to the pattern observed in wild-type siblings (Figure 9C3). These data suggest that *dmd* mutants have smaller, spheroidal nuclei compared to wild-type siblings, and eNMES is capable of elongating the nuclei, and increasing their volumes and surface areas. Since nuclear size affects DNA organization, transcriptional and translational processes, and nuclear import and export activities [435], minor changes in size correlate with reduced muscle function and fiber performance [436]. Therefore, these improvements in muscle nuclei following eNMES may direct improvements in the muscle structure and function that we observed.

5.3.3 Time-Lapse Analyses Suggest Less Muscle Degeneration and Improved Regeneration Capabilities With eNMES

From the changes in sarcomere lengths and muscle nuclei at 8 dpf, we next asked what is happening daily in the muscle structure that lead up to these improvements. We performed confocal time-lapse analyses using transgenic zebrafish to track individual fast-twitch muscle fibers immediately following each session of eNMES as well as the days following completion of eNMES training. Again, disease onset in these transgenic zebrafish is at 3 dpf; thus, NMES sessions are at 3, 4 and 5 dpf while the recovery period extends from 6 through 9 dpf. At 3 dpf, there was not a clear difference in muscle degeneration between treated and control mutants. However, by 4 dpf, control mutants exhibited initial signs of muscle degeneration (Figure 9D1c

and D1d). eNMES mutants showed less degeneration, suggesting that eNMES delays degeneration (Figure 9D2c and D2d). Whereas degenerated fibers persist in control mutants for days (Figure 9D1f - g), degenerated segments are cleared more quickly in eNMES-treated mutants (Figure 9D2f - g). Finally, more robust regeneration was observed in eNMES-treated mutants (Figure 9D2h). Taken together, these data suggest that eNMES improves muscle homeostasis. To elucidate potential molecular mechanisms that may underly these improvements in muscle health and function, as well as determine whether eNMES is enhancing regeneration, we performed RNAseq at 7 dpf.

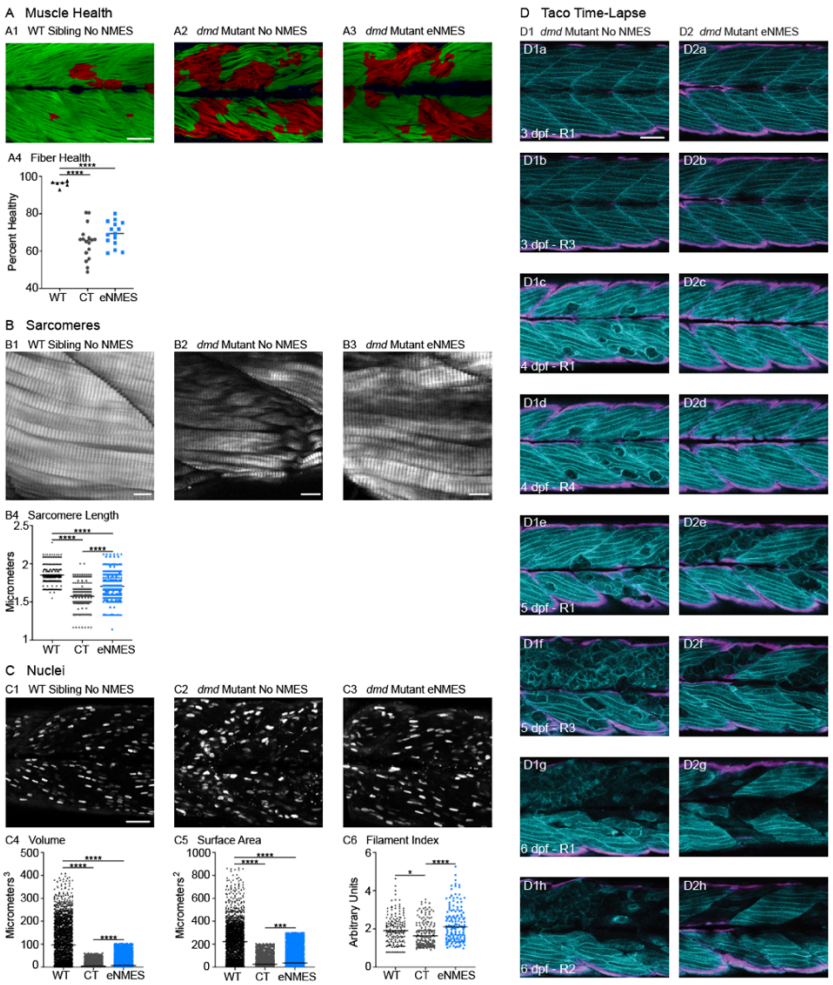

Figure 9: eNMES improves multiple components of muscle health in *dmd* mutants.

(A) Machine learning was used to quantify muscle health pixel-by-pixel. Green indicates healthy pixels while red indicates unhealthy pixels. (A4) The percent of healthy muscle following eNMES

trends to be higher in *dmd* mutants compared to *dmd* mutant controls. Scale bar is 50 micrometers. (B) Second harmonic generation microscopy was used to quantify sarcomere length at 8 dpf. Representative SHG images of WT sibling control (B1), *dmd* mutant controls (B2), and *dmd* mutants that completed eNMES training. Anterior left, dorsal top, side mounted. Scale bars are 10 micrometers. (B4) Sarcomere length is significantly shorter in *dmd* mutant controls compared to WT sibling controls. However, eNMES significantly improves sarcomere length, bringing it closer to WT lengths. Each point represents a single sarcomere along a predetermined length of a muscle fiber. Multiple muscle fibers were measured per zebrafish. (C) Muscle nuclei were imaged at 8 dpf as a potential mechanism for improved muscle health. Anterior left, dorsal top, side mounted. Scale bar is 50 micrometers. (C1) Representative image of WT sibling control demonstrates healthy ellipsoidal nuclei organized along the length of the muscle fibers. (C2) Representative image of *dmd* mutant control demonstrates fragmented punctae as well as more spherical nuclei that clustering within the muscle segments. (C3) Representative image of *dmd* mutant that completed eNMES training demonstrates healthier, ellipsoidal nuclei that appear more organized within the muscle segments. Quantification of nuclear size indicates that eNMES significantly increases the volume (C4) and surface area (C5) of muscle nuclei compared to *dmd* mutant controls. However, nuclei are still significantly smaller compared to WT sibling controls. visually appear to have an increased number of myonuclei compared to unstimulated *dmd* mutants. (C6) Filament index was used to assess circularity, specifically the departure from a circle. Filament index is significantly higher in *dmd* mutants that completed eNMES training, indicating that nuclei are more elongated compared to *dmd* mutant controls. Each point represents a single nuclei within a z-stack. (D) Transgenic *dmd* mutants (mylpfa:lyn-cyan, smych1:GFP) were used to visualize changes in structural integrity of fast- and slow-twitch muscle fibers across three days. Anterior left, dorsal top, side mounted. Scale bar is 50 micrometers. Images were taken around the 12th myotome. (D1) Representative *dmd* mutant control. (D1a – D1b) At 3 dpf, there is no dystrophy in the imaged

myotomes. (D1c – D1e) At 4 dpf and the beginning of 5 dpf, dystrophy is minimal with relatively few detaching muscle fibers. (D1f) However, massive muscle degeneration occurs between the first found of imaging and the third round of imaging at 5 dpf. (D1g – D1h) Fiber degeneration is present, suggesting that the damaged muscle fibers have not been cleared and regeneration is unlikely. (D2) Representative *dmd* mutant that is undergoing eNMES training. (D2a – D2b) The first session of eNMES at 3 dpf does not result in immediate damage to the muscle. (D2c – D2d) Similarly, following the second session of eNMES at 4 dpf, there is no immediate muscle damage occurring in the imaged myotomes. (D2e) At 5 dpf, following the third session of eNMES, muscle fiber degeneration is evident but by the third round of imaging (D2f), these damaged areas are being cleared and there is evidence of regeneration. (D2g – D2h) At 6 dpf, previously damaged muscle segments have new muscle fibers present. All data were analyzed using either an ordinary one-way ANOVA with Tukey's multiple comparisons test or a Kruskal-Wallis test with Dunn's multiple-comparison test.* $p < 0.05$, ** $p < 0.01$, *** $p < 0.001$, **** $p < 0.0001$.

5.3.4 eNMES Elicits a Molecular Response in Wild-Type Siblings Indicative of Exercise

In our RNAseq analysis, we first asked whether eNMES initiates a molecular response that emulates exercise in wild-type siblings. PCA analysis revealed that wild-type siblings that underwent three sessions of eNMES cluster completely separate from those in the control group (Figure 17), suggesting that wild-type siblings that complete three sessions of eNMES have an unique expression profile compared to controls. Of the total 25,863 genes identified across the RNAseq analysis, 932 genes were differentially expressed between wild-type siblings in the eNMES and control groups (Figure 10A1). Of these 932 genes, 306 genes were upregulated and 626 genes were downregulated (Figure 10A3). Using Gene Ontology (GO) enrichment analysis, 24 enriched categories were identified, including regulation of metabolic processes, regulation of MAP kinase activity, regulation of transcription, and circadian rhythms. Future

studies will compare these differentially expressed genes to those identified in human NMES studies to better understand these eNMES-induced molecular patterns.

5.3.5 DMD Zebrafish Do Not Respond to eNMES in the Same Manner as Wild-Type Siblings

Interestingly, the differentially expressed genes suggest that eNMES may be eliciting changes in WT versus *dmd* mutants through different mechanisms. Based on the number of genes differentially expressed, *dmd* mutants do not respond to eNMES in the same manner as wild-type siblings (Figure 10A2). Specifically, 123 genes were differentially expressed (FDR < 0.1 and abs(log2(Fold Change)) > 0.6) between *dmd* mutants that completed three eNMES sessions versus *dmd* mutant controls (Figure 10A4). This is much lower than the 932 differentially expressed genes in wild-type siblings. Additionally, *dmd* mutants have more genes that are increased (n = 84) than decreased (n = 39), which is the opposite of wild-type siblings, further suggesting that *dmd* mutants do not respond through the same signaling pathways as their healthy counterparts. Unfortunately, GO analyses did not reveal specific cellular processes in which these genes may participate in to positively impact muscle health. Therefore, we chose to examine genes individually, looking specifically at how their increase or decrease could influence *dmd* muscle.

Only 4 genes of the 1,048 differentially expressed genes elicited by eNMES in both *dmd* mutants and wild-type siblings shared the same expression pattern (Figure 10B). Three genes, including heme oxygenase 1a (*hmox1a*), calcium release activated channel regulator 2Ab (*cracr2ab*), and retinaldehyde binding protein 1b (*rlbp1b*) were increased and 1 gene, melanotransferrin (*meltf*), was decreased with eNMES. This lack of overlap between differentially expressed genes further indicates that *dmd* mutants do not respond similarly to eNMES as wild-type siblings.

Interestingly, we found 3 genes that exhibited opposite expression between genotypes (*dmd* mutants vs wild-type) and eNMES (*dmd* mutants vs wild-type siblings after eNMES) (Figure 10C). That is, a gene may be decreased in *dmd* mutants compared to wild-type siblings,

but eNMES increased its expression in *dmd* mutants while decreasing its expression in wild-type siblings. These genes included interferon induced transmembrane protein 1 (*ifitm1*), gamma-glutamyltransferase 1a (*ggt1a*), and Cabz01046949.1. Additionally, 3 genes were decreased in *dmd* mutants compared to wild-type siblings but eNMES decreased its expression in *dmd* mutants and had no effect in wild-type siblings. These genes included serpin peptidase inhibitor, clade B (ovalbumin), member 1, like 4 (*serpinb1l4*), kazal-type serine peptidase inhibitor domain 3 (*kazald3*), and cystathionase (cystathionine gamma-lyase), like (*cthl*). Lastly, 1 gene, si:ch1073-13h15.3, was increased in *dmd* mutants compared to wild-type siblings and was decreased in both wild-type siblings and *dmd* mutants following eNMES (Figure 10C7. Altogether, these data suggest the possibility that eNMES may partially improve dmd muscle structure and function by returning *dmd* mutants to more wild-type-like expression profiles.

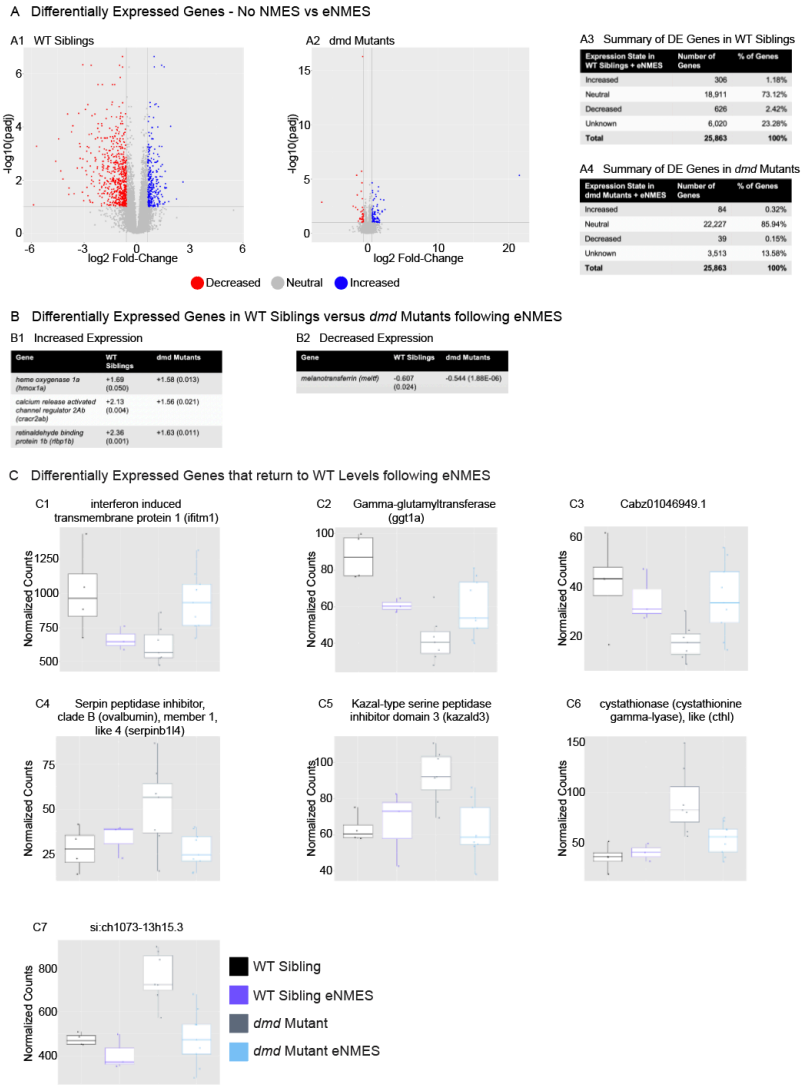

Figure 10: *dmd* mutants do not respond to eNMES in the same manner as WT siblings. RNAseq analysis was performed at 7 dpf in wild-type siblings and *dmd* mutants that completed eNMES training and their expression patterns were compared with their respective controls. (A1) Volcano plot showing significantly and biologically increased (blue dots) and decreased (red dots) genes in WT siblings that completed eNMES versus those that did not. (A2) Volcano plot showing significantly and biologically increased (blue dots) and decreased (red dots) genes in *dmd* mutants that completed eNMES versus those that did not. (A3 – A4) Summary of differentially expressed genes in WT siblings (A3) and *dmd* mutants (A4). WT siblings had 932 differentially expressed genes compared to 123 differentially expressed genes in *dmd* mutants,

suggesting that *dmd* muscle responds differently to eNMES and the genes responsible for eliciting beneficial effects on muscle structure and function are different. (B) Differentially expressed genes in WT siblings versus *dmd* mutants following eNMES that increased in expression (B1), decreased in expression (B2). Values are presented as Fold Change (FDR). The relatively few genes that were significantly differentially expressed in both data sets further suggests that *dmd* mutants respond differently to eNMES than WT siblings. (C) Selected differentially expressed genes in *dmd* mutants following eNMES to show how expression levels return to those of wild-type controls.

5.3.6 eNMES May Alter the ECM in *dmd* Mutants

The ECM surrounding muscle fibers is a critical component of muscle fiber health. Protein complexes spanning the sarcolemma and ECM serve as mechanical linkages and allow the muscle fiber to attach to the skeleton via the MTJ and to each other via the costamere [42]. Additionally, ECM proteins play a prominent role in muscle regeneration by promoting satellite cell division, differentiation and fusion into mature muscle fibers [437]. More importantly, though, many ECM proteins play dual roles in improving cell adhesion and promoting fibrosis. Since changes to the ECM, especially its mechanical stiffness, are well documented during disease and following exercise, we next asked whether ECM proteins are differentially expressed in our *dmd* mutants following eNMES and what consequences these expression patterns may have on muscle health. It should be noted that our RNAseq data represent a snapshot in time, and since the ECM is a highly dynamic tissue, mRNA expression is not the best way to capture physical changes to the ECM. Further, since zebrafish larvae are a developmental model, it is possible that we are capturing developmental changes rather than responses to eNMES. However, for the genes being discussed below, we see similar changes in wild-type siblings and *dmd* mutants, suggesting that expression changes may be more in response to eNMES than development.

Transforming growth factor beta induced (TGFBI) is an extracellular matrix protein that accumulates at the MTJ in high levels as well as in the ECM where it is associated with micro-fibrillar structures, and responsible for collagen deposition. In our RNAseq data, *transforming growth factor beta induced* (*tgfbi*) is significantly higher in *dmd* mutants compared to wild-type controls. However, eNMES reduces the levels of *tgfbi* in both *dmd* mutants and wild-type siblings (Figure 11A1). In studies looking at molecular signatures characterizing DMD muscle, *tgfbi* is highly upregulated compared to healthy muscle [438,439]. This is also true when comparing *tgfbi* expression in mdx muscle versus muscle from *fiona* mice (mdx mice overexpressing utrophin) [440]. TGFBI binds to type I, II and IV collagens as well as several integrins. In vitro, TGFBI mediates integrin α7-dependent adhesion of myoblasts and myotubes [441]. In zebrafish, morpholino-mediated knockdown of *tgfbi* resulted in normal MTJ formation and myofibril assembly in the sarcolemmal space but these myofibrils did not remain attached to the sarcolemma, leading to a significant reduction in myofibril content [442]. Therefore, TGFBI plays an intricate role in balancing fibrosis and cell adhesion. In our *dmd* mutants, the downregulation of *tgfbi* following eNMES may reflect a decrease in excessive ECM deposition and fibrosis rather than a loss in cell adhesion.

Periostin (postnb) is a TGFBI-related protein that is highly involved in modeling the ECM and connective tissue architecture during development and regeneration, serving specifically as a mediator of fibrosis in injury and disease [443]. Notably, RNAseq data indicate that *postnb* shares a similar expression pattern to *tgfbi* with increased expression in *dmd* mutants compared to wild-type siblings and a reduction in this expression following eNMES in both groups (Figure 11A2). Morpholino-mediated knockdown in zebrafish results in disrupted myoseptum formation and muscle fiber attachment [444]. Periostin directly interacts with other ECM proteins, including fibronectin, tenascin-C, collagen I and V, and heparin, to alter the ECM by changing the properties and/or assembly of these proteins [445]. In adult muscle, periostin is maintained at very low levels but becomes strongly expressed in fibroblasts and secreted into the ECM upon

acute injury [446,447]. Interestingly, periostin is linked to fibrosis induced by eccentric exercise [448]. Similarly, in individuals with DMD, periostin mRNA is significantly upregulated, especially in young children [439], and muscle biopsies confirm that periostin is upregulated and accumulates in the ECM, especially in areas of muscle fiber degeneration and dropout [449]. In periostin-deficient mice, however, the strength of the collagen network is significantly reduced as a result of disorganized and dysfunctional collagen fibrils [450,451]. Further, in δ-sarcoglycan-null mice, deletion of *Postn* resulted in significant reductions in muscle pathology of the diaphragm, gastrocnemius and quadriceps muscles at 6 weeks and 6 months of age [449]. Also, the pseudohypertrophy observed in the muscles of δ-sarcoglycan-null mice, which is often the result of extensive fibrosis, was no longer present in the absence of periostin [449]. These data suggest that while periostin negatively impacts disease pathogenesis, its absence significantly enhances muscle fiber health in dystrophic muscle [449]. Therefore, in combination with the downregulation of *tgfbi*, it is likely that eNMES decreases ECM deposition and fibrosis in *dmd* mutants without altering cell adhesion.

Integrin-β1 (*itgb1b.2*) is also significantly upregulated in *dmd* mutants compared to wild-type siblings, but is reduced with eNMES (Figure 11A3). In skeletal muscle, integrins represent the family of cell surface adhesion molecules that mediate cell-matrix interactions. Integrins are heterodimeric, transmembrane glycoproteins that are made up of an α and β subunit. Notably, the integrin-β1 family constitutes the largest group of receptors in the ECM, including at the costameres, NMJ, and MTJ, during development and in mature muscle [452]. Integrin-α5β1 is the classical fibronectin receptor while α6β1 and α7β1 are laminin receptors [452]. During development, α5β1, α6β1, and α7β1 mediate aspects of myoblast fusion and myotube formation [453–457]. In adult muscle, however, α7β1 is the major integrin receptor located peripherally around muscle fibers and is highly enriched at the MTJs [458] and NMJ [459]. Notably, integrin-α7β1 participates in both outside-in and inside-out signal transduction

processes and is involved in several muscle diseases [460]. In individuals with DMD and in mdx mice, integrin-α7β1 is increased compared to healthy muscle, and it is suggested that this increase may compensate for the absence of dystrophin [460]. In mdx muscles, activating integrin-β1 ameliorates the dystrophic pathology, restores muscle strength, and improves regeneration [461]. Similarly, in mdx-utrophin double knockout mice, overexpression of integrin-α7β1 ameliorates the development of muscular dystrophy and increases lifespan [462]. These improvements are likely the consequences of enhanced fiber integrity, especially at the MTJ and NMJ, which is suggested by the restoration of the highly folded sarcolemmal structure unique to these locations [462]. Additionally, the enhanced laminin organization in the ECM may support satellite cell proliferation and regenerative capacity [462]. In healthy muscle, integrin-α7β1 is increased at the MTJ following injury-producing exercise [463]. Interestingly, overexpression of integrin-α7β1 prior to exercise protected the muscle from this exercise-induced damage [463]. These data suggest that integrin may serve as a mechano-sensor and likely plays an important role in muscle regeneration [462,464]. The downregulation of *itgb1b.2* in *dmd* mutants as a consequence of eNMES is puzzling since we would expect that it would play a protective role in *dmd* muscle. Further studies should unravel the role that integrin-β1 may play in improving muscle health in *dmd* mutants following eNMES. Altogether, though, these data suggest that cell-ECM interactions and the composition of the ECM are changed with eNMES.

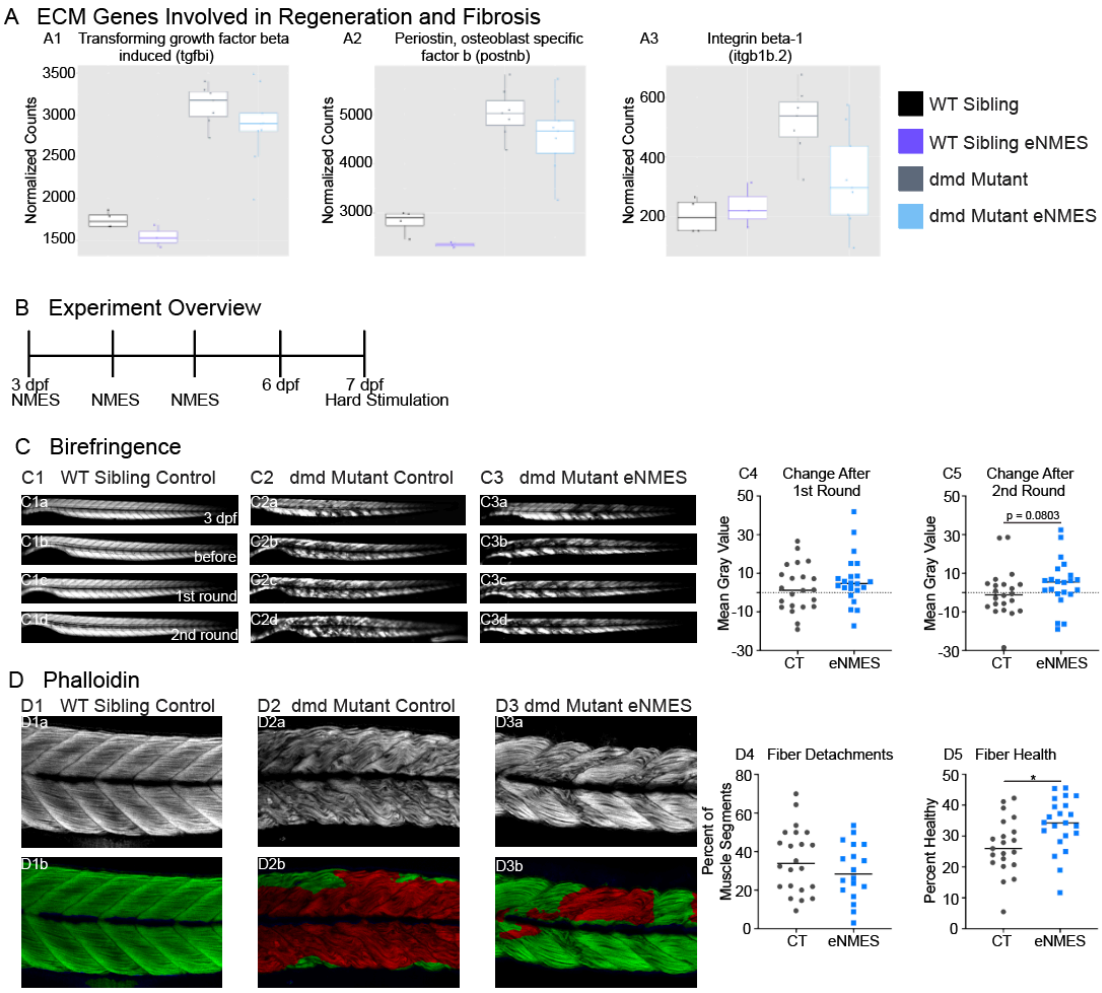

Figure 11: Modulation of ECM genes involved in regeneration and fibrosis following eNMES may lead to observed improvements in muscle resilience in *dmd* mutants. We identified three ECM genes, tgfbi (A1), postnb (A2), itgb1b.2 (A3) that are significantly upregulated in *dmd* mutants compared to WT siblings and trend to be downregulated with eNMES in *dmd* mutants. (B) Experiment overview. At 3 dpf (disease onset), birefringence images are taken followed by the first session of eNMES. At 4 and 5 dpf, zebrafish undergo the second and third NMES sessions, respectively. At 7 dpf, muscle resilience was tested using an electrical stimulation paradigm intended to cause fiber detachments. (C) Birefringence images were taken at 3 dpf, before the first session and after the first and second sessions. (C1) No visible changes in birefringence are observed in WT siblings after the two stimulation sessions.

(C2) For *dmd* mutant controls, the first round of stimulation did not result in visible changes to birefringence (C2c) but, after the second round, areas of muscle degeneration are visible (C2d). Conversely, in *dmd* mutants that completed three sessions of eNMES, the first (C3c) and second (C3d) rounds of stimulation did not result in visible changes to birefringence. (C4, C5) Change in birefringence from before to after the first round (C4) and second (C5) of stimulation suggests that eNMES training may improve muscle resilience. (D) Phalloidin was used to visualize individual muscle fibers. (D1a) Representative image of a WT sibling control demonstrates healthy, organized muscle fibers and myotomes. (D2a) Representative image of a *dmd* mutant control highlights disorganized and wavy muscle fibers and fiber detachments. (D3a) Representative image of a *dmd* mutant that completed eNMES demonstrates some wavy muscle fibers and detached fibers intermixed with relatively healthy myotomes. (D4) The percent of muscle segments with detached fibers following the hard stimulation is reduced in *dmd* mutants that complete eNMES training compared to *dmd* mutant controls. A muscle segment is defined as half of a myotome. (D1b, D2b, D3b) Machine learning was used to quantify muscle health pixel-by-pixel. Green indicates healthy pixels while red indicates unhealthy pixels. (D5) The percent of healthy muscle following the hard stimulation is significantly higher in *dmd* mutants that completed eNMES compared to *dmd* mutant controls. All data were analyzed using two-sided t tests. * $p < 0.05$.

5.3.7 eNMES May Reduce Susceptibility to Contraction-Induced Injury in *dmd* Mutants

As mentioned above, analysis of expression levels of cell-matrix adhesion proteins does not always indicate the physiological impact of these changes because the ECM supports muscle homeostasis but can also result in fibrosis. Cell-matrix adhesion is often negatively affected in various models of muscular dystrophy and restoration of adhesion improves muscle structure and function [465,466]. Therefore, the downregulation of key cell adhesion proteins following eNMES was puzzling and led us to ask whether muscle cell-matrix adhesion was

altered by eNMES. We did this by subjecting zebrafish to a hard stimulation paradigm designed to make muscle fibers detach from the MTJ [467] for two back-to-back sessions (Fig. 11B).

For this experiment, zebrafish completed three sessions of eNMES. Two days after completing the third session, zebrafish were subjected to a relatively hard stimulation paradigm designed to make muscle fibers detach from the MTJ for two back-to-back sessions (Figure 12A). This stimulation paradigm was defined by a frequency of 4 pulses per second, a delay of 60 ms, a duration of 2 ms, and a voltage of 30 volts, which is similar to that known to initiate muscle fiber detachment from the MTJ [467]. Dmd mutants were stimulated for 1 minute. Birefringence images were taken before and after each session. To ensure consistency in imaging, zebrafish were mounted laterally with the head on the left and dorsal up, and the same imaging parameters were used for each zebrafish across all imaging sessions. We then analyzed the change in mean gray values before stimulation compared to after the first or second session. Nearly half of control mutants (10/22) had decreased mean gray values after the first session (Figure 11C4), and slightly over half (13/22) had decreased mean gray values after the second session (Figure 11C5). In contrast, just under 25% of eNMES treated mutants (5/22) had a decreased mean gray value after the first session (Figure 11C4) and slightly under a third had a decreased mean gray value after the second session (7/22; Figure 11C5). While there are no differences in absolute mean gray values between control and eNMES mutants before and after the first round of stimulation (Fig. 11C4), the change in mean gray values for eNMES-treated *dmd* mutants is higher following the second round of stimulation (Fig. 11C5). These data suggest that eNMES may improve cell-adhesion.

In order to examine the impact of eNMES on muscle homeostasis in response to a hard stimulation more thoroughly, zebrafish were immediately fixed and stained with phalloidin after the last round of birefringence imaging. Similar to the birefringence data, the percent of muscle segments with detachments is lower in *dmd* mutants that completed eNMES compared to control *dmd* mutants (Figure 11D4). Notably, when we used machine learning to assess overall

muscle health, *dmd* mutants that completed eNMES had a significantly higher percentage of healthy muscle compared to control *dmd* mutants (Figure 11D5). These data suggest that *dmd* mutants that complete eNMES can withstand contraction-induced injury better than *dmd* mutant controls.

5.3.8 Paxillin Overexpression Does Not Improve the Benefits of Endurance NMES in *dmd* Mutants

With the improved cell adhesion following eNMES, we next asked if paxillin overexpression would further improve muscle resilience. Paxillin is an important mediator of cell-matrix adhesion and costamere formation [468,469]. For this experiment, we used transgenic *dmd* mutants that overexpress paxillin (actb2:pxn-EGFP) [470]. Zebrafish completed three sessions of eNMES at 2, 3 and 4 dpf. Three days after completing the third session, zebrafish were subjected to the cell adhesion stimulation paradigm for two back-to-back sessions with birefringence images taken before and after each session (Figure 12A). Surprisingly, paxillin overexpression negatively affected *dmd* muscle resilience in both groups, as indicated by the negative changes in mean gray values before versus after the second round of stimulation (Figure 12B4 and B5). Further, *dmd* mutants that completed eNMES have a higher percentage of muscle segments with detachments (Figure 12C4), suggesting that paxillin overexpression resulted in significant deterioration of muscle health and cell adhesion. These data also suggest that eNMES finely tunes the ECM, and any interference, such as overexpression of a cell adhesion protein, may negatively disrupt muscle's response to stimulation.

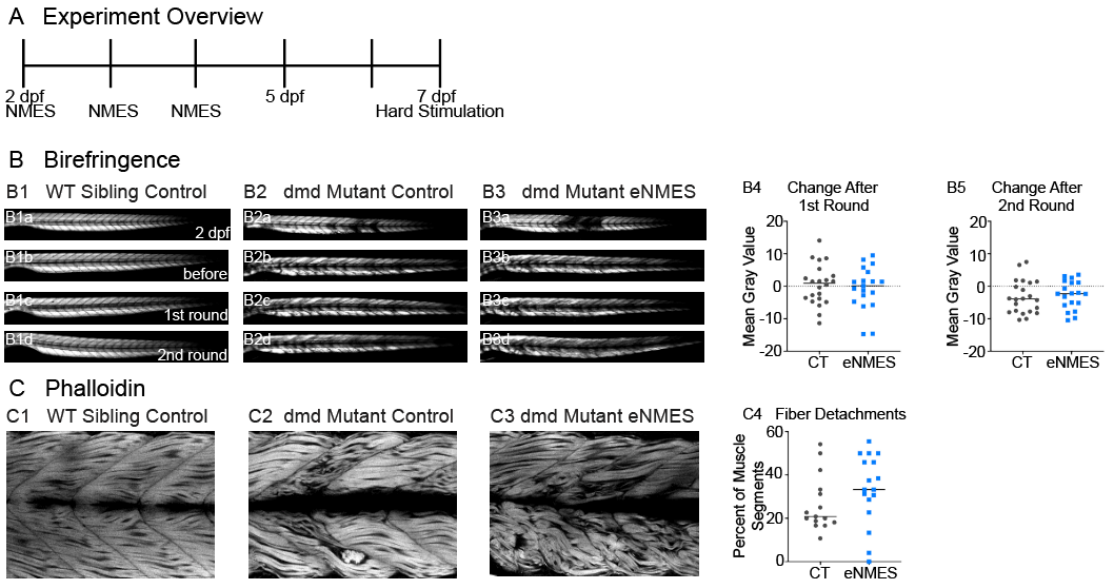

Figure 12: Paxillin overexpression decreases muscle resilience in *dmd* mutants.

(A) Experiment overview. Transgenic *dmd* mutants that overexpression paxillin completed 3 sessions of NMES at 2, 3, and 4 dpf. On 7 dpf, *dmd* mutants completed two back-to-back sessions of the cell adhesion stimulation paradigm. (B) Birefringence images were taken at 2 dpf, before the first session and after the first and second sessions of the hard stimulation. (B1) No visible changes in birefringence are observed in WT siblings after the two stimulation sessions. (B2) For *dmd* mutant controls, the first round of stimulation did not result in visible changes to birefringence (B2c) but, after the second round, new areas of muscle degeneration are visible (B2d). Similarly, in *dmd* mutants that completed three sessions of eNMES, the first (B3c) round of stimulation did not result in visible changes to birefringence but the second round (B3d) resulted in significant fiber damage. (B4, B5) Change in birefringence from before to after the first round (B4) and second (B5) of stimulation suggests that overexpression of paxillin does not protect the muscle from damage and may negatively affect its resilience. (C) Phalloidin was used to visualize individual muscle fibers. (C1a) Representative image of a WT sibling control demonstrates healthy, organized muscle fibers and myotomes. (C2a) Representative image of a *dmd* mutant control highlights some wavy muscle fibers with few fiber detachments. (C3a) Representative image of a *dmd* mutant that completed eNMES demonstrates vast muscle

disorganization and detached fibers. (C4) The percent of muscle segments with detached fibers following the hard stimulation is increased, but not significantly, in *dmd* mutants that complete eNMES training compared to *dmd* mutant controls. A muscle segment is defined as half of a myotome. All data were analyzed using two-sided t tests.

5.3.9 Genes in Our RNAseq Data Correspond With Those Identified in Pathway-Based Approaches for Developing Therapies for DMD

We next asked whether differentially expressed genes in our RNAseq datasets coincide with those being investigated as potential therapeutic targets in pre-clinical models. Immediately, we found three genes of interest: heme oxygenase 1a (*hmox1a*), inducible nitric oxide synthase 2a (*nos2a*), and beta-1,3-N-acetylglucosaminyltransferase 3 (*b3gnt3*) (Figure 13). These three genes are either being targeted directly or share unique features with those under investigation. A discussion of their current roles in DMD and how eNMES may initiate these same roles is provided below.

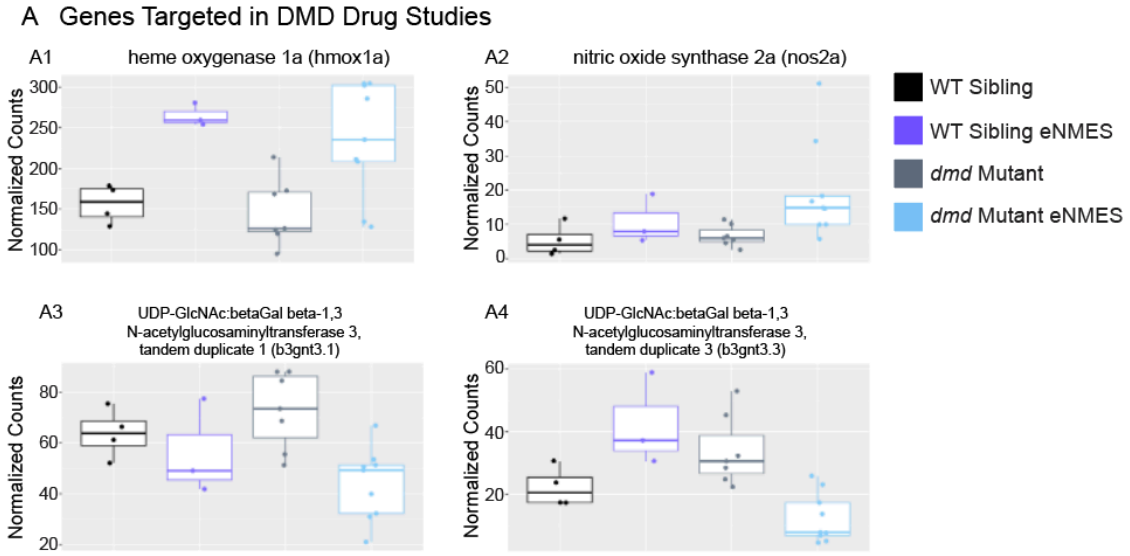

Figure 13: Potential genes that may be initiating the beneficial effects in muscle structure and function coincide with those identified in DMD drug studies.

Genes targeted in DMD drug studies. We identified two genes, hmox1a (A1) and nos2a (A2), that were significantly upregulated in *dmd* mutants following eNMES, and have been identified

as potential drug targets in pre-clinical trials to ameliorate disease progression in DMD. (A3 – A4) We also identified two genes, b3gnt3.1 (A3) and b3gnt3.3 (A4), with glycosyltransferase activity that is share to those responsible for the glycosylation of alpha-dystroglycan, which is another therapeutic target for DMD.

5.3.9.1 Sildenafil Citrate Targets NOS and HMOX1 and Improves DMD Phenotype

Sildenafil citrate is a phosphodiesterase-5 inhibitor that catalyzes the breakdown of cGMP, which is the primary player in smooth muscle relaxation [471]. Sildenafil citrate was initially introduced as a potential therapy for DMD due to its role as a potent vasodilator and its ability to enhance nitric oxide (NO) signaling. In dystrophic muscle, NO production is significantly reduced as a consequence of the mis-localization of neuronal nitric oxide synthase (nNOS) at the sarcolemma. Specifically, the absence of dystrophin disrupts the recruitment of nNOS to the sarcolemma, and therefore, negatively affects NO production [472]. Ultimately, the reduction in NO leads to functional ischemia [473–477] due to persistent vasoconstriction. Additionally, the lack of nNOS results in hyper-nitrosylation of ryanodine receptors, which causes a persistent Ca^{+2} leak [478]. Both of these events result in muscle damage, reduced force production and contraction-induced injury [475,476]. Numerous studies have demonstrated positive effects of the administration of sildenafil citrate on respiratory [479] and cardiac dysfunction [480–482], as well as sarcolemmal integrity and muscle fibrosis in the diaphragm muscles of mdx mice [479]. Further, sildenafil citrate was shown to reduce muscle damage following a single bout of downhill running and improve exercise performance in these mice, possibly through enhanced microvascular function [483]. Similarly, studies have shown that sildenafil citrate ameliorates the *dmd* phenotype in zebrafish and enhances survival [484,485]. These positive results have led to clinical trials in humans [486]. Notably, two genes targeted by sildenafil citrate, *nos2a* and *hmox1a*, are significantly upregulated following eNMES in *dmd* mutants (Figure 13A1 and A2).

5.3.9.2 HMOX1 is a Strong Therapeutic Target for DMD

HMOX1 is an anti-inflammatory and cytoprotective enzyme that attenuates both oxidative stress and inflammatory reaction, and increases cell survival [487]. Kawahara and colleagues (2014) [485] identified HMOX1 as a target of sildenafil citrate in zebrafish, demonstrating a second mechanism in which sildenafil citrate elicits beneficial effects on dystrophic muscle. Specifically, overexpression of HMOX1 significantly reduced the ability to distinguish *dmd* mutants from wild-type siblings using birefringence, indicating improved muscle structure and fewer muscle detachments. More importantly, though, overexpression of HMOX1 significantly extended survival in these zebrafish. Conversely, by administrating a morpholino targeting the *hmox1* transcript, these improvements were no longer observed. Similarly, in mdx mice, pharmacological inhibition or genetic ablation of *hmox1* aggravated muscle damage and inflammation, and severely impaired exercise capacity compared to control mdx mice [488]. HMOX1 has been shown to play numerous roles in the body, including the regulation of blood vessel formation and angiogenesis as well as muscle regeneration [489,490]. In regards to muscle regeneration, the timing of hmox1 expression is critical. Specifically, short-term expression of hmox1 promotes myoblast proliferation and subsequent muscle regeneration [489], but long-term expression inhibits myoblast differentiation and negatively affects regeneration [491]. Further, in hmox1-deficient satellite cells, higher activation and proliferation rates are observed following injury, suggesting that hmox1 may prevent exhaustion of the satellite cell niche [490]. Similarly, enhanced activation and differentiation is observed in satellite cells isolated from mdx-hmox1 double knockout mice, but satellite cell activity was normalized by supplementing cells with carbon monoxide, which is the product of HMOX1 activity [488]. Lastly, HMOX1 may play a protective role from oxidative stress by regulating mitochondrial quality and influencing the processes of biogenesis, dynamics, and mitophagy, especially in the cardiac muscle [492,493]. In our *dmd* mutants and wild-type siblings, eNMES significantly increased *hmox1a* expression compared to their respective controls (Figure 13A1), suggesting

a potential role for heme oxygenase signaling in eliciting the beneficial effects of eNMES on muscle structure, function, and survival. Preliminary data suggest that *dmd* mutants have impaired mitochondrial activity prior to disease onset (data not shown). Additionally, eNMES increases mitochondrial copy number at 8 dpf (data not shown). From these data, combined with our time-lapse analyses suggesting improved regeneration, we hypothesize that eNMES reduces oxidative stress by improving mitochondrial function and this could improve regeneration and muscle function. Future experiments should test whether eNMES and HMOX1 improve angiogenesis, mitochondrial activity, and/or regenerative capacities in *dmd* mutants.

5.3.9.3 Role of iNOS in DMD Pathology is Not Well Understood

nNOS is the principle isoform, or isozyme, expressed in skeletal muscle and has been extensively studied in DMD research. Transgenic expression of nNOS in the mdx mouse normalized NO production and reduced the occurrence of disease pathology, including the number of centrally located nuclei, inflammation, variability in muscle fiber size and the amount of sarcolemmal damage [274]. Similar results, including reduced fibrosis and increased life-span, were obtained in the mdx-utrophin double knockout mice [494]. Conversely, nNOS deficiency in mdx muscle exacerbated disease pathology, and it was hypothesized that disrupted blood flow and/or angiogenesis were the underlying mechanisms leading to this phenotype [126,495]. The role of iNOS, however, as a potential target for improving the dystrophic phenotype is less studied [496–498]. Inducible NOS is upregulated in DMD muscle fibers [496,498], suggesting a potential compensatory mechanism for maintaining homeostatic levels of NO [496]. Inducible NOS is also upregulated in infiltrating macrophages responsible for NO-dependent lysis of muscle fibers [497,499]. These studies suggest that iNOS-expressing macrophages may accelerate inflammation and disease pathology in dystrophic muscle. Conversely, it was recently shown that iNOS is required for effective muscle regeneration following acute injury in healthy muscle and that iNOS-derived NO plays a non-redundant role in skeletal muscle repair by regulating myogenic precursor cell function and shaping the

inflammatory infiltrate [500]. Surprisingly, healthy fast-twitch muscles subjected to electrical stimulation exhibit enhanced vasodilation via the NO-cGMP cascade [501,502], but whether nNOS or iNOS is responsible for the production of NO has yet to be determined. Therefore, the increased expression of *nos2a* transcript in *dmd* mutants following eNMES (Figure 13A2) should be investigated further to unravel its potential role in eliciting the positive benefits observed in muscle structure, function and survival. Specifically, is the upregulation in iNOS after eNMES supporting regeneration by regulating satellite cell activation or is iNOS maintaining homeostatic NO levels that support improved muscle function?

5.3.9.4 Glycosylation Events are Emerging as Major Players in Muscular Dystrophy Research

Mutations in proteins responsible for glycosylation and the production of glycosidic linkages are responsible for multiple types of muscular dystrophy [503,504]. Additionally, these proteins are also emerging as potential therapeutic targets for various muscular dystrophies, including DMD, since many of these proteins target α-dystroglycan and enhance its ability to bind to ECM ligands [503,504]. In our RNAseq data, two isoforms of β-1,3-N-acetylglucosaminyltransferase 3 (B3GNT3) are downregulated following eNMES in *dmd* mutants, including b3gnt3.1 and b3gnt3.3 (Figure 13A3 and A4). Currently, there are no studies linking these proteins to skeletal muscle health or neuromuscular diseases. However, their similarity with two well-established proteins in muscular dystrophy research warrants further discussion and future experiments to unravel their potential roles.

5.3.9.5 B3GNT3 and B3GNT1 Synthesize the Same Disaccharide

The B3GNT1 gene encodes a type II transmembrane protein essential for the synthesis of poly-N-acetyllactosamine residues. Interestingly, mutations in *b3gnt1* gene result in Walker-Warburg Syndrome, which is the most severe clinical form of secondary dystroglycanopathies [505]. Secondary dystroglycanopathies are a group of muscular dystrophies caused by abnormal glycosylation of α-dystroglycan. Knockdown of *b3gnt1* in zebrafish results in skeletal

muscle defects, including disrupted MTJs, compromised structural integrity, as well as reduced α-dystroglycan expression [505]. Studies have proposed that B3GNT1 forms a complex with LARGE and this interaction is required for LARGE's glycosyltransferase activity, especially the laminin-binding glycans on α-dystroglycan [506–508]. Interestingly, mutations in the *Large* gene also result in secondary dystroglycanopathy. Therefore, the significance of downregulating *b3gnt3.1* and *b3gnt3.3* following eNMES should be evaluated, especially to determine whether this protein plays an important role in glycosylation or cell-ECM interactions. Additionally, since glycosidic linkages are important for cell-adhesion, we further question how downregulating key ECM proteins following eNMES improves cell adhesion and allows for improvements in muscle function and survival.

5.3.9.6 B4GALNT2 is a Targeted Therapy for DMD

Similar to B3GNT1, the B4GALNT2 gene encodes a type II transmembrane protein essential for the synthesis of N-acetylgalactosamine residue, which is responsible for glycosylating a small number of glycoproteins, including α-dystroglycan [291,509]. More importantly, though, B4GALNT2 is confined to the neuromuscular junction in adult animals [509]. The B4GALNT2 (formerly GALGT2) protein plays an important role in improving DMD muscle phenotype [291,293,510,511] and is now undergoing clinical trials. B4GALNT2 is a great example for highlighting the fine balance in protein expression in muscle health. Specifically, in healthy muscle fibers, transgenic overexpression of B4GALNT2 in extra-synaptic regions dramatically reduced muscle fiber diameter and increased satellite cell activation [509]. Additionally, these muscle fibers exhibited significantly reduced numbers of secondary folds at the NMJ that were often misaligned with active zones as well as mis-localization of critical synaptic proteins, including laminin α4 and α5, utrophin and NCAM [509]. However, overexpression of B4GALNT2 in mdx muscle from embryonic time points onward is extremely effective at delaying the onset of dystrophy [291]. These same effects are also observed with

postnatal overexpression, delaying muscle pathology up to 18 months of age [510]. Early embryonic expression of B4GALNT2 increased the expression of utrophin and many dystrophin-associated proteins, including dystroglycan, sarcoglycans, and dystrobrevins along the length of the muscle fibers in mdx mice [291]. These improvements translated to protection from eccentric contraction-induced injury in mdx mice [293]. Interestingly, postnatal overexpression of B4GALNT2 may or may not require utrophin or α-dystroglycan to initiate the positive benefits on muscle health [510,511]. These data further support the idea that diseased muscle responds differently to treatments, whether it is a pharmacological or non-pharmacological intervention. Again, while there is no direct evidence establishing an interaction between or overlapping role of B3GNT3 and B4GALNT2, further investigations should be conducted to evaluate the significance of its downregulation following eNMES, especially since glycosylation proteins demonstrate a significant impact on skeletal muscle health and disease progression, and may require precise dosing to elicit beneficial versus detrimental effects.

5.4 Perspective

Basic fundamental studies are necessary to elucidate both the positive and negative physiological adaptations at the molecular, cellular, and tissue levels to resistance training and inactivity in dystrophic muscle. Our results demonstrate that *dmd* mutants play an integral role in understanding neuromuscular plasticity in dystrophic muscle. Specifically, by employing the zebrafish model to understand how eNMES impacts dystrophic muscle we have identified numerous potential mechanisms for improving muscle structure and function in dystrophic muscle. The data presented above demonstrate that eNMES positively benefits disease progression by increasing sarcomere lengths, improving muscle nuclei health, and creating an environment that supports regeneration. RNAseq data identify potential molecular mechanisms that may allow us to see these improvements, and often these mechanisms are simply restoring gene expression levels back to wild-type levels.

Re-evaluating the impact of NMES on the progression of DMD is critical for three reasons: (1) there are still extremely limited gene therapies, (2) inactivity negatively impacts disease progression, and (3) when an effective gene therapy is available, the next step will be to strengthen these muscles. Therefore, having an established NMES training program that improves muscle health is highly beneficial as it creates a starting point for when these gene therapies become available. The results from this study demonstrate that eNMES improves muscle health and is better for disease progression in *dmd* mutants, and that the zebrafish model is an extremely valuable tool in elucidating the mechanisms of skeletal muscle plasticity in healthy and diseased muscle.

CHAPTER 6

ANSWERING THE UNKNOWNS: HOW CAN WE LEVERAGE ZEBRAFISH TO UNDERSTAND NEUROMUSCULAR PLASTICITY?

6.1 Summary

The experiments conducted within this dissertation demonstrate that

- The zebrafish model for DMD exhibits phenotypic variation in disease progression.
- Periods of inactivity are extremely detrimental to dmd muscle health and survival.
- NMES initiates changes in gene expression in wild-type siblings, indicating that the zebrafish model is a valuable model to study skeletal muscle plasticity.
- Endurance NMES positively benefits muscle health, function, and survival in *dmd* mutants, and these changes are accompanied by improvements in NMJ abundance, nuclear shape and size, and sarcomere lengths.
- *Dmd* mutants respond to NMES differently than wild-type siblings, indicating that healthy and diseased muscle use different mechanisms to maintain homeostasis.

We created an experimental design that leverages the power of the zebrafish model's ability to perform in-vivo analyses of numerous components of organismal health across time in individual zebrafish. Ultimately, this design should be applied to pre-clinical drug studies for various zebrafish models of muscular dystrophy as it provides a more comprehensive understanding of the impacts an intervention may have immediately and across time. Further, no studies to our knowledge have established zebrafish as a model for studying NMES. By establishing zebrafish as a model for studying NMES, we can conduct comprehensive analyses at the functional, structural, and molecular levels using a well-controlled experimental set-up with high power analyses. These analyses will provide a more in depth understanding of the

effects of NMES on skeletal muscle with the potential of unveiling new mechanisms and key components in muscle growth. Most importantly, though, these findings indicate that the zebrafish model is a valuable tool for studying skeletal muscle plasticity.

6.2 How Can We Leverage Zebrafish to Understand Neuromuscular Plasticity?

6.2.1 Elucidate Mechanisms for Disease Variation and Response to Interventions

No two individuals are alike. This statement is easily accepted when discussing the human population but it is most often refuted when discussing animal models, such as the mouse and zebrafish. While humans, mice and zebrafish are all very different from each other in their size and biomechanics, it is possible that clinical trials, especially for muscular dystrophies, are less successful because researchers tend to not address the possibility of variation in inbred organisms.

The implications of variation in disease progression are not fully understood but make it difficult to predict response to potential treatments. As demonstrated in Chapter 2, we see two visibly and quantitatively distinct phenotypes at disease onset in our *dmd* mutants. We see a mild phenotype, where very few muscle segments have visible signs of dystrophy, and a severe phenotype, where multiple muscle segments have muscle fiber detachments and disorganized fibers. Additionally, we see that in our transgenic zebrafish, which harbor the same point-mutation, disease onset is delayed from 2 dpf to 3 dpf but the same mild and severe phenotypes are still present. This variation at disease onset is extremely important to be aware of since disease progression, especially in the first three days after disease onset, is different. Specifically, mild *dmd* mutants are degenerating while severe *dmd* mutants are regenerating. Even though mild and severe mutants arrive at the same muscle structure at 8 dpf, their initial severity level continues to affect their muscle function. Further studies will determine whether initial disease severity also affects survival.

Studies have identified disease modifiers in the human population, and these genes correlate with severity and muscle function, suggesting that our *dmd* mutants may also harbor

disease modifiers. We performed a preliminary investigation using RNAseq data from the eNMES experiment. Since we paired the zebrafish based on their birefringence at disease onset, we were able to compare differentially expressed genes in mild versus severe *dmd* mutants. To perform this analysis, we combined all of the mild replicates, regardless if they were in the control or eNMES group, into an analysis group (n = 9 replicates), and combined all of the severe replicates, regardless if they were in the control or eNMES group, into another analysis group (n = 7 replicates), and compare these two groups directly. Overall 76 genes were statistically and biologically significant in their increase or decrease between mild and severe mutants. These genes were associated with multiple GO terms, most notably are those associated with memory and learning (or more broadly neurological) and the regulation of transcription by RNA polymerase II. Two genes that immediately piqued our interest were *npas4*, which regulates gene transcription for genes controlling inhibitory synapse development and plasticity as well as *cdkn1a*, which stimulates protein breakdown and inhibits anabolic signaling, protein synthesis, and PGC1-alpha expression. Both were decreased in severe *dmd* mutants. Further, *klf2a* was decreased in severe mutants compared to mild mutants while *il1b* and *cd83* were upregulated. Interestingly, *klf2a* is involved in NO biosynthesis process while *il1b* and *cd83* are involved in the immune response. While these data are preliminary and represent only a snapshot in disease progression, they suggest that the zebrafish model may be a great model for studying variation and the underlying mechanisms of variation in disease.

To better understand neuromuscular plasticity in *dmd* muscle, future studies should look at gene expression changes at 2, 5, and 8 dpf, since these time points are found to be most critical in disease progression for mild versus severe *dmd* mutants. Differentially expressed genes could unveil potential biomarkers for neuromuscular plasticity and their potential roles in muscle structure, function and survival. Most importantly, though, these data could be valuable when evaluating pharmacological interventions as some may have differential effects based on the current expression levels of the targeted proteins in mild versus severe *dmd* mutants.

Combined with the potential biomarker data, it may be possible to predict responders from non-responders or create a drug program that targets specific genes at certain times depending on the disease stage.

6.2.2 Model Inactivity and Exercise to Unravel the Delicate Equilibrium in Diseased Muscle

Zebrafish have been used to study various components of the exercise response [512–515] as well as the impact of mechanical loading on development and tissue architecture [514,516,517]. In adult zebrafish, swimming at an optimal speed for 6 hours per day for 20 days significantly increased muscle fiber cross-sectional area, perimeter, and density, and promoted capillarization within the muscle [512]. These adaptations to swim training were also observed at the gene expression level. Specifically, swim training modulated the expression of genes involved in the activation of neuromuscular communication, excitation-contraction coupling, sarcomere contraction, cytoskeletal transmission of contractile force to the sarcolemma, and ECM remodeling [512]. Genes involved in muscle growth and development, angiogenesis, metabolism, inflammation, and protein synthesis and degradation were also altered by swim training [512]. Lastly, adult swim training increased the expression of genes involved in generating the slow muscle fiber phenotype [516]. Similarly, zebrafish larvae demonstrate these same adaptations to swim training [513]. Beginning at 5 dpf, zebrafish completed three 3-hour training sessions each day for up to 10 days. Following swim training, qPCR, in situ hybridization and whole genome microarray analyses were performed, and data suggest that molecular adaptations occurred in the brain, kidneys, pancreas, intestines and skeletal muscle. Molecular changes in the gastrointestinal system suggest that larvae were able to physiologically adapt to the increasing energy demands of the active muscles. Most importantly, though, zebrafish larvae exhibited molecular changes that support muscle growth and shift in muscle fiber types to support aerobic training. Most importantly, growth and survival were not affected by swim training. Collectively, these data support the idea that zebrafish are a valuable model for assessing the immediate and long-term physiological effects of aerobic exercise. In

addition to being a valuable model for aerobic exercise, we believe zebrafish are exceptional animals for elucidating mechanisms of neuromuscular plasticity in response to inactivity and NMES, especially in healthy and diseased muscle.

NMES allows us to employ a concrete definition of exercise that can easily translate across studies and across animal models. In Chapter 4, we explored how four NMES paradigms influence components of muscle structure, function and survival and in Chapter 5, we explored potential mechanisms that could lead to improvements in all three of these components in response to only one NMES paradigm. There are numerous questions that remain unanswered, such as how NMES improves structure but not function, or how NMES negatively affects function but enhances survival. Performing additional analyses from Chapter 5 in *dmd* mutants that underwent hypertrophy, strength and power NMES could help define the delicate equilibrium we observe for neuromuscular plasticity in *dmd* mutants.

6.2.3 Understand the Importance of Time in Neuromuscular Plasticity

We created a high-throughput system to test the effects of electrical stimulation on numerous components of muscle health but focused solely on a single time point, which is 8 dpf. We know that critical changes occur in *dmd* muscle from disease onset to this point. Thus, it is important to look at additional time points in order to paint a better picture of how *dmd* mutants arrive at this 8 dpf stage. Specifically, we have the ability to perform live SHG imaging to elucidate changes in sarcomeres during and after NMES and utilize transgenic zebrafish harboring fluorescent markers for pre- and post-synaptic proteins to monitor changes in NMJ distributions. Additional confocal time-lapse analyses using our transgenic fish will also help capture critical periods in which the muscle's response to NMES is decided.

The ECM is highly dynamic and is constantly responding to signals from outside the cell as well as to signals from inside the cell. In muscle, the ECM incorporates these signals to provide a scaffold that supports regeneration or fibrosis to prevent further damage. Our RNAseq data suggest that ECM remodeling is critical to *dmd* mutant phenotype and response to

eNMES. Unfortunately, though, a single measure of gene expression at 8 dpf, does not allow us to elucidate how the ECM responds to eNMES and if this response is the same immediately following NMES versus three days post-NMES. In most exercise studies, gene expression is evaluated at multiple time points after exercise to capture the evolving ECM dynamics. Based on our taco time-lapse analysis, there is a critical period between 5 and 6 dpf where *dmd* mutant controls are slow to respond to damaged muscle segments while *dmd* mutants that underwent eNMES respond to and repair the damage. Evaluating gene expression during these time points could shed light on what determines the fate of the ECM. Ultimately, these could identify therapeutic targets that may support improvements in structure, function, and survival.

6.2.4 Target Newly Identified Genes to Understand Their Roles in Improving Muscle Structure, Function, and Survival in *dmd* Mutants

Our RNAseq data provide us with a foundation to begin testing how certain genes influence neuromuscular plasticity, especially in response to eNMES. First, we must confirm that these genes and their respective proteins are differentially expressed using qPCR and Western blot. Additionally, we need to identify where these genes are being expressed using in-situ hybridization. Once these data are confirmed, the next step is to perform studies that examine how manipulating their expression impacts eNMES-induced benefits in *dmd* muscle. For example, 1400W dihydrochloride is a potent, highly selective iNOS inhibitor. Our data demonstrate that *nos2a* is significantly upregulated in *dmd* mutants following eNMES. By administering this drug during the training period, we would be able to determine whether iNOS plays a fundamental role in eliciting the benefits observed with eNMES. Specifically, if eNMES is no longer beneficial, we know that *nos2a* expression is important and additional experiments can then be performed to determine the underlying mechanisms in which iNOS is driving these improvements. Also, if *nos2a* is responsible, we can perform overexpression studies with our inactivity paradigm to determine whether iNOS preserves muscle resilience. Similar studies can be performed for HMOX1.

6.3 Moving Forward

The purpose of this project stemmed from questions concerning the limitations of previous studies addressing the effects of exercise in dystrophic muscle and the difficulties of accepting inactivity as the best recommendation for care. Disease-modifying therapies are within the drug development pipeline for DMD. However, we are still unsure what the underlying mechanisms for neuromuscular plasticity in dystrophic muscle are and how these muscles may respond to changes in the demands imposed upon it, especially after the restoration of dystrophin. We believe that identifying these basic mechanisms is a crucial first step for evaluating potential therapies and driving research forward. The long-term impact of this project is the establishment of a model system that provides a sustained and powerful influence within the field of neuromuscular plasticity in healthy versus diseased muscle. It is likely that the mechanisms in which our NMES programs benefit muscle health in *dmd* muscle may have therapeutic potential in non-dystrophic muscle wasting conditions, including cardiovascular disease, chronic obstructive pulmonary disease, diabetes, cancer, and long-term inactivity due to trauma. Therefore, we believe that our study will help guide future efforts in the more time- and resource-intensive mouse model studies and human patient trials.

REFERENCES

1. Mukund K, Subramaniam S. Skeletal muscle: A review of molecular structure and function, in health and disease. WIREs Syst Biol Med. 2019; doi:10.1002/wsbm.1462

2. Pedersen BK. Muscles and their myokines. Journal of Experimental Biology. 2011;214: 337–346. doi:10.1242/jeb.048074

3. Pedersen BK, Åkerström TCA, Nielsen AR, Fischer CP. Role of myokines in exercise and metabolism. Journal of Applied Physiology. 2007;103: 1093–1098. doi:10.1152/japplphysiol.00080.2007

4. Leal LG, Lopes MA, Batista ML. Physical Exercise-Induced Myokines and Muscle-Adipose Tissue Crosstalk: A Review of Current Knowledge and the Implications for Health and Metabolic Diseases. Front Physiol. 2018;9: 1307. doi:10.3389/fphys.2018.01307

5. Pillon NJ, Krook A. Innate immune receptors in skeletal muscle metabolism. Experimental Cell Research. 2017;360: 47–54. doi:10.1016/j.yexcr.2017.02.035

6. Febbraio MA, Pedersen BK. Contraction-Induced Myokine Production and Release: Is Skeletal Muscle an Endocrine Organ?: Exercise and Sport Sciences Reviews. 2005;33: 114–119. doi:10.1097/00003677-200507000-00003

7. Schnyder S, Handschin C. Skeletal muscle as an endocrine organ: PGC-1α, myokines and exercise. Bone. 2015;80: 115–125. doi:10.1016/j.bone.2015.02.008

8. Pedersen BK, Febbraio M. Muscle-derived interleukin-6: a possible link between skeletal muscle, adipose tissue, liver, and brain. Brain Behav Immun. 2005;19: 371–376. doi:10.1016/j.bbi.2005.04.008

9. Frontera WR, Ochala J. Skeletal Muscle: A Brief Review of Structure and Function. Calcif Tissue Int. 2015;96: 183–195. doi:10.1007/s00223-014-9915-y

10. Yan Z, Okutsu M, Akhtar YN, Lira VA. Regulation of exercise-induced fiber type transformation, mitochondrial biogenesis, and angiogenesis in skeletal muscle. Journal of Applied Physiology. 2011;110: 264–274. doi:10.1152/japplphysiol.00993.2010

11. Margolis LM, Rivas DA. Implications of Exercise Training and Distribution of Protein Intake on Molecular Processes Regulating Skeletal Muscle Plasticity. Calcif Tissue Int. 2015;96: 211–221. doi:10.1007/s00223-014-9921-0

12. Knierim J. Motor Units and Muscle Receptors (Section 3, Chapter 1) Neuroscience Online: An Electronic Textbook for the Neurosciences | Department of Neurobiology and Anatomy - The University of Texas Medical School at Houston. Available: https://nba.uth.tmc.edu/neuroscience/m/s3/chapter01.html

13. Folker E, Baylies M. Nuclear positioning in muscle development and disease. Front Physiol. 2013;4. doi:10.3389/fphys.2013.00363

14. Dahl R, Larsen S, Dohlmann TL, Qvortrup K, Helge JW, Dela F, et al. Three-dimensional reconstruction of the human skeletal muscle mitochondrial network as a tool to assess mitochondrial content and structural organization. Acta Physiologica. 2015;213: 145–155. doi:10.1111/apha.12289

15. Denker A, Rizzoli SO. Synaptic Vesicle Pools: An Update. Front Synaptic Neurosci. 2010;2. doi:10.3389/fnsyn.2010.00135

16. Rizzoli SO, Betz WJ. Synaptic vesicle pools. Nature Reviews Neuroscience. 2005;6: 57-.

17. Nishimune H. Active zones of mammalian neuromuscular junctions: formation, density, and aging. Annals of the New York Academy of Sciences. 2012;1274: 24–32. doi:10.1111/j.1749-6632.2012.06836.x

18. Kramer IjM. Chapter 4 - Cholinergic Signaling and Muscle Contraction. In: Kramer IjM, editor. Signal Transduction (Third Edition). Boston: Academic Press; 2016. pp. 263–327. doi:10.1016/B978-0-12-394803-8.00004-8

19. Jayasinghe ID, Launikonis BS. Three-dimensional reconstruction and analysis of the tubular system of vertebrate skeletal muscle. J Cell Sci. 2013;126: 4048–4058. doi:10.1242/jcs.131565

20. Ottenheijm CAC, Granzier H. Lifting the Nebula: Novel Insights into Skeletal Muscle Contractility. Physiology. 2010;25: 304–310. doi:10.1152/physiol.00016.2010

21. Monroy JA, Powers KL, Gilmore LA, Uyeno TA, Lindstedt SL, Nishikawa KC. What Is the Role of Titin in Active Muscle? Exercise and Sport Sciences Reviews. 2012;40: 73–78. doi:10.1097/JES.0b013e31824580c6

22. Kontrogianni-Konstantopoulos A, Ackermann MA, Bowman AL, Yap SV, Bloch RJ. Muscle Giants: Molecular Scaffolds in Sarcomerogenesis. Physiol Rev. 2009;89: 1217–1267. doi:10.1152/physrev.00017.2009

23. Xiao S, Gräter F. Molecular Basis of the Mechanical Hierarchy in Myomesin Dimers for Sarcomere Integrity. Biophysical Journal. 2014;107: 965–973. doi:10.1016/j.bpj.2014.06.043

24. Wallimann T, Eppenberger HM. Localization and function of M-line-bound creatine kinase. M-band model and creatine phosphate shuttle. Cell Muscle Motil. 1985;6: 239–285. doi:10.1007/978-1-4757-4723-2_8

25. Wallimann T, Schlösser T, Eppenberger HM. Function of M-line-bound creatine kinase as intramyofibrillar ATP regenerator at the receiving end of the phosphorylcreatine shuttle in muscle. J Biol Chem. 1984;259: 5238–5246.

26. Humphrey JD, Dufresne ER, Schwartz MA. Mechanotransduction and extracellular matrix homeostasis. Nat Rev Mol Cell Biol. 2014;15: 802–812. doi:10.1038/nrm3896

27. Grzelkowska-Kowalczyk K. The Importance of Extracellular Matrix in Skeletal Muscle Development and Function. Composition and Function of the Extracellular Matrix in the Human Body. 2016. doi:10.5772/62230

28. Aya KL, Stern R. Hyaluronan in wound healing: Rediscovering a major player. Wound Repair and Regeneration. 2014;22: 579–593. doi:10.1111/wrr.12214

29. Li Y, Li J, Zhu J, Sun B, Branca M, Tang Y, et al. Decorin Gene Transfer Promotes Muscle Cell Differentiation and Muscle Regeneration. Molecular Therapy. 2007;15: 1616–1622. doi:10.1038/sj.mt.6300250

30. Schultz GS, Wysocki A. Interactions between extracellular matrix and growth factors in wound healing. Wound Repair and Regeneration. 2009;17: 153–162. doi:10.1111/j.1524-475X.2009.00466.x

31. Gelse K, Pöschl E, Aigner T. Collagens—structure, function, and biosynthesis. Advanced Drug Delivery Reviews. 2003;55: 1531–1546. doi:10.1016/j.addr.2003.08.002

32. Gordon MK, Hahn RA. Collagens. Cell Tissue Res. 2010;339: 247–257. doi:10.1007/s00441-009-0844-4

33. Fox MA, Ho MS, Smyth N, Sanes JR. A synaptic nidogen: Developmental regulation and role of nidogen-2 at the neuromuscular junction. Neural Development. 2008;3: 24. doi:10.1186/1749-8104-3-24

34. Ho MSP, Böse K, Mokkapati S, Nischt R, Smyth N. Nidogens—Extracellular matrix linker molecules. Microscopy Research and Technique. 2008;71: 387–395. doi:10.1002/jemt.20567

35. Halper J, Kjaer M. Basic Components of Connective Tissues and Extracellular Matrix: Elastin, Fibrillin, Fibulins, Fibrinogen, Fibronectin, Laminin, Tenascins and Thrombospondins. In: Halper J, editor. Progress in Heritable Soft Connective Tissue Diseases. Dordrecht: Springer Netherlands; 2014. pp. 31–47. doi:10.1007/978-94-007-7893-1_3

36. Arpino V, Brock M, Gill SE. The role of TIMPs in regulation of extracellular matrix proteolysis. Matrix Biology. 2015;44–46: 247–254. doi:10.1016/j.matbio.2015.03.005

37. Murphy S, Ohlendieck K. The Extracellular Matrix Complexome from Skeletal Muscle. Composition and Function of the Extracellular Matrix in the Human Body. 2016. doi:10.5772/62253

38. Flaumenhaft R, Rifkin DB. Extracellular matrix regulation of growth factor and protease activity. Current Opinion in Cell Biology. 1991;3: 817–823. doi:10.1016/0955-0674(91)90055-4

39. Ervasti JM. Costameres: the Achilles' Heel of Herculean Muscle. J Biol Chem. 2003;278: 13591–13594. doi:10.1074/jbc.R200021200

40. Pardo JV, Siliciano JD, Craig SW. A vinculin-containing cortical lattice in skeletal muscle: transverse lattice elements ("costameres") mark sites of attachment between myofibrils and sarcolemma. Proc Natl Acad Sci U S A. 1983;80: 1008–1012.

41. Danowski BA, Imanaka-Yoshida K, Sanger JM, Sanger JW. Costameres are sites of force transmission to the substratum in adult rat cardiomyocytes. J Cell Biol. 1992;118: 1411–1420.

42. Bloch RJ, Gonzalez-Serratos H. Lateral Force Transmission Across Costameres in Skeletal Muscle. Exercise and Sport Sciences Reviews. 2003;31: 73–78.

43. Street SF. Lateral transmission of tension in frog myofibers: a myofibrillar network and transverse cytoskeletal connections are possible transmitters. Journal of cellular physiology. 1983;114: 346.

44. Grounds MD, Sorokin L, White J. Strength at the extracellular matrix-muscle interface. Scand J Med Sci Sports. 2005;15: 381–391. doi:10.1111/j.1600-0838.2005.00467.x

45. Ervasti JM, Ohlendieck K, Kahl SD, Gaver MG, Campbell KP. Deficiency of a glycoprotein component of the dystrophin complex in dystrophic muscle. Nature. 1990;345: 315–319. doi:10.1038/345315a0

46. Ervasti J, Campbell K. A role for the dystrophin-glycoprotein complex as a transmembrane linker between laminin and actin. The Journal of Cell Biology. 1993;122: 809–823. doi:10.1083/jcb.122.4.809

47. Constantin B. Dystrophin complex functions as a scaffold for signalling proteins. Biochimica et Biophysica Acta (BBA) - Biomembranes. 2014;1838: 635–642. doi:10.1016/j.bbamem.2013.08.023

48. Gao Q, McNally, EM. The Dystrophin Complex- structure, function and implications for therapy. Compr Physiol. 2015;5:1223-1239. doi:10.1002/cphy.c140048

49. Staub V, Campbell KP. Muscular dystrophies and the dystrophin-glycoprotein complex. Current Opinion in Neurology. 1997;10: 168-175. doi: 10.1097/00019052-199704000-0016

50. Sunada Y, Campbell KP. Dystrophin-glycoprotein complex: molecular organization and critical roles in skeletal muscle. Current Opinion in Neurology. 1995;8: 279-384

51. Winder SJ, Gibson TJ, Kendrick-Jones J. Dystrophin and utrophin: the missing links! FEBS Letters. 1995;369: 27–33. doi:10.1016/0014-5793(95)00398-S

52. Way M, Pope B, Cross RA, Kendrick-Jones J, Weeds AG. Expression of the N-terminal domain of dystrophin in E. coli and demonstration of binding to F-actin. FEBS Letters. 1992;301: 243–245. doi:10.1016/0014-5793(92)80249-G

53. Stone MR, O'Neill A, Catino D, Bloch RJ. Specific Interaction of the Actin-binding Domain of Dystrophin with Intermediate Filaments Containing Keratin 19. Mol Biol Cell. 2005;16: 4280–4293. doi:10.1091/mbc.E05-02-0112

54. Stone MR, O'Neill A, Lovering RM, Strong J, Resneck WG, Reed PW, et al. Absence of keratin 19 in mice causes skeletal myopathy with mitochondrial and sarcolemmal reorganization. Journal of Cell Science. 2007;120: 3999–4008. doi:10.1242/jcs.009241

55. Koenig M, Kunkel LM. Detailed analysis of the repeat domain of dystrophin reveals four potential hinge segments that may confer flexibility. J Biol Chem. 1990;265: 4560–4566.

56. Amann KJ, Renley BA, Ervasti JM. A Cluster of Basic Repeats in the Dystrophin Rod Domain Binds F-actin through an Electrostatic Interaction. J Biol Chem. 1998;273: 28419–28423. doi:10.1074/jbc.273.43.28419

57. Belanto JJ, Mader TL, Eckhoff MD, Strandjord DM, Banks GB, Gardner MK, et al. Microtubule binding distinguishes dystrophin from utrophin. Proc Natl Acad Sci U S A. 2014;111: 5723–5728. doi:10.1073/pnas.1323842111

58. Prins KW, Humston JL, Mehta A, Tate V, Ralston E, Ervasti JM. Dystrophin is a microtubule-associated protein. J Cell Biol. 2009;186: 363–369. doi:10.1083/jcb.200905048

59. Rybakova IN, Patel JR, Ervasti JM. The Dystrophin Complex Forms a Mechanically Strong Link between the Sarcolemma and Costameric Actin. J Cell Biol. 2000;150: 1209–1214.

60. Bork P, Sudol M. The WW domain: a signalling site in dystrophin? Trends in Biochemical Sciences. 1994;19: 531–533. doi:10.1016/0968-0004(94)90053-1

61. Koenig M, Monaco AP, Kunkel LM. The complete sequence of dystrophin predicts a rod-shaped cytoskeletal protein. Cell. 1988;53: 219–228. doi:10.1016/0092-8674(88)90383-2

62. Ponting CP, Blake DJ, Davies KE, Kendrick-Jones J, Winder SJ. ZZ and TAZ: new putative zinc fingers in dystrophin and other proteins. Trends Biochem Sci. 1996;21: 11–13.

63. Anderson JT, Rogers RP, Jarrett HW. Ca-Calmodulin Binds to the Carboxyl-terminal Domain of Dystrophin. J Biol Chem. 1996;271: 6605–6610. doi:10.1074/jbc.271.12.6605

64. Ayalon G, Davis JQ, Scotland PB, Bennett V. An ankyrin-based mechanism for functional organization of dystrophin and dystroglycan. Cell. 2008;135: 1189–1200. doi:10.1016/j.cell.2008.10.018

65. Bhosle RC, Michele DE, Campbell KP, Li Z, Robson RM. Interactions of intermediate filament protein synemin with dystrophin and utrophin. Biochem Biophys Res Commun. 2006;346: 768–777. doi:10.1016/j.bbrc.2006.05.192

66. Tinsley JM, Blake DJ, Roche A, Fairbrother U, Riss J, Byth BC, et al. Primary structure of dystrophin-related protein. Nature. 1992;360: 591–593. doi:10.1038/360591a0

67. Blake DJ, Tinsley JM, Davies KE, Knight AE, Winder SJ, Kendrick-Jones J. Coiled-coil regions in the carboxy-terminal domains of dystrophin and related proteins: potentials for protein-protein interactions. Trends Biochem Sci. 1995;20: 133–135. doi:10.1016/s0968-0004(00)88986-0

68. Sadoulet-Puccio HM, Rajala M, Kunkel LM. Dystrobrevin and dystrophin: an interaction through coiled-coil motifs. Proc Natl Acad Sci USA. 1997;94: 12413–12418. doi:10.1073/pnas.94.23.12413

69. Weller B, Karpati G, Carpenter S. Dystrophin-deficient mdx muscle fibers are preferentially vulnerable to necrosis induced by experimental lengthening contractions. Journal of the Neurological Sciences. 1990;100: 9–13. doi:10.1016/0022-510X(90)90005-8

70. Clarke MS, Khakee R, McNeil PL. Loss of cytoplasmic basic fibroblast growth factor from physiologically wounded myofibers of normal and dystrophic muscle. Journal of Cell Science. 1993;106: 121–133.

71. Cox GA, Cole NM, Matsumura K, Phelps SF, Hauschka SD, Campbell KP, et al. Overexpression of dystrophin in transgenic mdx mice eliminates dystrophic symptoms without toxicity. Nature. 1993;364: 725–729. doi:10.1038/364725a0

72. Karpati G, Carpenter S. Small-caliber skeletal muscle fibers do not suffer deleterious consequences of dystrophic gene expression. Am J Med Genet. 1986;25: 653–658. doi:10.1002/ajmg.1320250407

73. Mizuno Y. Prevention of myonecrosis in mdx mice: effect of immobilization by the local tetanus method. Brain Dev. 1992;14: 319–322. doi:10.1016/s0387-7604(12)80151-3

74. Vilquin JT, Brussee V, Asselin I, Kinoshita I, Gingras M, Tremblay JP. Evidence of mdx mouse skeletal muscle fragility in vivo by eccentric running exercise. Muscle Nerve. 1998;21: 567–576. doi:10.1002/(sici)1097-4598(199805)21:5<567::aid-mus2>3.0.co;2-6

75. Mokhtarian A, Lefaucheur JP, Even PC, Sebille A. Hindlimb immobilization applied to 21-day-old mdx mice prevents the occurrence of muscle degeneration. J Appl Physiol. 1999;86: 924–931. doi:10.1152/jappl.1999.86.3.924

76. Petrof BJ, Shrager JB, Stedman HH, Kelly AM, Sweeney HL. Dystrophin protects the sarcolemma from stresses developed during muscle contraction. Proc Natl Acad Sci USA. 1993;90: 3710–3714.

77. Moens P, Baatsen PH, Maréchal G. Increased susceptibility of EDL muscles from mdx mice to damage induced by contractions with stretch. J Muscle Res Cell Motil. 1993;14: 446–451. doi:10.1007/BF00121296

78. Le S, Yu M, Hovan L, Zhao Z, Ervasti J, Yan J. Dystrophin As A Molecular Shock Absorber. ACS Nano. 2018;12: 12140–12148. doi:10.1021/acsnano.8b05721

79. Ervasti JM, Campbell KP. A role for the dystrophin-glycoprotein complex as a transmembrane linker between laminin and actin. J Cell Biol. 1993;122: 809–823.

80. Ervasti JM, Campbell KP. Membrane organization of the dystrophin-glycoprotein complex. Cell. 1991; 66: 1121-1131. Available: http://web.mit.edu/7.61/restricted/readings/ervasti.pdf

81. Brancaccio A, Schulthess T, Gesemann M, Engel J. The N-terminal Region of α-Dystroglycan is an Autonomous Globular Domain. European Journal of Biochemistry. 1997;246: 166–172. doi:10.1111/j.1432-1033.1997.00166.x

82. Bozic D, Sciandra F, Lamba D, Brancaccio A. The Structure of the N-terminal Region of Murine Skeletal Muscle α-Dystroglycan Discloses a Modular Architecture. J Biol Chem. 2004;279: 44812–44816. doi:10.1074/jbc.C400353200

83. Bowe MA, Mendis DB, Fallon JR. The Small Leucine-Rich Repeat Proteoglycan Biglycan Binds to α-Dystroglycan and Is Upregulated in Dystrophic Muscle. J Cell Biol. 2000;148: 801–810.

84. Di Stasio E, Sciandra F, Maras B, Di Tommaso F, Petrucci TC, Giardina B, et al. Structural and Functional Analysis of the N-Terminal Extracellular Region of β-Dystroglycan. Biochemical and Biophysical Research Communications. 1999;266: 274–278. doi:10.1006/bbrc.1999.1803

85. Boffi A, Bozzi M, Sciandra F, Woellner C, Bigotti MG, Ilari A, et al. Plasticity of secondary structure in the N-terminal region of beta-dystroglycan. Biochim Biophys Acta. 2001;1546: 114–121. doi:10.1016/s0167-4838(01)00131-5

86. Suzuki A, Yoshida M, Yamamoto H, Ozawa E. Glycoprotein-binding site of dystrophin is confined to the cysteine-rich domain and the first half of the carboxy-terminal domain. FEBS Letters. 1992;308: 154–160. doi:10.1016/0014-5793(92)81265-N

87. Ishikawa-Sakurai M, Yoshida M, Imamura M, Davies KE, Ozawa E. ZZ domain is essentially required for the physiological binding of dystrophin and utrophin to β-dystroglycan. Hum Mol Genet. 2004;13: 693–702. doi:10.1093/hmg/ddh087

88. Sotgia F, Lee JK, Das K, Bedford M, Petrucci TC, Macioce P, et al. Caveolin-3 Directly Interacts with the C-terminal Tail of β-Dystroglycan IDENTIFICATION OF A CENTRAL WW-LIKE DOMAIN WITHIN CAVEOLIN FAMILY MEMBERS. J Biol Chem. 2000;275: 38048–38058. doi:10.1074/jbc.M005321200

89. Durbeej M, Larsson E, Ibraghimov-Beskrovnaya O, Roberds SL, Campbell KP, Ekblom P. Non-muscle alpha-dystroglycan is involved in epithelial development. J Cell Biol. 1995;130: 79–91. doi:10.1083/jcb.130.1.79

90. Deng W-M, Schneider M, Frock R, Castillejo-Lopez C, Gaman EA, Baumgartner S, et al. Dystroglycan is required for polarizing the epithelial cells and the oocyte in Drosophila. Development. 2003;130: 173–184. doi:10.1242/dev.00199

91. Weir ML, Oppizzi ML, Henry MD, Onishi A, Campbell KP, Bissell MJ, et al. Dystroglycan loss disrupts polarity and β-casein induction in mammary epithelial cells by perturbing laminin anchoring. Journal of Cell Science. 2006;119: 4047–4058. doi:10.1242/jcs.03103

92. Cartaud A, Coutant S, Petrucci TC, Cartaud J. Evidence for in Situ and in VitroAssociation between β-Dystroglycan and the Subsynaptic 43K Rapsyn Protein CONSEQUENCE FOR ACETYLCHOLINE RECEPTOR CLUSTERING AT THE SYNAPSE. J Biol Chem. 1998;273: 11321–11326. doi:10.1074/jbc.273.18.11321

93. Constantin B. Dystrophin complex functions as a scaffold for signalling proteins. Biochim Biophys Acta. 2014;1838: 635–642. doi:10.1016/j.bbamem.2013.08.023

94. Newey SE, Benson MA, Ponting CP, Davies KE, Blake DJ. Alternative splicing of dystrobrevin regulates the stoichiometry of syntrophin binding to the dystrophin protein complex. Curr Biol. 2000;10: 1295–1298. doi:10.1016/s0960-9822(00)00760-0

95. Newbell BJ, Anderson JT, Jarrett HW. Ca2+-calmodulin binding to mouse alpha1 syntrophin: syntrophin is also a Ca2+-binding protein. Biochemistry. 1997;36: 1295–1305. doi:10.1021/bi962452n

96. Iwata Y, Pan Y, Yoshida T, Hanada H, Shigekawa M. Alpha1-syntrophin has distinct binding sites for actin and calmodulin. FEBS Lett. 1998;423: 173–177. doi:10.1016/s0014-5793(98)00085-4

97. Okumura A, Nagai K, Okumura N. Interaction of α1-syntrophin with multiple isoforms of heterotrimeric G protein α subunits. The FEBS Journal. 2008;275: 22–33. doi:10.1111/j.1742-4658.2007.06174.x

98. Hashida-Okumura A, Okumura N, Iwamatsu A, Buijs RM, Romijn HJ, Nagai K. ␣1-Syntrophin in Rat Brain. : 7.

99. Brenman JE, Chao DS, Gee SH, McGee AW, Craven SE, Santillano DR, et al. Interaction of nitric oxide synthase with the postsynaptic density protein PSD-95 and alpha1-syntrophin mediated by PDZ domains. Cell. 1996;84: 757–767. doi:10.1016/s0092-8674(00)81053-3

100. Kameya S, Miyagoe Y, Nonaka I, Ikemoto T, Endo M, Hanaoka K, et al. α1-Syntrophin Gene Disruption Results in the Absence of Neuronal-type Nitric-oxide Synthase at the Sarcolemma but Does Not Induce Muscle Degeneration. J Biol Chem. 1999;274: 2193–2200. doi:10.1074/jbc.274.4.2193

101. Gee SH, Madhavan R, Levinson SR, Caldwell JH, Sealock R, Froehner SC. Interaction of Muscle and Brain Sodium Channels with Multiple Members of the Syntrophin Family of Dystrophin-Associated Proteins. J Neurosci. 1998;18: 128–137. doi:10.1523/JNEUROSCI.18-01-00128.1998

102. Sabourin J, Lamiche C, Vandebrouck A, Magaud C, Rivet J, Cognard C, et al. Regulation of TRPC1 and TRPC4 Cation Channels Requires an α1-Syntrophin-dependent Complex in Skeletal Mouse Myotubes. J Biol Chem. 2009;284: 36248–36261. doi:10.1074/jbc.M109.012872

103. Roberds SL, Anderson RD, Ibraghimov-Beskrovnaya O, Campbell KP. Primary structure and muscle-specific expression of the 50-kDa dystrophin-associated glycoprotein (adhalin). J Biol Chem. 1993;268: 23739–23742.

104. Lim LE, Duclos F, Broux O, Bourg N, Sunada Y, Allamand V, et al. Beta-sarcoglycan: characterization and role in limb-girdle muscular dystrophy linked to 4q12. Nat Genet. 1995;11: 257–265. doi:10.1038/ng1195-257

105. Noguchi S, McNally EM, Othmane KB, Hagiwara Y, Mizuno Y, Yoshida M, et al. Mutations in the Dystrophin-Associated Protein γ-Sarcoglycan in Chromosome 13 Muscular Dystrophy. Science. 1995;270: 819–822. doi:10.1126/science.270.5237.819

106. Nigro V, Piluso G, Belsito A, Politano L, Puca AA, Papparella S, et al. Identification of a novel sarcoglycan gene at 5q33 encoding a sarcolemmal 35 kDa glycoprotein. Hum Mol Genet. 1996;5: 1179–1186. doi:10.1093/hmg/5.8.1179

107. Crosbie RH, Lebakken CS, Holt KH, Venzke DP, Straub V, Lee JC, et al. Membrane targeting and stabilization of sarcospan is mediated by the sarcoglycan subcomplex. J Cell Biol. 1999;145: 153–165. doi:10.1083/jcb.145.1.153

108. Ozawa E, Mizuno Y, Hagiwara Y, Sasaoka T, Yoshida M. Molecular and cell biology of the sarcoglycan complex. Muscle Nerve. 2005;32: 563–576. doi:10.1002/mus.20349

109. Yoshida T, Pan Y, Hanada H, Iwata Y, Shigekawa M. Bidirectional signaling between sarcoglycans and the integrin adhesion system in cultured L6 myocytes. J Biol Chem. 1998;273: 1583–1590. doi:10.1074/jbc.273.3.1583

110. Chen J, Skinner MA, Shi W, Yu Q-C, Wildeman AG, Chan YM. The 16 kDa subunit of vacuolar H+-ATPase is a novel sarcoglycan-interacting protein. Biochim Biophys Acta. 2007;1772: 570–579. doi:10.1016/j.bbadis.2007.01.014

111. Crosbie RH, Heighway J, Venzke DP, Lee JC, Campbell KP. Sarcospan, the 25-kDa transmembrane component of the dystrophin-glycoprotein complex. J Biol Chem. 1997;272: 31221–31224. doi:10.1074/jbc.272.50.31221

112. Marshall JL, Crosbie-Watson RH. Sarcospan: a small protein with large potential for Duchenne muscular dystrophy. Skeletal Muscle. 2013;3: 1. doi:10.1186/2044-5040-3-1

113. Miura P, Jasmin BJ. Utrophin upregulation for treating Duchenne or Becker muscular dystrophy: how close are we? Trends Mol Med. 2006;12: 122–129. doi:10.1016/j.molmed.2006.01.002

114. Fairclough RJ, Perkins KJ, Davies KE. Pharmacologically targeting the primary defect and downstream pathology in Duchenne muscular dystrophy. Curr Gene Ther. 2012;12: 206–244. doi:10.2174/156652312800840595

115. Peters MF, Adams ME, Froehner SC. Differential Association of Syntrophin Pairs with the Dystrophin Complex. J Cell Biol. 1997;138: 81–93. doi:10.1083/jcb.138.1.81

116. Sadoulet-Puccio HM, Rajala M, Kunkel LM. Dystrobrevin and dystrophin: an interaction through coiled-coil motifs. Proc Natl Acad Sci USA. 1997;94: 12413–12418. doi:10.1073/pnas.94.23.12413

117. Grady RM, Akaaboune M, Cohen AL, Maimone MM, Lichtman JW, Sanes JR. Tyrosine-phosphorylated and nonphosphorylated isoforms of α-dystrobrevin roles in skeletal muscle and its neuromuscular and myotendinous junctions. J Cell Biol. 2003;160: 741–752. doi:10.1083/jcb.200209045

118. Grady RM, Zhou H, Cunningham JM, Henry MD, Campbell KP, Sanes JR. Maturation and Maintenance of the Neuromuscular Synapse: Genetic Evidence for Roles of the Dystrophin–Glycoprotein Complex. Neuron. 2000;25: 279–293. doi:10.1016/S0896-6273(00)80894-6

119. Gingras J, Gawor M, Bernadzki KM, Grady RM, Hallock P, Glass DJ, et al. α-Dystrobrevin-1 recruits Grb2 and α-catulin to organize neurotransmitter receptors at the neuromuscular junction. J Cell Sci. 2016;129: 898–911. doi:10.1242/jcs.181180

120. Galbiati F, Lisanti MP. Caveolin-3 and Limb-Girdle Muscular Dystrophy. Landes Bioscience; 2013. Available: https://www.ncbi.nlm.nih.gov/books/NBK6073/

121. Song KS, Scherer PE, Tang Z, Okamoto T, Li S, Chafel M, et al. Expression of caveolin-3 in skeletal, cardiac, and smooth muscle cells. Caveolin-3 is a component of the sarcolemma and co-fractionates with dystrophin and dystrophin-associated glycoproteins. J Biol Chem. 1996;271: 15160–15165. doi:10.1074/jbc.271.25.15160

122. Parton RG, Way M, Zorzi N, Stang E. Caveolin-3 Associates with Developing T-tubules during Muscle Differentiation. J Cell Biol. 1997;136: 137–154.

123. Scherer PE, Lisanti MP. Association of phosphofructokinase-M with caveolin-3 in differentiated skeletal myotubes. Dynamic regulation by extracellular glucose and intracellular metabolites. J Biol Chem. 1997;272: 20698–20705. doi:10.1074/jbc.272.33.20698

124. García-Cardeña G, Martasek P, Masters BS, Skidd PM, Couet J, Li S, et al. Dissecting the interaction between nitric oxide synthase (NOS) and caveolin. Functional significance of the nos caveolin binding domain in vivo. J Biol Chem. 1997;272: 25437–25440. doi:10.1074/jbc.272.41.25437

125. Venema VJ, Ju H, Zou R, Venema RC. Interaction of neuronal nitric-oxide synthase with caveolin-3 in skeletal muscle. Identification of a novel caveolin scaffolding/inhibitory domain. J Biol Chem. 1997;272: 28187–28190. doi:10.1074/jbc.272.45.28187

126. Thomas GD, Sander M, Lau KS, Huang PL, Stull JT, Victor RG. Impaired metabolic modulation of alpha-adrenergic vasoconstriction in dystrophin-deficient skeletal muscle. Proc Natl Acad Sci USA. 1998;95: 15090–15095. doi:10.1073/pnas.95.25.15090

127. Galpin AJ, Raue U, Jemiolo B, Trappe TA, Harber MP, Minchev K, et al. Human skeletal muscle fiber type specific protein content. Anal Biochem. 2012;425: 175–182. doi:10.1016/j.ab.2012.03.018

128. Lamboley CR, Murphy RM, McKenna MJ, Lamb GD. Sarcoplasmic reticulum Ca2+ uptake and leak properties, and SERCA isoform expression, in type I and type II fibres of human skeletal muscle. J Physiol. 2014;592: 1381–1395. doi:10.1113/jphysiol.2013.269373

129. Schiaffino S, Reggiani C. Fiber Types in Mammalian Skeletal Muscles. Physiological Reviews. 2011;91: 1447–1531. doi:10.1152/physrev.00031.2010

130. Ackermann F, Waites CL, Garner CC. Presynaptic active zones in invertebrates and vertebrates. EMBO Rep. 2015;16: 923–938. doi:10.15252/embr.201540434

131. Alabi AA, Tsien RW. Perspectives on kiss-and-run: role in exocytosis, endocytosis, and neurotransmission. Annu Rev Physiol. 2013;75: 393–422. doi:10.1146/annurev-physiol-020911-153305

132. Wu L-G, Hamid E, Shin W, Chiang H-C. Exocytosis and endocytosis: modes, functions, and coupling mechanisms. Annu Rev Physiol. 2014;76: 301–331. doi:10.1146/annurev-physiol-021113-170305

133. Soreq H, Seidman S. Acetylcholinesterase--new roles for an old actor. Nat Rev Neurosci. 2001;2: 294–302. doi:10.1038/35067589

134. Awad SS, Lightowlers RN, Young C, Chrzanowska-Lightowlers ZMA, Lømo T, Slater CR. Sodium Channel mRNAs at the Neuromuscular Junction: Distinct Patterns of Accumulation and Effects of Muscle Activity. J Neurosci. 2001;21: 8456–8463. doi:10.1523/JNEUROSCI.21-21-08456.2001

135. Rebbeck RT, Karunasekara Y, Board PG, Beard NA, Casarotto MG, Dulhunty AF. Skeletal muscle excitation-contraction coupling: who are the dancing partners? Int J Biochem Cell Biol. 2014;48: 28–38. doi:10.1016/j.biocel.2013.12.001

136. Galińska-Rakoczy A, Engel P, Xu C, Jung H, Craig R, Tobacman LS, et al. Structural Basis for the Regulation of Muscle Contraction by Troponin and Tropomyosin. J Mol Biol. 2008;379: 929–935. doi:10.1016/j.jmb.2008.04.062

137. Fitts RH. The cross-bridge cycle and skeletal muscle fatigue. J Appl Physiol. 2008;104: 551–558. doi:10.1152/japplphysiol.01200.2007

138. Huxley HE. The Mechanism of Muscular Contraction. Science. 1969;164: 1356–1366. doi:10.1126/science.164.3886.1356

139. Huxley HE, Kress M. Crossbridge behaviour during muscle contraction. J Muscle Res Cell Motil. 1985;6: 153–161. doi:10.1007/BF00713057

140. Fulford J, Eston RG, Rowlands AV, Davies RC. Assessment of magnetic resonance techniques to measure muscle damage 24 h after eccentric exercise. Scand J Med Sci Sports. 2015;25: e28-39. doi:10.1111/sms.12234

141. Romijn JA, Coyle EF, Sidossis LS, Gastaldelli A, Horowitz JF, Endert E, et al. Regulation of endogenous fat and carbohydrate metabolism in relation to exercise intensity and duration. Am J Physiol. 1993;265: E380-391. doi:10.1152/ajpendo.1993.265.3.E380

142. Bansal D, Miyake K, Vogel SS, Groh S, Chen C-C, Williamson R, et al. Defective membrane repair in dysferlin-deficient muscular dystrophy. Nature. 2003;423: 168–172. doi:10.1038/nature01573

143. Anderson LV, Davison K, Moss JA, Young C, Cullen MJ, Walsh J, et al. Dysferlin is a plasma membrane protein and is expressed early in human development. Hum Mol Genet. 1999;8: 855–861. doi:10.1093/hmg/8.5.855

144. Achanzar WE, Ward S. A nematode gene required for sperm vesicle fusion. J Cell Sci. 1997;110 (Pt 9): 1073–1081.

145. Davis DB, Doherty KR, Delmonte AJ, McNally EM. Calcium-sensitive phospholipid binding properties of normal and mutant ferlin C2 domains. J Biol Chem. 2002;277: 22883–22888. doi:10.1074/jbc.M201858200

146. Matsuda C, Hayashi YK, Ogawa M, Aoki M, Murayama K, Nishino I, et al. The sarcolemmal proteins dysferlin and caveolin-3 interact in skeletal muscle. Hum Mol Genet. 2001;10: 1761–1766. doi:10.1093/hmg/10.17.1761

147. Huang Y, Verheesen P, Roussis A, Frankhuizen W, Ginjaar I, Haldane F, et al. Protein studies in dysferlinopathy patients using llama-derived antibody fragments selected by phage display. Eur J Hum Genet. 2005;13: 721–730. doi:10.1038/sj.ejhg.5201414

148. Lennon NJ, Kho A, Bacskai BJ, Perlmutter SL, Hyman BT, Brown RH. Dysferlin Interacts with Annexins A1 and A2 and Mediates Sarcolemmal Wound-healing. J Biol Chem. 2003;278: 50466–50473. doi:10.1074/jbc.M307247200

149. Huang Y, Laval SH, van Remoortere A, Baudier J, Benaud C, Anderson LVB, et al. AHNAK, a novel component of the dysferlin protein complex, redistributes to the cytoplasm with dysferlin during skeletal muscle regeneration. FASEB J. 2007;21: 732–742. doi:10.1096/fj.06-6628com

150. McNeil AK, Rescher U, Gerke V, McNeil PL. Requirement for annexin A1 in plasma membrane repair. J Biol Chem. 2006;281: 35202–35207. doi:10.1074/jbc.M606406200

151. Wallace GQ, McNally EM. Mechanisms of Muscle Degeneration, Regeneration, and Repair in the Muscular Dystrophies. Annu Rev Physiol. 2009;71: 37–57. doi:10.1146/annurev.physiol.010908.163216

152. Detrait ER, Yoo S, Eddleman CS, Fukuda M, Bittner GD, Fishman HM. Plasmalemmal repair of severed neurites of PC12 cells requires Ca(2+) and synaptotagmin. J Neurosci Res. 2000;62: 566–573. doi:10.1002/1097-4547(20001115)62:4<566::AID-JNR11>3.0.CO;2-4

153. Huang Y, de Morrée A, van Remoortere A, Bushby K, Frants RR, den Dunnen JT, et al. Calpain 3 is a modulator of the dysferlin protein complex in skeletal muscle. Hum Mol Genet. 2008;17: 1855–1866. doi:10.1093/hmg/ddn081

154. Han R, Campbell KP. Dysferlin and muscle membrane repair. Current Opinion in Cell Biology. 2007;19: 409–416. doi:10.1016/j.ceb.2007.07.001

155. Weisleder N, Takeshima H, Ma J. Mitsugumin 53 (MG53) facilitates vesicle trafficking in striated muscle to contribute to cell membrane repair. Commun Integr Biol. 2009;2: 225–226. doi:10.4161/cib.2.3.8077

156. Cao C-M, Zhang Y, Weisleder N, Ferrante C, Wang X, Lv F, et al. MG53 constitutes a primary determinant of cardiac ischemic preconditioning. Circulation. 2010;121: 2565–2574. doi:10.1161/CIRCULATIONAHA.110.954628

157. Cai C, Masumiya H, Weisleder N, Matsuda N, Nishi M, Hwang M, et al. MG53 nucleates assembly of cell membrane repair machinery. Nat Cell Biol. 2009;11: 56–64. doi:10.1038/ncb1812

158. Cai C, Masumiya H, Weisleder N, Pan Z, Nishi M, Komazaki S, et al. MG53 regulates membrane budding and exocytosis in muscle cells. J Biol Chem. 2009;284: 3314–3322. doi:10.1074/jbc.M808866200

159. Wang X, Xie W, Zhang Y, Lin P, Han L, Han P, et al. Cardioprotection of ischemia/reperfusion injury by cholesterol-dependent MG53-mediated membrane repair. Circ Res. 2010;107: 76–83. doi:10.1161/CIRCRESAHA.109.215822

160. Südhof TC, Rothman JE. Membrane fusion: grappling with SNARE and SM proteins. Science. 2009;323: 474–477. doi:10.1126/science.1161748

161. Südhof TC, Rizo J. Synaptotagmins: C2-domain proteins that regulate membrane traffic. Neuron. 1996;17: 379–388. doi:10.1016/s0896-6273(00)80171-3

162. Han R. Muscle membrane repair and inflammatory attack in dysferlinopathy. Skeletal Muscle. 2011;1: 10. doi:10.1186/2044-5040-1-10

163. St Pierre BA, Tidball JG. Differential response of macrophage subpopulations to soleus muscle reloading after rat hindlimb suspension. J Appl Physiol. 1994;77: 290–297. doi:10.1152/jappl.1994.77.1.290

164. St Pierre BA, Tidball JG. Macrophage activation and muscle remodeling at myotendinous junctions after modifications in muscle loading. Am J Pathol. 1994;145: 1463–1471.

165. McLennan IS. Degenerating and regenerating skeletal muscles contain several subpopulations of macrophages with distinct spatial and temporal distributions. J Anat. 1996;188: 17–28.

166. Hikida RS. Aging changes in satellite cells and their functions. Curr Aging Sci. 2011;4: 279–297. doi:10.2174/1874609811104030279

167. Macaluso F, Myburgh KH. Current evidence that exercise can increase the number of adult stem cells. J Muscle Res Cell Motil. 2012;33: 187–198. doi:10.1007/s10974-012-9302-0

168. Philippou A, Maridaki M, Theos A, Koutsilieris M. Cytokines in muscle damage. Adv Clin Chem. 2012;58: 49–87. doi:10.1016/b978-0-12-394383-5.00010-2

169. Scharner J, Zammit PS. The muscle satellite cell at 50: the formative years. Skelet Muscle. 2011;1: 28. doi:10.1186/2044-5040-1-28

170. Lander AD, Kimble J, Clevers H, Fuchs E, Montarras D, Buckingham M, et al. What does the concept of the stem cell niche really mean today? BMC Biol. 2012;10: 19. doi:10.1186/1741-7007-10-19

171. Dumont NA, Wang YX, Rudnicki MA. Intrinsic and extrinsic mechanisms regulating satellite cell function. Development. 2015;142: 1572–1581. doi:10.1242/dev.114223

172. Yin H, Price F, Rudnicki MA. Satellite Cells and the Muscle Stem Cell Niche. Physiological Reviews. 2013;93: 23–67. doi:10.1152/physrev.00043.2011

173. Hindi SM, Kumar A. Toll-like receptor signalling in regenerative myogenesis: friend and foe. The Journal of Pathology. 2016;239: 125–128. doi:10.1002/path.4714

174. Lotze MT, Zeh HJ, Rubartelli A, Sparvero LJ, Amoscato AA, Washburn NR, et al. The grateful dead: damage-associated molecular pattern molecules and reduction/oxidation regulate immunity. Immunol Rev. 2007;220: 60–81. doi:10.1111/j.1600-065X.2007.00579.x

175. Allen RE, Boxhorn LK. Regulation of skeletal muscle satellite cell proliferation and differentiation by transforming growth factor-beta, insulin-like growth factor I, and fibroblast growth factor. J Cell Physiol. 1989;138: 311–315. doi:10.1002/jcp.1041380213

176. Christov C, Chrétien F, Abou-Khalil R, Bassez G, Vallet G, Authier F-J, et al. Muscle satellite cells and endothelial cells: close neighbors and privileged partners. Mol Biol Cell. 2007;18: 1397–1409. doi:10.1091/mbc.e06-08-0693

177. Li Y-P. TNF-alpha is a mitogen in skeletal muscle. Am J Physiol, Cell Physiol. 2003;285: C370-376. doi:10.1152/ajpcell.00453.2002

178. Sheehan SM, Allen RE. Skeletal muscle satellite cell proliferation in response to members of the fibroblast growth factor family and hepatocyte growth factor. J Cell Physiol. 1999;181: 499–506. doi:10.1002/(SICI)1097-4652(199912)181:3<499::AID-JCP14>3.0.CO;2-1

179. Tidball JG, Villalta SA. Regulatory interactions between muscle and the immune system during muscle regeneration. Am J Physiol Regul Integr Comp Physiol. 2010;298: R1173-1187. doi:10.1152/ajpregu.00735.2009

180. Tajbakhsh S. Skeletal muscle stem cells in developmental versus regenerative myogenesis. J Intern Med. 2009;266: 372–389. doi:10.1111/j.1365-2796.2009.02158.x

181. Moreira-Pais A, Amado F, Vitorino R, Coriolano H-JA, Duarte JA, Ferreira R. The Signaling Pathways Involved in the Regulation of Skeletal Muscle Plasticity. In: Silva JV, Freitas MJ, Fardilha M, editors. Tissue-Specific Cell Signaling. Cham: Springer International Publishing; 2020. pp. 383–408. doi:10.1007/978-3-030-44436-5_14

182. Ruegsegger GN, Booth FW. Health Benefits of Exercise. Cold Spring Harb Perspect Med. 2018;8. doi:10.1101/cshperspect.a029694

183. Wei M, Kampert JB, Barlow CE, Nichaman MZ, Gibbons LW, Paffenbarger RS, et al. Relationship between low cardiorespiratory fitness and mortality in normal-weight, overweight, and obese men. JAMA. 1999;282: 1547–1553. doi:10.1001/jama.282.16.1547

184. Kodama S, Saito K, Tanaka S, Maki M, Yachi Y, Asumi M, et al. Cardiorespiratory fitness as a quantitative predictor of all-cause mortality and cardiovascular events in healthy men and women: a meta-analysis. JAMA. 2009;301: 2024–2035. doi:10.1001/jama.2009.681

185. Kaminsky LA, Arena R, Beckie TM, Brubaker PH, Church TS, Forman DE, et al. The importance of cardiorespiratory fitness in the United States: the need for a national registry: a policy statement from the American Heart Association. Circulation. 2013;127: 652–662. doi:10.1161/CIR.0b013e31827ee100

186. Garber CE, Blissmer B, Deschenes MR, Franklin BA, Lamonte MJ, Lee I-M, et al. American College of Sports Medicine position stand. Quantity and quality of exercise for developing and maintaining cardiorespiratory, musculoskeletal, and neuromotor fitness in apparently healthy adults: guidance for prescribing exercise. Med Sci Sports Exerc. 2011;43: 1334–1359. doi:10.1249/MSS.0b013e318213fefb

187. Bateman LA, Slentz CA, Willis LH, Shields AT, Piner LW, Bales CW, et al. Comparison of aerobic versus resistance exercise training effects on metabolic syndrome (from the Studies of a Targeted Risk Reduction Intervention Through Defined Exercise - STRRIDE-AT/RT). Am J Cardiol. 2011;108: 838–844. doi:10.1016/j.amjcard.2011.04.037

188. Joseph A-M, Pilegaard H, Litvintsev A, Leick L, Hood DA. Control of gene expression and mitochondrial biogenesis in the muscular adaptation to endurance exercise. Essays Biochem. 2006;42: 13–29. doi:10.1042/bse0420013

189. Rose AJ, Richter EA. Regulatory mechanisms of skeletal muscle protein turnover during exercise. J Appl Physiol. 2009;106: 1702–1711. doi:10.1152/japplphysiol.91375.2008

190. Yan Z, Lira VA, Greene NP. Exercise training-induced regulation of mitochondrial quality. Exerc Sport Sci Rev. 2012;40: 159–164. doi:10.1097/JES.0b013e3182575599

191. Baar K, Wende AR, Jones TE, Marison M, Nolte LA, Chen M, et al. Adaptations of skeletal muscle to exercise: rapid increase in the transcriptional coactivator PGC-1. FASEB J. 2002;16: 1879–1886. doi:10.1096/fj.02-0367com

192. Rivas DA, Lessard SJ, Saito M, Friedhuber AM, Koch LG, Britton SL, et al. Low intrinsic running capacity is associated with reduced skeletal muscle substrate oxidation and lower mitochondrial content in white skeletal muscle. Am J Physiol Regul Integr Comp Physiol. 2011;300: R835-843. doi:10.1152/ajpregu.00659.2010

193. Kraemer WJ, Ratamess NA. Fundamentals of Resistance Training: Progression and Exercise Prescription. Med Sci Sports Exerc. 2004; 36(4): 674-688.

194. J F Steven, William K. Designing Resistance Training Programs, 4E. Human Kinetics; 2014.

195. Dudley GA, Tesch PA, Miller BJ, Buchanan P. Importance of eccentric actions in performance adaptations to resistance training. Aviat Space Environ Med. 1991;62: 543–550.

196. Kanehisa H, Miyashita M. Specificity of velocity in strength training. Europ J Appl Physiol. 1983;52: 104–106. doi:10.1007/BF00429034

197. Knapik JJ, Mawdsley RH, Ramos MU. Angular Specificity and Test Mode Specificity of Isometric and Isokinetic Strength Training *. J Orthop Sports Phys Ther. 1983;5: 58–65. doi:10.2519/jospt.1983.5.2.58

198. Kraemer WJ, Nindl BC, Ratamess NA, Gotshalk LA, Volek JS, Fleck SJ, et al. Changes in muscle hypertrophy in women with periodized resistance training. Med Sci Sports Exerc. 2004;36: 697–708. doi:10.1249/01.mss.0000122734.25411.cf

199. Kraemer WJ, Noble BJ, Clark MJ, Culver BW. Physiologic responses to heavy-resistance exercise with very short rest periods. Int J Sports Med. 1987;8: 247–252. doi:10.1055/s-2008-1025663

200. Schuenke MD, Mikat RP, McBride JM. Effect of an acute period of resistance exercise on excess post-exercise oxygen consumption: implications for body mass management. Eur J Appl Physiol. 2002;86: 411–417. doi:10.1007/s00421-001-0568-y

201. Campos GER, Luecke TJ, Wendeln HK, Toma K, Hagerman FC, Murray TF, et al. Muscular adaptations in response to three different resistance-training regimens: specificity of repetition maximum training zones. Eur J Appl Physiol. 2002;88: 50–60. doi:10.1007/s00421-002-0681-6

202. Rhea MR, Alvar BA, Ball SD, Burkett LN. Three sets of weight training superior to 1 set with equal intensity for eliciting strength. J Strength Cond Res. 2002;16: 525–529.

203. Schlumberger A, Stec J, Schmidtbleicher D. Single- vs. multiple-set strength training in women. J Strength Cond Res. 2001;15: 284–289.

204. Sale DG. Neural adaptation to resistance training. Med Sci Sports Exerc. 1988;20: S135-145. doi:10.1249/00005768-198810001-00009

205. Kraemer WJ, Patton JF, Gordon SE, Harman EA, Deschenes MR, Reynolds K, et al. Compatibility of high-intensity strength and endurance training on hormonal and skeletal muscle adaptations. J Appl Physiol. 1995;78: 976–989. doi:10.1152/jappl.1995.78.3.976

206. Phillips SM. Short-term training: when do repeated bouts of resistance exercise become training? Can J Appl Physiol. 2000;25: 185–193. doi:10.1139/h00-014

207. Staron RS, Karapondo DL, Kraemer WJ, Fry AC, Gordon SE, Falkel JE, et al. Skeletal muscle adaptations during early phase of heavy-resistance training in men and women. J Appl Physiol. 1994;76: 1247–1255. doi:10.1152/jappl.1994.76.3.1247

208. Guthold R, Stevens GA, Riley LM, Bull FC. Worldwide trends in insufficient physical activity from 2001 to 2016: a pooled analysis of 358 population-based surveys with 1·9 million participants. Lancet Glob Health. 2018;6: e1077–e1086. doi:10.1016/S2214-109X(18)30357-7

209. Mansoubi M, Pearson N, Biddle SJH, Clemes S. The relationship between sedentary behaviour and physical activity in adults: a systematic review. Prev Med. 2014;69: 28–35. doi:10.1016/j.ypmed.2014.08.028

210. Biswas A, Oh PI, Faulkner GE, Bajaj RR, Silver MA, Mitchell MS, et al. Sedentary time and its association with risk for disease incidence, mortality, and hospitalization in adults: a systematic review and meta-analysis. Ann Intern Med. 2015;162: 123–132. doi:10.7326/M14-1651

211. Barnes DE, Yaffe K. The projected effect of risk factor reduction on Alzheimer's disease prevalence. Lancet Neurol. 2011;10: 819–828. doi:10.1016/S1474-4422(11)70072-2

212. Norton S, Matthews FE, Barnes DE, Yaffe K, Brayne C. Potential for primary prevention of Alzheimer's disease: an analysis of population-based data. Lancet Neurol. 2014;13: 788–794. doi:10.1016/S1474-4422(14)70136-X

213. Bergouignan A, Rudwill F, Simon C, Blanc S. Physical inactivity as the culprit of metabolic inflexibility: evidence from bed-rest studies. J Appl Physiol. 2011;111: 1201–1210. doi:10.1152/japplphysiol.00698.2011

214. Trappe SW, Trappe TA, Lee GA, Widrick JJ, Costill DL, Fitts RH. Comparison of a space shuttle flight (STS-78) and bed rest on human muscle function. J Appl Physiol. 2001;91: 57–64. doi:10.1152/jappl.2001.91.1.57

215. Alkner BA, Tesch PA. Knee extensor and plantar flexor muscle size and function following 90 days of bed rest with or without resistance exercise. Eur J Appl Physiol. 2004;93: 294–305. doi:10.1007/s00421-004-1172-8

216. Rittweger J, Möller K, Bareille M-P, Felsenberg D, Zange J. Muscle X-ray attenuation is not decreased during experimental bed rest. Muscle Nerve. 2013;47: 722–730. doi:10.1002/mus.23644

217. Trappe S, Trappe T, Gallagher P, Harber M, Alkner B, Tesch P. Human single muscle fibre function with 84 day bed-rest and resistance exercise. J Physiol (Lond). 2004;557: 501–513. doi:10.1113/jphysiol.2004.062166

218. Convertino VA, Bloomfield SA, Greenleaf JE. An overview of the issues: physiological effects of bed rest and restricted physical activity. Med Sci Sports Exerc. 1997;29: 187–190. doi:10.1097/00005768-199702000-00004

219. Convertino VA, Bisson R, Bates R, Goldwater D, Sandler H. Effects of antiorthostatic bedrest on the cardiorespiratory responses to exercise. Aviat Space Environ Med. 1981;52: 251–255.

220. Greenleaf JE, Vernikos J, Wade CE, Barnes PR. Effect of leg exercise training on vascular volumes during 30 days of 6 degrees head-down bed rest. J Appl Physiol. 1992;72: 1887–1894. doi:10.1152/jappl.1992.72.5.1887

221. Convertino VA. Effects of exercise and inactivity on intravascular volume and cardiovascular control mechanisms. Acta Astronaut. 1992;27: 123–129. doi:10.1016/0094-5765(92)90188-o

222. Greenleaf JE, Wade CE, Leftheriotis G. Orthostatic responses following 30-day bed rest deconditioning with isotonic and isokinetic exercise training. Aviat Space Environ Med. 1989;60: 537–542.

223. Buchanan P, Convertino VA. A study of the effects of prolonged simulated microgravity on the musculature of the lower extremities in man: an introduction. Aviat Space Environ Med. 1989;60: 649–652.

224. Gogia P, Schneider VS, LeBlanc AD, Krebs J, Kasson C, Pientok C. Bed rest effect on extremity muscle torque in healthy men. Arch Phys Med Rehabil. 1988;69: 1030–1032.

225. Greenleaf JE, Van Beaumont W, Convertino VA, Starr JC. Handgrip and general muscular strength and endurance during prolonged bedrest with isometric and isotonic leg exercise training. Aviat Space Environ Med. 1983;54: 696–700.

226. Greenleaf JE. Intensive exercise training during bed rest attenuates deconditioning. Med Sci Sports Exerc. 1997;29: 207–215. doi:10.1097/00005768-199702000-00007

227. Greenleaf JE, Bernauer EM, Ertl AC, Bulbulian R, Bond M. Isokinetic strength and endurance during 30-day 6 degrees head-down bed rest with isotonic and isokinetic exercise training. Aviat Space Environ Med. 1994;65: 45–50.

228. Ellis S, Kirby LC, Greenleaf JE. Lower extremity muscle thickness during 30-day 6 degrees head-down bed rest with isotonic and isokinetic exercise training. Aviat Space Environ Med. 1993;64: 1011–1015.

229. LeBlanc A, Gogia P, Schneider V, Krebs J, Schonfeld E, Evans H. Calf muscle area and strength changes after five weeks of horizontal bed rest. Am J Sports Med. 1988;16: 624–629. doi:10.1177/036354658801600612

230. Crandall CG, Johnson JM, Convertino VA, Raven PB, Engelke KA. Altered thermoregulatory responses after 15 days of head-down tilt. J Appl Physiol. 1994;77: 1863–1867. doi:10.1152/jappl.1994.77.4.1863

231. Greenleaf JE, Reese RD. Exercise thermoregulation after 14 days of bed rest. J Appl Physiol Respir Environ Exerc Physiol. 1980;48: 72–78. doi:10.1152/jappl.1980.48.1.72

232. DeRoshia CW, Greenleaf JE. Performance and mood-state parameters during 30-day 6 degrees head-down bed rest with exercise training. Aviat Space Environ Med. 1993;64: 522–527.

233. Gustafsson T, Osterlund T, Flanagan JN, von Waldén F, Trappe TA, Linnehan RM, et al. Effects of 3 days unloading on molecular regulators of muscle size in humans. J Appl Physiol. 2010;109: 721–727. doi:10.1152/japplphysiol.00110.2009

234. Zhang P, Chen X, Fan M. Signaling mechanisms involved in disuse muscle atrophy. Medical Hypotheses. 2007;69: 310–321. doi:10.1016/j.mehy.2006.11.043

235. Haus JM, Carrithers JA, Carroll CC, Tesch PA, Trappe TA. Contractile and connective tissue protein content of human skeletal muscle: effects of 35 and 90 days of simulated microgravity and exercise countermeasures. Am J Physiol Regul Integr Comp Physiol. 2007;293: R1722-1727. doi:10.1152/ajpregu.00292.2007

236. Morey-Holton ER, Globus RK. Hindlimb unloading rodent model: technical aspects. J Appl Physiol. 2002;92: 1367–1377. doi:10.1152/japplphysiol.00969.2001

237. Haida N, Fowler WM, Abresch RT, Larson DB, Sharman RB, Taylor RG, et al. Effect of hind-limb suspension on young and adult skeletal muscle. I. Normal mice. Exp Neurol. 1989;103: 68–76. doi:10.1016/0014-4886(89)90187-8

238. McCarthy JJ, Fox AM, Tsika GL, Gao L, Tsika RW. beta-MHC transgene expression in suspended and mechanically overloaded/suspended soleus muscle of transgenic mice. Am J Physiol. 1997;272: R1552-1561. doi:10.1152/ajpregu.1997.272.5.R1552

239. Thomason DB, Booth FW. Atrophy of the soleus muscle by hindlimb unweighting. J Appl Physiol. 1990;68: 1–12. doi:10.1152/jappl.1990.68.1.1

240. Stelzer JE, Widrick JJ. Effect of hindlimb suspension on the functional properties of slow and fast soleus fibers from three strains of mice. J Appl Physiol. 2003;95: 2425–2433. doi:10.1152/japplphysiol.01091.2002

241. Baehr LM, West DWD, Marshall AG, Marcotte GR, Baar K, Bodine SC. Muscle-specific and age-related changes in protein synthesis and protein degradation in response to hindlimb unloading in rats. Journal of Applied Physiology. 2017;122: 1336–1350. doi:10.1152/japplphysiol.00703.2016

242. Simske SJ, Greenberg AR, Luttges MW. Effects of suspension-induced osteopenia on the mechanical behaviour of mouse long bones. J Mater Sci Mater Med. 1991;2: 43–50. doi:10.1007/BF00701686

243. Bowden Davies KA, Pickles S, Sprung VS, Kemp GJ, Alam U, Moore DR, et al. Reduced physical activity in young and older adults: metabolic and musculoskeletal implications. Therapeutic Advances in Endocrinology. 2019;10: 2042018819888824. doi:10.1177/2042018819888824

244. Kang PB, Griggs RC. Advances in Muscular Dystrophies. JAMA Neurol. 2015;72: 741–742. doi:10.1001/jamaneurol.2014.4621

245. Waldrop MA, Flanigan KM. Update in Duchenne and Becker muscular dystrophy: Current Opinion in Neurology. 2019;32: 722–727. doi:10.1097/WCO.0000000000000739

246. Tidball JG, Welc SS, Wehling-Henricks M. Immunobiology of Inherited Muscular Dystrophies. In: Pollock DM, editor. Comprehensive Physiology. Hoboken, NJ, USA: John Wiley & Sons, Inc.; 2018. pp. 1313–1356. doi:10.1002/cphy.c170052

247. Den Dunnen JT, Grootscholten PM, Bakker E, Blonden LA, Ginjaar HB, Wapenaar MC, et al. Topography of the Duchenne muscular dystrophy (DMD) gene: FIGE and cDNA analysis of 194 cases reveals 115 deletions and 13 duplications. Am J Hum Genet. 1989;45: 835–847.

248. Coffey AJ, Roberts RG, Green ED, Cole CG, Butler R, Anand R, et al. Construction of a 2.6-Mb contig in yeast artificial chromosomes spanning the human dystrophin gene using an STS-based approach. Genomics. 1992;12: 474–484. doi:10.1016/0888-7543(92)90437-w

249. Monaco AP, Walker AP, Millwood I, Larin Z, Lehrach H. A yeast artificial chromosome contig containing the complete Duchenne muscular dystrophy gene. Genomics. 1992;12: 465–473. doi:10.1016/0888-7543(92)90436-v

250. Roberts RG, Coffey AJ, Bobrow M, Bentley DR. Determination of the exon structure of the distal portion of the dystrophin gene by vectorette PCR. Genomics. 1992;13: 942–950. doi:10.1016/0888-7543(92)90005-d

251. Tennyson CN, Klamut HJ, Worton RG. The human dystrophin gene requires 16 hours to be transcribed and is cotranscriptionally spliced. Nat Genet. 1995;9: 184–190. doi:10.1038/ng0295-184

252. Bushby K, Finkel R, Birnkrant DJ, Case LE, Clemens PR, Cripe L, et al. Diagnosis and management of Duchenne muscular dystrophy, part 2: implementation of multidisciplinary care. Lancet Neurol. 2010;9: 177–189. doi:10.1016/S1474-4422(09)70272-8

253. Matsumura T, Saito T, Fujimura H, Shinno S, Sakoda S. [A longitudinal cause-of-death analysis of patients with Duchenne muscular dystrophy]. Rinsho Shinkeigaku. 2011;51: 743–750. doi:10.5692/clinicalneurol.51.743

254. Connolly AM, Keeling RM, Mehta S, Pestronk A, Sanes JR. Three mouse models of muscular dystrophy: the natural history of strength and fatigue in dystrophin-, dystrophin/utrophin-, and laminin alpha2-deficient mice. Neuromuscul Disord. 2001;11: 703–712. doi:10.1016/s0960-8966(01)00232-2

255. Desguerre I, Mayer M, Leturcq F, Barbet J-P, Gherardi RK, Christov C. Endomysial fibrosis in Duchenne muscular dystrophy: a marker of poor outcome associated with macrophage alternative activation. J Neuropathol Exp Neurol. 2009;68: 762–773. doi:10.1097/NEN.0b013e3181aa31c2

256. Frascarelli M, Rocchi L, Feola I. EMG computerized analysis of localized fatigue in Duchenne muscular dystrophy. Muscle Nerve. 1988;11: 757–761. doi:10.1002/mus.880110712

257. Marshall PA, Williams PE, Goldspink G. Accumulation of collagen and altered fiber-type ratios as indicators of abnormal muscle gene expression in the mdx dystrophic mouse. Muscle Nerve. 1989;12: 528–537. doi:10.1002/mus.880120703

258. Nagel A, Lehmann-Horn F, Engel AG. Neuromuscular transmission in the mdx mouse. Muscle Nerve. 1990;13: 742–749. doi:10.1002/mus.880130813

259. Rybalka E, Timpani CA, Cooke MB, Williams AD, Hayes A. Defects in mitochondrial ATP synthesis in dystrophin-deficient mdx skeletal muscles may be caused by complex I insufficiency. PLoS ONE. 2014;9: e115763. doi:10.1371/journal.pone.0115763

260. Sander M, Chavoshan B, Harris SA, Iannaccone ST, Stull JT, Thomas GD, et al. Functional muscle ischemia in neuronal nitric oxide synthase-deficient skeletal muscle of children with Duchenne muscular dystrophy. Proceedings of the National Academy of Sciences. 2000;97: 13818–13823. doi:10.1073/pnas.250379497

261. Shiao T, Fond A, Deng B, Wehling-Henricks M, Adams ME, Froehner SC, et al. Defects in neuromuscular junction structure in dystrophic muscle are corrected by expression of a NOS transgene in dystrophin-deficient muscles, but not in muscles lacking alpha- and beta1-syntrophins. Hum Mol Genet. 2004;13: 1873–1884. doi:10.1093/hmg/ddh204

262. van der Pijl EM, van Putten M, Niks EH, Verschuuren JJGM, Aartsma-Rus A, Plomp JJ. Characterization of neuromuscular synapse function abnormalities in multiple Duchenne muscular dystrophy mouse models. Eur J Neurosci. 2016;43: 1623–1635. doi:10.1111/ejn.13249

263. Webster C, Blau HM. Accelerated age-related decline in replicative life-span of Duchenne muscular dystrophy myoblasts: implications for cell and gene therapy. Somat Cell Mol Genet. 1990;16: 557–565. doi:10.1007/BF01233096

264. Wehling-Henricks M, Oltmann M, Rinaldi C, Myung KH, Tidball JG. Loss of positive allosteric interactions between neuronal nitric oxide synthase and phosphofructokinase contributes to defects in glycolysis and increased fatigability in muscular dystrophy. Hum Mol Genet. 2009;18: 3439–3451. doi:10.1093/hmg/ddp288

265. Willcocks RJ, Triplett WT, Forbes SC, Arora H, Senesac CR, Lott DJ, et al. Magnetic resonance imaging of the proximal upper extremity musculature in boys with Duchenne muscular dystrophy. J Neurol. 2017;264: 64–71. doi:10.1007/s00415-016-8311-0

266. Panicker JB, Chacko G, Patil AKB, Alexander M, Muliyil J. Immunohistochemical differentiation of inflammatory myopathies. Neurology India. 2011;59: 513. doi:10.4103/0028-3886.84329

267. Murahashi M, Wakayama Y, Kumagai T, Kobayashi T, Yamashita S, Misugi N, et al. Observations of muscle plasma membrane undercoats in Duchenne and fukuyama muscula dystrophies. Med Electron Microsc. 1995;28: 102–110. doi:10.1007/BF02348027

268. Ervasti JM, Sonnemann KJ. Biology of the striated muscle dystrophin-glycoprotein complex. Int Rev Cytol. 2008;265: 191–225. doi:10.1016/S0074-7696(07)65005-0

269. Allen DG, Gervasio OL, Yeung EW, Whitehead NP. Calcium and the damage pathways in muscular dystrophy. Can J Physiol Pharmacol. 2010;88: 83–91. doi:10.1139/Y09-058

270. Ambrosio F, Ferrari RJ, Fitzgerald GK, Carvell G, Boninger ML, Huard J. Functional Overloading of Dystrophic Mice Enhances Muscle-Derived Stem Cell Contribution to Muscle Contractile Capacity. Archives of Physical Medicine and Rehabilitation. 2009;90: 66–73. doi:10.1016/j.apmr.2008.06.035

271. Johnson BD, Scheuer T, Catterall WA. Convergent regulation of skeletal muscle Ca2+ channels by dystrophin, the actin cytoskeleton, and cAMP-dependent protein kinase. Proc Natl Acad Sci USA. 2005;102: 4191–4196. doi:10.1073/pnas.0409695102

272. Ratel S, Duché P, Williams CA. Muscle Fatigue during High-Intensity Exercise in Children. Sports Med. 2006;36: 1031–1065. doi:10.2165/00007256-200636120-00004

273. Kaczor JJ, Hall JE, Payne E, Tarnopolsky MA. Low intensity training decreases markers of oxidative stress in skeletal muscle of mdx mice. Free Radical Biology and Medicine. 2007;43: 145–154. doi:10.1016/j.freeradbiomed.2007.04.003

274. Wehling M, Spencer MJ, Tidball JG. A nitric oxide synthase transgene ameliorates muscular dystrophy in mdx mice. J Cell Biol. 2001;155: 123–131. doi:10.1083/jcb.200105110

275. Gosselin LE, McCormick KM. Targeting the immune system to improve ventilatory function in muscular dystrophy. Med Sci Sports Exerc. 2004;36: 44–51. doi:10.1249/01.MSS.0000106185.22349.2C

276. Lovering RM, Michaelson L, Ward CW. Malformed mdx myofibers have normal cytoskeletal architecture yet altered EC coupling and stress-induced Ca2+ signaling. American Journal of Physiology-Cell Physiology. 2009;297: C571–C580. doi:10.1152/ajpcell.00087.2009

277. Percival JM, Anderson KNE, Gregorevic P, Chamberlain JS, Froehner SC. Functional Deficits in nNOSμ-Deficient Skeletal Muscle: Myopathy in nNOS Knockout Mice. Andreu AL, editor. PLoS ONE. 2008;3: e3387. doi:10.1371/journal.pone.0003387

278. Rando TA, Disatnik M-H, Yu Y, Franco A. Muscle cells from mdx mice have an increased susceptibility to oxidative stress. Neuromuscular Disorders. 1998;8: 14–21. doi:10.1016/S0960-8966(97)00124-7

279. Monaco AP, Neve RL, Colletti-Feener C, Bertelson CJ, Kurnit DM, Kunkel LM. Isolation of candidate cDNAs for portions of the Duchenne muscular dystrophy gene. Nature. 1986;323: 646–650. doi:10.1038/323646a0

280. Hoffman EP, Brown RH, Kunkel LM. Dystrophin: the protein product of the Duchenne muscular dystrophy locus. Cell. 1987;51: 919–928. doi:10.1016/0092-8674(87)90579-4

281. Hoffman EP, Knudson CM, Campbell KP, Kunkel LM. Subcellular fractionation of dystrophin to the triads of skeletal muscle. Nature. 1987;330: 754–758. doi:10.1038/330754a0

282. Guiraud S, Aartsma-Rus A, Vieira NM, Davies KE, van Ommen G-JB, Kunkel LM. The Pathogenesis and Therapy of Muscular Dystrophies. Annu Rev Genomics Hum Genet. 2015;16: 281–308. doi:10.1146/annurev-genom-090314-025003

283. Duan D. Systemic AAV Micro-dystrophin Gene Therapy for Duchenne Muscular Dystrophy. Mol Ther. 2018;26: 2337–2356. doi:10.1016/j.ymthe.2018.07.011

284. Chamberlain JR, Chamberlain JS. Progress toward Gene Therapy for Duchenne Muscular Dystrophy. Mol Ther. 2017;25: 1125–1131. doi:10.1016/j.ymthe.2017.02.019

285. Mendell JR, Goemans N, Lowes LP, Alfano LN, Berry K, Shao J, et al. Longitudinal effect of eteplirsen versus historical control on ambulation in Duchenne muscular dystrophy. Ann Neurol. 2016;79: 257–271. doi:10.1002/ana.24555

286. Kinane TB, Mayer OH, Duda PW, Lowes LP, Moody SL, Mendell JR. Long-Term Pulmonary Function in Duchenne Muscular Dystrophy: Comparison of Eteplirsen-Treated Patients to Natural History. J Neuromuscul Dis. 2018;5: 47–58. doi:10.3233/JND-170272

287. Law DJ, Allen DL, Tidball JG. Talin, vinculin and DRP (utrophin) concentrations are increased at mdx myotendinous junctions following onset of necrosis. J Cell Sci. 1994;107 (Pt 6): 1477–1483.

288. Hodges BL, Hayashi YK, Nonaka I, Wang W, Arahata K, Kaufman SJ. Altered expression of the alpha7beta1 integrin in human and murine muscular dystrophies. J Cell Sci. 1997;110 (Pt 22): 2873–2881.

289. Hanft LM, Rybakova IN, Patel JR, Rafael-Fortney JA, Ervasti JM. Cytoplasmic gamma-actin contributes to a compensatory remodeling response in dystrophin-deficient muscle. Proc Natl Acad Sci USA. 2006;103: 5385–5390. doi:10.1073/pnas.0600980103

290. Call JA, Mckeehen JN, Novotny SA, Lowe DA. Progressive resistance voluntary wheel running in the mdx mouse. Muscle Nerve. 2010;42: 871–880. doi:10.1002/mus.21764

291. Nguyen HH, Jayasinha V, Xia B, Hoyte K, Martin PT. Overexpression of the cytotoxic T cell GalNAc transferase in skeletal muscle inhibits muscular dystrophy in mdx mice. Proc Natl Acad Sci U S A. 2002;99: 5616–5621. doi:10.1073/pnas.082613599

292. Xu R, Jia Y, Zygmunt DA, Martin PT. rAAVrh74.MCK.GALGT2 Protects against Loss of Hemodynamic Function in the Aging mdx Mouse Heart. Mol Ther. 2019;27: 636–649. doi:10.1016/j.ymthe.2019.01.005

293. Martin PT, Xu R, Rodino-Klapac LR, Oglesbay E, Camboni M, Montgomery CL, et al. Overexpression of Galgt2 in skeletal muscle prevents injury resulting from eccentric contractions in both mdx and wild-type mice. Am J Physiol, Cell Physiol. 2009;296: C476-488. doi:10.1152/ajpcell.00456.2008

294. Vo AH, McNally EM. Modifier genes and their effect on Duchenne muscular dystrophy. Curr Opin Neurol. 2015;28: 528–534. doi:10.1097/WCO.0000000000000240

295. Eagle M. Report on the muscular dystrophy campaign workshop: exercise in neuromuscular diseases Newcastle, January 2002. Neuromuscul Disord. 2002;12: 975–983. doi:10.1016/s0960-8966(02)00136-0

296. Alemdaroğlu I, Karaduman A, Yilmaz ÖT, Topaloğlu H. Different types of upper extremity exercise training in Duchenne muscular dystrophy: effects on functional performance, strength, endurance, and ambulation. Muscle Nerve. 2015;51: 697–705. doi:10.1002/mus.24451

297. Bushby K, Finkel R, Birnkrant DJ, Case LE, Clemens PR, Cripe L, et al. Diagnosis and management of Duchenne muscular dystrophy, part 1: diagnosis, and pharmacological and psychosocial management. Lancet Neurol. 2010;9: 77–93. doi:10.1016/S1474-4422(09)70271-6

298. Brooke MH, Fenichel GM, Griggs RC, Mendell JR, Moxley RT, Miller JP, et al. Clinical investigation of Duchenne muscular dystrophy. Interesting results in a trial of prednisone. Arch Neurol. 1987;44: 812–817. doi:10.1001/archneur.1987.00520200016010

299. Mendell JR, Moxley RT, Griggs RC, Brooke MH, Fenichel GM, Miller JP, et al. Randomized, double-blind six-month trial of prednisone in Duchenne's muscular dystrophy. N Engl J Med. 1989;320: 1592–1597. doi:10.1056/NEJM198906153202405

300. Griggs RC, Miller JP, Greenberg CR, Fehlings DL, Pestronk A, Mendell JR, et al. Efficacy and safety of deflazacort vs prednisone and placebo for Duchenne muscular dystrophy. Neurology. 2016;87: 2123–2131. doi:10.1212/WNL.0000000000003217

301. Buckner JL, Bowden SA, Mahan JD. Optimizing Bone Health in Duchenne Muscular Dystrophy. Int J Endocrinol. 2015;2015. doi:10.1155/2015/928385

302. Wang RT, Silverstein Fadlon CA, Ulm JW, Jankovic I, Eskin A, Lu A, et al. Online self-report data for duchenne muscular dystrophy confirms natural history and can be used to assess for therapeutic benefits. PLoS Curr. 2014;6. doi:10.1371/currents.md.e1e8f2be7c949f9ffe81ec6fca1cce6a

303. Bello L, Gordish-Dressman H, Morgenroth LP, Henricson EK, Duong T, Hoffman EP, et al. Prednisone/prednisolone and deflazacort regimens in the CINRG Duchenne Natural History Study. Neurology. 2015;85: 1048–1055. doi:10.1212/WNL.0000000000001950

304. Griggs RC, Herr BE, Reha A, Elfring G, Atkinson L, Cwik V, et al. Corticosteroids in Duchenne muscular dystrophy: major variations in practice. Muscle Nerve. 2013;48: 27–31. doi:10.1002/mus.23831

305. Griggs RC, Moxley RT, Mendell JR, Fenichel GM, Brooke MH, Pestronk A, et al. Duchenne dystrophy: randomized, controlled trial of prednisone (18 months) and azathioprine (12 months). Neurology. 1993;43: 520–527. doi:10.1212/wnl.43.3_part_1.520

306. Escolar DM, Hache LP, Clemens PR, Cnaan A, McDonald CM, Viswanathan V, et al. Randomized, blinded trial of weekend vs daily prednisone in Duchenne muscular dystrophy. Neurology. 2011;77: 444–452. doi:10.1212/WNL.0b013e318227b164

307. Connolly AM, Zaidman CM, Golumbek PT, Cradock MM, Flanigan KM, Kuntz NL, et al. Twice-weekly glucocorticosteroids in infants and young boys with Duchenne muscular dystrophy. Muscle Nerve. 2019;59: 650–657. doi:10.1002/mus.26441

308. Leigh F, Ferlini A, Biggar D, Bushby K, Finkel R, Morgenroth LP, et al. Neurology Care, Diagnostics, and Emerging Therapies of the Patient With Duchenne Muscular Dystrophy. Pediatrics. 2018;142: S5–S16. doi:10.1542/peds.2018-0333C

309. Scott OM, Vrbová G, Hyde SA, Dubowitz V. Responses of muscles of patients with Duchenne muscular dystrophy to chronic electrical stimulation. J Neurol Neurosurg Psychiatry. 1986;49: 1427–1434. doi:10.1136/jnnp.49.12.1427

310. Jansen M, van Alfen N, Geurts ACH, de Groot IJM. Assisted bicycle training delays functional deterioration in boys with Duchenne muscular dystrophy: the randomized controlled trial “no use is disuse.” Neurorehabil Neural Repair. 2013;27: 816–827. doi:10.1177/1545968313496326

311. McDonald CM, Jaffe KM, Mosca VS, Shurtleff DB. Ambulatory outcome of children with myelomeningocele: effect of lower-extremity muscle strength. Dev Med Child Neurol. 1991;33: 482–490. doi:10.1111/j.1469-8749.1991.tb14913.x

312. McDonald CM, Abresch RT, Carter GT, Fowler WM, Johnson ER, Kilmer DD, et al. Profiles of neuromuscular diseases. Duchenne muscular dystrophy. Am J Phys Med Rehabil. 1995;74: S70-92. doi:10.1097/00002060-199509001-00003

313. McDonald CM, Widman LM, Walsh DD, Walsh SA, Abresch RT. Use of step activity monitoring for continuous physical activity assessment in boys with Duchenne muscular dystrophy. Arch Phys Med Rehabil. 2005;86: 802–808. doi:10.1016/j.apmr.2004.10.012

314. Jeannet P-Y, Aminian K, Bloetzer C, Najafi B, Paraschiv-Ionescu A. Continuous monitoring and quantification of multiple parameters of daily physical activity in ambulatory Duchenne muscular dystrophy patients. Eur J Paediatr Neurol. 2011;15: 40–47. doi:10.1016/j.ejpn.2010.07.002

315. McDonald CM. Physical Activity, Health Impairments, and Disability in Neuromuscular Disease: American Journal of Physical Medicine & Rehabilitation. 2002;81: S108–S120. doi:10.1097/00002060-200211001-00012

316. Jansen M, de Groot IJ, van Alfen N, Geurts AC. Physical training in boys with Duchenne Muscular Dystrophy: the protocol of the No Use is Disuse study. BMC Pediatr. 2010;10: 55. doi:10.1186/1471-2431-10-55

317. Markert CD, Ambrosio F, Call JA, Grange RW. Exercise and duchenne muscular dystrophy: Toward evidence-based exercise prescription. Muscle Nerve. 2011;43: 464–478. doi:10.1002/mus.21987

318. Wagner MB, Vignos PJ, Fonow DC. Serial isokinetic evaluations used for a patient with scapuloperoneal muscular dystrophy. A case report. Phys Ther. 1986;66: 1110–1113. doi:10.1093/ptj/66.7.1110

319. Vignos PJ, Watkins MP. The Effect of Exercise in Muscular Dystrophy. JAMA. 1966; 197: 121-126.

320. Effect on maximal strength of submaximal exercise in Duchenne muscular dystrophy. - Abstract - Europe PMC. [cited 2 Jun 2020]. Available: https://europepmc.org/article/med/434131

321. Scott OM, Hyde SA, Goddard C, Jones R, Dubowitz V. Effect of exercise in Duchenne muscular dystrophy. Physiotherapy. 1981;67: 174–176.

322. Munn J, Herbert RD, Gandevia SC. Contralateral effects of unilateral resistance training: a meta-analysis. Journal of Applied Physiology. 2004;96: 1861–1866. doi:10.1152/japplphysiol.00541.2003

323. Bulfield G, Siller WG, Wight PA, Moore KJ. X chromosome-linked muscular dystrophy (mdx) in the mouse. Proc Natl Acad Sci USA. 1984;81: 1189–1192. doi:10.1073/pnas.81.4.1189

324. Sicinski P, Geng Y, Ryder-Cook AS, Barnard EA, Darlison MG, Barnard PJ. The molecular basis of muscular dystrophy in the mdx mouse: a point mutation. Science. 1989;244: 1578–1580. doi:10.1126/science.2662404

325. Manning J, O'Malley D. What has the mdx mouse model of Duchenne muscular dystrophy contributed to our understanding of this disease? J Muscle Res Cell Motil. 2015;36: 155–167. doi:10.1007/s10974-015-9406-4

326. McGreevy JW, Hakim CH, McIntosh MA, Duan D. Animal models of Duchenne muscular dystrophy: from basic mechanisms to gene therapy. Dis Model Mech. 2015;8: 195–213. doi:10.1242/dmm.018424

327. Hayes A, Williams DA. Contractile function and low-intensity exercise effects of old dystrophic (*mdx*) mice. American Journal of Physiology-Cell Physiology. 1998;274: C1138–C1144. doi:10.1152/ajpcell.1998.274.4.C1138

328. Fowler WM, Abresch RT, Larson DB, Sharman RB, Entrikin RK. High-repetitive submaximal treadmill exercise training: effect on normal and dystrophic mice. Ach Phys Med Rehabil. 1990; 71: 552-557.

329. Kobayashi YM, Rader EP, Crawford RW, Campbell KP. Endpoint measures in the mdx mouse relevant for muscular dystrophy pre-clinical studies. Neuromuscul Disord. 2012;22: 34–42. doi:10.1016/j.nmd.2011.08.001

330. Call JA, Voelker KA, Wolff AV, McMillan RP, Evans NP, Hulver MW, et al. Endurance capacity in maturing mdx mice is markedly enhanced by combined voluntary wheel running and green tea extract. Journal of Applied Physiology. 2008;105: 923–932. doi:10.1152/japplphysiol.00028.2008

331. Hulmi JJ, Oliveira BM, Silvennoinen M, Hoogaars WMH, Pasternack A, Kainulainen H, et al. Exercise restores decreased physical activity levels and increases markers of autophagy and oxidative capacity in myostatin/activin-blocked mdx mice. Am J Physiol Endocrinol Metab. 2013;305: E171-182. doi:10.1152/ajpendo.00065.2013

332. Baltgalvis KA, Call JA, Cochrane GD, Laker RC, Yan Z, Lowe DA. Exercise training improves plantar flexor muscle function in mdx mice. Med Sci Sports Exerc. 2012;44: 1671–1679. doi:10.1249/MSS.0b013e31825703f0

333. Burdi R, Rolland J-F, Fraysse B, Litvinova K, Cozzoli A, Giannuzzi V, et al. Multiple pathological events in exercised dystrophic mdx mice are targeted by pentoxifylline: outcome of a large array of in vivo and ex vivo tests. J Appl Physiol. 2009;106: 1311–1324. doi:10.1152/japplphysiol.90985.2008

334. Faist V, König J, Höger H, Elmadfa I. Decreased mitochondrial oxygen consumption and antioxidant enzyme activities in skeletal muscle of dystrophic mice after low-intensity exercise. Ann Nutr Metab. 2001;45: 58–66. doi:10.1159/000046707

335. Louboutin JP, Fichter-Gagnepain V, Thaon E, Fardeau M. Morphometric analysis of mdx diaphragm muscle fibres. Comparison with hindlimb muscles. Neuromuscul Disord. 1993;3: 463–469. doi:10.1016/0960-8966(93)90098-5

336. Brussee V, Tardif F, Tremblay JP. Muscle fibers of mdx mice are more vulnerable to exercise than those of normal mice. Neuromuscular Disorders. 1997;7: 487–492. doi:10.1016/S0960-8966(97)00115-6

337. Nakamura A, Yoshida K, Takeda S, Dohi N, Ikeda S. Progression of dystrophic features and activation of mitogen-activated protein kinases and calcineurin by physical exercise, in hearts of *mdx* mice. FEBS Letters. 2002;520: 18–24. doi:10.1016/S0014-5793(02)02739-4

338. Nakamura A, Yoshida K, Ueda H, Takeda S, Ikeda S. Up-regulation of mitogen activated protein kinases in mdx skeletal muscle following chronic treadmill exercise. Biochimica et Biophysica Acta (BBA) - Molecular Basis of Disease. 2005;1740: 326–331. doi:10.1016/j.bbadis.2004.12.003

339. Okano T, Yoshida K, Nakamura A, Sasazawa F, Oide T, Takeda S, et al. Chronic exercise accelerates the degeneration–regeneration cycle and downregulates insulin-like growth factor-1 in muscle ofmdx mice. Muscle Nerve. 2005;32: 191–199. doi:10.1002/mus.20351

340. Radley-Crabb H, Terrill J, Shavlakadze T, Tonkin J, Arthur P, Grounds M. A single 30min treadmill exercise session is suitable for 'proof-of concept studies' in adult mdx mice: A comparison of the early consequences of two different treadmill protocols. Neuromuscular Disorders. 2012;22: 170–182. doi:10.1016/j.nmd.2011.07.008

341. Camerino GM, Cannone M, Giustino A, Massari AM, Capogrosso RF, Cozzoli A, et al. Gene expression in mdx mouse muscle in relation to age and exercise: aberrant mechanical–metabolic coupling and implications for pre-clinical studies in Duchenne muscular dystrophy. Human Molecular Genetics. 2014;23: 5720–5732. doi:10.1093/hmg/ddu287

342. Schill KE, Altenberger AlexR, Lowe J, Periasamy M, Villamena FA, Rafael-Fortney JiA, et al. Muscle damage, metabolism, and oxidative stress in *mdx* mice: Impact of aerobic running: Impact Of Aerobic Running IN *MDX* Mice. Muscle Nerve. 2016;54: 110–117. doi:10.1002/mus.25015

343. Gaiad TP, Oliveira MX, Lobo-Jr AR, Libório LR, Pinto PAF, Fernandes DC, et al. Low-intensity training provokes adaptive extracellular matrix turnover of a muscular dystrophy model. J Exerc Rehabil. 2017;13: 693–703. doi:10.12965/jer.1735094.547

344. Zelikovich AS, Quattrocelli M, Salamone IM, Kuntz NL, McNally EM. Moderate exercise improves function and increases adiponectin in the mdx mouse model of muscular dystrophy. Sci Rep. 2019;9: 5770. doi:10.1038/s41598-019-42203-z

345. Capogrosso RF, Mantuano P, Cozzoli A, Sanarica F, Massari AM, Conte E, et al. Contractile efficiency of dystrophic mdx mouse muscle: in vivo and ex vivo assessment of adaptation to exercise of functional end points. Journal of Applied Physiology. 2017;122: 828–843. doi:10.1152/japplphysiol.00776.2015

346. Carter GT, Wineinger MA, Walsh SA, Horasek SJ, Abresch RT, Fowler WM. Effect of voluntary wheel-running exercise on muscles of the mdx mouse. Neuromuscular Disorders. 1995;5: 323–332. doi:10.1016/0960-8966(94)00063-F

347. Hayes A, Williams DA. Beneficial effects of voluntary wheel running on the properties of dystrophic mouse muscle. Journal of Applied Physiology. 1996;80: 670–679. doi:10.1152/jappl.1996.80.2.670

348. Wineinger MA, Abresch RT, Walsh SA, Carter GT. Effects of aging and voluntary exercise on the function of dystrophic muscle from mdx mice. Am J Phys Med Rehabil. 1998; 77: 20-27.

349. Landisch RM, Kosir AM, Nelson SA, Baltgalvis KA, Lowe DA. Adaptive and nonadaptive responses to voluntary wheel running by *mdx* mice. Muscle Nerve. 2008;38: 1290–1293. doi:10.1002/mus.21141

350. Smythe GM, White JD. Voluntary wheel running in dystrophin-deficient (mdx) mice: Relationships between exercise parameters and exacerbation of the dystrophic phenotype. PLoS Curr. 2012;3: RRN1295. doi:10.1371/currents.RRN1295

351. Hourdé C, Joanne P, Medja F, Mougenot N, Jacquet A, Mouisel E, et al. Voluntary Physical Activity Protects from Susceptibility to Skeletal Muscle Contraction–Induced Injury But Worsens Heart Function in mdx Mice. The American Journal of Pathology. 2013;182: 1509–1518. doi:10.1016/j.ajpath.2013.01.020

352. Selsby JT, Acosta P, Sleeper MM, Barton ER, Sweeney HL. Long-term wheel running compromises diaphragm function but improves cardiac and plantarflexor function in the mdx mouse. Journal of Applied Physiology. 2013;115: 660–666. doi:10.1152/japplphysiol.00252.2013

353. Gordon BS, Lowe DA, Kostek MC. Exercise increases utrophin protein expression in the *mdx* mouse model of Duchenne muscular dystrophy: Short Reports. Muscle Nerve. 2014;49: 915–918. doi:10.1002/mus.24151

354. Ferry A, Benchaouir R, Joanne P, Peat RA, Mougenot N, Agbulut O, et al. Effect of voluntary physical activity initiated at age 7 months on skeletal hindlimb and cardiac muscle function in *mdx* mice of both genders: Physical Activity in *mdx* Mice. Muscle Nerve. 2015;52: 788–794. doi:10.1002/mus.24604

355. Hayes A, Lynch GS, Williams D. The effects of endurance exercise on dystrophic *mdx* mice. I. Contractile and histochemical properties of intact muscles. Proc R Soc Lond B. 1993;253: 19–25. doi:10.1098/rspb.1993.0077

356. Lynch GS, Hayes A, Lam M, Williams D. The effects of endurance exercise on dystrophic *mdx* mice. II. Contractile properties of skinned muscle fibres. Proc R Soc Lond B. 1993;253: 27–33. doi:10.1098/rspb.1993.0078

357. Hyzewicz J, Tanihata J, Kuraoka M, Ito N, Miyagoe-Suzuki Y, Takeda S. Low intensity training of mdx mice reduces carbonylation and increases expression levels of proteins involved in energy metabolism and muscle contraction. Free Radical Biology and Medicine. 2015;82: 122–136. doi:10.1016/j.freeradbiomed.2015.01.023

358. Frinchi M, Macaluso F, Licciardi A, Perciavalle V, Coco M, Belluardo N, et al. Recovery of Damaged Skeletal Muscle in mdx Mice through Low-intensity Endurance Exercise. Int J Sports Med. 2013;35: 19–27. doi:10.1055/s-0033-1343405

359. Fontana S, Schillaci O, Frinchi M, Giallombardo M, Morici G, Liberto VD, et al. Reduction in mdx mouse muscle degeneration by low-intensity endurance exercise: a proteomic

analysis in quadriceps muscle of exercised compared with sedentary mdx mice. Bioscience Reports. 2015;35: e00213. doi:10.1042/BSR20150013

360. Morici G, Frinchi M, Pitruzzella A, Di Liberto V, Barone R, Pace A, et al. Mild Aerobic Exercise Training Hardly Affects the Diaphragm of *mdx* Mice: DIAPHRAGM AFTER MILD TRAINING IN *mdx* MICE. J Cell Physiol. 2017;232: 2044–2052. doi:10.1002/jcp.25573

361. Fridén J, Lieber RL. Structural and mechanical basis of exercise-induced muscle injury. Med Sci Sports Exerc. 1992;24: 521–530.

362. Lieber RL, Fridén J. Mechanisms of muscle injury after eccentric contraction. Journal of Science and Medicine in Sport. 1999;2: 253–265. doi:10.1016/S1440-2440(99)80177-7

363. Brown SJ, Child RB, Day SH, Donnelly AE. Indices of skeletal muscle damage and connective tissue breakdown following eccentric muscle contractions. Eur J Appl Physiol. 1997;75: 369–374. doi:10.1007/s004210050174

364. Crameri RM, Aagaard P, Qvortrup K, Langberg H, Olesen J, Kjær M. Myofibre damage in human skeletal muscle: effects of electrical stimulation versus voluntary contraction. The Journal of Physiology. 2007;583: 365–380. doi:10.1113/jphysiol.2007.128827

365. Quinlan JG, Wong BL, Niemeier RT, McCullough AS, Levin L, Emanuele M. Poloxamer 188 failed to prevent exercise-induced membrane breakdown in mdx skeletal muscle fibers. Neuromuscular Disorders. 2006;16: 855–864. doi:10.1016/j.nmd.2006.09.016

366. Whitehead NP, Streamer M, Lusambili LI, Sachs F, Allen DG. Streptomycin reduces stretch-induced membrane permeability in muscles from mdx mice. Neuromuscular Disorders. 2006;16: 845–854. doi:10.1016/j.nmd.2006.07.024

367. Mathur S, Vohra RS, Germain SA, Forbes S, Bryant ND, Vandenborne K, et al. Changes in muscle T2 and tissue damage after downhill running in mdx Mice. Muscle & Nerve. 2011;43: 878–886. doi:10.1002/mus.21986

368. Terrill JR, Radley-Crabb HG, Grounds MD, Arthur PG. N-Acetylcysteine treatment of dystrophic mdx mice results in protein thiol modifications and inhibition of exercise induced myofibre necrosis. Neuromuscular Disorders. 2012;22: 427–434. doi:10.1016/j.nmd.2011.11.007

369. Hyzewicz J, Ruegg UT, Takeda S. Comparison of Experimental Protocols of Physical Exercise for mdx Mice and Duchenne Muscular Dystrophy Patients. J Neuromuscul Dis. 2015;2: 325–342. doi:10.3233/JND-150106

370. Dupont-Versteegden EE, McCarter RJ, Katz MS. Voluntary exercise decreases progression of muscular dystrophy in diaphragm of mdx mice. Journal of Applied Physiology. 1994; 77(4): 1736-1741.

371. Anziska Y, Sternberg A. Exercise in neuromuscular disease: Exercise in Neuromuscular Disease. Muscle Nerve. 2013;48: 3–20. doi:10.1002/mus.23771

372. Markert CD, Case LE, Carter GT, Furlong PA, Grange RW. Exercise and duchenne muscular dystrophy: Where we have been and where we need to go: Issues & Opinions: Exercise and DMD Roundtable. Muscle Nerve. 2012;45: 746–751. doi:10.1002/mus.23244

373. Voet NB, van der Kooi EL, Riphagen II, Lindeman E, van Engelen BG, Geurts AC. Strength training and aerobic exercise training for muscle disease. Cochrane Neuromuscular Group, editor. Cochrane Database of Systematic Reviews. 2013 [cited 2 Jun 2020]. doi:10.1002/14651858.CD003907.pub4

374. Howe K, Clark MD, Torroja CF, Torrance J, Berthelot C, Muffato M, et al. The zebrafish reference genome sequence and its relationship to the human genome. Nature. 2013;496: 498–503. doi:10.1038/nature12111

375. Gibbs EM, Horstick EJ, Dowling JJ. Swimming into prominence: the zebrafish as a valuable tool for studying human myopathies and muscular dystrophies. FEBS J. 2013;280: 4187–4197. doi:10.1111/febs.12412

376. Berger J, Currie PD. Zebrafish models flex their muscles to shed light on muscular dystrophies. Disease Models & Mechanisms. 2012;5: 726–732. doi:10.1242/dmm.010082

377. Berger J, Berger S, Hall TE, Lieschke GJ, Currie PD. Dystrophin-deficient zebrafish feature aspects of the Duchenne muscular dystrophy pathology. Neuromuscular Disorders. 2010;20: 826–832. doi:10.1016/j.nmd.2010.08.004

378. Telfer WR, Busta AS, Bonnemann CG, Feldman EL, Dowling JJ. Zebrafish models of collagen VI-related myopathies. Hum Mol Genet. 2010;19: 2433–2444. doi:10.1093/hmg/ddq126

379. Lieschke GJ, Currie PD. Animal models of human disease: zebrafish swim into view. Nat Rev Genet. 2007;8: 353–367. doi:10.1038/nrg2091

380. Santoriello C, Zon LI. Hooked! Modeling human disease in zebrafish. J Clin Invest. 2012;122: 2337–2343. doi:10.1172/JCI60434

381. Parsons MJ, Campos I, Hirst EMA, Stemple DL. Removal of dystroglycan causes severe muscular dystrophy in zebrafish embryos. Development. 2002;129: 3505–3512.

382. Guyon JR, Mosley AN, Zhou Y, O'Brien KF, Sheng X, Chiang K, et al. The dystrophin associated protein complex in zebrafish. Hum Mol Genet. 2003;12: 601–615.

383. Hirata H, Watanabe T, Hatakeyama J, Sprague SM, Saint-Amant L, Nagashima A, et al. Zebrafish relatively relaxed mutants have a ryanodine receptor defect, show slow swimming and provide a model of multi-minicore disease. Development. 2007;134: 2771–2781. doi:10.1242/dev.004531

384. Dou Y, Andersson-Lendahl M, Arner A. Structure and function of skeletal muscle in zebrafish early larvae. J Gen Physiol. 2008;131: 445–453. doi:10.1085/jgp.200809982

385. Dowling JJ, Vreede AP, Low SE, Gibbs EM, Kuwada JY, Bonnemann CG, et al. Loss of myotubularin function results in T-tubule disorganization in zebrafish and human myotubular myopathy. PLoS Genet. 2009;5: e1000372. doi:10.1371/journal.pgen.1000372

386. Widrick JJ, Alexander MS, Sanchez B, Gibbs DE, Kawahara G, Beggs AH, et al. Muscle dysfunction in a zebrafish model of Duchenne muscular dystrophy. Physiol Genomics. 2016;48: 850–860. doi:10.1152/physiolgenomics.00088.2016

387. Saint-Amant L, Drapeau P. Time course of the development of motor behaviors in the zebrafish embryo. J Neurobiol. 1998;37: 622–632. doi:10.1002/(sici)1097-4695(199812)37:4<622::aid-neu10>3.0.co;2-s

388. Granato M, van Eeden FJ, Schach U, Trowe T, Brand M, Furutani-Seiki M, et al. Genes controlling and mediating locomotion behavior of the zebrafish embryo and larva. Development. 1996;123: 399–413.

389. Bassett DI, Bryson-Richardson RJ, Daggett DF, Gautier P, Keenan DG, Currie PD. Dystrophin is required for the formation of stable muscle attachments in the zebrafish embryo. Development. 2003;130: 5851–5860. doi:10.1242/dev.00799

390. Bassett D, Currie PD. Identification of a Zebrafish Model of Muscular Dystrophy. Clinical and Experimental Pharmacology and Physiology. 2004;31: 537–540. doi:10.1111/j.1440-1681.2004.04030.x

391. Subramanian A, Schilling TF. Thrombospondin-4 controls matrix assembly during development and repair of myotendinous junctions. eLife. 2014;3: e02372. doi:10.7554/eLife.02372

392. Pette D, Vrbová G. Neural control of phenotypic expression in mammalian muscle fibers. Muscle Nerve. 1985;8: 676–689. doi:10.1002/mus.880080810

393. Scott OM, Hyde SA, Vrbová G, Dubowitz V. Therapeutic possibilities of chronic low frequency electrical stimulation in children with Duchenne muscular dystrophy. Journal of the Neurological Sciences. 1990;95: 171–182. doi:10.1016/0022-510X(90)90240-N

394. Fitts RH, Riley DR, Widrick JJ. Physiology of a microgravity environment invited review: microgravity and skeletal muscle. J Appl Physiol. 2000;89: 823–839. doi:10.1152/jappl.2000.89.2.823

395. Fitts RH, Trappe SW, Costill DL, Gallagher PM, Creer AC, Colloton PA, et al. Prolonged space flight-induced alterations in the structure and function of human skeletal muscle fibres. J Physiol (Lond). 2010;588: 3567–3592. doi:10.1113/jphysiol.2010.188508

396. Freilinger G, Mayr W. Electrical stimulation as a countermeasure to muscle alteration in space. J Gravit Physiol. 2002;9: P319-322.

397. Gibson JN, Halliday D, Morrison WL, Stoward PJ, Hornsby GA, Watt PW, et al. Decrease in human quadriceps muscle protein turnover consequent upon leg immobilization. Clin Sci. 1987;72: 503–509. doi:10.1042/cs0720503

398. Chang DG, Healey RM, Snyder AJ, Sayson JV, Macias BR, Coughlin DG, et al. Lumbar Spine Paraspinal Muscle and Intervertebral Disc Height Changes in Astronauts After Long-Duration Spaceflight on the International Space Station. Spine. 2016;41: 1917–1924. doi:10.1097/BRS.0000000000001873

399. Dirks ML, Groen BBL, Franssen R, van Kranenburg J, van Loon LJC. Neuromuscular electrical stimulation prior to presleep protein feeding stimulates the use of protein-derived amino acids for overnight muscle protein synthesis. J Appl Physiol. 2017;122: 20–27. doi:10.1152/japplphysiol.00331.2016

400. Gibson JN, Smith K, Rennie MJ. Prevention of disuse muscle atrophy by means of electrical stimulation: maintenance of protein synthesis. Lancet. 1988;2: 767–770. doi:10.1016/s0140-6736(88)92417-8

401. Glover EI, Phillips SM, Oates BR, Tang JE, Tarnopolsky MA, Selby A, et al. Immobilization induces anabolic resistance in human myofibrillar protein synthesis with low and high dose amino acid infusion. J Physiol (Lond). 2008;586: 6049–6061. doi:10.1113/jphysiol.2008.160333

402. Gobbo M, Maffiuletti NA, Orizio C, Minetto MA. Muscle motor point identification is essential for optimizing neuromuscular electrical stimulation use. J Neuroeng Rehabil. 2014;11: 17. doi:10.1186/1743-0003-11-17

403. Gondin J, Cozzone PJ, Bendahan D. Is high-frequency neuromuscular electrical stimulation a suitable tool for muscle performance improvement in both healthy humans and athletes? Eur J Appl Physiol. 2011;111: 2473–2487. doi:10.1007/s00421-011-2101-2

404. Gregory CM, Bickel CS. Recruitment patterns in human skeletal muscle during electrical stimulation. Phys Ther. 2005;85: 358–364.

405. Hackney KJ, Scott JM, Hanson AM, English KL, Downs ME, Ploutz-Snyder LL. The Astronaut-Athlete: Optimizing Human Performance in Space. J Strength Cond Res. 2015;29: 3531–3545. doi:10.1519/JSC.0000000000001191

406. Hargens AR, Richardson S. Cardiovascular adaptations, fluid shifts, and countermeasures related to space flight. Respir Physiol Neurobiol. 2009;169 Suppl 1: S30-33. doi:10.1016/j.resp.2009.07.005

407. Jones S, Man WD-C, Gao W, Higginson IJ, Wilcock A, Maddocks M. Neuromuscular electrical stimulation for muscle weakness in adults with advanced disease. Cochrane Database Syst Rev. 2016;10: CD009419. doi:10.1002/14651858.CD009419.pub3

408. Gould N, Donnermeyer D, Pope M, Ashikaga T. Transcutaneous muscle stimulation as a method to retard disuse atrophy. Clin Orthop Relat Res. 1982; 215–220.

409. Green DA, Scott JPR. Spinal Health during Unloading and Reloading Associated with Spaceflight. Front Physiol. 2017;8: 1126. doi:10.3389/fphys.2017.01126

410. Sheffler LR, Chae J. Neuromuscular electrical stimulation in neurorehabilitation. Muscle Nerve. 2007;35: 562–590. doi:10.1002/mus.20758

411. Theurel J, Lepers R, Pardon L, Maffiuletti NA. Differences in cardiorespiratory and neuromuscular responses between voluntary and stimulated contractions of the quadriceps femoris muscle. Respir Physiol Neurobiol. 2007;157: 341–347. doi:10.1016/j.resp.2006.12.002

412. De l'électrisation localisée et de son application à la pathologie et à la thérapeutique - Digital Collections - National Library of Medicine. [cited 2 Jun 2020]. Available: https://collections.nlm.nih.gov/catalog/nlm:nlmuid-63860920R-bk

413. Botelho SY, Beckett SB, Bendler E. Mechanical and electrical responses of intact thenar muscles to indirect stimuli: study of patients with pseudohypertrophic muscular dystrophy. Neurology. 1960;10: 601–612. doi:10.1212/wnl.10.6.601

414. Desmedt JE, Emeryk B. Disorder of muscle contraction processes in sex-linked (Duchenne) muscular dystrophy, with correlative electromyographic study of myopathic involvement in small hand muscles. Am J Med. 1968;45: 853–872. doi:10.1016/0002-9343(68)90184-8

415. Buchthal F, Schmalbruch H, Kamieniecka Z. Contraction times and fiber types in patients with progressive muscular dystrophy. Neurology. 1971;21: 131–139. doi:10.1212/wnl.21.2.131

416. McComas AJ, Sica RE, Currie S. An electrophysiological study of Duchenne dystrophy. J Neurol Neurosurg Psychiatry. 1971;34: 461–468. doi:10.1136/jnnp.34.4.461

417. Reichmann H, Pette D, Vrbová G. Effects of low frequency electrical stimulation on enzyme and isozyme patterns of dystrophic mouse muscle. FEBS Lett. 1981;128: 55–58. doi:10.1016/0014-5793(81)81078-2

418. Barnard EA, Barnard PJ, Jarvis JC, Lai J. Low frequency chronic electrical stimulation of normal and dystrophic chicken muscle. J Physiol. 1986;376: 377–409.

419. Zupan A. Long-term electrical stimulation of muscles in children with Duchenne and Becker muscular dystrophy. Muscle Nerve. 1992;15: 362–367. doi:10.1002/mus.880150316

420. Zupan A, Gregorič M, Valenčič V, Vandot S. Effects of Electrical Stimulation on Muscles of Children with Duchenne and Becker Muscular Dystrophy. Neuropediatrics. 1993;24: 189–192. doi:10.1055/s-2008-1071537

421. Luthert P, Vrbova G, Ward KM. Effects of slow frequency electrical stimulation on muscles of dystrophic mice. Journal of Neurology, Neurosurgery & Psychiatry. 1980;43: 803–809. doi:10.1136/jnnp.43.9.803

422. Vrbová G, Ward K. Observations on the effects of low frequency electrical stimulation on fast muscles of dystrophic mice. J Neurol Neurosurg Psychiatry. 1981;44: 1002–1006.

423. Dangain J, Vrbova G. Long term effect of low frequency chronic electrical stimulation on the fast hind limb muscles of dystrophic mice. J Neurol Neurosurg Psychiatry. 1989;52: 1382–1389. doi:10.1136/jnnp.52.12.1382

424. Fujita N, Murakami S, Fujino H. The Combined Effect of Electrical Stimulation and High-Load Isometric Contraction on Protein Degradation Pathways in Muscle Atrophy Induced by Hindlimb Unloading. Journal of Biomedicine and Biotechnology. 2011;2011: 1–8. doi:10.1155/2011/401493

425. Kern H, Barberi L, Löfler S, Sbardella S, Burggraf S, Fruhmann H, et al. Electrical Stimulation Counteracts Muscle Decline in Seniors. Front Aging Neurosci. 2014;6. doi:10.3389/fnagi.2014.00189

426. Gondin J, Brocca L, Bellinzona E, D'Antona G, Maffiuletti NA, Miotti D, et al. Neuromuscular electrical stimulation training induces atypical adaptations of the human skeletal muscle phenotype: a functional and proteomic analysis. J Appl Physiol. 2011;110: 433–450. doi:10.1152/japplphysiol.00914.2010

427. Donoghue P, Doran P, Dowling P, Ohlendieck K. Differential expression of the fast skeletal muscle proteome following chronic low-frequency stimulation. Biochimica et Biophysica Acta (BBA) - Proteins and Proteomics. 2005;1752: 166–176. doi:10.1016/j.bbapap.2005.08.005

428. Donoghue P, Doran P, Wynne K, Pedersen K, Dunn MJ, Ohlendieck K. Proteomic profiling of chronic low-frequency stimulated fast muscle. PROTEOMICS. 2007;7: 3417–3430. doi:10.1002/pmic.200700262

429. Moo EK, Herzog W. Single sarcomere contraction dynamics in a whole muscle. Scientific Reports. 2018;8: 15235. doi:10.1038/s41598-018-33658-7

430. Gordon AM, Huxley AF, Julian FJ. The variation in isometric tension with sarcomere length in vertebrate muscle fibres. The Journal of Physiology. 1966;184: 170–192. doi:10.1113/jphysiol.1966.sp007909

431. Huang S-H, Hsiao C-D, Lin D-S, Chow C-Y, Chang C-J, Liau I. Imaging of Zebrafish In Vivo with Second-Harmonic Generation Reveals Shortened Sarcomeres Associated with Myopathy Induced by Statin. PLOS ONE. 2011;6: e24764. doi:10.1371/journal.pone.0024764

432. Malfatti E, Romero NB. Diseases of the skeletal muscle. Handb Clin Neurol. 2017;145: 429–451. doi:10.1016/B978-0-12-802395-2.00030-4

433. Schreiber KH, Kennedy BK. When lamins go bad: nuclear structure and disease. Cell. 2013;152: 1365–1375. doi:10.1016/j.cell.2013.02.015

434. Bruusgaard JC, Liestøl K, Ekmark M, Kollstad K, Gundersen K. Number and spatial distribution of nuclei in the muscle fibres of normal mice studied in vivo. J Physiol. 2003;551: 467–478. doi:10.1113/jphysiol.2003.045328

435. Levy DL, Heald R. Mechanisms of intracellular scaling. Annu Rev Cell Dev Biol. 2012;28: 113–135. doi:10.1146/annurev-cellbio-092910-154158

436. Windner SE, Manhart A, Brown A, Mogilner A, Baylies MK. Nuclear Scaling Is Coordinated among Individual Nuclei in Multinucleated Muscle Fibers. Dev Cell. 2019;49: 48-62.e3. doi:10.1016/j.devcel.2019.02.020

437. Csapo R, Gumpenberger M, Wessner B. Skeletal Muscle Extracellular Matrix – What Do We Know About Its Composition, Regulation, and Physiological Roles? A Narrative Review. Front Physiol. 2020;11. doi:10.3389/fphys.2020.00253

438. Coles CA, Gordon L, Hunt LC, Webster T, Piers AT, Kintakas C, et al. Expression profiling in exercised mdx suggests a role for extracellular proteins in the dystrophic muscle immune response. Hum Mol Genet. 2020;29: 353–368. doi:10.1093/hmg/ddz266

439. Pescatori M, Broccolini A, Minetti C, Bertini E, Bruno C, D'amico A, et al. Gene expression profiling in the early phases of DMD: a constant molecular signature characterizes DMD muscle from early postnatal life throughout disease progression. The FASEB Journal. 2007;21: 1210–1226. doi:10.1096/fj.06-7285com

440. Baban D, Davies KE. Microarray analysis of mdx mice expressing high levels of utrophin: Therapeutic implications for dystrophin deficiency. Neuromuscular Disorders. 2008;18: 239–247. doi:10.1016/j.nmd.2007.11.011

441. Ferguson JW, Thoma BS, Mikesh MF, Kramer RH, Bennett KL, Purchio A, et al. The extracellular matrix protein betaIG-H3 is expressed at myotendinous junctions and supports muscle cell adhesion. Cell Tissue Res. 2003;313: 93–105. doi:10.1007/s00441-003-0743-z

442. Kim HR, Ingham PW. The extracellular matrix protein TGFBI promotes myofibril bundling and muscle fibre growth in the zebrafish embryo. Dev Dyn. 2009;238: 56–65. doi:10.1002/dvdy.21812

443. Özdemir C, Akpulat U, Sharafi P, Yıldız Y, Onbaşılar İ, Kocaefe Ç. Periostin is temporally expressed as an extracellular matrix component in skeletal muscle regeneration and differentiation. Gene. 2014;553: 130–139. doi:10.1016/j.gene.2014.10.014

444. Kudo H, Amizuka N, Araki K, Inohaya K, Kudo A. Zebrafish periostin is required for the adhesion of muscle fiber bundles to the myoseptum and for the differentiation of muscle fibers. Dev Biol. 2004;267: 473–487. doi:10.1016/j.ydbio.2003.12.007

445. Norris RA, Moreno-Rodriguez R, Hoffman S, Markwald RR. The many facets of the matricelluar protein periostin during cardiac development, remodeling, and pathophysiology. J Cell Commun Signal. 2009;3: 275–286. doi:10.1007/s12079-009-0063-5

446. Marotta M, Ruiz-Roig C, Sarria Y, Peiro JL, Nuñez F, Ceron J, et al. Muscle genome-wide expression profiling during disease evolution in mdx mice. Physiol Genomics. 2009;37: 119–132. doi:10.1152/physiolgenomics.90370.2008

447. Kruzynska-Frejtag A, Machnicki M, Rogers R, Markwald RR, Conway SJ. Periostin (an osteoblast-specific factor) is expressed within the embryonic mouse heart during valve formation. Mech Dev. 2001;103: 183–188. doi:10.1016/s0925-4773(01)00356-2

448. Rani S, Barbe MF, Barr AE, Litvin J. Induction of Periostin-like Factor and Periostin in Forearm Muscle, Tendon, and Nerve in an Animal Model of Work-related Musculoskeletal Disorder. J Histochem Cytochem. 2009;57: 1061–1073. doi:10.1369/jhc.2009.954081

449. Lorts A, Schwanekamp JA, Baudino TA, McNally EM, Molkentin JD. Deletion of periostin reduces muscular dystrophy and fibrosis in mice by modulating the transforming growth factor- pathway. Proceedings of the National Academy of Sciences. 2012;109: 10978–10983. doi:10.1073/pnas.1204708109

450. Kii I, Nishiyama T, Li M, Matsumoto K, Saito M, Amizuka N, et al. Incorporation of Tenascin-C into the Extracellular Matrix by Periostin Underlies an Extracellular Meshwork Architecture. J Biol Chem. 2010;285: 2028–2039. doi:10.1074/jbc.M109.051961

451. Norris RA, Damon B, Mironov V, Kasyanov V, Ramamurthi A, Moreno-Rodriguez R, et al. Periostin regulates collagen fibrillogenesis and the biomechanical properties of connective tissues. J Cell Biochem. 2007;101: 695–711. doi:10.1002/jcb.21224

452. Mayer U. Integrins: Redundant or Important Players in Skeletal Muscle? J Biol Chem. 2003;278: 14587–14590. doi:10.1074/jbc.R200022200

453. Bronner-Fraser M, Artinger M, Muschler J, Horwitz AF. Developmentally regulated expression of alpha 6 integrin in avian embryos. Development. 1992;115: 197–211.

454. Blaschuk KL, Holland PC. The regulation of α5β1 integrin expression in human muscle cells. Developmental Biology. 1994;164: 475–483. doi:10.1006/dbio.1994.1217

455. Boettiger D, Enomoto-Iwamoto M, Yoon HY, Hofer U, Menko AS, Chiquet-Ehrismann R. Regulation of Integrin α5β1 Affinity during Myogenic Differentiation. Developmental Biology. 1995;169: 261–272. doi:10.1006/dbio.1995.1142

456. Song WK, Wang W, Sato H, Bielser DA, Kaufman SJ. Expression of alpha 7 integrin cytoplasmic domains during skeletal muscle development: alternate forms, conformational change, and homologies with serine/threonine kinases and tyrosine phosphatases. J Cell Sci. 1993;106 (Pt 4): 1139–1152.

457. Yao CC, Ziober BL, Sutherland AE, Mendrick DL, Kramer RH. Laminins promote the locomotion of skeletal myoblasts via the alpha 7 integrin receptor. J Cell Sci. 1996;109 (Pt 13): 3139–3150.

458. Bao ZZ, Lakonishok M, Kaufman S, Horwitz AF. Alpha 7 beta 1 integrin is a component of the myotendinous junction on skeletal muscle. J Cell Sci. 1993;106 (Pt 2): 579–589.

459. Martin PT, Kaufman SJ, Kramer RH, Sanes JR. Synaptic Integrins in Developing, Adult, and Mutant Muscle: Selective Association of α1, α7A, and α7B Integrins with the Neuromuscular Junction. Developmental Biology. 1996;174: 125–139. doi:10.1006/dbio.1996.0057

460. Burkin DJ, Kaufman SJ. The α7β1 integrin in muscle development and disease. Cell and Tissue Research. 1999;296: 183–190. doi:10.1007/s004410051279

461. Rozo M, Li L, Fan C-M. Targeting β1-Integrin Signaling Enhances Regeneration in Aged and Dystrophic Muscle in Mice. Nat Med. 2016;22: 889–896. doi:10.1038/nm.4116

462. Burkin DJ, Wallace GQ, Milner DJ, Chaney EJ, Mulligan JA, Kaufman SJ. Transgenic expression of {alpha}7{beta}1 integrin maintains muscle integrity, increases regenerative capacity, promotes hypertrophy, and reduces cardiomyopathy in dystrophic mice. Am J Pathol. 2005;166: 253–263.

463. Boppart MD, Volker SE, Alexander N, Burkin DJ, Kaufman SJ. Exercise promotes α7 integrin gene transcription and protection of skeletal muscle. American Journal of Physiology-Regulatory, Integrative and Comparative Physiology. 2008;295: R1623–R1630. doi:10.1152/ajpregu.00089.2008

464. Järvinen TA, Kannus P, Järvinen TL, Jozsa L, Kalimo H, Järvinen M. Tenascin-C in the pathobiology and healing process of musculoskeletal tissue injury. Scand J Med Sci Sports. 2000;10: 376–382. doi:10.1034/j.1600-0838.2000.010006376.x

465. Goody MF, Kelly MW, Reynolds CJ, Khalil A, Crawford BD, Henry CA. NAD+ Biosynthesis Ameliorates a Zebrafish Model of Muscular Dystrophy. Kunkel LM, editor. PLoS Biology. 2012;10: e1001409. doi:10.1371/journal.pbio.1001409

466. Van Ry PM, Fontelonga TM, Barraza-Flores P, Sarathy A, Nunes AM, Burkin DJ. ECM-Related Myopathies and Muscular Dystrophies: Pros and Cons of Protein Therapies. Compr Physiol. 2017;7: 1519–1536. doi:10.1002/cphy.c150033

467. Subramanian A, Schilling TF. Thrombospondin-4 controls matrix assembly during development and repair of myotendinous junctions. eLife. 2014;3. doi:10.7554/eLife.02372

468. Flück M, Carson JA, Gordon SE, Ziemiecki A, Booth FW. Focal adhesion proteins FAK and paxillin increase in hypertrophied skeletal muscle. American Journal of Physiology-Cell Physiology. 1999;277: C152–C162. doi:10.1152/ajpcell.1999.277.1.C152

469. Quach NL, Rando TA. Focal adhesion kinase is essential for costamerogenesis in cultured skeletal muscle cells. Developmental Biology. 2006;293: 38–52. doi:10.1016/j.ydbio.2005.12.040

470. Goody MF, Kelly MW, Lessard KN, Khalil A, Henry CA. Nrk2b-mediated NAD+ production regulates cell adhesion and is required for muscle morphogenesis in vivo. Dev Biol. 2010;344: 809–826. doi:10.1016/j.ydbio.2010.05.513

471. Boolell M, Allen MJ, Ballard SA, Gepi-Attee S, Muirhead GJ, Naylor AM, et al. Sildenafil: an orally active type 5 cyclic GMP-specific phosphodiesterase inhibitor for the treatment of penile erectile dysfunction. Int J Impot Res. 1996;8: 47–52.

472. Ramachandran J, Schneider JS, Crassous P-A, Zheng R, Gonzalez JP, Xie L-H, et al. Nitric Oxide Signaling Pathway in Duchenne Muscular Dystrophy Mice: Upregulation of L-arginine Transporters. Biochem J. 2013;449: 133–142. doi:10.1042/BJ20120787

473. Chang WJ, Iannaccone ST, Lau KS, Masters BS, McCabe TJ, McMillan K, et al. Neuronal nitric oxide synthase and dystrophin-deficient muscular dystrophy. Proc Natl Acad Sci USA. 1996;93: 9142–9147. doi:10.1073/pnas.93.17.9142

474. Brenman JE, Chao DS, Xia H, Aldape K, Bredt DS. Nitric oxide synthase complexed with dystrophin and absent from skeletal muscle sarcolemma in Duchenne muscular dystrophy. Cell. 1995;82: 743–752. doi:10.1016/0092-8674(95)90471-9

475. Li D, Yue Y, Lai Y, Hakim CH, Duan D. Nitrosative stress elicited by nNOSμ delocalization inhibits muscle force in dystrophin-null mice. J Pathol. 2011;223: 88–98. doi:10.1002/path.2799

476. Asai A, Sahani N, Kaneki M, Ouchi Y, Martyn JAJ, Yasuhara SE. Primary role of functional ischemia, quantitative evidence for the two-hit mechanism, and phosphodiesterase-5 inhibitor therapy in mouse muscular dystrophy. PLoS ONE. 2007;2: e806. doi:10.1371/journal.pone.0000806

477. Thomas GD, Sander M, Lau KS, Huang PL, Stull JT, Victor RG. Impaired metabolic modulation of alpha-adrenergic vasoconstriction in dystrophin-deficient skeletal muscle. Proc Natl Acad Sci USA. 1998;95: 15090–15095. doi:10.1073/pnas.95.25.15090

478. Bellinger AM, Reiken S, Carlson C, Mongillo M, Liu X, Rothman L, et al. Hypernitrosylated ryanodine receptor calcium release channels are leaky in dystrophic muscle. Nature Medicine. 2009;15: 325–330. doi:10.1038/nm.1916

479. Percival JM, Whitehead NP, Adams ME, Adamo CM, Beavo JA, Froehner SC. Sildenafil reduces respiratory muscle weakness and fibrosis in the mdx mouse model of Duchenne muscular dystrophy. J Pathol. 2012;228: 77–87. doi:10.1002/path.4054

480. Adamo CM, Dai D-F, Percival JM, Minami E, Willis MS, Patrucco E, et al. Sildenafil reverses cardiac dysfunction in the mdx mouse model of Duchenne muscular dystrophy. Proc Natl Acad Sci U S A. 2010;107: 19079–19083. doi:10.1073/pnas.1013077107

481. Khairallah M, Khairallah RJ, Young ME, Allen BG, Gillis MA, Danialou G, et al. Sildenafil and cardiomyocyte-specific cGMP signaling prevent cardiomyopathic changes associated with dystrophin deficiency. Proc Natl Acad Sci USA. 2008;105: 7028–7033. doi:10.1073/pnas.0710595105

482. Parchen CM, Dai D-F, Percival JM, Willis M, Froehner SC, Beavo JA. Sildenafil ameliorates cardiomyopathy in dystrophin-null (mdx) mice. BMC Pharmacol. 2009;9: P53. doi:10.1186/1471-2210-9-S1-P53

483. Batra A, Vohra RS, Chrzanowski SM, Hammers DW, Lott DJ, Vandenborne K, et al. Effects of PDE5 inhibition on dystrophic muscle following an acute bout of downhill running and endurance training. Journal of Applied Physiology. 2019;126: 1737–1745. doi:10.1152/japplphysiol.00664.2018

484. Kawahara G, Karpf JA, Myers JA, Alexander MS, Guyon JR, Kunkel LM. Drug screening in a zebrafish model of Duchenne muscular dystrophy. PNAS. 2011;108: 5331–5336. doi:10.1073/pnas.1102116108

485. Kawahara G, Gasperini MJ, Myers JA, Widrick JJ, Eran A, Serafini PR, et al. Dystrophic muscle improvement in zebrafish via increased heme oxygenase signaling. Human Molecular Genetics. 2014;23: 1869–1878. doi:10.1093/hmg/ddt579

486. Nelson MD, Rader F, Tang X, Tavyev J, Nelson SF, Miceli MC, et al. PDE5 inhibition alleviates functional muscle ischemia in boys with Duchenne muscular dystrophy. Neurology. 2014;82: 2085–2091. doi:10.1212/WNL.0000000000000498

487. Loboda A, Jazwa A, Grochot-Przeczek A, Rutkowski AJ, Cisowski J, Agarwal A, et al. Heme Oxygenase-1 and the Vascular Bed: From Molecular Mechanisms to Therapeutic Opportunities. Antioxidants & Redox Signaling. 2008;10: 1767–1812. doi:10.1089/ars.2008.2043

488. Pietraszek-Gremplewicz K, Kozakowska M, Bronisz-Budzynska I, Ciesla M, Mucha O, Podkalicka P, et al. Heme Oxygenase-1 Influences Satellite Cells and Progression of Duchenne Muscular Dystrophy in Mice. Antioxid Redox Signal. 2018;29: 128–148. doi:10.1089/ars.2017.7435

489. Jazwa A, Stepniewski J, Zamykal M, Jagodzinska J, Meloni M, Emanueli C, et al. Pre-emptive hypoxia-regulated HO-1 gene therapy improves post-ischaemic limb perfusion and tissue regeneration in mice. Cardiovasc Res. 2013;97: 115–124. doi:10.1093/cvr/cvs284

490. Kozakowska M, Pietraszek-Gremplewicz K, Ciesla M, Seczynska M, Bronisz-Budzynska I, Podkalicka P, et al. Lack of Heme Oxygenase-1 Induces Inflammatory Reaction and Proliferation of Muscle Satellite Cells after Cardiotoxin-Induced Skeletal Muscle Injury. Am J Pathol. 2018;188: 491–506. doi:10.1016/j.ajpath.2017.10.017

491. Kozakowska M, Ciesla M, Stefanska A, Skrzypek K, Was H, Jazwa A, et al. Heme Oxygenase-1 Inhibits Myoblast Differentiation by Targeting Myomirs. Antioxid Redox Signal. 2012;16: 113–127. doi:10.1089/ars.2011.3964

492. Hull TD, Boddu R, Guo L, Tisher CC, Traylor AM, Patel B, et al. Heme oxygenase-1 regulates mitochondrial quality control in the heart. JCI Insight. 1. doi:10.1172/jci.insight.85817

493. Piantadosi Claude A., Carraway Martha Sue, Babiker Abdelwahid, Suliman Hagir B. Heme Oxygenase-1 Regulates Cardiac Mitochondrial Biogenesis via Nrf2-Mediated Transcriptional Control of Nuclear Respiratory Factor-1. Circulation Research. 2008;103: 1232–1240. doi:10.1161/01.RES.0000338597.71702.ad

494. Wehling-Henricks M, Tidball JG. Neuronal nitric oxide synthase-rescue of dystrophin/utrophin double knockout mice does not require nNOS localization to the cell membrane. PLoS ONE. 2011;6: e25071. doi:10.1371/journal.pone.0025071

495. Sander M, Chavoshan B, Harris SA, Iannaccone ST, Stull JT, Thomas GD, et al. Functional muscle ischemia in neuronal nitric oxide synthase-deficient skeletal muscle of children with Duchenne muscular dystrophy. Proc Natl Acad Sci USA. 2000;97: 13818–13823. doi:10.1073/pnas.250379497

496. Buchwalow IB, Minin EA, Müller F-U, Lewin G, Samoilova VE, Schmitz W, et al. Nitric oxide synthase in muscular dystrophies: a re-evaluation. Acta Neuropathol. 2006;111: 579–588. doi:10.1007/s00401-006-0069-5

497. Villalta SA, Nguyen HX, Deng B, Gotoh T, Tidball JG. Shifts in macrophage phenotypes and macrophage competition for arginine metabolism affect the severity of muscle pathology in muscular dystrophy. Hum Mol Genet. 2009;18: 482–496. doi:10.1093/hmg/ddn376

498. Louboutin JP, Rouger K, Tinsley JM, Halldorson J, Wilson JM. iNOS expression in dystrophinopathies can be reduced by somatic gene transfer of dystrophin or utrophin. Mol Med. 2001;7: 355–364.

499. Nguyen HX, Tidball JG. Interactions between neutrophils and macrophages promote macrophage killing of rat muscle cells in vitro. J Physiol (Lond). 2003;547: 125–132. doi:10.1113/jphysiol.2002.031450

500. Rigamonti E, Touvier T, Clementi E, Manfredi AA, Brunelli S, Rovere-Querini P. Requirement of Inducible Nitric Oxide Synthase for Skeletal Muscle Regeneration after Acute Damage. J Immunol. 2013;190: 1767–1777. doi:10.4049/jimmunol.1202903

501. Lau KS, Grange RW, Isotani E, Sarelius IH, Kamm KE, Huang PL, et al. nNOS and eNOS modulate cGMP formation and vascular response in contracting fast-twitch skeletal muscle. Physiol Genomics. 2000;2: 21–27. doi:10.1152/physiolgenomics.2000.2.1.21

502. Grange RW, Isotani E, Lau KS, Kamm KE, Huang PL, Stull JT. Nitric oxide contributes to vascular smooth muscle relaxation in contracting fast-twitch muscles. Physiol Genomics. 2001;5: 35–44. doi:10.1152/physiolgenomics.2001.5.1.35

503. Wells L. The o-mannosylation pathway: glycosyltransferases and proteins implicated in congenital muscular dystrophy. J Biol Chem. 2013;288: 6930–6935. doi:10.1074/jbc.R112.438978

504. Muntoni F, Torelli S, Wells DJ, Brown SC. Muscular dystrophies due to glycosylation defects: diagnosis and therapeutic strategies. Curr Opin Neurol. 2011;24: 437–442. doi:10.1097/WCO.0b013e32834a95e3

505. Buysse K, Riemersma M, Powell G, van Reeuwijk J, Chitayat D, Roscioli T, et al. Missense mutations in β-1,3-N-acetylglucosaminyltransferase 1 (B3GNT1) cause Walker-Warburg syndrome. Hum Mol Genet. 2013;22: 1746–1754. doi:10.1093/hmg/ddt021

506. Bao X, Kobayashi M, Hatakeyama S, Angata K, Gullberg D, Nakayama J, et al. Tumor suppressor function of laminin-binding alpha-dystroglycan requires a distinct beta3-N-acetylglucosaminyltransferase. Proc Natl Acad Sci USA. 2009;106: 12109–12114. doi:10.1073/pnas.0904515106

507. Hu H, Li J, Zhang Z, Yu M. Pikachurin interaction with dystroglycan is diminished by defective O-mannosyl glycosylation in congenital muscular dystrophy models and rescued by LARGE overexpression. Neurosci Lett. 2011;489: 10–15. doi:10.1016/j.neulet.2010.11.056

508. Grewal PK, Holzfeind PJ, Bittner RE, Hewitt JE. Mutant glycosyltransferase and altered glycosylation of α-dystroglycan in the myodystrophy mouse. Nature Genetics. 2001;28: 151–154. doi:10.1038/88865

509. Xia B, Hoyte K, Kammesheidt A, Deerinck T, Ellisman M, Martin PT. Overexpression of the CT GalNAc Transferase in Skeletal Muscle Alters Myofiber Growth, Neuromuscular Structure, and Laminin Expression. Developmental Biology. 2002;242: 58–73. doi:10.1006/dbio.2001.0530

510. Xu R, Camboni M, Martin PT. Postnatal Overexpression of the CT GalNAc Transferase Inhibits Muscular Dystrophy in mdx mice without Altering Muscle Growth or Neuromuscular Development. Neuromuscul Disord. 2007;17: 209–220. doi:10.1016/j.nmd.2006.12.004

511. Durko M, Allen C, Nalbantoglu J, Karpati G. CT-GalNAc transferase overexpression in adult mice is associated with extrasynaptic utrophin in skeletal muscle fibres. J Muscle Res Cell Motil. 2010;31: 181–193. doi:10.1007/s10974-010-9222-9

512. Palstra AP, Rovira M, Rizo-Roca D, Torrella J, Spaink HP, Planas JV. Swimming-induced exercise promotes hypertrophy and vascularization of fast skeletal muscle fibres and activation of myogenic and angiogenic transcriptional programs in adult zebrafish. BMC Genomics. 2014;15: 1136. doi:10.1186/1471-2164-15-1136

513. Fiaz AW, Léon-Kloosterziel KM, van Leeuwen JL, Kranenbarg S. Exploring the effect of exercise on the transcriptome of zebrafish larvae (*Danio rerio*). J Appl Ichthyol. 2014;30: 728–739. doi:10.1111/jai.12509

514. Fiaz AW, Léon-Kloosterziel KM, Gort G, Schulte-Merker S, van Leeuwen JL, Kranenbarg S. Swim-Training Changes the Spatio-Temporal Dynamics of Skeletogenesis in Zebrafish Larvae (Danio rerio). PLoS ONE. 2012;7: e34072. doi:10.1371/journal.pone.0034072

515. Simmonds AIM, Miln C, Seebacher F. Zebrafish (*Danio rerio)* as a Model for Sprint Exercise Training. Zebrafish. 2019;16: 1–7. doi:10.1089/zeb.2018.1646

516. van der Meulen T, Schipper H, van den Boogaart JGM, Huising MO, Kranenbarg S, van Leeuwen JL. Endurance exercise differentially stimulates heart and axial muscle development in zebrafish (*Danio rerio*). American Journal of Physiology-Regulatory, Integrative and Comparative Physiology. 2006;291: R1040–R1048. doi:10.1152/ajpregu.00116.2006

517. Bagatto B, Pelster B, Burggren WW. Growth and metabolism of larval zebrafish: effects of swim training. Journal of Experimental Biology. 2001; 204: 4335-4343.

518. Smith LL, Beggs AH, Gupta VA. Analysis of Skeletal Muscle Defects in Larval Zebrafish by Birefringence and Touch-evoke Escape Response Assays. JoVE (Journal of Visualized Experiments). 2013; e50925. doi:10.3791/50925

519. Berger J, Sztal T, Currie PD. Quantification of birefringence readily measures the level of muscle damage in zebrafish. Biochemical and Biophysical Research Communications. 2012;423: 785–788. doi:10.1016/j.bbrc.2012.06.040

520. Smith SJ, Horstick EJ, Davidson AE, Dowling J. Analysis of Zebrafish Larvae Skeletal Muscle Integrity with Evans Blue Dye. JoVE. 2015; 53183. doi:10.3791/53183

521. Chen L-C, Papandreou G, Schroff F, Adam H. Rethinking Atrous Convolution for Semantic Image Segmentation. ArXiv. 2017.

522. He K, Zhang X, Ren S, Sun J. Deep Residual Learning for Image Recognition. 2016 IEEE Conference on Computer Vision and Pattern Recognition (CVPR). Las Vegas, NV, USA: IEEE; 2016. pp. 770–778. doi:10.1109/CVPR.2016.90

523. Bailey EC, Alrowaished SS, Kilroy EA, Crooks ES, Drinkert DM, Karunasiri CM, et al. NAD+ improves neuromuscular development in a zebrafish model of FKRP-associated dystroglycanopathy. Skeletal Muscle. 2019;9: 21. doi:10.1186/s13395-019-0206-1

524. Babraham Bioinformatics - FastQC A Quality Control tool for High Throughput Sequence Data. [cited 10 Jun 2020]. Available: http://www.bioinformatics.babraham.ac.uk/projects/fastqc/

525. Bolger AM, Lohse M, Usadel B. Trimmomatic: a flexible trimmer for Illumina sequence data. Bioinformatics. 2014;30: 2114–2120. doi:10.1093/bioinformatics/btu170

526. GRCz11 - danRer11 - Genome - Assembly - NCBI. [cited 10 Jun 2020]. Available: https://www.ncbi.nlm.nih.gov/assembly/GCF_000002035.6/

527. Li B, Dewey CN. RSEM: accurate transcript quantification from RNA-Seq data with or without a reference genome. BMC Bioinformatics. 2011;12: 323. doi:10.1186/1471-2105-12-323

528. Langmead B, Trapnell C, Pop M, Salzberg SL. Ultrafast and memory-efficient alignment of short DNA sequences to the human genome. Genome Biol. 2009;10: R25. doi:10.1186/gb-2009-10-3-r25

529. Love MI, Huber W, Anders S. Moderated estimation of fold change and dispersion for RNA-seq data with DESeq2. Genome Biol. 2014;15: 550. doi:10.1186/s13059-014-0550-8

530. Eden E, Lipson D, Yogev S, Yakhini Z. Discovering Motifs in Ranked Lists of DNA Sequences. PLOS Computational Biology. 2007;3: e39. doi:10.1371/journal.pcbi.0030039

531. Eden E, Navon R, Steinfeld I, Lipson D, Yakhini Z. GOrilla: a tool for discovery and visualization of enriched GO terms in ranked gene lists. BMC Bioinformatics. 2009;10: 48. doi:10.1186/1471-2105-10-48

532. Mi H, Poudel S, Muruganujan A, Casagrande JT, Thomas PD. PANTHER version 10: expanded protein families and functions, and analysis tools. Nucleic Acids Res. 2016;44: D336-342. doi:10.1093/nar/gkv1194

533. Smith RN, Aleksic J, Butano D, Carr A, Contrino S, Hu F, et al. InterMine: a flexible data warehouse system for the integration and analysis of heterogeneous biological data. Bioinformatics. 2012;28: 3163–3165. doi:10.1093/bioinformatics/bts577

APPENDIX A: MATERIALS

This section provides detailed protocols for making the solutions used throughout the experiments performed in the above chapters.

A.1 1X ERM

To prepare a 20X stock solution the following was added to 800 mL of ddH_2O: 17.5 g NaCl, 0.75 g KCl, 2.9 g CaCl-$2H_2O$, 0.41 g KH_2PO_4, 0.142 g Na_2HPO_4 anhydrous, and 4.9 g $MgSO_4$-$7H_2O$. Once in solution, ddH2O was used to fill up to 1 L. This solution was then filter sterilized into an autoclaved 1-L flask and stored at +4C. 1X ERM was prepared by adding 50 mL of the 20X stock solution, 0.3 g of $NaHCO_3$, and one drop of methylene blue to 950 mL of autoclaved ddH_2O. 1X ERM was stored at room temperature.

A.2 Tricaine

A stock solution of triciane (MS-222) was prepared by adding 400 mg of powered tricaine and 800 mg of Na_2HP0_4 (Anhydrous) to 100 mL ddH_20. The pH was adjusted to 7.0 if necessary with 1M HCl or 1M NaOH. The stock solution was aliquoted and stored at -20C. Working solutions were prepared daily for live imaging and/or NMES by adding 400 μL of the stock solution to 10 mL of 1X ERM (612 μM). For the inactivity studies, working solutions were prepared daily by adding 200 μL of the stock solution to 10 mL of 1X ERM (306 μM).

A.3 Agarose

For long-term live imaging on the confocal, we found the best concentration for agarose to be 0.05%. In a 50-mL conical, 50 mg of low-melt agarose (Boston Bioproducts) was added to 10 mL of 1X ERM. The solution was then warmed in the microwave until the agarose was completely dissolved. After the agarose cooled, but before it solidified, 400 μL of tricaine was

added. For confocal imaging of fixed zebrafish, 50 mg of low-melt agarose was added to 10 mL of 1X PBS and warmed in the microwave until it was dissolved.

A.4 Evan's Blue Dye

Evan's Blue Dye (EBD) was prepared in 0.9% saline solution. To make the 0.9% saline solution, 9 g NaCl was dissolved in 700 mL dd H_2O, and the final volume was brought to 1 L using ddH_2O and filter sterilized into an autoclaved 1 L flask. To make 1% EBD stock solution, 100 mg of EBD powder was added to 10 mL of 0.9% saline solution. This stock solution was diluted to a final working solution of 0.1% by adding 1 mL of stock solution to 9 mL of 0.9% saline solution. EBD remained wrapped in tin foil to avoid exposure to light.

A.5 Buffers

A 10X PBS stock solution was made by adding 74.0 g NaCl, 19.4 g Na_2HPO_4•$7H_2O$, and 4.37 g NaH_2PO_4•H_2O to 800 mL ddH_2O. Once dissolved, ddH_2O was used to fill up to 1 L and the pH is adjusted to 7.4. This solution is then autoclaved. A 1X PBS solution was made by adding 100 mL of 10X PBS to 900 mL of ddH_2O. Similarly, a 2X PBS solution was made by adding 200 mL of 10X PBS to 800 mL of ddH_2O.

The 1X PBS-0.01% tween (PBS-tw) solution was prepared by adding 10 mL of Tween20 to 990 mL of 1X PBS. Similarly, the 1X PBS-2% triton (PBS-tx) solution was prepared by adding 20 mL of Triton X-100 to 980 mL of 1X PBS.

A.6 Paraformaldehyde

To prepare a 4% solution, 15 mL of ddH2O and 10 drops of 1M NaOH was added to 2 g of powdered PFA in a 50-mL conical. The conical was placed in a hot bath with a stir bar until the PFA was dissolved. Once dissolved, ddH2O was added up to 25-mL line, and the solution

was filtered into a clean 50-mL conical. Next, 25 mL of 2X PBS was added followed by 12 drops of 1M HCl. The pH was further adjusted until it was between 7.2 and 7.4.

A.7 Antibody Block

In a 50-mL conical, 2.5 g of Bovine Serum Albumin was dissolved in 30 mL of 1X PBS. Once BSA was in solution, 500 μL of DMSO, 500 μL of Triton and 100 mg of saponin was added. The final volume was brought up to 50-mL mark on the conical with 1X PBS.

APPENDIX B: METHODS

This section provides detailed descriptions for the assays and analyses performed throughout the experiments described in the above chapters. For every experiment, the same protocol was followed unless explicitly stated.

B.1 Zebrafish Husbandry and Handling

Zebrafish embryos were retrieved from natural spawns of adult zebrafish maintained on a 14-h light/10-h dark cycle. We used sapje^{ta222a} zebrafish [390] for most experiments. For live imaging studies, we used a transgenic sapje^{ta222a} zebrafish expressing mylpfa:lyn-cyan, smych1:GFP, myog:H2B:RFP (gift from Drs. Sharon Amacher and Jared Talbot). For the cell adhesion study, we used sapje^{ta222a} zebrafish overexpressing paxillin (actb2:pxn-EGFP) [470]. Embryos were grown in embryo rearing media (ERM) with methylene blue at 28.5 degrees Celsius. Embryos were manually dechorionated at 1 day post fertilization (dpf). Zebrafish were fed once daily beginning at 5 dpf. For survival studies, zebrafish were housed in 20 mm petri dishes with 10 mL of system water per dish beginning at 8 dpf. Survival checks were performed in the morning and at night. All protocols conform to the University of Maine Institutional Animal Care and Use Committee's Guidelines.

B.2 Birefringence Analysis

Birefringence is unique, physical property of highly organized matter, such as sarcomeres, in which light is rotated as it passes through it [518]. The optical transparency of zebrafish larvae allows birefringence to be used as a quick, rudimentary assessment of muscle defects [518,519], and we use it in our experiments to quantitatively assess the daily progression of dystrophy. Zebrafish were placed in tricaine (612 μM in 1X ERM) immediately prior to imaging and then transferred to a 35-mm glass bottom dish. Birefringence images were taken on a Leica MZ10 F Stereomicroscope with a Zeiss AxioCam MRm or Leica DMC5400

camera attached. An analyzer in a rotatable mount (Leica) was attached to the objective and the glass-bottom petri dish was placed on the polarized glass stage. Larvae showing consistently bright (white in color), well organized myotomes are classified as unaffected, wild-type siblings. Those displaying patchy areas (gray to black in color) of disrupted and disorganized myotomes are classified as affected *dmd* mutants. These gaps or lesions are the result of muscle fiber detachments from the myotendinous junction or disorganized and wavy muscle fibers [389]. Images were taken at the same time every day within an experiment. Imaging parameters were consistent for all zebrafish and across all days.

Mean gray values were calculated using FIJI software as described previously [519]. All images were blinded prior to measurements. Briefly, the body of the zebrafish was outlined from the 6th to the 25th myotome using the “Polygon selections” tool and then the mean gray value was measured. Three separate outlines were drawn to obtain three separate measures, and the average was used for calculations. All birefringence data were normalized to the average wild-type birefringence in each imaging session. Mean gray values are presented as a percentage of the average mean gray value of wild-type siblings in the control group (equation in Figure 1A). Birefringence was used as the metric to assess changes in overall muscle structure from 5 dpf to 8 dpf. A positive change in birefringence (increase in mean gray value) meant that there was increased birefringence at 8 dpf compared to 5 dpf and thus muscle structure improved. A negative change (decrease in mean gray value) meant that there was decreased birefringence and that muscle structure was worse.

B.3 DanioVision Analysis

The DanioVision system and EthoVision XT 13.0 software (Noldus Information, Inc) was used to conduct high-throughput locomotion tracking studies to better characterize the impact of NMES on zebrafish swimming activity. DanioVision uses a high-speed, infrared-sensitive camera to track individual zebrafish movement. For experiments, we kept zebrafish in their

respective wells of a 12-well plate and placed the 12-well plate into the DanioVision observation chamber. The temperature control unit was set to 28 degrees Celsius, ensuring that the temperature of the ERM in the well plate was maintained throughout the recording period. All zebrafish had five minutes to acclimate to the chamber. Using the EthoVision software, we created a white-light routine that included a 5 minute period in the dark followed by two light-on/off cycles, where the white light turned on at 100% intensity for 5 minutes and then turned off for 5 minutes. The total recording time was 25 minutes. Recordings were made at the same time each day.

At the end of the recording period, the raw data for each well was exported as an Excel file. This raw data file includes the distance moved and mean velocity across 0.033-second periods. For each fish, the average total distance and mean velocity across 1 minute intervals were calculated. Total distance and mean velocity during the dark periods (when fish are most active) was then calculated for each experimental group using the average total distance and mean velocity for each fish across the three 5-minute intervals.

B.4 Evan's Blue Dye Analysis

Evan's blue dye is a membrane impermeable dye used to assess membrane damage. In *dmd* mutants, EBD is used to assess muscle fiber integrity [520]. We used EBD to assess fiber integrity pre- and post-NMES using the methods described by [520]. Zebrafish were placed in tricaine (612 μM) for 4 minutes. At the end of the 4 minutes, zebrafish were aligned on a 1% agarose-lined Petri dish in a minimal volume of ERM. EBD was loaded into an injection needle pulled from glass capillary tubes on a Sutter Flaming/Brown Micropipette Puller. The needle was gently inserted into the peri-cardial space and EBD was ejected using a MPPI-3 pressure injector (ASI). Zebrafish were allowed to recover for 3 hours, providing ample time for the dye to circulate the body and enter damaged muscle fibers. Zebrafish were prepared for live imaging as described above for birefringence. An ET DSR fluorescent filter (Leica) was used to visualize

EBD. After imaging the initial dye amount in each zebrafish, zebrafish underwent 1 session of NMES as described above. Immediately after the NMES session, zebrafish were again prepared for live imaging. This allowed us to observe whether NMES caused additional dye entry into the muscle. The next day, zebrafish were imaged pre- and post-NMES using the same methods. Imaging parameters remained the same for all zebrafish and imaging sessions. Zebrafish were mounted laterally with the head on the left and dorsal up. To quantify EBD entry, mean gray values were calculated using the same methods described for birefringence except the outline was drawn from the first visible somite to the last visible somite. All images were blinded prior to analysis using a Perl script. Data is presented as the average mean gray value of the three separate measurements.

B.5 NMES

Zebrafish were subjected to NMES in groups of four using our 3D printed ‘gym’ (Figure 4B). The rectangular gym is divided into 6 rectangular wells that measure 4.7625 mm (length), 1.5875 mm (width), and 1.5875 mm (depth). Two tunnels run parallel to the smaller sides of the rectangular wells and the positive and negative electrodes slide through these tunnels such that they are exposed only in the wells. This allows the delivery of electrical pulses to each zebrafish simultaneously. Prior to the NMES session, zebrafish were transferred to tricaine solution (612 μM in 1X ERM) for 4 minutes. At the end of the 4 minutes, each zebrafish was placed into a well with its head facing the positive electrode and its tail facing the negative electrode. The positive and negative electrodes are attached to a Grass SD9 Stimulator, which is used to generate the electrical pulses. Each NMES session lasts 1 minute. Following each NMES session, zebrafish are removed from the gym and placed back into their respective well plates.

B.6 Immunostaining

Zebrafish were fixed in 4% Paraformaldehyde (PFA) for 4 h at room temperature. After fixation, embryos were rinsed in PBS-0.1% Tween 20 (PBS-tw). For visualizing muscle structure, phalloidin was used. Zebrafish were first permeabilized in PBS-2% Triton-X-100 for 1.5 h and then placed in 1:20 phalloidin (Invitrogen) in PBS-tw for 4 hours on the rocker at room temperature. Zebrafish were rinsed out of phalloidin using PBS-tw and stored in PBS-tw until imaged. For visualizing neuromuscular junctions, zebrafish were stained with alpha-bungarotoxin and SV2. Zebrafish were first permeabilized in 1 mg/ml collagenase in 1X PBS for 1.5 h, and then stained with 1:500 alpha-bungarotoxin-647 (Molecular Probes) and 1:20 phalloidin in antibody block for 2 h at room temperature. Zebrafish were rinsed using PBS-tw, and placed in antibody block overnight at 4°C. Zebrafish were then stained with 1:50 SV2 (DSHB) in antibody block for 3 days at 4°C. Upon removal from SV2, zebrafish were rinsed using PBS-tw and then placed in antibody block for 8 h at room temperature. This was followed by an overnight incubation in 1:200 GAM (Invitrogen) in antibody block. Zebrafish were then rinsed out of secondary antibody using PBS-tw and stored in PBS-tw until imaged. Phalloidin-488 or -546 and GAM-488 or -546 were used interchangeably with no differences in staining observed.

B.7 Confocal Imaging

Confocal imaging was used to visualize phalloidin and NMJ staining. Fixed and stained zebrafish were deyolked and then mounted in 0.5% low-melt agarose in 1X PBS in a 24-well glass bottom plate. Fluorescent images were captured using a 25x water objective on a Leica SP8 confocal microscope.

For live imaging, zebrafish were anesthetized in tricaine solution (612 μM in 1X ERM) for 4 minutes and then mounted 24-well glass bottom plate using 0.5% low-melt agarose in 1X ERM (with 612 μM tricaine). Two or three zebrafish were placed in each well. Zebrafish were mounted anterior left and dorsal up to ensure the same side of the fish was imaged each day.

Finally, a small amount of tricaine solution (612 μM in 1X ERM) was added to prevent the agarose from evaporating and to ensure the zebrafish remained anesthetized throughout the imaging session. Upon completion of imaging, zebrafish were gently removed from the agarose using fine fishing line and returned to their respective wells.

B.8 Second Harmonic Generation

Fixed zebrafish were deyolked and then mounted in 1.0% low-melt agarose in 1XPBS glass bottom 30-mm petri dish. The petri dish was then filled with PBS. Images were acquired using a custom-built two-photon microscope. This system uses a modified Olympus FV300 system with an upright BX50WI microscope stand and a mode-locked Ti:Sapphire laser. Laser power was modulated via an electro-optic modulator.

The SHG signals were collected in a non-descanned geometry using a single PMT. Emission wavelengths were separated from excitation wavelengths using a 665 nm dichroic beam splitter followed by a 448/20 nm bandpass filters for SHG signals. Images were acquired using circular polarization with excitation power ranging from 1 to 50 mW and a 40x 0.8 NA water immersion objective with 3x optical zoom and scanning speeds of 2.71s/frame. All images were 512 x 512 pixels with a field of view of 85 micrometers.

To calculate sarcomere distance, SHG images were first imported into ImageJ, and then, using the Freehand selection tool, two lines were drawn to indicate the outer boundaries (top and bottom) of the muscle fiber being analyzed. The Freehand selections were converted into .txt files and imported into LabVIEW VI. Using LabVIEW, the midline of the two selections (top and bottom) was determined. The midline was then imported back into ImageJ over the original photo, and positioned in the center of the sarcomeres. Next, the Plot Profile tool and Peak Finder tool were then used to determine the peaks, which correspond to sarcomere length. Since the Peak Finder tool gives distance in pixels, a conversion factor was used to

convert pixels to micrometers based on the objective and optical zoom used. Multiple muscle fibers are analyzed for each zebrafish.

B.9 Image Analysis

All images were blinded using a Perl script prior to analysis. Phalloidin images were used to assess muscle fiber degeneration. The percent of myotomes with muscle fiber detachments was calculated manually by counting the number of muscle segments with visibly detached fiber(s). Muscle segments are defined as half myotomes. Additionally, we used machine learning to identify healthy versus unhealthy muscle fibers. For these analyses, we used MATLAB to implement a deep learning approach to segment images of phalloidin stained fish into healthy muscle, sick muscle, and background. We used the DeepLab v3+ system with an underlying Resnet18 network [521,522]. We defined the ground truth dataset manually using LabelBox (labelbox.com). Training images and ground truth images were broken down into 256 x 256 pixel images for training. The training dataset was divided into 60% training, 20% validation and 20% test data. Median frequency weighting was used to balance the classes. Each fish was oriented such that the head of the fish would be at the left of the image. Data was augmented to translate the images by 10 pixels vertically and horizontally. Rotation was found to make the network less accurate as orientation angle of the muscle fibers relative to the body orientation is important to assessing their health. The stochastic gradient descent with momentum (SGDM) optimizer was selected with 0.9 momentum. The maximum number of epochs was 100, and the mini-batch size was 8. In every epoch, the training dataset was shuffled. The number of iterations between evaluations of validation metrics was 315. The patience of validation stopping of network training is set up to 4. The initial learning rate used for training was 0.001. The learning rate was dropped 0.3 fold piecewise during training every10 epochs. The Factor for L2 regularization (weight decay) was 0.005. The training set reached an accuracy of 97%. Images were then segmented by the MATLAB *semanticseg* command, which

produced 8-bit unsigned integer segmentations. The fraction of each fish that was determined to be healthy was reported as a fraction of the total muscle. Pixels determined to be background (i.e. not muscle) were excluded from this calculation.

For NMJ analyses, we used the method that was recently published by our laboratory [523]. To prepare images for analysis, a custom Fiji macro was written in order to keep image processing consistent throughout all experiments. First, the raw .lif file is opened in FIJI and the image is split into its respective channels (phalloidin, AChR, and SV2). The phalloidin channel is immediately saved as a .tif file and closed. For the AChR and SV2 channels, duplicate z stacks are created and a 10 pixel radius Gaussian blur is applied. These blurred images are then subtracted from their original images, respectively. The resulting images are then merged to a single image and a maximum intensity projection is generated. This maximum intensity projection is saved as a .tif file and closed. For each experiment, the maximum intensity projections are combined into a single .tif file using a custom MATLAB script. This file is then opened in FIJI and three separate masks, marking the fish body, horizontal myoseptum and myoseptal innervation, are drawn on the projected images using the Pencil tool. These masks were used to define muscle segments, where a muscle segment represents half of a single myotome. Using a custom MatLab script, skeleton number and skeleton length were then calculated for each muscle segment across all zebrafish analyzed. To do this, masks were imported back into MATLAB for segmentation of the AChR and SV2 channels. Images were further processed using the adaptive histogram equalization (“adapthisteq” function) to enhance the images followed by a 1 pixel radius Gaussian blur (‘imguassfilt’ function) to denoise the images. The now defined muscle segments were then skeletonized, cleaned, and despurred (“bwmorph” function). Finally, skeleton number and length were calculated within each muscle segment of a single fish and averaged across all fish within each experimental group.

Muscle nuclei were analyzed using FIJI’s 3D Object Counter as well as the basic Measure tool. To prepare images for analysis we first reduced background noise by duplicating

the image (z stack), performing a 10 pixel Gaussian blur on the duplicated image, and subtracting the blurred image from the original image. We then performed a 1 pixel Gaussian blur on this image and set a threshold using 'max entropy' setting. With this image, we used the "Analyze Particles" tool to generate masks to use with "3D Object Counter" tool as well as the "Measure" tool. The 3D Objects Counter tool provided surface area and volume measurements while the Measure tool provided perimeter, area, and major axis measurements. These latter measurements were used to calculate filament index.

B.10 Statistical Analysis

All statistical analyses were performed in Graphpad Prism. Normality was first assessed for all data using the Shapiro-Wilk test. If data passed this normality test, an unpaired two-tailed t test was performed between two data sets (i.e., *dmd* mutant control vs *dmd* mutant eNMES) while an ordinary one-way ANOVA was performed followed by a Tukey's multiple comparison test between three data sets (i.e., WT sibling control vs *dmd* mutant control vs *dmd* mutant eNMES). Conversely, if data failed the normality test, a Mann-Whitney U test was performed for comparing two data sets while a Kruskal-Wallis test was performed for comparing three data sets. Significance for all tests was set to $p < 0.05$.

B.11 RNA Extraction and Analysis

Total RNA was extracted from whole zebrafish at 7 dpf from replicate samples using the Zymo Direct-zol RNA microprep kit. Each biological replicate consisted of two zebrafish. For wild-type siblings, there were 4 replicates for the control group and 3 replicates for the eNMES group, and for *dmd* mutants, there were 8 replicates for the control group and 10 replicates for the eNMES group. Prior to performing RNA extractions, zebrafish within the eNMES and control groups were paired based on their severity at disease onset and the calculated change in their birefringence from 5 dpf to 7 dpf. RNA was kept at -80°C until it was shipped to Quick Biology

(Pasadena, CA) for sequencing. Following RNA quality control using an Agilent BioAnalyzer 2100 (), polyA+ RNA-seq libraries were prepared for each sample using the KAPA Stranded RNA-Seq Kit (KAPA Biosystems, Wilmington, MA). Final library quality and quantity were analyzed by Agilent Bioanalyzer 2100 and Life Technologies Qubit3.0 Fluorometer. 150 bp reads were sequenced on Illumina HighSeq 4000 (Illumnia Inc., San Diego, CA). Each library was sequenced using 150bp paired-end reads using an Illumina HiSeq4000.

Analyses of RNA-Seq reads were completed on the Advanced Computing Group Linux cluster at the University of Maine. To determine the quality of the RNA sequencing reads before further processing, FastQC version 0.11.8 was utilized [524]. Following this quality assessment, reads were concatenated tail-to-head to produce one forward FASTQ file and one reverse FASTQ file for each replicate sample. These FASTQ files were then trimmed of adapter sequences, and low quality leading and trailing ends were removed using Trimmomatic version 0.36.0 [525]. Trimmed paired-end reads mapped to the Ensembl-annotated zebrafish transcriptome [526] (Ensembl version 95) to generate read counts per gene using RSEM version 1.2.31 [527] with bowtie version 1.1.2 [528]. Read counts were analyzed using the DESeq2 version 1.22.2 [529] to analyze gene expression, p-value, and false discovery rate (FDR). Genes with fewer than ten mapped reads across all samples were excluded. For each pairwise comparison of treatment groups, differentially expressed genes were determined using FDR p-value cutoff of 0.1 and requiring at least a 0.6 $\log_2$ fold-change (in either direction). Resulting lists were used for Gene Ontology enrichment analysis and set analysis for each pair-wise comparison.

Sets of differentially expressed genes (both up and down regulated) were analyzed to test for enriched GO Biological Process terms (FDR < 0.1) using GOrilla [530,531] (http://cbl-gorilla.cs.technion.ac.il/) for enrichment in Biological Processes. For this analysis, the entire set of expressed genes were used a background. In cases where Gorilla found no enriched terms, PantherDB's overrepresentation test on Biological Processes [532] (http://pantherdb.org/) was

used. Again, the entire set of expressed genes list was used as the backround, and results were evaluated using Panther's Fisher's Exact Test and p-values were adjusted for multiple testing using FDR.

Ensembl gene IDs were mapped to gene symbols and names using zebrafishMine's Analyse feature [533] (http://www.zebrafishmine.org/). In some cases, manual mapping was used by comparing Zfin.org gene search and Ensembl gene search results. Summarized gene expression data are available at the Gene Expression Omnibus (accession number GSE155465), and FASTQ files are available at the Short Read Archive (accession number SRP274405).

APPENDIX C: SUPPLEMENTAL FIGURES

Figure 14: Variation at disease onset in *dmd* mutants affects swimming activity throughout disease progression.

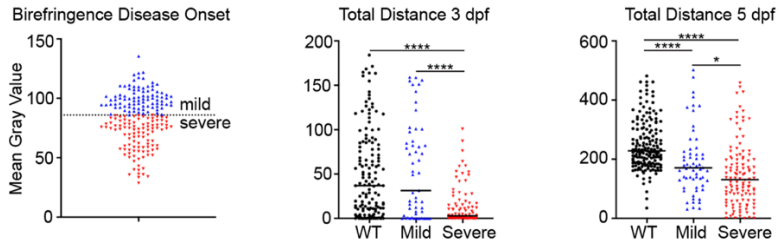

Figure 15: Swimming activity is negatively affected by extended inactivity at 5 dpf.

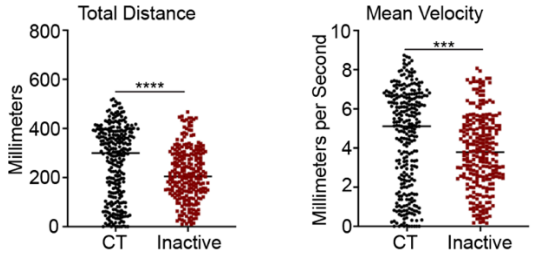

Figure 16: Percentage of *dmd* mutants that exhibited a negative change in mean gray value from 5 to 8 dpf following NMES or extended inactivity.

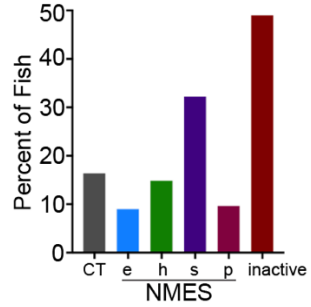

Figure 17: Principal component analysis highlights clustering of replicates for WT siblings and *dmd* mutants with and without eNMES.

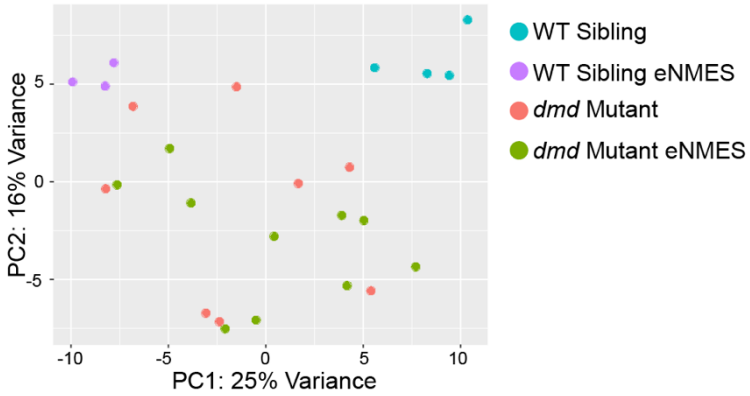

BIOGRAPHY OF THE AUTHOR

Elisabeth Kilroy was born in February of 1992. Since the age of 16, she has dedicated herself to understanding how muscle grows in size, how it is able to increase the force it generates, and how it recovers from injury. Watching her brother and father battle an unknown type of muscular dystrophy further fueled her commitment to understanding skeletal muscle and searching for a cure. She graduated from James Island Charter High School in Charleston, South Carolina in June of 2010 with an International Baccalaureate Diploma. In December of 2014, she graduated *summa cum laude* with a GPA of 3.968 from the College of Charleston with a Bachelor of Science degree in Exercise Science and a minor in Neuroscience. For her accomplishments in the classroom, Elisabeth received the Outstanding Student in Exercise Science award and the Teacher's Pet award. Her career as a researcher began in the laboratory of Dr. Gary Aston-Jones at the Medical University of South Carolina. For 3.5 years she volunteered as an undergraduate research assistant under the mentorship of Drs. David Moorman and Benjamin Zimmer, studying the role of orexinergic neurons in alcohol and cocaine addiction. As an undergraduate, Elisabeth published one first author manuscript titled "The effect of single-leg stance on dancer and control group static balance" (*International Journal of Exercise Science*) and co-authored two manuscripts titled "Orexin/hypocretin neuron activation is correlated with alcohol seeking and preference in a topographically specific manner" (*European Journal of Neuroscience* 2016) and "Orexin/hypocretin-1 receptor antagonism reduces ethanol self-administration and reinstatement in highly-motivated rats" (*Brain Research* 2017).

In August of 2015, Elisabeth started in the Graduate School of Biomedical Science and Engineering at University of Maine. Even though she had no idea what a zebrafish was or how it could be used to understand skeletal muscle and muscular dystrophy, she joined the laboratory of Dr. Clarissa Henry. During her first summer in the laboratory, Dr. Henry left Elisabeth unattended and it was during this time that Elisabeth, with the help of her brother, Keegan,

conceptualized her dissertation project. Elisabeth was awarded the prestigious National Science Foundation Graduate Research Fellowship during her second year as a graduate student. In addition to her own research, she assisted with other laboratory projects, and co-authored two manuscripts titled “NAD+ improves neuromuscular development in a zebrafish model of FKRP associated dystroglycanopathy” (*Skeletal Muscle*) and “A novel drug-combination screen in zebrafish identifies epigenetic small molecule candidates for Duchenne muscular dystrophy” (*Skeletal Muscle*), and one review paper titled ‘Muscling’ through life: integrating studies of muscular development, homeostasis, and disease in zebrafish” (*Current Topics in Developmental Biology*). Outside of the laboratory, Elisabeth served as the Vice President of Graduate Student Government for two years and the Student Body President of her graduate program for one year. While in these leadership roles, she dedicated herself to increasing professional development opportunities for graduate students. Elisabeth also volunteered her time with the Muscular Dystrophy Association, serving as a summer camp counselor, team captain for the annual Muscle Walk, and advocate. For her commitment to research and service, Elisabeth was awarded the Dan Sandweiss Graduate Student Advocacy Award, the UMaine GSBSE Student Service Award, the UMaine College of Natural Sciences, Forestry and Agriculture Outstanding Service Award, and the UMaine Tyler-Glanz Prize for Excellence in Animal Research. Lastly, for her commitment to finding a cure for muscular dystrophy, she received the first ever research grant from the Morgan Hoffmann Foundation. Elisabeth is a candidate for the Doctor of Philosophy degree in Biomedical Science from the University of Maine in August 2020.